DEPARTMENT OF PHYSICS

CONTROLLING ELECTRON AND EXCITON TRANSFER PATHS IN MOLECULAR SYSTEMS

DOCTOR OF PHILOSOPHY DISSERTATION

PANAYIOTIS ANTONIOU

2017

DEPARTMENT OF PHYSICS

CONTROLLING ELECTRON AND EXCITON TRANSFER PATHS IN MOLECULAR SYSTEMS

PANAYIOTIS ANTONIOU

A Dissertation Submitted to the University of Cyprus in Partial Fulfillment of the Requirements for the Degree of Doctor of Philosophy

April 2017

VALIDATION PAGE

Doctoral Candidate: Panayiotis Antoniou

Doctoral Thesis Title: Controlling Electron and Exciton Transfer Paths in Molecular Systems

The present Doctoral Dissertation was submitted in partial fulfillment of the requirements for the Degree of Doctor of Philosophy at the ***Department of Physics*** *and was approved on the 24/04/2017 by the members of the* ***Examination Committee****.*

Examination Committee:

Research Supervisor: Spiros Skourtis (Assoc. Prof., Dep. of Physics, UCY)

Committee Member: Uri Peskin (Prof., Dep. of Chemistry, Technion – Israel Institute of Technology)

Committee Member: Georgios Archontis (Assoc. Prof., Dep. of Physics, UCY)

Committee Member: Nicolaos Toumbas (Assoc. Prof., Dep. of Physics, UCY)

Committee Member: Anastasios Keramidas (Prof., Dep. of Chemistry, UCY)

DECLARATION OF DOCTORAL CANDIDATE

The present doctoral dissertation was submitted in partial fulfillment of the requirements for the degree of Doctor of Philosophy of the University of Cyprus. It is a product of original work of my own, unless otherwise mentioned through references, notes, or any other statements.

Panayiotis Antoniou

Περίληψη

Η παρούσα Διδακτορική Διατριβή επικεντρώνεται στη μελέτη των μηχανισμών αντιδράσεων μεταφοράς ηλεκτρονίου (ΜΗΛ) και μεταφοράς ενέργειας (ΜΕΝ) σε μοριακά συστήματα. Ο κύριος στόχος της ερευνητικής μου δραστηριότητας ήταν να αναπτύξω καλύτερη φυσική κατανόηση όσον αφορά τον ενεργό έλεγχο των αντιδράσεων ΜΗΛ και ΜΕΝ σε μοριακά σύμπλοκα. Ο έλεγχος των μηχανισμών ΜΗΛ και ΜΕΝ είναι ζωτικής σημασίας σε βιολογικά και τεχνητά φωτοβολταϊκά υλικά καθώς και στον ευρύτερο τομέα της μοριακής ηλεκτρονικής. Χρησιμοποιώντας θεωρητικά μοριακά μοντέλα, δότη (ΔΟ) – γέφυρας (ΓΕ) – δέκτη (ΔΕ), και πραγματοποιώντας προσομοιώσεις, υπολογισμούς *ab initio* σε πραγματικά μόρια και αναλυτικές μεθοδολογίες, αναπτύξαμε ένα φορμαλισμό και υπολογιστικά εργαλεία που μας δίνουν τη δυνατότητα ανάλυσης του ελέγχου διαδικασιών ΜΗΛ και ΜΕΝ σε μόρια.

Η κύρια ερευνητική συνιστώσα της παρούσας Διατριβής, αφορά το πεδίο του ελέγχου μοριακών αντιδράσεων ΜΗΛ μέσω εφαρμογής υπέρυθρων (IR) παλμών διέγερσης που διαταράσσουν τις δονήσεις του μορίου. Η βασική ιδέα μπορεί διαισθητικά να περιγραφεί με ένα μόριο ΔΟ-ΓΕ-ΔΕ το οποίο πραγματοποιεί ΜΗΛ μέσω φωτοδιέγερσης από το ΔΟ στο ΔΕ διαμέσου των ενδιάμεσων ηλεκτρονιακών καταστάσεων της ΓΕ. Η επιλεκτική διέγερση συγκεκριμένων δονητικών καταστάσεων ΓΕ με παλμούς IR προκαλεί χρονοεξαρτημένες μεταβολές στις ενέργειες των ηλεκτρονιακών καταστάσεων ΓΕ καθώς και στις ηλεκτρονιακές συζεύξεις μεταξύ των καταστάσεων DO-ΓΕ και ΔΕ-ΓΕ, επηρεάζοντας έτσι το ρυθμό ΜΗΛ. Αυτού του είδους ο έλεγχος είναι ιδιαίτερα επωφελής, αφού η διέγερση IR είναι σχετικά μη επιβλαβής, υπό την έννοια ότι δεν μεταβάλλει τις ηλεκτρονιακές καταστάσεις του συστήματος ΔΟ-ΓΕ-ΔΕ και κυρίως δεν προκαλεί μη αντιστρεπτές αλλαγές στη μοριακή δομή. Έχουν πραγματοποιηθεί μερικά πειράματα δονητικού ελέγχου ΜΗΛ χρησιμοποιώντας δράση παλμών IR. Τα πειράματα πραγματοποιήθηκαν σε διαφορετικά μοριακά συστήματα και όλα παρουσιάζουν σημαντική αλλά διαφορετικού βαθμού επίδραση της διέγερσης IR στο ρυθμό ΜΗΛ. Στη δική μου ερευνητική εργασία χρησιμοποιήσαμε θεωρητικά μοριακά μοντέλα ΔΟ-ΓΕ-ΔΕ και υπολογισμούς *ab initio* σε συγκεκριμένα μόρια, για να διερευνήσουμε τους περιορισμούς που υπάρχουν στη δυνατότητα να επηρεαστεί σημαντικά ο ρυθμός ΜΗΛ μέσω δονητικής διέγερσης με δράση παλμού IR. Οι περισσότεροι περιορισμοί προέρχονται από τη φύση του μοριακού δονητικού φάσματος, την ισχύ της σύζευξης ηλεκτρονίου-

δονήσεων, την ισχύ της αλληλεπίδρασης μεταξύ μοριακών δονήσεων και ακτινοβολίας IR και την ισχύ της αλληλεπίδρασης μορίου-διαλύματος. Επίσης, υπάρχουν περιορισμοί που προέρχονται από τη πειραματική διάταξη και οι οποίοι καθορίζουν τα χαρακτηριστικά των παλμών IR διέγερσης. Έχοντας αυτούς τους περιορισμούς υπόψη, προτείνουμε εύρος παραμέτρων και μοριακές αρχιτεκτονικές που αυξάνουν το δονητικό έλεγχο των ΜΗΛ για γρήγορες διαδικασίες ΜΗΛ.

Επιπρόσθετα στη παρούσα Διατριβή μελετήσαμε αντιδράσεις ΜΕΝ (ή μεταφοράς εξιτονίων) τριπλής κατάστασης μέσω του μηχανισμού Dexter. Οι μοριακές ΜΕΝ σε μόρια ΔΟ-ΓΕ-ΔΕ, πραγματοποιούνται μέσω των ενδιάμεσων καταστάσεων εξιτονίων της ΓΕ. Η μεταφορά εξιτονίου είναι συνδυασμένη μεταφορά δύο σωματιδίων, ενός ηλεκτρονίου και μίας οπής, μεταξύ διαφορετικών εντοπισμένων περιοχών του μορίου. Η συνδυασμένη μεταφορά δύο σωματιδίων είναι πολύ πιο πολύπλοκη από τη μεταφορά ενός σωματιδίου (ηλεκτρονίου ή οπής). Στην ερευνητική εργασία αναπτύξαμε μια νέα θεωρητική και υπολογιστική περιγραφή μονοπατιών σύζευξης μέσω καταστάσεων ΓΕ για μηχανισμούς ΜΕΝ σήραγγος (tunneling). Είναι σημαντικό να αναφέρω ότι ο θεωρητικός φορμαλισμός που έχουμε αναπτύξει, λαμβάνει υπόψη τη συνεισφορά εξιτονίων ΓΕ στη σύζευξη ΜΕΝ (οι συνεισφορές εξιτονίων ΓΕ έχουν αγνοηθεί από προηγούμενες θεωρίες). Έχουμε παρατηρήσει δύο ανταγωνιστικούς μηχανισμούς μονοπατιών σύζευξης. Σε μόρια με μικρές ΓΕ ή/και μεγάλα ενεργειακά φράγματα δυναμικού στη ΓΕ (tunneling barriers), οι εξιτονικές καταστάσεις ΔΟ-ΔΕ καθορίζουν κυρίως τη σύζευξη. Εν αντιθέσει σε μόρια με μεγαλύτερες ΓΕ ή/και μικρότερα φράγματα δυναμικού στη ΓΕ η σύζευξη ΜΕΝ εξιτονίων τριπλής κατάστασης πραγματοποιείται κυρίως μέσω των εξιτονικών καταστάσεων ΓΕ. Επιπρόσθετα έχουμε αναπτύξει αναλυτικά μοντέλα ΔΟ-ΓΕ-ΔΕ για να κατανοήσουμε τη συμπεριφορά των μονοπατιών ΔΟ-ΔΕ και ΓΕ ως συνάρτηση του μήκους της ΓΕ και των ενεργειακών καταστάσεων της γέφυρας.

Abstract

This Ph.D. Thesis focuses on electron transfer (ET) and energy transfer (EnT) mechanisms in molecular systems. The main objective of my research work was to develop a physical understanding of how to control actively electron and energy propagation through molecules. Such control of ET and EnT flow is vital in biological and artificial solar energy conversion materials and in molecular electronics. Using theoretical models of donor (D) – bridge (B) – acceptor (A) molecules, and employing simulations, *ab initio* computations on real molecules and analytical methodologies, I described frameworks that enable the active control of ET and EnT reactions.

A major component of this Thesis is in the field of vibrational control of molecular ET reactions by application of infrared (IR) pulses. The basic idea can be intuitively described by a D-B-A molecule that undergoes photoinduced bridge-mediated D-to-A ET. Selective IR (vibrational) excitation of specific bridge vibrational modes influences the ET rate by modulating the bridge electronic state energies and the bridge-mediated D-to-A electronic coupling. This type of ET rate control is exciting since IR excitation is chemically innocent, in the sense that it does not alter the electronic states of the D-B-A system and neither does it cause irreversible changes to the molecular structure. Some experiments of vibrationally-controlled molecular ET using IR pulses have been realized. The experiments were performed on different molecular systems and all of them demonstrated significant but different levels of IR-induced ET rate modulation. In my research work we used theoretical models of D-B-A molecules and *ab initio* computations on specific classes of molecules, to explore the constraints on achieving enhanced vibrational perturbation of ET rates with application of IR excitation pulses. Most of the constraints stem from molecule-specific characteristics, such as the nature of molecular vibrational spectra, the strengths of the electron–vibrational coupling, the interaction strengths between molecular vibrations and IR radiation and the strength of the molecule-solvent interaction. There also constraints that stem from experimental setups that produce the IR excitation pulses characteristics. Having these constraints in mind, we suggest parameter regimes and molecular architectures that may enhance the vibrational control of ET for fast ET reactions.

Another part of this Thesis is devoted for triplet exciton ("Dexter") EnT and in particular on bridge-mediated Dexter EnT systems. The simplest intuitive way to describe EnT is to consider it as a coupled motion of two particles, an electron and a hole, between different localized molecular regions. This adds considerable richness to the mediation process, compared to single-particle (electron or hole) transfer. In this research work we developed a single-particle coupling-pathway theory for bridge-mediated triplet EnT and provided formulas and computational schemes to assess the bridge exciton contribution to the triplet-exciton coupling (ignored by earlier theories). We find two competing coupling pathway mechanisms. At shorter distances and/or high tunneling gaps, donor-acceptor charge-transfer exciton virtual states dominate the triplet EnT coupling. At longer distances and/or lower tunneling gaps, virtual exciton states of the bridge (with both electron and hole on the bridge), mediate the transport. We further developed D-B-A models to illustrate single-particle and two-particle (exchange) EnT pathways and to formulate an intuitive framework of EnT pathways that demonstrates strong analogies to ET pathways and their interferences.

Acknowledgements

First and foremost, I would like to express my sincerest gratitude to my Thesis advisor, and my mentor, Prof. Spiros S. Skourtis for his constant enthusiasm guidance, support and encouragement throughout this long journey of my Master and Ph.D. studies. It has been an honor for me to work under his supervision all these years.

I am especially grateful to Prof. David N. Beratan and to all of his group members at Duke University: Dr. Peng Zhang, Chaoren Liu and Zheng Ma for good advice and great collaborations.

I would like to thank my Thesis committee members: Profs. Uri Peskin, Georgios Archontis, Nicolaos Toumbas and Anastasios Keramidas, for honoring me with their acceptance to join my Thesis committee.

I would also like to express my sincere thanks to all of my friends and fellow students for their friendship, support, and for making my student life enjoyable.

Last, I am deeply grateful to my beloved family, my parents and my brother for their unconditional love and support, especially for their encouragement and patience during the "dark" periods of my Ph.D. studies.

Table of Contents

List of Figures

List of Tables

Chapter 1: Introduction

Molecular electron transfer and energy transfer reactions are of tremendous importance in molecular and chemical science, in engineering and biology, e.g., in biological and artificial solar energy conversion materials and molecular electronics [1-4]. An exciting topic of intensive study, especially the last few years, is the development of new experimental and theoretical/computational methodologies that give the necessary tools to control actively charge and energy flow in molecular systems [1,5].

Theoretical studies by S. Skourtis, D. Beratan and colleagues, e.g., [6-8] predicted that infrared (IR) excitation of spatially-localized vibrational modes of electron transfer (ET) molecules may be used to control ET kinetics. The idea is as follows: if we consider an electron donor (D) – bridge (B) – electron acceptor (A) molecule that undergoes photoinduced D-to-A ET mediated by the electronic states of the intervening B, the IR excitation of the B vibrational modes before or after initiation of ET could make it possible to control the D-to-A ET rate by modulating the molecular structure. This type of ET rate control is advantageous because it does not alter the electronic state of the molecular ET system or irreversibly change its molecular structure. It is, therefore, reversible and repeatable without inducing photodamage.

Motivated by these ideas, I. Rubtsov and co-workers performed in 2009 the first experiment of vibrationally-controlled molecular ET using IR laser pulses [9]. The ET system consists of an anthracene-derived acceptor connected to a dimethylaniline-containing donor linked by guanosine-cytidine (GC) hydrogen bonds. Selective IR excitation of the bridge G-C H-bonds reduces the D-to-A ET rate by 60%. It took up to 2014-15 to obtain further solid verification of the original idea from new experiments [10-12] that achieved a high IR-perturbation effect on molecular ET rates (from 28% [11] to 100% [10]). J. Weinstein and co-workers [10] demonstrated 100% switch off of D-to-A ET by IR excitation of the high-frequency bridge carbon-carbon triple-bond vibrations for an electronically excited covalent trans-acetylide platinum(II) D-B-A system. The ability to switch off ET is exciting, but it is also of essential importance to be able to switch on ET. In addition, I. Rubtsov and co-workers [11] reported IR-induced enhanced ET rate modulations in Re(I) D-A complexes. Specifically, IR excitation of the bipyridine ring stretching modes on the acceptor, exhibit 28% faster D-to-A ET. The new experimental

successes and the status of the field are described in two recent news articles in the journals Nature Chemistry [13] and Physics Today [14]. Despite of the recent experimental progress in controlling molecular ET rates by IR excitation, a full theoretical understanding of all the factors that determine the ET rate modulations is lacking. Detailed understanding of the IR modulation mechanism is needed to explain the ET rate changes induced by the IR excitation and to design structures with specific ET properties that enable enhanced control of the ET rates by IR excitation

A large components of my research work as a Ph.D. student was in this field under the supervision of Prof. S. Skourtis and in collaboration with Prof. D. Beratan and his group at Duke University USA. The collaboration was funded by the Cyprus Research Promotion Foundation, through the project "Vibrational Control of Electron Transfer" ΔΙΕΘΝΗΣ/ ΣΤΟΧΟΣ/0311/04. I used theoretical models of D-B-A molecules and *ab initio* computations on real molecules to explore the constraints on achieving strong vibrational perturbation of ET rates with IR pulses. These constraints stem from molecule-specific characteristics, such as the nature of molecular vibrational spectra and the strengths of the electron–vibrational coupling, and from the interaction strengths between molecular vibrations and infrared radiation. In this research work, I suggested parameter regimes and molecular architectures that may enhance the vibrational control of ET for fast ET reactions. The suggested molecular architectures may allow the control of ET pathways in multiple B ($D–B_i–A$) systems *via* selective IR excitations of B modes. The advantage of using B vibrations to perturb bridge-mediated ET rates is due to the possibility to manipulate ET pathways selectively, without altering the electronic states of the molecular ET system or causing irreversible photochemical changes to the ET structures. Specifically, I find that the IR-induced ET rate perturbation is enhanced if the ET mechanism is coherent resonant through-bridge tunneling and if the timescales of ET and vibrational relaxation of the IR-excited B mode are of the same order. This work has been cited by some of the main experimentalists in the field [12] who performed the experiment in [10]. I will extensively discuss this research work in Chapter 4.

In addition, part of my research work was dedicated to triplet-energy (exciton) transfer models, for bridge-mediated exciton transfer systems (the so-called Dexter energy transfer systems). When the exciton donor and the exciton acceptor states are triplets, a one-electron tunneling and a two-electron exchange interaction enable the energy transfer from donor to acceptor. In many molecular energy transfer systems the donor and acceptor

molecules are connected by a bridge which mediates donor-to-acceptor triplet energy transfer [15-20].

In collaboration with Prof. D. Beratan and his group at Duke University USA we developed a coupling-pathway theory for bridge-mediated triplet energy transfer, a process controlled by the structure of the bridge between donor and acceptor species. In this research work we provide formulas and computational schemes to assess the bridge exciton contribution to the triplet-exciton coupling, which earlier theories did not account for. Our description of the exciton coupling pathways relies on a configuration-interaction single-excitations (CIS) framework, which tracks the coupled motion of two particles (electron and hole). We find two competing coupling pathway mechanisms. At shorter distances and/or high tunneling gaps, the electron and hole propagate sequentially from donor to acceptor, accessing donor-acceptor charge-transfer exciton virtual states. In this regime the relevant virtual exciton states of the bridge have either a single electron or a single hole. At longer distances and/or lower tunneling gaps, virtual exciton states of the bridge mediate the transport, where both electron and hole reside on the bridge. Molecular design strategies can modulate these competing mechanisms and their distinctive dependences on molecular structure. Our coupling-pathway theory enables a structure-function analysis of the triplet energy transfer coupling at the atomic-level, a step forward to our task to control energy transfer reactions in a wide range of energy transfer systems. It may also explain the enhanced triplet energy transfer rates non-compatible with the standard energy transfer theories [21,22]. My own contribution to this project was to develop and to code Green's function formulas for the exciton-pathway analysis of the bridge-mediated triplet-exciton coupling. I also analyzed some simple models for the triplet exciton bridge pathways and for their interferences.

In the remaining of this first Chapter, I give an introductory theoretical description of electron transfer and energy transfer procedures in molecular systems, essential for the following Chapters.

1.1 Electron Transfer in Molecules

This section is a brief overview of some of the basic concepts of molecular electron transfer reactions. The electron transfer process can be understood as a spontaneous electron transition from an initial state spatially localized at the electron donor part of the molecular system to a final state spatially localized at the acceptor part of the system. The electronic transition dynamics are always accompanied by instantaneous nuclear rearrangement and by the interplay between electronic and nuclear dynamics. In the following, theories of electron transfer rates will be discussed accompanied by presentations of the different regimes of electron transfer rates.

1.1.1 Molecular Hamiltonian

Let us first consider a molecule composed of N_{el} electrons and N_{nuc} nuclei atoms. The Cartesian coordinates and momenta will be denoted as $\vec{r}_j$ and $\vec{p}_j$, for electrons, and $\vec{R}_n$, $\vec{P}_n$ for the nuclei, respectively. The total molecular Hamiltonian operator has the general form

$$\hat{H}_{mol} = \hat{T}_{el} + \hat{T}_{nuc} + \hat{V} . \tag{1.1}$$

$\hat{T}_{el}$ is the electron kinetic energy, $\hat{T}_{nuc}$ is the nuclear kinetic energy and $\hat{V}$ is the potential energy of the system. The kinetic energies of the electrons and nuclei are given by

$$\hat{T}_{el} = \sum_{j=1}^{N_{el}} \frac{p_j^2}{2m_{el}} \quad , \quad \hat{T}_{nuc} = \sum_{n=1}^{N_{nuc}} \frac{P_n^2}{2M_n} \ , \tag{1.2}$$

where m_{el} is the electron mass and M_n the mass of the *n*th nucleus. The potential energy includes electron-electron and nuclear-nuclear Coulomb repulsion interactions and the corresponding attractive Coulomb interactions between electrons and nuclei

$$\hat{V}_{el-el} = \frac{1}{2}\sum_{i\neq j}^{N_{el}} \frac{e^2}{4\pi\varepsilon_0 \left|\vec{r}_i - \vec{r}_j\right|} \ , \ \hat{V}_{nuc-nuc} = \frac{1}{2}\sum_{m\neq n}^{N_{nuc}} \frac{z_m z_n e^2}{4\pi\varepsilon_0 \left|\vec{R}_m - \vec{R}_n\right|} \ , \ \hat{V}_{el-nuc} = -\sum_{j}^{N_{el}}\sum_{n}^{N_{nuc}} \frac{z_n e^2}{4\pi\varepsilon_0 \left|\vec{r}_j - \vec{R}_n\right|} . \tag{1.3}$$

z_m, z_n are the atomic numbers of the *m*th and *n*th nucleus.

The time independent molecular Schrödinger equation is

$$\hat{H}_{mol}\Psi\left(\vec{r};\vec{R}\right)=\mathcal{E}\,\Psi\left(\vec{r};\vec{R}\right). \tag{1.4}$$

Ψ is a multi-particle wavefunction, where $\vec{r}=\left(\vec{r}_1,\vec{r}_2,...,\vec{r}_{N_{el}}\right)$ and $\vec{R}=\left(\vec{R}_1,\vec{R}_2,...,\vec{R}_{N_{nuc}}\right)$ denote the electronic and nuclear Cartesian coordinates, respectively. $\mathcal{E}$ denotes the energy of either the ground or any of the excited eigenstates of the system.

1.1.2 Born-Oppenheimer Approximation

Solving eq. (1.4) is a highly difficult task and due to the large numbers of particles the Schrödinger equation cannot be solved analytically and approximations are required. One first adopts the Born-Oppenheimer approximation which is based on the large mass difference of electrons and nuclei $\left(M_n \geq 2000\,m_{el}\right)$. Due to this difference, electrons can be considered to move much faster than nuclei and to respond almost instantaneously to any changes in the nuclear configuration [1,2,23]. This further implies that the nuclear motion alters electron-nuclear interactions only adiabatically and does not trigger transitions between different electronic states [1]. Thus, we can separate the wavefunction $\Psi\left(\vec{r};\vec{R}\right)$ into two components (the so-called Born-Oppenheimer Separation), i.e.,

$$\Psi^{BO}\left(\vec{r};\vec{R}\right)=\psi_{el}\left(\vec{r};\vec{R}\right)\varphi_{vib}\left(\vec{R}\right), \tag{1.5}$$

where $\psi_{el}\left(\vec{r};\vec{R}\right)$ is the electronic wavefunction at each nuclear geometry and $\varphi_{vib}\left(\vec{R}\right)$ is the nuclear wavefunction. Importantly, the electronic wavefunction will only parametrically depend on the nuclear coordinates.

Following the arguments above, we can ignore the nuclear kinetic energy operator as compared to the electron kinetic energy operator ($\hat{T}_{nuc} \ll \hat{T}_{el}$, since $M_n \geq 2000\,m_{el}$). This approximation leads us to the definition of the Born-Oppenheimer Hamiltonian $\hat{H}^{BO}=\hat{H}_{mol}-\hat{T}_{nuc}$. Hence,

$$\hat{H}^{BO}\left(\vec{r};\vec{R}\right)=\hat{H}^{el}\left(\vec{r};\vec{R}\right)+\hat{V}_{nuc-nuc}, \tag{1.6a}$$

$$\hat{H}^{el}\left(\vec{r};\vec{R}\right)=\hat{T}_{el}+\hat{V}_{el-nuc}+\hat{V}_{el-el}. \tag{1.6b}$$

The Born-Oppenheimer Hamiltonian $\hat{H}^{BO}$ is comprised of the electronic Hamiltonian $\hat{H}^{el}$ and the nuclear-nuclear repulsion interactions $\hat{V}_{nuc-nuc}$. $\hat{H}^{el}$ consists of the kinetic energy operator of the electrons $\hat{T}_{el}$, the attractive interactions between electrons and nuclei $\hat{V}_{el-nuc}$ and the electron-electron repulsion interactions $\hat{V}_{el-el}$. Both of the Hamiltonians, $\hat{H}^{BO}$ and $\hat{H}^{el}$ carry a parametric dependence on the nuclear coordinates.

Therefore, instead of solving the Schrödinger equation for the total molecular Hamiltonian eq. (1.4), we solve the respective Schrödinger equation within the Born-Oppenheimer approximation

$$\hat{H}^{BO}\Psi^{BO}\left(\vec{r};\vec{R}\right)=E^{BO}\left(\vec{R}\right)\Psi^{BO}\left(\vec{r};\vec{R}\right) \tag{1.7}$$

where, $E^{BO}\left(\vec{R}\right)$ are the eigenenergies of the $\hat{H}^{BO}$. $E^{BO}\left(\vec{R}\right)$ defines a hypersurface in the space of nuclear coordinates $\vec{R}$, the potential energy surface (PES) for the nuclear motions in a specific electronic state. If we consider the nuclei as classical particles, then the total force exerted on every individual nucleus from the N_{el} electrons and the remaining $N_{nuc}-1$ nuclei atoms will be

$$\vec{F}_n=-\vec{\nabla}_{R_n}E^{BO}\left(\vec{R}\right) \tag{1.8}$$

for nucleus n. Equation (1.8) is proved using the Feynman-Hellmann theorem, that considers a system with a Hamiltonian $\hat{H}\{L_i\}$ that depends on some parameters $\{L_i\}$. The respective Hamiltonian eigenstates Ψ and eigenvalues E also depend on parameters $\{L_i\}$.

$$\hat{H}\{L_i\}\left|\Psi\{L_i\}\right\rangle=E\{L_i\}\left|\Psi\{L_i\}\right\rangle. \tag{1.9}$$

The Feynman-Hellmann theorem states that

$$\frac{\partial}{\partial L_i}E\{L_i\}=\left\langle\Psi\{L_i\}\right|\frac{\partial}{\partial L_i}\hat{H}\{L_i\}\left|\Psi\{L_i\}\right\rangle, \tag{1.10}$$

which directly relates the derivative of the total energy of the system to the expectation value of the derivative of the Hamiltonian with respect to a general parameter L_i. The Feynman-Hellmann theorem demonstrates that all the forces in the system can be

calculated using classical electrostatics (e.g., eq. (1.8)), as long as the electron densities are computed from the Schrödinger equation.

To prove eq. (1.8) we set in eqs. (1.9) and (1.10) $\hat{H}\{L_i\} = \hat{H}^{BO}(\vec{R})$, $E\{L_i\} = E^{BO}(\vec{R})$, $|\Psi\{L_i\}\rangle = |\Psi^{BO}(\vec{R})\rangle$ and eq. (1.8) becomes

$$-\vec{\nabla}_{R_n} E^{BO}(\vec{R}) = \langle \Psi^{BO}(\vec{r};\vec{R}) | (-\vec{\nabla}_{R_n} \hat{H}^{BO}) | \Psi^{BO}(\vec{r};\vec{R}) \rangle \tag{1.11}$$

where, $\vec{\nabla}_{R_n} \hat{H}^{BO} = \vec{\nabla}_{R_n} \hat{V}_{el-nuc} + \vec{\nabla}_{R_n} \hat{V}_{nuc-nuc}$ and eq. (1.11) will be

$$\begin{aligned} -\vec{\nabla}_{R_n} E^{BO}(\vec{R}) &= \langle \Psi^{BO}(\vec{r};\vec{R}) | (-\vec{\nabla}_{R_n} \hat{V}_{el-nuc} - \vec{\nabla}_{R_n} \hat{V}_{nuc-nuc}) | \Psi^{BO}(\vec{r};\vec{R}) \rangle \\ &= \langle \Psi^{BO}(\vec{r};\vec{R}) | (\vec{F}_{el-n}) | \Psi^{BO}(\vec{r};\vec{R}) \rangle + \langle \Psi^{BO}(\vec{r};\vec{R}) | (\vec{F}_{n-m}) | \Psi^{BO}(\vec{r};\vec{R}) \rangle. \end{aligned} \tag{1.12}$$

The first term on the right-hand site of eq. (1.12) $\langle \vec{F}_{el-n} \rangle$ is the average attractive force exerted on nucleus n from the N_{el} electrons and the second term $\langle \vec{F}_{n-m} \rangle$ is the average repulsive force exerted on nucleus n from the remaining $N_{nuc} - 1$ nuclei atoms $(m \neq n)$. Thus the summation of these two terms gives the total force exerted on every individual nucleus n from the N_{el} electrons and the remaining $N_{nuc} - 1$ nuclei atoms, demonstrating eq. (1.8).

1.1.3 Diabatic and Adiabatic States

Let us now consider the simplest case scenario of a molecule consisting of donor and acceptor parts with respective donor-localized (D) and acceptor-localized (A) diabatic electronic states. Often in ET experiments the molecule is photoexcited by a laser pulse to prepare the initial donor state. Subsequently, a second laser pulse is applied to monitor the decay of the donor state and/or the rise of the acceptor state (pump-probe experiment). The ET from donor to acceptor parts is carried by an electronic coupling between donor and acceptor states. We present the simplest two-state model for the ET problem (Fig. 1.1). The electronic Hamiltonian in the donor-acceptor diabatic representation is generally given by

$$\hat{H}^{el} = E_D(R)|D\rangle\langle D| + E_A(R)|A\rangle\langle A| + V_{DA}(|D\rangle\langle A| + |A\rangle\langle D|), \tag{1.13}$$

where V_{DA} is the D-A electronic coupling matrix element. $E_D(R)$, $E_A(R)$ are the D and A diabatic PES energies (solid lines in Fig. 1.1) and R is a collective coordinate (normal mode) [1,2,24] that modulates $E_D(R)$ and $E_A(R)$ (Fig. 1.1). The above model is the simplest model, because it assumes two electronic states and a single reaction coordinate.

Diagonalization of $\hat{H}^{el}$ (eq. (1.13)) for every R gives the adiabatic representation of $\hat{H}^{el}$. The adiabatic $\hat{H}^{el}$ is written as

$$\hat{H}^{el} = E_g(R)|g\rangle\langle g| + E_e(R)|e\rangle\langle e|, \tag{1.14}$$

where $|g\rangle$ and $|e\rangle$ are the ground and excited adiabatic electronic states, with energies $E_g(R)$ and $E_e(R)$, respectively (dashed lines in Fig. 1.1). The ground adiabatic PES $E_g(R)$ is well described by the double well potential in Fig. 1.1 (lower dashed line curve) with respect to a single reaction coordinate. Also the excited adiabatic PES $E_e(R)$ (upper dashed line curve) can be seen in Fig. 1.1. Even though, most of the electronic structure calculations initially compute the adiabatic states, several diabatization procedures exist [25-31], to obtain the respective diabatic states.

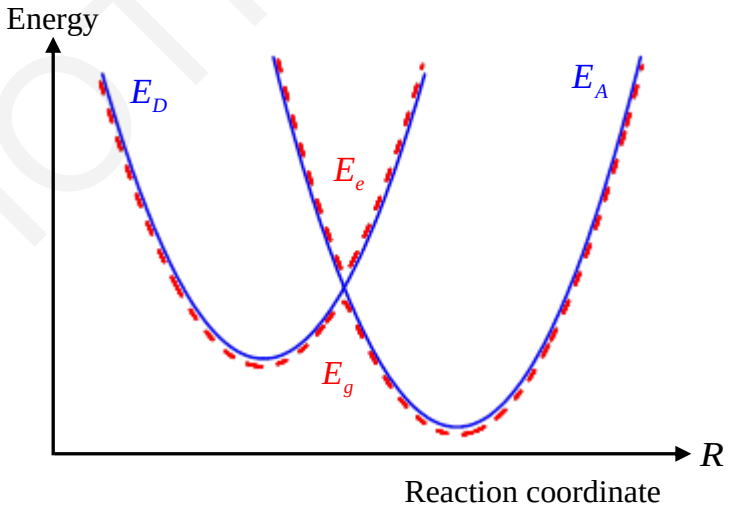

Figure 1.1: Adiabatic and diabatic representation of PES versus reaction coordinate R which can be some collective nuclear coordinate. The adiabatic (red dashed line) curves, for the ground E_g and excited E_e states, and the diabatic (blue solid line) curves for donor E_D and acceptor E_A states are shown.

1.1.4 Regimes of Electron Transfer

To give a qualitative description and to further distinguish the different (nonadiabatic and adiabatic) ET regimes, in the following we will apply a theoretical treatment, based on the Landau-Zener theory [1,2,24,32-36] of ET in which the D and A electronic state energies are time dependent and cross. We first describe the D-A ET system within a single classical reaction coordinate which is time dependent (i.e., $R = R(t)$). The respective diabatic D-A electronic Hamiltonian is given by

$$\hat{H}^{el} = E_D\left(R(t)\right)|D\rangle\langle D| + E_A\left(R(t)\right)|A\rangle\langle A| + V_{DA}\left(|D\rangle\langle A| + |A\rangle\langle D|\right), \tag{1.15}$$

where $E_D\left(R(t)\right)$, $E_A\left(R(t)\right)$ represents diabatic PES localized at D and A, respectively (Fig. 1.1). Initially we assume that the electronic state is D and that the reaction coordinate (and respective energies) start to move on the D PES far away from the crossing point $\left(R_{res}\right)$ with the A PES. At a time window t_{res} the reaction coordinate reaches the resonance region $\left(R(t_{res}) = R_{res}\right)$ during which the D and A electronic energies cross, such that $E_D\left(R_{res}\right) = E_A\left(R_{res}\right) = E_{res}$.

The D to A transition probability for this crossing event can be estimated adopting the Landau-Zener approach which assumes a linear time dependence of the reaction coordinate around the resonance region. We thus perform a Taylor expansion around the resonance region for both PES, i.e.,

$$E_{D/A}\left(R(t)\right) = E_{res} + \left\{\left.\frac{dE_{D/A}}{dR}\right|_{R_{res}}\right\} \times \left\{\left.\frac{dR}{dt}\right|_{t_{res}}\right\} \times \left(t - t_{res}\right). \tag{1.16}$$

The D to A Landau-Zener transfer probability is given by

$$P_{DA} = 1 - \exp\left[\left(2\pi\right)^2 \gamma\right], \tag{1.17}$$

where $\gamma = \tau_{LZ}/\tau_{Rabi}$ is the Landau-Zener (or the so-called Massey) parameter written as a ratio of two times, the Rabi time and the Landau-Zener time. The Rabi time is $\tau_{Rabi} = h/|V_{DA}|$, which applied to a resonant time-independent D-A system. This time interval is a good estimate for the time required in a (time-independent) resonant D-A

system, i.e., when $|E_D - E_A| \le |V_{DA}|$, to induce a complete donor to acceptor transition $(P_{DA} \approx 1)$. In addition the Landau-Zener time

$$\tau_{LZ} = \frac{|V_{DA}|}{\left| \{dR/dt\}_{t_{res}} \{dE_D/dR - dE_A/dR\}_{R_{res}} \right|}, \tag{1.18}$$

is the time spent by the D and A energies in the resonance region in a time-dependent D-A system described by eq. (1.16).

In the nonadiabatic limit the motion of the reaction coordinate in the crossing-resonance region ($|E_D - E_A| \le |V_{DA}|$) is so fast such that the D and A energies do not remain in resonance for long enough time in order to induce a complete D to A transition, i.e., $\gamma = \tau_{LZ}/\tau_{Rabi} \ll 1$. In this nonadiabatic ET regime the exponent in eq. (1.17) can be expanded in a Taylor series such that the D to A transition probability becomes proportional to the square of the electronic coupling $\left(P_{DA} \approx (2\pi)^2 \gamma \approx |V_{DA}|^2\right)$ and the corresponding nonadiabatic ET rate is proportional to $|V_{DA}|^2$ (e.g., eq. (1.19)). In the nonadiabatic limit the probability of electron transfer for every energy crossing is small.

In the opposite limit $(\gamma = \tau_{LZ}/\tau_{Rabi} \gg 1)$ the ET is called adiabatic. The D and A energies remain in resonance for long enough time, i.e., $\gamma = \tau_{LZ}/\tau_{Rabi} \gg 1$ and induce a complete D to A transition. The probability of electron transfer is 100% for each crossing $(P_{DA} \approx 1)$. Adiabatic ET can be visualized as the rearrangement of the reaction coordinate from the D minimum diabatic PES to the A minimum diabatic PES by crossing the intermediate potential barrier (e.g., see E_g adiabatic PES in Fig. 1.1). The respective adiabatic ET rate can be expressed as a standard Arrhenius type $k_{DA} \sim e^{-E_{act}/K_B T}$, where E_{act} is the activation energy to reach the resonance region.

1.1.5 Classical Marcus Electron Transfer Theory in Nonadiabatic Regime

Let us now present a description of ET reactions rates, starting our considerations in the high temperature limit. Despite the fact that molecular nuclear motions are of quantum nature the (classical) high temperature limit is applicable if the energy of a characteristic

vibrational quantum $\hbar\omega$ of the reaction coordinate R is much smaller than the thermal energy K_BT $\left(K_BT \gg \hbar\omega\right)$. In this situation (Figs. 1.1 and 1.2) the vibrational dynamics of the system along R (vibrational modes) can be described using classical physics.

In molecular ET reactions the observable quantity is often the D to A ET rate and the main model describing ET reactions is the nonadiabatic Marcus-rate expression [1,2,24,32-37]. The ET rate is a product of a classical Boltzmann factor (see eq. (1.20)) and a tunneling probability

$$k_{DA} = \frac{2\pi}{\hbar}\left|V_{DA}\right|^2 \rho_{FC}\,. \tag{1.19}$$

It is worth mentioning that in nonadiabatic ET reactions the tunneling matrix elements (electronic couplings V_{DA}) that induce ET from D to A are weak and therefore the ET rate is limited by these electronic couplings.

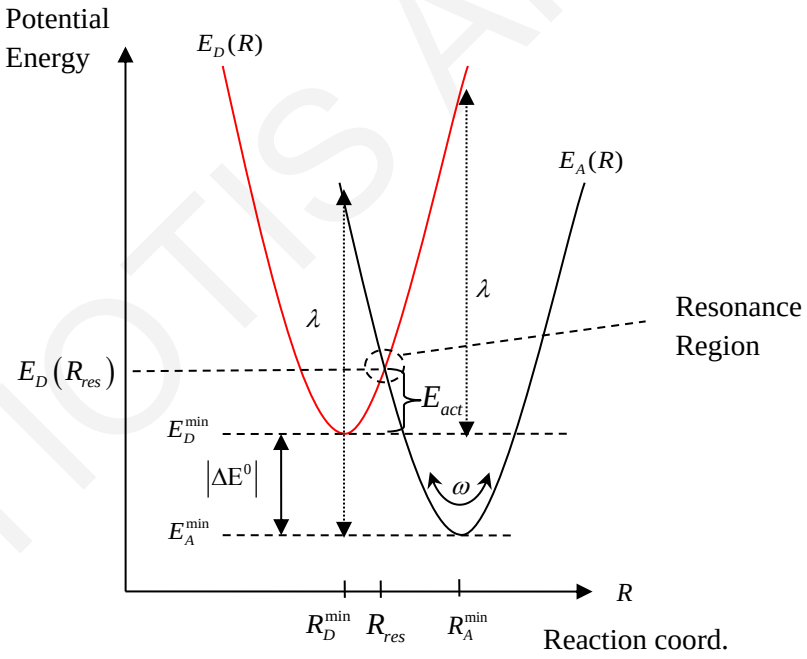

Figure 1.2: Potential energy surfaces of the ET system when the electron is at the initial (D) and the final (A) electronic states (E_D and E_A respectively).

The potential energy (diabatic Born-Oppenheimer, Fig. 1.2) surfaces seen by the ET system when the electron is at the D or at the A electronic state generally present different energetic characteristics, i.e., different minimum energy values $E_D^{\min} \neq E_A^{\min}$, where

$E_D^{\min} = E_D\left(R_D^{\min}\right)$, $E_A^{\min} = E_A\left(R_A^{\min}\right)$ and different reaction-coordinate values $R_D^{\min} \neq R_A^{\min}$ (see Fig. 1.2). With the electron at D, the reaction coordinate fluctuates around the conformation that minimizes E_D, more precisely around $R_D^{\min}$, which is not a D-A resonance conformation $\left(R_D^{\min} \neq R_{res}\right)$ and the system has to wait for a thermal fluctuation of the reaction coordinate to bring D and A to resonance. The classical (high-temperature) Boltzmann probability (or the classical Franck-Condon factor) for this activation step to the resonance conformation is [1,2,24,32-37]

$$\rho_{FC} = \frac{1}{\sqrt{4\pi\lambda K_B T}} \exp\left[-E_{act} / K_B T\right], \tag{1.20}$$

$$E_{act} = \frac{\left(\left|\Delta E^0\right| + \lambda\right)^2}{4\lambda} \quad , \quad \left|\Delta E^0\right| = \left|E_{\mathrm{A}}^{\min} - E_D^{\min}\right|. \tag{1.21}$$

E_{act} is the activation energy to reach the resonance conformation R_{res} (Fig. 1.2) $\left(E_{res} = E_D\left(R_{res}\right) = E_A\left(R_{res}\right)\right)$. $\left|\Delta E^0\right|$ is the energetic difference between the D and A minimum energy conformations, which is frequently called as the driving force of the ET reaction and λ denotes the reorganization energy given by $\lambda = E_{D/A}\left(R_{A/D}^{\min}\right) - E_{D/A}\left(R_{D/A}^{\min}\right)$ or, equivalently, by $\lambda = m\omega^2\left(R_A - R_D\right)^2/2$, where $E_{D/A}$, $R_{D/A}$ are the electronic state energies and reaction coordinates for D and A respectively. The reorganization energy is defined as the energy required to "reorganize" the system to the new equilibrium coordinate conformation.

D to A ET may only proceed if the total energy of the system (ET molecule and solvent) is conserved. Energy-conserving ET occurs when the D and A electronic state energies E_D and E_A are in resonance $\left(E_D = E_A\right)$.

Generally, a collective set of system motions, described by the reaction coordinates R, modulates the energies of the D and A electronic states, i.e., $E_D(t) = E_D\left(R(t)\right)$ and $E_A(t) = E_A\left(R(t)\right)$. Thermal fluctuations of the reaction coordinate bring the system to a D-to-A resonance conformation R_{res} for which $E_D\left(R_{res}\right) = E_A\left(R_{res}\right)$ and thus enable ET. Thus, eqs. (1.19)-(1.21) can be derived from the Landau-Zener nonadiabatic result as follows. The D to A ET only proceeds if the system is in the resonance conformation R_{res}.

The total energy needed for the reaction coordinate R to reach R_{res} should be $E^{tot} \geq E_D^{\min} + E_{act}$ (see Fig. 1.2). If $E^{tot} \geq E_D^{\min} + E_{act}$ then the reaction coordinate R will pass through R_{res} two times per period $2\pi/\omega$. For every time $\left(t_{res}\right)$ R_{res} is reached, the D to A transfer probability will be given by the Landau-Zener transfer probability in the nonadiabatic limit

$$P_{DA}\left(E^{tot}\right) = \frac{2\pi \left|V_{DA}\right|^2}{\hbar \left| \left\{dR/dt\right\}_{t_{res}} \left\{dE_D/dR - dE_A/dR\right\}_{R_{res}} \right|}, \tag{1.22}$$

and the respective D to A Landau-Zener ET rate will be given by

$$k_{DA}\left(E^{tot}\right) = 2 \times P_{DA}\left(E^{tot}\right) \times \frac{\omega}{2\pi}, \tag{1.23}$$

since the resonance conformation R_{res} is reached two times per period, when the total energy is $E^{tot} \geq E_D^{\min} + E_{act}$.

For an ensemble of D-A molecules, the ET rate is given by a product of a Boltzmann probability average over the D PES and the D to A Landau-Zener ET rate eq. (1.23) for every energy crossing

$$k_{DA} = \int_{E_D(R_{res})}^{\infty} dE^{tot}\, k_{DA}\left(E^{tot}\right) \times P_{Boltz}\left(E^{tot}\right), \tag{1.24a}$$

$$P_{Boltz}\left(E^{tot}\right) = \frac{e^{-E^{tot}/K_BT}}{\int_{E_D^{\min}}^{\infty} dE^{tot}\, e^{-E^{tot}/K_BT}}, \tag{1.24b}$$

where $E^{tot} = E_D^{\min} + E_{act}$. This calculation leads to the Marcus rate expression eq. (1.19).

1.1.6 Quantum Electron Transfer Theory in Nonadiabatic Regime

In the foregoing discussion it was assumed that the nuclear motion (reaction coordinate R) is classical. Next we assume that $K_BT \leq \hbar\omega$ holds for all the vibrational degrees of freedom participating in the ET reaction and change to a quantum description of nuclear motion [1,2,32-34]. For simplicity we assume that there is one high frequency vibrational mode whose equilibrium position (minimum conformation energy with the electron at D or

A) changes upon ET from D to A. In the quantum mechanical description of the process the total Hamiltonian of the system will be (Fig. 1.3)

$$\hat{H} = \hat{H}^{el} + \hat{H}^{vi} + \hat{H}^{el-vi}, \tag{1.25}$$

where "el" denotes electronic, "vi" vibrational and "el-vi" electronic-vibrational couplings. The electronic Hamiltonian is

$$\hat{H}^{el} = E_D^{\min} |D\rangle\langle D| + E_A^{\min} |A\rangle\langle A| + V_{DA}\left(|D\rangle\langle A| + |A\rangle\langle D|\right), \tag{1.26}$$

where $E_D^{\min}$, $E_A^{\min}$ describes the D and A electronic site energies and V_{DA} the intersite electronic coupling between D and A. The respective vibrational Hamiltonian is given by

$$\begin{aligned} &\hat{H}^{vi} = \hat{H}_D^{vi} + \hat{H}_A^{vi}, \\ &\hat{H}_K^{vi} = \frac{\hat{P}_R^2}{2m}|K\rangle\langle K| + \frac{m\omega^2}{2}\left(R - R_K\right)^2 |K\rangle\langle K| = \sum_{n_K} \hbar\omega\left(n_K + \frac{1}{2}\right)|n_K\rangle\langle n_K| \quad (K = D, A), \end{aligned} \tag{1.27}$$

where $|n_K\rangle$ denotes the vibrational eigenstates when the electron is in D or A and $\hbar\omega\left(n_K + 1/2\right)$ the respective vibrational eigenenergies. Further, we assume linear electron-vibrational coupling and the corresponding electron-vibrational Hamiltonian is given by

$$\hat{H}^{el-vi} = \left(|A\rangle\langle A|\right) \otimes \left[-\Delta F_A\left(R - R_A\right)\right], \tag{1.28}$$

where ΔF_A is the force exerted on the vibrational mode as the electron transfers from D to A.

Having established the Hamiltonian (eqs. (1.25)–(1.28)) for the desired ET system we can now further split the Hamiltonian into two parts

$$\hat{H} = \hat{H}^{(0)} + \hat{V} \quad , \quad \hat{H}^{(0)} = \hat{H}_D^{(0)} + \hat{H}_A^{(0)} \quad , \quad \hat{V} = V_{DA}\left(|D\rangle\langle A| + |A\rangle\langle D|\right), \tag{1.29a}$$

$$\hat{H}_D^{(0)} = \left\{E_D^{\min} + \frac{\hat{P}_R^2}{2m} + \frac{m\omega^2}{2}\left(R - R_D\right)^2\right\}|D\rangle\langle D|, \tag{1.29b}$$

$$\hat{H}_A^{(0)} = \left\{E_A^{\min} + \frac{\hat{P}_R^2}{2m} + \frac{m\omega^2}{2}\left(R - R_A\right)^2 - \frac{\Delta F_A^2}{2m\omega^2}\right\}|A\rangle\langle A|, \tag{1.29c}$$

where $\hat{H}^{(0)}$ is the time independent unperturbed Hamiltonian and $\hat{V}$ is a weak time independent perturbation.

The eigenstates and eigenvalues of the unperturbed Hamiltonian will be

$$\left|\psi_k\right\rangle = \begin{Bmatrix} \left|n_D\right\rangle\left|D\right\rangle \\ \left|n_A\right\rangle\left|A\right\rangle \end{Bmatrix} \quad , \quad E_k = \begin{Bmatrix} E_D^{\min} + \hbar\omega\left(n_D + 1/2\right),\ n_D = 0,1,... \\ E_A^{\min} + \hbar\omega\left(n_A + 1/2\right) - \lambda,\ n_A = 0,1,... \end{Bmatrix}, \tag{1.30}$$

where $\left|\psi_k\right\rangle$ are electron-vibrational (vibronic) states and λ is the corresponding reorganization energy and is defined as $\lambda = m\omega^2\left(R_A - R_D\right)^2/2 = \Delta F_A^2/2m\omega^2$.

The D-to-A ET rate is given by the Fermi golden-rule for time independent perturbation

$$k_{DA} = \frac{2\pi}{\hbar}\sum_{n_D}\sum_{n_A}\frac{e^{-E_{n_D}/K_BT}}{Z}\left|\left\langle D\left|\hat{V}\right|A\right\rangle\right|^2\left|\left\langle n_D\middle|n_A\right\rangle\right|^2\delta\left(E_D^{\min} + E_{n_D} - \left(E_A^{\min} + E_{n_A}\right)\right), \tag{1.31}$$

where, $E_{n_D} = \hbar\omega\left(n_D + 1/2\right)$, $E_{n_A} = \hbar\omega\left(n_A + 1/2\right)$ and $Z = \sum_{n_D} e^{-E_{n_D}/K_BT}$.

$\left\langle D\left|\hat{V}\right|A\right\rangle$ is the electronic coupling between D and A. $\left\langle n_D\middle|n_A\right\rangle$ is the overlap between the vibrational eigenstates $\left(X_{n_D}\left(R-R_D\right),\ X_{n_A}\left(R-R_A\right)\right)$ and in the form of an integral $\left\langle n_D\middle|n_A\right\rangle = \int_{-\infty}^{\infty} dR\left\{X_{n_D}\left(R-R_D\right)\right\}^* X_{n_A}\left(R-R_A\right)$.

The square of the overlap integral is the Franck-Condon factor, which is given by [38,39]

$$\left|\left\langle n_D\middle|n_A\right\rangle\right|^2 = \exp\left[-\frac{\lambda}{\hbar\omega}\right]\times\left(\frac{\lambda}{\hbar\omega}\right)^{\left(n_D-n_A\right)}\times\left(\frac{n_A!}{n_D!}\right)\times\left[L_{n_A}^{\left(n_D-n_A\right)}\left(-\frac{\lambda}{\hbar\omega}\right)\right]^2 \tag{1.32}$$

where, λ is the reorganization energy and $L_{n_A}^{\left(n_D-n_A\right)}$ the Laguerre polynomial $L_p^q\left(x\right) = \sum_{k=0}^{p}\frac{\left(-x\right)^k}{k!}\left[\frac{\left(p+q\right)!}{\left(q+k\right)!\left(p-k\right)!}\right]$.

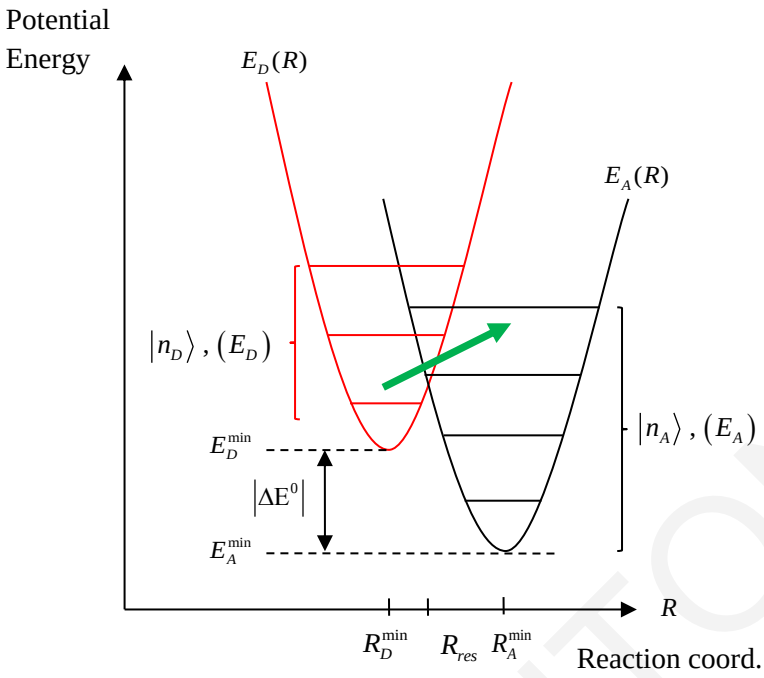

Figure 1.3: Potential energy surfaces of the ET system when the electron is at the initial $(|D\rangle|n_D\rangle)$ and the final $(|A\rangle|n_A\rangle)$ vibronic state.

1.1.7 Through-Bridge Electron Transfer Mechanisms

The simple picture of direct D to A ET, discussed in previous sections, in many molecular ET systems is not directly applicable to systems where D and A are connected by a bridge and the ET reactions proceed through the intermediate bridging units connecting D with A. Due to the large variety of molecular ET structures and architectures, the mechanisms of bridge-mediated biomolecular and molecular ET are variable and include coherent deep tunneling, coherent resonant tunneling and thermally activated hopping [1,2,24,32-35,37], where the term "coherent", refers to the electron's propagation through the molecular bridge.

Coherent deep tunneling is the transfer mechanism where the intermediate bridge (B) states between donor (D) and acceptor (A) states presents a tunneling barrier for the transferring electron (Fig. 1.4) with a height ΔE_B. ΔE_B is the average D/A to B energy gap and is much greater than K_BT (K_B is Boltzmann's constant and T is the temperature). Thermal fluctuations bring D and A into resonance, while the B sites remain off-resonant, causing the electron to tunnel through the B. During the tunneling process the electron occupies the B electronic states with very low probabilities and for very short times. The B states are

not perturbed by the transferring electron and the electronic coherence in the B is maintained.

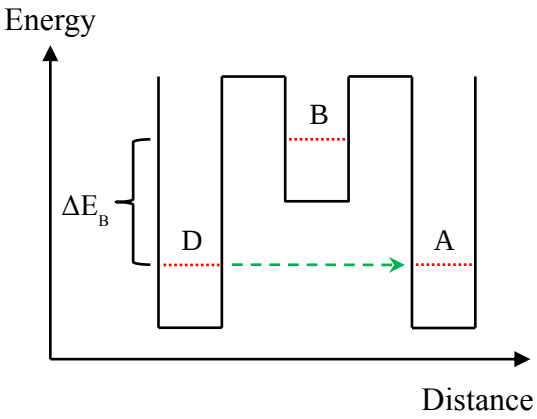

Figure 1.4: Coherent deep tunneling mechanism $\left(\Delta E_B \gg K_B T\right)$. The B electronic states are energetically higher than the D and A states which are in a resonant conformation. ET from D to A is induced by a tunneling matrix element eq. (1.33) between D and A states.

Bridge-mediated ET, especially in the coherent deep tunneling regime, a process controlled by the structure of the bridge medium between D and A sites, influence the D-A electronic coupling. Bridge-mediated ET often involves long distance ET and due to the large D-A separations the direct D-A electronic coupling (V_{DA}) is negligibly weak and the ET takes place in the nonadiabatic regime. The effective electronic coupling (T_{DA}) that induces ET from D to A is described by a tunneling matrix element [1,2,24,32-35,37]

$$T_{DA} \propto \exp\left[-\left(\sqrt{2m_e \Delta E_B}/\hbar\right) R_{DA}\right], \tag{1.33}$$

where R_{DA} is the D to A distance and $\beta_{el} \propto \sqrt{2m_e \Delta E_B}/\hbar$ is an electron tunneling decay constant. Equation (1.33) is based on a simple average-tunneling-barrier model that provides an intuitive understanding of effective D-A electronic coupling (T_{DA}) but fails to give an accurate description of the D-A coupling in different molecular systems with different system specific characteristics.

To compute a more accurate expression of the D-A effective tunneling matrix element (T_{DA}) consider for instance a D-B-A molecular system in the coherent deep tunneling regime (Fig. 1.4) in which D and A states are in resonance conformation and B states are off resonant in respect to D and A. The D-B-A system's electronic Hamiltonian is given by

$$\hat{H}^{el} = \hat{H}_{DA} + \hat{H}_B + \hat{V}, \tag{1.34}$$

where $\hat{H}_{DA}$ is the D-A subsystem Hamiltonian, $\hat{H}_B$ is the B subsystem Hamiltonian and $\hat{V}$ is the interaction Hamiltonian between D-A and B subsystems. The D-A Hamiltonian is

$$\hat{H}_{DA} = E_{res}\left|D\right\rangle\left\langle D\right| + E_{res}\left|A\right\rangle\left\langle A\right| + V_{DA}\left(\left|D\right\rangle\left\langle A\right| + \left|A\right\rangle\left\langle D\right|\right), \tag{1.35}$$

where the direct D-A electronic coupling (V_{DA}) is weak and can be neglected for large D-A separations. The B Hamiltonian is

$$\hat{H}_B = \sum_{i=1}^{N_B} E_{B_i}\left|B_i\right\rangle\left\langle B_i\right| + \sum_{i=1}^{N_B-1}\sum_{j>i}^{N_B} V_{B_i,B_j}\left(\left|B_i\right\rangle\left\langle B_j\right| + \left|B_j\right\rangle\left\langle B_i\right|\right), \tag{1.36}$$

where N_B is the number of bridge states. The interaction Hamiltonian between D-A and B subsystems is

$$\hat{V} = \sum_{i=1}^{N_B}\left[V_{D,B_i}\left(\left|D\right\rangle\left\langle B_i\right| + \left|B_i\right\rangle\left\langle D\right|\right) + V_{A,B_i}\left(\left|A\right\rangle\left\langle B_i\right| + \left|B_i\right\rangle\left\langle A\right|\right)\right]. \tag{1.37}$$

The bridge-mediated D to A effective tunneling matrix element is given by [32,40]

$$T_{DA} = \left\langle D\middle|\hat{V}\,\hat{G}_B\left(E_{tun}\right)\hat{V}\middle|A\right\rangle, \tag{1.38}$$

where $E_{tun} = E_{res}$ and

$$\hat{G}_B\left(E_{tun}\right) = \left(E_{tun}\,\hat{I} - \hat{H}_B\right)^{-1} = \sum_k \frac{\left|\psi_k^{(B)}\right\rangle\left\langle\psi_k^{(B)}\right|}{E_{tun} - E_k^{(B)}}, \tag{1.39}$$

where $\hat{G}_B$ is the bridge Green function and $\left|\psi_k^{(B)}\right\rangle$, $E_k^{(B)}$ denote the eigenstates and eigenenergies of $\hat{H}_B$, respectively. The above expressions are valid for the tunneling limit [32,40], i.e., $\left\langle D\middle|\hat{V}\middle|\psi_k^{(B)}\right\rangle \Big/ \left|E_{tun} - E_k^{(B)}\right| < 1$ and $\left\langle A\middle|\hat{V}\middle|\psi_k^{(B)}\right\rangle \Big/ \left|E_{tun} - E_k^{(B)}\right| < 1$.

For simplicity let's assume a D-B-A molecular system with a single bridge unit. For such a situation the bridge Hamiltonian becomes $\hat{H}_B = E_B\left|B\right\rangle\left\langle B\right|$ and according to eqs. (1.38) and (1.39) the bridge-mediated D to A effective tunneling matrix element is obtained as

$$T_{DA} \approx \frac{V_{DB}V_{BA}}{E_{res} - E_B}, \tag{1.40}$$

for the case of a single bridge unit. For the more general case of a larger number of bridge units the bridge-mediated D to A effective tunneling matrix element will be of the form

$$T_{DA} \approx \frac{V_{D,B_1}}{E_{res} - E_{B_1}} \frac{V_{B_1,B_2}}{E_{res} - E_{B_2}} \cdots \frac{V_{B_{N_B-1},B_{N_B}}}{E_{res} - E_{B_{N_B}}} V_{B_{N_B},A} \tag{1.41}$$

for N_B bridge units [1,2,33,40,41].

In the opposite limit when the bridge electronic states can be brought to resonance with the D and A states (by thermal fluctuations) we consider briefly two other mechanisms. Let's start our discussion with the coherent resonant tunneling mechanism [1,2,24,32-37]. In the resonant tunneling regime (Fig. 1.5a) ET from D to A take place when thermal fluctuations (structural and solvent) bring the B electronic states in resonance with the D and/or A states $\left(\Delta E_B \le K_B T\right)$. In this case the B electronic states are occupied by the transferring electron with high probability. Similar to the deep tunneling regime the B occupation time is too short for the B to respond to the transferring electronic charge and the coherence in the B is maintained.

The thermally activated hopping mechanism $\left(\Delta E_B \le K_B T\right)$ can become relevant for ET reactions in molecular systems with longer bridges and at higher temperatures [1,2,24,32-37]. In the hopping regime (Fig. 1.5b) the D and the nearest neighbor B site get into resonance and the electron tunnels from D to the B. Now the electron stays long enough in the B and the B responds to the electronic charge, trapping the electron in a B electronic state. ET from B to A may occur if a thermally activation event brings the B electronic state occupied by the electron in energetic resonance with the A electronic state.

The determinants of ET mechanisms include the molecular (electronic) structure, the structure of the solvent and their dynamics. The D, A moieties of an ET molecular system can be metal atoms, aminoacids or other small organic molecules. The deep tunneling mechanism where the D and A electronic states are energetically well separated from B electronic states, usually involves metal D and A moieties embedded in an organic bridge. The resonant tunneling and hopping mechanisms, where the D and A electronic states have

similar energies to the B electronic states, often involve D, A and B electronic states that are either all metal or all organic.

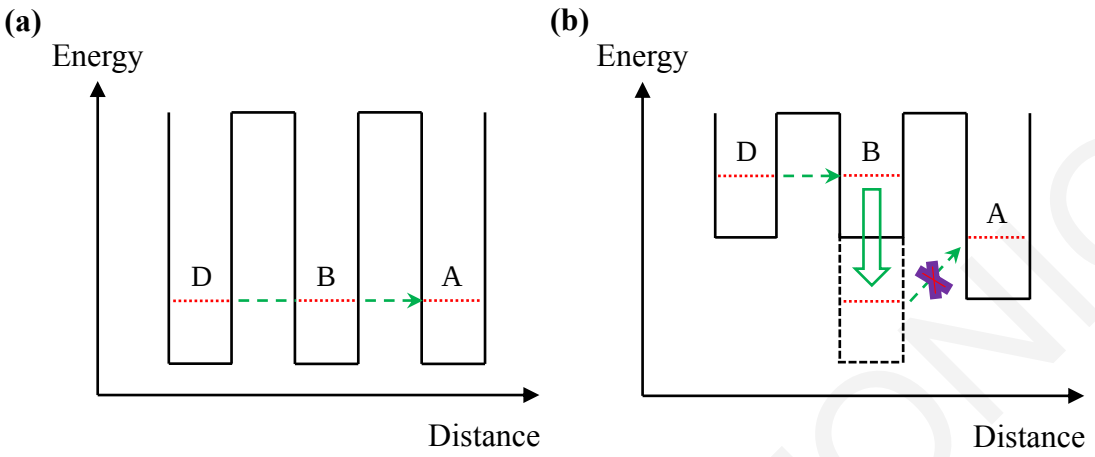

Figure 1.5: (a) Coherent resonant tunneling mechanism. ET from D to A take place when thermal fluctuations bring the B states in resonance with the D and/or A states. Electronic coherence in the B is maintained because the occupation time of B states is too short for the B to respond. (b) In the thermally activated hopping mechanism, ET can be visualized to take place as a sequence of multiple consecutive tunneling steps. Initially the D and the nearest neighbor B site get into resonance and the electron tunnels to the B. Due to the long occupation time of the B, the B responds to the electronic charge and traps the electron in the B. An activation step is necessary for ET to A.

The ET mechanisms introduced in this section, apply to ET reactions for which the time scale of ET is long compared to the time scale of thermal relaxation. For example eqs. (1.19)-(1.21) and (1.31) further assumes that the reaction coordinate dynamics of the system is thermally equilibrated prior to ET and this assumption leads to the Boltzmann (Franck-Condon) activation factors in the rate expressions (eqs. (1.19), (1.31)). For fast ET reactions for which the time scale of ET is similar to the time scale of thermal relaxation, this assumption is not valid. In this situation complete thermalization of the reaction coordinate is not possible prior to ET. This is often the case with fast (*psec*) photo-excited ET where ET competes with vibrational relaxation. These cases need theoretical and computational methods that go beyond the Marcus-type nonadiabatic rate expressions and this regime of ET will be extensively described in the following Chapters (Chapter 2 and 4).

1.2 Energy Transfer in Molecules

This section is a brief introduction to energy transfer reactions between and within molecules. In addition to ET, energy transfer (EnT) processes occur in many molecular systems. Both ET and EnT can be viewed as special cases of nonradiative decay of an excited electronic state and often offer independent excited states deactivation pathways [35]. EnT involves the transfer of both an electron and a hole from an initial to a final electronic state, as compared to the single particle electron or hole transfer (ET or HT), respectively. More precisely, in EnT reactions the initial photoexcitation (absorption) leads to the formation of a bound electron-hole pair, the so-called donor exciton which is subsequently transferred to a different location in the molecule or to another molecule, forming the acceptor exciton. There are three mechanisms (types of electronic donor-acceptor couplings) that mediate EnT reactions. The one-electron mediated tunneling and the two-electron Coulomb and exchange mechanisms.

Consider two molecules or molecular fragments, in close proximity to each other. Initially, the D molecule is photoexcited by an external laser pulse and the A molecule is unaffected and still in its ground electronic state. Electronic interactions among the D and A molecules lead to the transfer of an electron-hole pair from D to A. The Hamiltonian of the system is given by (eq. (1.6b))

$$\hat{H} = \hat{h}^{(1e)} + \hat{V}^{(2e)}, \tag{1.42}$$

where $\hat{h}^{(1e)}$ is an one-electron operator and $\hat{V}^{(2e)}$ is a two-electron operator. $\hat{h}^{(1e)}$ describes the electron kinetic energy $\left(\hat{T}_{el}\right)$ and the Coulomb attraction interaction between the electrons with the nuclei $\left(\hat{V}_{el-nuc}\right)$. $\hat{V}^{(2e)}$ describes the electron-electron repulsive interactions $\left(\hat{V}_{el-el}\right)$. In the following section we will compute the Hamiltonian matrix elements between exciton states in a localized basis using a simple model for the cases when the exciton donor and exciton acceptor are: i) singlet states $\left|{}^1\Psi_D\right\rangle$, $\left|{}^1\Psi_A\right\rangle$ and ii) triplet states $\left|{}^3\Psi_D\right\rangle$, $\left|{}^3\Psi_A\right\rangle$ (e.g., Fig. 1.6).

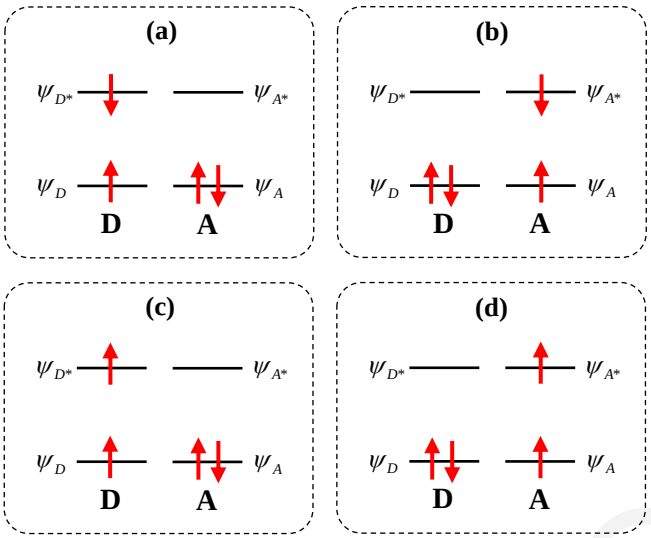

Figure 1.6: Schematic diagram demonstrating singlet and triplet states. a) Donor singlet state $\left|{}^1\Psi_D\right\rangle$, b) Acceptor singlet state $\left|{}^1\Psi_A\right\rangle$, c) Donor triplet state $\left|{}^3\Psi_D\right\rangle$ and d) Acceptor triplet state $\left|{}^3\Psi_A\right\rangle$.

1.2.1 The Matrix Elements between Donor and Acceptor Exciton States: A Simple Model

Consider a four-electron donor-exciton (D), acceptor-exciton (A) system where now each of the fragments, are described by two orbitals (Fig. 1.7), the highest occupied molecular orbital (HOMO) denoted as ψ_D and ψ_A and the lowest unoccupied molecular orbital (LUMO) denoted as ψ_{D^*} and ψ_{A^*}, respectively. Figure 1.7a shows the donor and acceptor fragments in their ground many-electron state configuration. Initially the D molecule is excited by an external laser pulse, in which one electron has been promoted from the HOMO (ψ_D) to the LUMO (ψ_{D^*}) and the A molecule remains in its ground electronic state and specifically in its HOMO (ψ_A) (Fig. 1.7b). Electronic interactions between the D and A fragments enable EnT from D to A in which D subsystem is in its ground state and the A subsystem in its excited state (Fig. 1.7c).

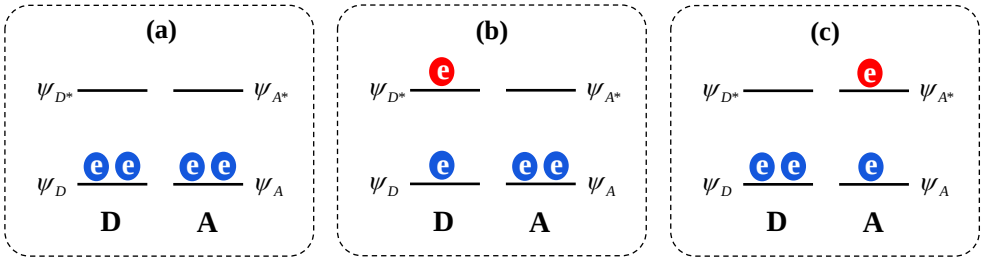

Figure 1.7: Schematic representation of the electronic structure of a four-electron D-A exciton system. Both of the fragments are described by two orbitals, the HOMO and the LUMO orbitals ψ_D, ψ_{D^*} and ψ_A, ψ_{A^*} for D and A fragments, respectively. a) Shows the ground state four-electron configuration of the D-A system. b) D is in its excited state and the A in its ground state. c) Energy is transferred from D to A through electronic interactions, in which D is in its ground state and the A in its excited state.

To describe the many-electron states we use Slater determinants. The ground state Ψ_0 is described by a single Slater determinant, which is an antisymmetrized product of four spin orbitals, each a product of a spatial orbital ψ and a spin function, one corresponding to spin up (α) and the other to spin down (β)

$$\left|\Psi_0\right\rangle = \left|\psi_D\alpha, \psi_D\beta, \psi_A\alpha, \psi_A\beta\right\rangle. \tag{1.43}$$

The excited donor many-electron state (Fig. 1.7b) is described by two possible Slater determinants, in which the electron spin (α or β) is interchanged between the ground ψ_D and excited ψ_D^* spatial orbital

$$\left|\Psi_{D_1}\right\rangle = \left|\psi_D\alpha, \psi_{D^*}\beta, \psi_A\alpha, \psi_A\beta\right\rangle, \tag{1.44a}$$

$$\left|\Psi_{D_2}\right\rangle = \left|\psi_{D^*}\alpha, \psi_D\beta, \psi_A\alpha, \psi_A\beta\right\rangle. \tag{1.44b}$$

Similarly, the excited acceptor many-electron state (Fig. 1.7c) is also described by two possible Slater determinants

$$\left|\Psi_{A_1}\right\rangle = \left|\psi_D\alpha, \psi_D\beta, \psi_A\alpha, \psi_{A^*}\beta\right\rangle, \tag{1.45a}$$

$$\left|\Psi_{A_2}\right\rangle = \left|\psi_D\alpha, \psi_D\beta, \psi_{A^*}\alpha, \psi_A\beta\right\rangle. \tag{1.45b}$$

By taking appropriate linear combinations of these determinants (eqs. (1.44) and (1.45)) we can form the respective singlet states

$$\left|{}^1\Psi_D\right\rangle = \frac{1}{\sqrt{2}}\left(\left|\Psi_{D_1}\right\rangle + \left|\Psi_{D_2}\right\rangle\right), \tag{1.46a}$$

$$\left|{}^1\Psi_A\right\rangle = \frac{1}{\sqrt{2}}\left(\left|\Psi_{A_1}\right\rangle + \left|\Psi_{A_2}\right\rangle\right), \tag{1.46b}$$

and triplet states

$$\left|{}^3\Psi_D\right\rangle = \frac{1}{\sqrt{2}}\left(\left|\Psi_{D_1}\right\rangle - \left|\Psi_{D_2}\right\rangle\right), \tag{1.47a}$$

$$\left|{}^3\Psi_A\right\rangle = \frac{1}{\sqrt{2}}\left(\left|\Psi_{A_1}\right\rangle - \left|\Psi_{A_2}\right\rangle\right). \tag{1.47b}$$

Now we are in position to compute the Hamiltonian matrix elements for our simple four-electron model for the case when donor and acceptor are singlet and triplet states. Applying the Slater rules [42] and the orthonormality of the spin (e.g., $\langle\alpha|\alpha\rangle = \langle\beta|\beta\rangle = 1$ and $\langle\alpha|\beta\rangle = \langle\beta|\alpha\rangle = 0$) we obtain for the singlet case

$$\left\langle {}^1\Psi_D\left|\hat{H}\right|{}^1\Psi_A\right\rangle = \left\langle {}^1\Psi_D\left|\hat{h}^{(1e)}\right|{}^1\Psi_A\right\rangle + \left\langle {}^1\Psi_D\left|\hat{V}^{(2e)}\right|{}^1\Psi_A\right\rangle, \tag{1.48a}$$

$$\left\langle {}^1\Psi_D\left|\hat{h}^{(1e)}\right|{}^1\Psi_A\right\rangle = V^e_{D^*A^*}S_{DA} - V^h_{DA}S_{D^*A^*}, \tag{1.48b}$$

$$\left\langle {}^1\Psi_D\left|\hat{V}^{(2e)}\right|{}^1\Psi_A\right\rangle = 2\left(\psi_D\psi_{D^*}|\psi_A\psi_{A^*}\right) - \left(\psi_{D^*}\psi_{A^*}|\psi_D\psi_A\right), \tag{1.48c}$$

and for the triplet case

$$\left\langle {}^3\Psi_D\left|\hat{H}\right|{}^3\Psi_A\right\rangle = \left\langle {}^3\Psi_D\left|\hat{h}^{(1e)}\right|{}^3\Psi_A\right\rangle + \left\langle {}^3\Psi_D\left|\hat{V}^{(2e)}\right|{}^3\Psi_A\right\rangle, \tag{1.49a}$$

$$\left\langle {}^3\Psi_D\left|\hat{h}^{(1e)}\right|{}^3\Psi_A\right\rangle = V^e_{D^*A^*}S_{DA} - V^h_{DA}S_{D^*A^*}, \tag{1.49b}$$

$$\left\langle {}^3\Psi_D\left|\hat{V}^{(2e)}\right|{}^3\Psi_A\right\rangle = -\left(\psi_{D^*}\psi_{A^*}|\psi_D\psi_A\right), \tag{1.49c}$$

where $V^e_{D^*A^*}$ is the ET coupling matrix element between excited D (ψ_{D^*}) and A (ψ_{A^*}) orbitals and V^h_{DA} is the corresponding HT coupling matrix element between ground D (ψ_D) and A (ψ_A) orbitals. $S_{D^*A^*}$ and S_{DA} are the overlap matrix elements between the LUMO and HOMO orbitals, respectively. The two electron integrals

$$\left(\psi_D \psi_{D^*} \middle| \psi_A \psi_{A^*}\right) = k \int d^3 r_1 \, d^3 r_2 \, \psi_D(\vec{r}_1) \psi_{D^*}(\vec{r}_1) \, r_{12}^{-1} \psi_A(\vec{r}_2) \psi_{A^*}(\vec{r}_2), \quad (1.50a)$$

$$\left(\psi_{D^*} \psi_{A^*} \middle| \psi_D \psi_A\right) = k \int d^3 r_1 \, d^3 r_2 \, \psi_{D^*}(\vec{r}_1) \psi_{A^*}(\vec{r}_1) \, r_{12}^{-1} \psi_D(\vec{r}_2) \psi_A(\vec{r}_2), \quad (1.50b)$$

($k = e^2/4\pi\varepsilon_0$) are Coulombic matrix elements. The first two-electron integral $\left(\psi_D \psi_{D^*} \middle| \psi_A \psi_{A^*}\right)$ eq. (1.50a) is the Coulomb integral that describes the classical Coulomb repulsion interactions between electronic charge densities localized at D and A, respectively. The second two-electron integral $\left(\psi_{D^*} \psi_{A^*} \middle| \psi_D \psi_A\right)$ eq. (1.50b) is the exchange integral and does not have a simple classical interpretation. The $\psi_{D^*}(\vec{r}_1)\psi_{A^*}(\vec{r}_1)$ $\left(\psi_D(\vec{r}_2)\psi_A(\vec{r}_2)\right)$ terms are the overlap densities between the LUMO (HOMO) D and A molecular orbitals.

The one-electron contribution for both singlet (eq. (1.48b)) and triplet (eq. (1.49b)) cases are the same but the two-electron contributions are not. Comparing the two-electron contributions for the singlet (eq. (1.48c)) and for the triplet (eq. (1.49c)) cases we can see that the Coulomb contribution (eq. (1.50a)) is absent for the triplet case. The Coulomb interaction in eq. (1.50a) of the singlet case is the dominant contribution which is characteristic of Förster energy transfer mechanism for singlet states. In the triplet case only the exchange contribution eq. (1.50b) is present and this is the Dexter energy transfer historically associated with the EnT coupling of the Dexter mechanism.

1.2.2 Coulomb and Exchange Distance Dependencies

In the previous section we derived the Hamiltonian matrix elements between singlet and triplet D and A excitons. We now consider only the two-electron contributions, namely the Coulomb and exchange integrals (eqs. (1.50a), (1.50b)), in order to derive their distance dependencies of the Förster and Dexter EnT mechanisms, respectively. The one-electron contributions eqs. (1.48b) and (1.49b), common to both singlet and triplet cases, demonstrate an exponential D-A distance (R_{DA}) decay behavior and are well described by tunneling matrix elements of the form in eq. (1.33).

Let's first consider the $\left(\psi_D \psi_{D^*} \middle| \psi_A \psi_{A^*}\right)$ present only in the singlet case (eq. (1.48c)). This term can be written as

$$\left(\psi_D\,\psi_{D^*}\middle|\psi_A\,\psi_{A^*}\right)=\frac{1}{4\pi\varepsilon_0}\int d^3r_1\,d^3r_2\,\rho_{DD^*}\left(\vec{r}_1\right)\,r_{12}^{-1}\,\rho_{AA^*}\left(\vec{r}_2\right), \tag{1.51}$$

where $\rho_{DD^*}\left(\vec{r}_1\right)=-e\psi_D\left(\vec{r}_1\right)\psi_{D^*}\left(\vec{r}_1\right)$ and $\rho_{AA^*}\left(\vec{r}_2\right)=-e\psi_A\left(\vec{r}_2\right)\psi_{A^*}\left(\vec{r}_2\right)$ are called D and A transition charge densities and $r_{12}=\left|\vec{r}_2-\vec{r}_1\right|$. We further assume that the spatial extent (similar to the molecular sizes) of the ρ_{DD^*} and ρ_{AA^*} is much smaller than the D-A separation. Under these assumptions we may expand the Coulomb interaction eq. (1.51) in a multipole series with respect to the center of mass displacements $\delta\vec{r}_D=\vec{r}_1-\vec{R}_D$, $\delta\vec{r}_A=\vec{r}_2-\vec{R}_A$ where $\vec{R}_D$ and $\vec{R}_A$ are the center of masses of the two molecules. Thus, we express $r_{12}=\left|\delta\vec{r}_A+\vec{R}_{DA}-\delta\vec{r}_D\right|$ where $\left|\delta\vec{r}_D\right|$, $\left|\delta\vec{r}_A\right|\ll\left|\vec{R}_{DA}\right|$ ($\left|\vec{R}_{DA}\right|=\left|\vec{R}_A-\vec{R}_D\right|$ is the center of mass D-A distance). We further define the D and A transition dipole moments matrix elements as

$$\vec{\mu}_{DD^*}=\int d^3r_1\,\rho_{DD^*}\left(\vec{r}_1\right)\delta\vec{r}_D\quad,\quad\vec{\mu}_{AA^*}=\int d^3r_2\,\rho_{AA^*}\left(\vec{r}_2\right)\delta\vec{r}_A. \tag{1.52}$$

Performing initially a Taylor expansion for $\left|\delta\vec{r}_D\right|/\left|\vec{R}_{DA}\right|\ll1$ the r_{12}^{-1} term becomes

$$\frac{1}{r_{12}}=\frac{1}{\left|\delta\vec{r}_A+\vec{R}_{DA}-\delta\vec{r}_D\right|}\approx\frac{1}{\left|\delta\vec{r}_A+\vec{R}_{DA}\right|}+\frac{\left(\delta\vec{r}_A+\vec{R}_{DA}\right)}{\left|\delta\vec{r}_A+\vec{R}_{DA}\right|^3}\cdot\delta\vec{r}_D. \tag{1.53}$$

Subsequently, we perform Taylor expansions for $\left|\delta\vec{r}_A\right|/\left|\vec{R}_{DA}\right|\ll1$ on the components of eq. (1.53) to get

$$\frac{1}{\left|\delta\vec{r}_A+\vec{R}_{DA}\right|}\approx\frac{1}{\left|\vec{R}_{DA}\right|}-\frac{\vec{R}_{DA}\cdot\delta\vec{r}_A}{\left|\vec{R}_{DA}\right|^3}, \tag{1.54a}$$

$$\frac{\left(\delta\vec{r}_A+\vec{R}_{DA}\right)}{\left|\delta\vec{r}_A+\vec{R}_{DA}\right|^3}\cdot\delta\vec{r}_D\approx\frac{\vec{R}_{DA}\cdot\delta\vec{r}_D}{\left|\vec{R}_{DA}\right|^3}+\frac{\delta\vec{r}_D\cdot\delta\vec{r}_A}{\left|\vec{R}_{DA}\right|^3}-3\frac{\left(\vec{R}_{DA}\cdot\delta\vec{r}_D\right)\left(\vec{R}_{DA}\cdot\delta\vec{r}_A\right)}{\left|\vec{R}_{DA}\right|^5}, \tag{1.54b}$$

and the respective r_{12}^{-1} term becomes

$$\frac{1}{r_{12}}\approx\frac{1}{\left|\vec{R}_{DA}\right|}-\frac{\vec{R}_{DA}\cdot\delta\vec{r}_A}{\left|\vec{R}_{DA}\right|^3}+\frac{\vec{R}_{DA}\cdot\delta\vec{r}_D}{\left|\vec{R}_{DA}\right|^3}+\frac{\delta\vec{r}_D\cdot\delta\vec{r}_A}{\left|\vec{R}_{DA}\right|^3}-3\frac{\left(\vec{R}_{DA}\cdot\delta\vec{r}_D\right)\left(\vec{R}_{DA}\cdot\delta\vec{r}_A\right)}{\left|\vec{R}_{DA}\right|^5}. \tag{1.55}$$

Substituting eq. (1.55) into eq. (1.51) we see that the first three terms of eq. (1.55) do not contribute to the overall Coulomb interaction, since the molecular orbitals are orthonormal to each other, i.e., $\int d^3r_1\,\rho_{DD^*}(\vec{r}_1)=0$ and $\int d^3r_2\,\rho_{AA^*}(\vec{r}_2)=0$. This finally yields the D-A Coulomb interaction within the multipole expansion

$$\left(\psi_D\psi_{D^*}\middle|\psi_A\psi_{A^*}\right)=\frac{1}{4\pi\varepsilon_0}\left[\frac{\vec{\mu}_{DD^*}\cdot\vec{\mu}_{AA^*}-3\left(\vec{\mu}_{DD^*}\cdot\hat{R}_{DA}\right)\left(\vec{\mu}_{AA^*}\cdot\hat{R}_{DA}\right)}{\left|\vec{R}_{DA}\right|^3}\right], \tag{1.56}$$

where $\hat{R}_{DA}$ is a unit vector in the direction from D to A.

We have thus shown that the Coulomb $\left(\psi_D\psi_{D^*}\middle|\psi_A\psi_{A^*}\right)$ term eq. (1.56) is approximated by the dipole-dipole interaction, which is the crucial interaction among neutral D and A molecules. The dipole-dipole interaction decays as R_{DA}^{-3} and is directly depended on the orientation of the individual D and A transition dipole moments.

The exchange matrix element $\left(\psi_{D^*}\psi_{A^*}\middle|\psi_D\psi_A\right)$ eq. (1.50b) is a short range interaction and only contributes to the EnT coupling for short D-A separations, due to its strong dependence on the degree of overlap between the D and A molecular orbitals (see Fig. 1.8). The exchange interaction eq. (1.50b) may be rewritten as

$$\left(\psi_{D^*}\psi_{A^*}\middle|\psi_D\psi_A\right)=\frac{1}{4\pi\varepsilon_0}\int d^3r_1\,d^3r_2\,S^e_{D^*A^*}(\vec{r}_1)\,r_{12}^{-1}\,S^h_{DA}(\vec{r}_2), \tag{1.57}$$

where $S^e_{D^*A^*}(\vec{r}_1)=\psi_{D^*}(\vec{r}_1)\psi_{A^*}(\vec{r}_1)$ and $S^h_{DA}(\vec{r}_2)=\psi_D(\vec{r}_2)\psi_A(\vec{r}_2)$ are overlap densities (Fig. 1.8) between the LUMO (HOMO) D and A molecular orbitals. As the D-A distance increases the magnitude of the orbital overlap is approximately exponentially decreased, i.e., $S^e_{D^*A^*}\propto e^{-\beta_{el}R_{DA}}$ and $S^h_{DA}\propto e^{-\beta_{hole}R_{DA}}$, where β_{el}, β_{hole} are electron and hole tunneling decay constants. Due to this orbital overlap reduction, as a function of D-A distance, the exchange interaction contribution for large D-A separations is negligible and therefore can be ignored, compared to the Coulomb $\left(\psi_D\psi_{D^*}\middle|\psi_A\psi_{A^*}\right)$ term in eq. (1.48c) for the case of singlet EnT.

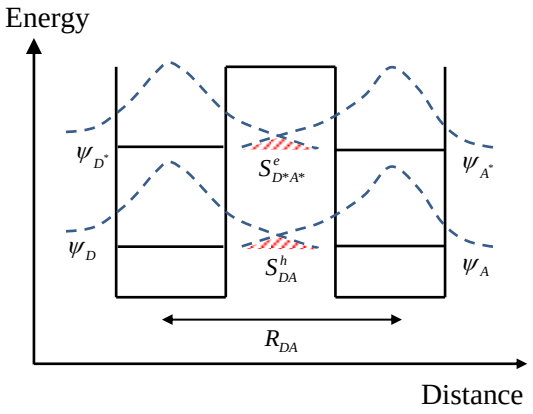

Figure 1.8: Electron and hole donor and acceptor molecular orbitals overlap densities (red areas), $S^e_{D^*A^*}$ and S^h_{DA}, respectively. The orbital overlap densities are approximately exponentially decreased as D-A separation R_{DA} increases.

Having now demonstrated the Coulomb and exchange two-electron contribution distance dependencies, we briefly discuss the effect of these two-electron terms in the D-to-A EnT process. Let's consider, EnT between D and A segments for the four-electron D-A exciton system (Fig. 1.7) of Section 1.2.1. Assume, initially that D fragment is excited (Fig. 1.7b). EnT from D-to-A may take place either with both (Coulomb and exchange) or only with one (exchange) two-electron interaction, depending on if we are dealing with singlet or triplet cases, respectively (see eqs. (1.48) and (1.49)).

1.2.3 Förster Energy Transfer Mechanism

The Förster EnT mechanism refers to singlet exciton transfer (Fig. 1.9) between D and A molecules in which the distance between D and A molecules is large enough, relative to their molecular sizes (thus physical contact between D and A is not a requirement for the EnT process to occur).

Förster's theory identifies the most dominant term in eqs. (1.48a)-(1.48c) to be the $2\left(\psi_D\psi_{D^*}\middle|\psi_A\psi_{A^*}\right)$ term in eq. (1.48c) which is approximated as a dipole-dipole interaction, i.e.,

$$\left\langle {}^1\Psi_D \middle| \hat{H} \middle| {}^1\Psi_A \right\rangle \approx 2\left(\psi_D \psi_{D^*} \middle| \psi_A \psi_{A^*}\right) \equiv V_S^{Förster} = \frac{1}{4\pi\varepsilon_0} \frac{\vec{\mu}_{DD^*} . \vec{\mu}_{AA^*} - 3\left(\vec{\mu}_{DD^*} . \hat{R}_{DA}\right)\left(\vec{\mu}_{AA^*} . \hat{R}_{DA}\right)}{R_{DA}^3} \quad (1.58)$$

where $\vec{\mu}_{DD^*}$ and $\vec{\mu}_{AA^*}$ are transition dipole moments of the D and A molecules, R_{DA} is the D to A distance and $\hat{R}_{DA}$ is a unit vector in the direction from D to A. Through the dipole-dipole interaction, the energy excitation initially localized at the D molecule is transferred to the A molecule or similar the initial singlet exciton state localized at D is transferred to A.

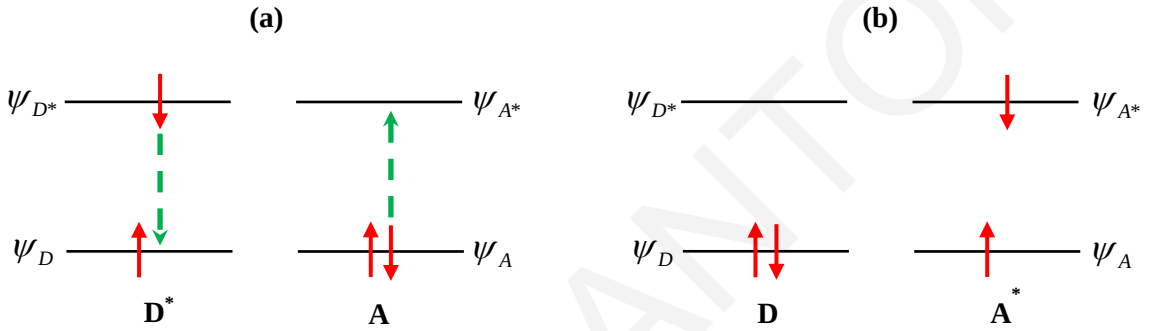

Figure 1.9: Schematic representation of Förster EnT. (a) Initially, the D molecule is excited and can be described by a singlet exciton state. Dipole-dipole Coulomb interactions trigger EnT from D to A. (b) The energy excitation initially localized at the D molecule is transferred to the A molecule. D molecule is now in its ground state and the A in its excited state which is described by a singlet exciton state.

The Förster EnT coupling eq. (1.58) R_{DA}^{-3} distance dependence enables EnT to occur efficiently for large D-A separations if appropriate conditions, such as good spectral overlap (see the following) and desirable EnT enhanced orientation of the individual transition dipole moments $\vec{\mu}_{DD^*}$ and $\vec{\mu}_{AA^*}$ are fulfilled. The Förster mechanism ignores the one-electron (eq. (1.48b)) and exchange ($(\psi_{D^*}\psi_{A^*}|\psi_D\psi_A)$ in eq. (1.48c)) terms because they decay exponentially with distance R_{DA} and thus show a weaker dependence than R_{DA}^{-3}.

1.2.4 Dexter Energy Transfer Mechanism

The Dexter EnT mechanism describes triplet to triplet EnT via two-electron exchange interactions between D and A molecules. The Dexter EnT mechanism is a short range mechanism and requires either physical contact between D and A molecules, so that direct overlap of D and A orbitals to be significant, or D and A molecules to be connected through a bond or other molecules that will act as an intermediate bridge for D-to-A EnT process to occur.

Figure 1.10 illustrates schematically triplet to triplet D-to-A EnT. Initially, D molecule is in its excited electronic state, described by a triplet exciton state (see eq. (1.47a)). The D-to-A EnT may be viewed as a double particle transfer process initiated through the exchange interaction among the particles. The exchange interaction $\left(\psi_{D^*}\psi_{A^*}\left|\psi_D\psi_A\right.\right)$ eq. (1.50b) enables simultaneously ET from D LUMO $\left(\psi_{D^*}\right)$ to A LUMO $\left(\psi_{A^*}\right)$ and HT from D HOMO $\left(\psi_D\right)$ to A HOMO $\left(\psi_A\right)$. In that way, via double particle exchange between the HOMO and LUMO orbitals of the D and A molecules the energy excitation initially localized at the D molecule is transferred to the A molecule or similar the initial triplet exciton state localized at D is transferred to A.

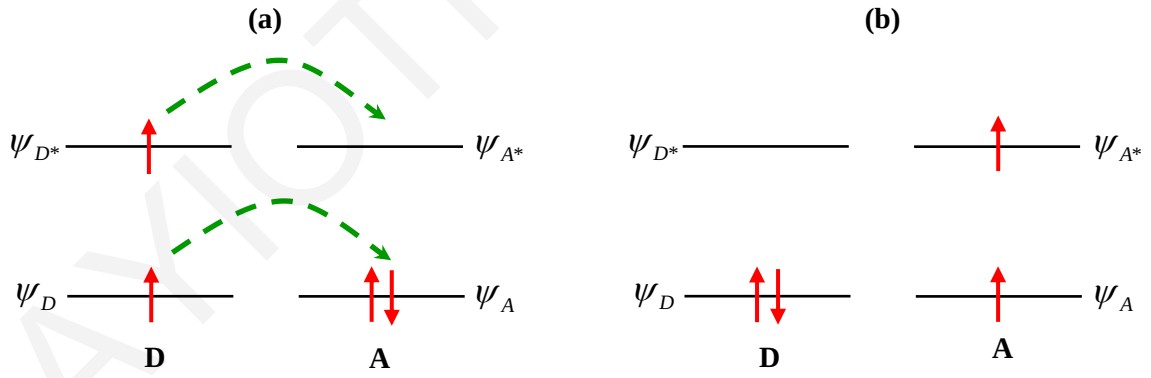

Figure 1.10: Schematic representation of Dexter EnT. a) Initially, the excited D molecule is described by a triplet exciton state. Exchange interactions enable EnT from D to A. b) The energy excitation initially localized at the D molecule is transferred to the A molecule. D molecule is now in its ground state and the A in its excited state which is described by a triplet exciton state.

The Dexter triplet-triplet EnT coupling is commonly given by an approximate expression [43], which in addition to the two-electron exchange contribution also takes into account one particle (ET and HT) contributions

$$\left\langle {}^3\Psi_D \left| \hat{H} \right| {}^3\Psi_A \right\rangle \approx V_{tr}^{Dexter} = \underbrace{2\frac{\left(V_{D^*A^*}^{e}\right)\times\left(V_{DA}^{h}\right)}{\Delta E_{CT}}}_{\left\langle {}^3\Psi_D \left| \hat{h}^{(1e)} \right| {}^3\Psi_A \right\rangle} - \left(\psi_{D^*}\psi_{A^*}\left|\psi_D\psi_A\right.\right), \tag{1.59}$$

where $\left(\psi_{D^*}\psi_{A^*}\left|\psi_D\psi_A\right.\right)$ is the two-electron exchange integral given by eq. (1.50b), $V_{D^*A^*}^{e} \propto e^{-\beta_{el}R_{DA}}$ is the ET coupling matrix element between excited D and A orbitals and $V_{DA}^{h} \propto e^{-\beta_{hole}R_{DA}}$ is the corresponding HT coupling matrix element between ground D and A orbitals. ΔE_{CT} is the energy difference between the triplet D-A charge-transfer configuration, in which a hole occupies the ground D (A) orbital and an electron the excited A (D) orbital, with locally triplet excited D configuration, in which both electron and hole occupies D ground and excited orbitals. Historically only the exchange term was considered for the Dexter EnT mechanism. However, the one-electron term can be of equal magnitude to the exchange term and it is often included when discussing the Dexter interaction.

Since both of the single particle electronic coupling matrix elements ($V_{D^*A^*}^{e}$, V_{DA}^{h}) and the exchange interaction, demonstrate exponentially D-A distance dependence (i.e., eq. (1.33)), the overall Dexter triplet-triplet EnT coupling approximately falls off exponentially with D-A distance [19] and eq. (1.59) suggest a distance decay constant approximately equal to the sum of the electron and hole decay constants [16]. Furthermore, the exponential sensitivity of the Dexter coupling to distance makes triplet-triplet EnT particularly sensitive to molecular structure and energetics. We show that eq. (1.59) does not provide a complete description of the triplet EnT coupling for bridge-mediated EnT and we suggest generalizations of the equations (Chapter 5).

1.2.5 Donor to Acceptor Energy Transfer Rate

In the nonadiabatic limit (weak electronic coupling) EnT can be described by the golden-rule approximation, similar to ET (eqs. (1.19) and (1.31)). The D-to-A EnT (golden-rule) rate expression is

$$k_{DA} = \frac{2\pi}{\hbar}\left|V_{DA}\right|^2 \rho_{FC}, \tag{1.60}$$

where V_{DA} is the D-A electronic coupling eq. (1.48) for singlet excitons and eq. (1.49) for triplet excitons. ρ_{FC} is an appropriate Franck-Condon factor for D and A exciton energies [1,2,35].

The Franck-Condon factor ρ_{FC} can be formulated in a way similar to ET, in its classical or quantum mechanical representation (eqs. (1.20) and (1.32)). The most important distinct feature of EnT in comparison to ET version of Franck-Condon factor (e.g., [44]), is that in EnT reactions the Franck-Condon factor can be approximated by the spectral overlap (Fig. 1.11) of donor emission (fluorescence) $F_{(D^*\to D)}$ spectrum with acceptor absorption $A_{(A\to A^*)}$ spectrum

$$\rho_{FC} = \int_{-\infty}^{\infty} dE\; F_{(D^*\to D)}(E) \times A_{(A\to A^*)}(E) \tag{1.61}$$

with (see Fig. 1.12),

$$F_{(D^*\to D)}(E) = \frac{1}{\sqrt{4\pi k_B T \lambda_{D^*D}}}\, exp\left[-\left(E - \Delta E_{D^*D} + \lambda_{D^*D}\right)^2 \Big/ 4\lambda_{D^*D} k_B T\right], \tag{1.62a}$$

$$A_{(A\to A^*)}(E) = \frac{1}{\sqrt{4\pi k_B T \lambda_{AA^*}}}\, exp\left[-\left(E - \Delta E_{AA^*} + \lambda_{AA^*}\right)^2 \Big/ 4\lambda_{AA^*} k_B T\right]. \tag{1.62b}$$

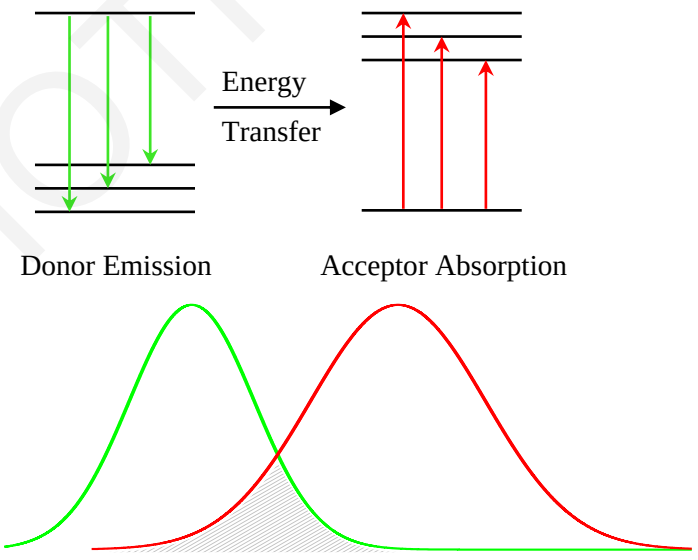

Figure 1.11: Schematic description of EnT (top) showing de-excitation (fluorescence) of the D to the ground state which is accompanied by excitation (absorption) of the A to the excited state. Both processes demonstrate transitions to multiple vibrational levels. Energy conservation is ensured by spectral overlap of D emission and A absorption (bottom).

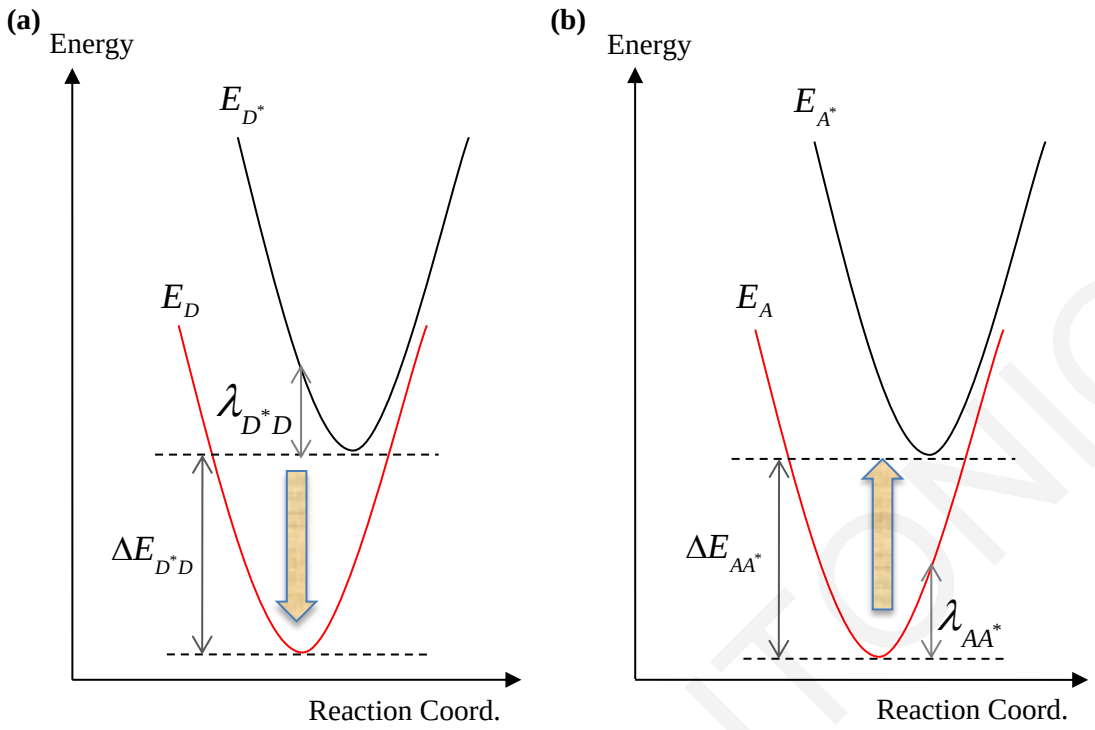

Figure 1.12: Potential energy surfaces when the D and A exciton states are singlets. (a) Donor emission (fluorescence) and (b) acceptor absorption. The reorganization energies and driving forces included in D emission eq. (1.62a) and A absorption eq. (1.62b) spectrum are shown.

The above equations correlate experimental observables, such as emission and absorption spectra, to complicated theoretical descriptions of nuclear overlap factors and nuclear reorganization energies included in the Franck-Condon factor.

In Chapter 5 we study bridge-mediated Dexter triplet energy transfer systems and further develop a general theoretical formulation to account for bridge-mediated exciton pathways contributions ignored by earlier theories (e.g., eq. (1.59)).

1.3 References

[1] V. May and O. Kühn, Charge and Energy Transfer Dynamics in Molecular Systems, Wiley-VCH, Weinheim, Germany, 2004.

[2] A. Nitzan, Chemical Dynamics in Condensed Phases, Oxford Univ. Press, Oxford, 2006.

[3] J. C. Cuevas and E. Sheer, Molecular Electronics: An Introduction to Theory and Experiment, World Scientific Publishing, 2010.

[4] S. S. Skourtis, D. H. Waldeck and D. N. Beratan, Annu. Rev. Phys. Chem., 2010, 61, 461–485.

[5] D. N. Beratan, C. Liu, A. Migliore, N. F. Polizzi, S. S. Skourtis, P. Zhang and Y. Zhang, Acc. Chem. Res., 2015, 48, 474–481.

[6] S. S. Skourtis, D. H. Waldeck and D. N. Beratan, J. Phys. Chem. B, 2004, 108, 15511–15518.

[7] D. Xiao, S. S. Skourtis, I. V. Rubtsov and D. N. Beratan, Nano Lett., 2009, 9, 1818–1823.

[8] H. Carias, D. N. Beratan and S. S. Skourtis, J. Phys. Chem. B, 2011, 115, 5510–5518.

[9] Z. Lin, C. M. Lawrence, D. Xiao, et al., J. Am. Chem. Soc., 2009, 131, 18060–18062.

[10] M. Delor, P. A. Scattergood, I. V. Sazanovich et al., Science, 2014, 346, 1492–1495.

[11] Y. Yue, T. Grusenmeyer, Z. Ma et al., Dalton Trans., 2015, 44, 8609–8616.

[12] M. Delor, T. Keane, P.A. Scattergood et al., Nat. Chem., 2015, 7, 689–695.

[13] I. V. Rubtsov, Nat. Chem., 2015, 7, 683–684, DOI:10.1038/nchem.2332.

[14] J. L. Miller, Physics Today, 2015, 68(3), 10, DOI: 10.1063/PT.3.2706.

[15] R. D. Harcourt, G. D. Scholes and K. P. Ghiggino, J. Chem. Phys., 1994, 101(12), 10521-10525.

[16] G. L. Closs, M. D. Johnson, J. R. Miller and P. Piotrowiak, J. Am. Chem. Soc., 1989, 111(10), 3751–3753.

[17] B. Albinsson, M. P. Eng, K. Pettersson and M. U. Winters, Phys. Chem. Chem. Phys., 2007, 9(44), 5847–5864.

[18] A. Harriman, A. Khatyr, R. Ziessel and A. C. Benniston, Angew. Chem. Int. Ed., 2000, 39(23), 4287–4290.

[19] S. Speiser, Chem. Rev., 1996, 96(6), 1953–1976.

[20] C. Mongin, S. Garakyaraghi, N. Razgoniaeva, M. Zamkov and F. N. Castellano, Science, 2016, 351(6271), 369–372.

[21] S. Speiser and F. Schael, J. Mol. Liq., 2000, 86, 25-35.

[22] N. Lokan, M. N. Paddon-Row, T. A. Smith, M. La Rosa, K. P. Ghiggino, and S. Speiser, J. Am. Chem. Soc., 1999, 121, 2917-2918.

[23] P. Atkins and R. Friedman, Molecular Quantum Mechanics, fifth edition, Oxford Univ. Press, New York, 2011.

[24] J. Blumberger, Chem. Rev., 2015, 115, 11191−11238.

[25] M. D. Newton, Chem. Rev., 1991, 91, 767−792.

[26] T. Pacher, L. S. Cederbaum and H. Köppel, J. Chem. Phys. 1988, 89, 7367−7381.

[27] R. J. Cave and M. D. Newton, J. Chem. Phys., 1997, 106, 9213−9226.

[28] Q. Wu and T. Van Voorhis, J. Chem. Phys., 2006, 125, 164105−9.

[29] J. E. Subotnik, S. Yeganeh, R. J. Cave and M. A. Ratner, J. Chem. Phys. 2008, 129, 244101−14.

[30] J. E Subotnik, R. J. Cave, R. P. Steele and N. Shenvi, J. Chem. Phys., 2009, 130, 234102−14.

[31] A. Migliore, J. Chem. Theory Comput., 2011, 7, 1712−1725.

[32] M. Mohseni, Y. Omar, G. Engel and M. B. Plenio, Quantum Effects in Biology, Cambridge Univ. Press, 2014.

[33] J. Jortner and M. Bixon, Electron Transfer: From Isolated Molecules to Biomolecules, Adv. Chem. Phys. Ser., Wiley Intersci., New York, 1999, vols. 106–107.

[34] A. M. Kuznetsov, J. Ulstrup, Electron Transfer in Chemistry and Biology, Wiley, Chichester, UK, 1999.

[35] V. Balzani et al., Electron Transfer in Chemistry, Wiley-VCH, Weinheim, vols. 1–4, 2001.

[36] R. A. Marcus and N. Sutin, Biochim. Biophys. Acta, 1985, 811, 265–322.

[37] S. S. Skourtis, Wiley Period., Inc. Biopol. Pept. Sci., 2013, 100, 82–92.

[38] C. Manneback, Elsevier Science B.V., Physica, 1951, 17, 11, 1001-1010.

[39] Don DeVault, Quantum-Mechanical Tunnelling in Biological Systems, Cambridge Univ. Press, second edition, 1984.

[40] S. S. Skourtis and D. N. Beratan, Adv. Chem. Phys.,1999, 106, 377-452.

[41] S. S. Skourtis, D. N. Beratan and J. N. Onuchic, Chem. Phys., 1993, 176, 501-520.

[42] A. Szabo and N. S. Ostlund, Modern Quantum Chemistry, Dover, Mineola, NY, 1996.

[43] G. D. Scholes, Annu. Rev. Phys. Chem., 2003, 54(18), 57–87.

[44] T. Förster, Ann. Phys., 1948, 2, 55–75.

Chapter 2: Theoretical Methodologies

Theoretical models with isolated systems that do not interact with the surrounding environment (thermal bath) are oversimplified models. A realistic description of molecular systems demands to take into account the interactions between the quantum system of interest with the surrounding environment. These interactions results in energy exchange between the system and its environment, which is frequently termed as relaxation or energy dissipation in general. A typical situation encountered in the condensed phase is a molecular system interacting with its surrounding environment (solvent). The system is experimentally investigated with spectroscopic techniques (e.g., pump-probe experiments, see Chapter 4) by means of external electromagnetic fields. Experimentalists seek to extract detail information from the experimentally obtained spectra, about the dynamics of the molecular system of interest under the influence of its solvent-environment. The corresponding theoretical description of these condensed phase experiments is the density matrix formalism, which will be discussed in detail in this Chapter (Section 2.1), specifically its reduced description (Section 2.2) that focuses on the molecular system degrees of freedom and traces over the respective environmental degrees of freedom. In the remaining of this Chapter we present the Lindblad form of the master equation that describes the time evolution of the reduced density matrix of a molecular quantum system coupled to a thermal bath.

2.1 Density Operator

Consider a quantum system characterized by a Hamiltonian operator $\hat{H}$, and a time dependent wavefunction $|\psi(t)\rangle$ which represents the quantum system's state. Further consider a dynamical variable A, described by an operator $\hat{A}$, whose expectation value at any time t is given by the matrix element

$$\left\langle \hat{A}(t) \right\rangle = \langle \psi(t) | \hat{A} | \psi(t) \rangle . \tag{2.1}$$

The wavefunction $|\psi(t)\rangle$, using an arbitrary orthonormal basis set $\{|n\rangle\}$, can be expanded as

$$|\psi(t)\rangle = \sum_n |n\rangle c_n(t) , \tag{2.2a}$$

and the respective Hermitian conjugate of the wavefunction will be

$$\langle \psi(t)| = \sum_m c_m^*(t) \langle m| . \tag{2.2b}$$

Substituting $|\psi(t)\rangle$ and $\langle \psi(t)|$ in the expectation value of operator $\hat{A}$ (eq. (2.1)) we get

$$\left\langle \hat{A}(t) \right\rangle = \sum_{n,m} c_n(t) c_m^*(t) \langle m | \hat{A} | n \rangle = \sum_{n,m} c_n(t) c_m^*(t) A_{mn} . \tag{2.3}$$

We can now introduce the density operator for the state $|\psi(t)\rangle$ [1,2] which is defined as the outer product of the wavefunction and its conjugate

$$\hat{\rho}(t) = |\psi(t)\rangle \langle \psi(t)| . \tag{2.4}$$

When the density operator is expanded in the basis set $\{|n\rangle\}$ we get

$$\hat{\rho}(t) = \sum_{n,m} c_n(t) c_m^*(t) |n\rangle \langle m| \equiv \sum_{n,m} \rho_{nm}(t) |n\rangle \langle m| \tag{2.5}$$

where, $\rho_{nm}(t) = c_n(t) c_m^*(t)$ is the density operator matrix element. The expectation value of operator $\hat{A}$ (eq. (2.3)) as a function of the density operator will be

$$\left\langle \hat{A}(t) \right\rangle = \sum_{n,m} A_{mn}\, \rho_{nm}(t) \equiv Tr\left[\hat{A}\hat{\rho}(t) \right], \tag{2.6}$$

where $Tr[\ldots]$ refers to tracing (summing) over the diagonal elements of the matrix.

Until this point we have considered an ensemble of identically prepared quantum systems all described by the same state (wavefunction) $|\psi(t)\rangle$, the so-called pure state. In the same manner the quantum systems ensemble is said to be in a pure state or, equivalently, that we have a pure-state ensemble. Generally, most of the quantum systems are not in a pure state. Their statistical ensembles consist of different quantum-states $|\psi_k(t)\rangle$ with probabilities P_k, i.e., the corresponding density operator is given by

$$\hat{\rho}(t) \equiv \sum_k P_k |\psi_k(t)\rangle\langle\psi_k(t)| \tag{2.7}$$

where, $P_k \geq 0$ and normalized $\sum_k P_K = 1$.

When $P_k = 0$ for $k \neq k'$ and $P_{k'} = 1$ then the system is in a pure state described by a single wavefunction $|\psi_{k'}\rangle$. If however, $P_k \neq 0$ for different $|\psi_k(t)\rangle$, $\hat{\rho}(t) \equiv \sum_k P_k |\psi_k(t)\rangle\langle\psi_k(t)|$ represents a system in a statistical mixture or a mixed ensemble (mixed state). The expectation value of operator $\hat{A}$ for a mixed state is given by

$$\left\langle \hat{A}(t) \right\rangle = \sum_k P_k \langle\psi_k(t)|\hat{A}|\psi_k(t)\rangle = Tr\left[\hat{A}\hat{\rho}(t) \right], \tag{2.8}$$

where the density operator is given by eq. (2.7).

2.1.1 Properties of the Density Operator

In the following we will introduce some of the most important properties of the density operator.

i. The density operator is always Hermitian

$$\hat{\rho}^{\dagger}(t) = \hat{\rho}(t). \tag{2.9}$$

ii. The density operator diagonal elements are real and positive

$$\rho_{nn}(t)=\sum_k P_k \langle n|\psi_k\rangle\langle\psi_k|n\rangle=\sum_k P_k \left|\langle n|\psi_k\rangle\right|^2 \geq 0. \tag{2.10}$$

The diagonal element ρ_{nn} give the probability to find the system in the corresponding quantum state $|n\rangle$ and for this reason, diagonal elements are referred to as populations. The off-diagonal elements $\rho_{mn}(t)$, where $n \neq m$ are complex numbers and most often contain time dependent phase factors that describe the evolution of coherent superposition and are referred to as coherences.

iii. The normalization condition is

$$Tr\left[\hat{\rho}(t)\right]=1. \tag{2.11}$$

iv. For a pure state,

$$Tr\left[\hat{\rho}^2(t)\right]=1, \tag{2.12}$$

whereas for mixed state

$$Tr\left[\hat{\rho}^2(t)\right]\leq 1 \tag{2.13}$$

2.1.2 Time Evolution of the Density Operator

The equation of motion for the density operator can be found from the time evolution of $|\psi(t)\rangle$ and the definition of density operator. For instance let's consider the pure state, where $\hat{\rho}(t)=|\psi(t)\rangle\langle\psi(t)|$. We get

$$\frac{d\hat{\rho}(t)}{dt}=\left(\frac{d}{dt}|\psi(t)\rangle\right)\langle\psi(t)|+|\psi(t)\rangle\left(\frac{d}{dt}\langle\psi(t)|\right). \tag{2.14}$$

Using the Scrödinger equation and its Hermitian conjugate

$$\frac{d}{dt}|\psi(t)\rangle=-\frac{i}{\hbar}\hat{H}|\psi(t)\rangle \quad , \quad \frac{d}{dt}\langle\psi(t)|=\frac{i}{\hbar}\langle\psi(t)|\hat{H}^{\dagger} \tag{2.15}$$

we get

$$\frac{d\hat{\rho}(t)}{dt}=-\frac{i}{\hbar}\hat{H}|\psi(t)\rangle\langle\psi(t)|+\frac{i}{\hbar}|\psi(t)\rangle\langle\psi(t)|\hat{H}^{\dagger}=-\frac{i}{\hbar}\left(\hat{H}\hat{\rho}(t)-\hat{\rho}(t)\hat{H}^{\dagger}\right), \tag{2.16}$$

and taking into account that the Hamiltonian is Hermitian, finally yields the quantum Liouville equation, also known as the Liouville - Von Neumann equation

$$\frac{d\hat{\rho}(t)}{dt} = -\frac{i}{\hbar}\left[\hat{H}, \hat{\rho}(t)\right] = -\frac{i}{\hbar}\hat{L}\hat{\rho}(t). \tag{2.17}$$

$\hat{L}$ is called Liouvillian superoperator, whose action on the density operator is given by the relationship

$$\hat{L}\hat{\rho}(t) \equiv \left[\hat{H}, \hat{\rho}(t)\right]. \tag{2.18}$$

Generally, the Liouville - Von Neumann equation (eq. (2.17)) also holds for a mixed state, $\hat{\rho}(t) \equiv \sum_k P_k \left|\psi_k(t)\right\rangle\left\langle\psi_k(t)\right|$. This applies because $\hat{\rho}_k(t) \equiv \left|\psi_k(t)\right\rangle\left\langle\psi_k(t)\right|$ satisfies the Liouville - Von Neumann equation.

2.1.3 Time Evolution of the Density Operator in Hilbert and Liouville space

A state $\left|\psi(t)\right\rangle$ evolves according to the time-dependent Scrödinger equation. For a time-independent Hamiltonian $\left|\psi(t)\right\rangle = \exp\left[-(i/\hbar)\hat{H}t\right]\left|\psi(0)\right\rangle$, so that the time evolution for the density operator of a pure state will be

$$\hat{\rho}(t) = \left|\psi(t)\right\rangle\left\langle\psi(t)\right| = \underbrace{e^{-i\hat{H}t/\hbar}}_{\hat{U}^H(t)} \underbrace{\left|\psi(0)\right\rangle\left\langle\psi(0)\right|}_{\hat{\rho}(0)} \underbrace{e^{i\hat{H}t/\hbar}}_{\hat{U}^{H\dagger}(t)} \tag{2.19}$$

where,

$$\hat{U}^H(t) = e^{-i\hat{H}t/\hbar}, \tag{2.20}$$

is the time evolution operator in Hilbert space. Equation (2.19) is often written as a function of the Liouvillian superoperator

$$\hat{\rho}(t) = \underbrace{e^{-i\hat{L}t/\hbar}}_{\hat{U}^L(t)} \hat{\rho}(0) \tag{2.21}$$

where,

$$\hat{U}^L(t) = e^{-i\hat{L}t/\hbar}, \tag{2.22}$$

is the time evolution superoperator in Liouville space which is defined as

$$e^{-i\hat{L}t/\hbar}\,\hat{\rho}(0) \equiv e^{-i\hat{H}t/\hbar}\,\hat{\rho}(0)\,e^{i\hat{H}t/\hbar}\,. \tag{2.23}$$

Equations (2.19) – (2.23) also holds for a mixed state, $\hat{\rho}(t) \equiv \sum_k P_k \left|\psi_k(t)\right\rangle\left\langle\psi_k(t)\right|$.

2.1.4 Liouville Space and Tetradic Notation

The space in which the density operator is represented by a vector is called Liouville space. We now consider a two-level system Hamiltonian, composed by an unperturbed Hamiltonian $\hat{H}^0$ and a perturbation $\hat{V}$

$$\hat{H} = \hat{H}^0 + \hat{V}\,. \tag{2.24}$$

The eigenvectors of the unperturbed Hamiltonian $\hat{H}^0$ are $|a\rangle$, $|b\rangle$ and the corresponding eigenvalues are E_a, E_b. We further assume that the total Hamiltonian in the unperturbed eigenvectors representation has the following form

$$\hat{H} = E_a\left|a\right\rangle\left\langle a\right| + E_b\left|b\right\rangle\left\langle b\right| + V_{ab}\left|a\right\rangle\left\langle b\right| + V_{ba}\left|b\right\rangle\left\langle a\right|, \tag{2.25}$$

and the respective density operator will be

$$\hat{\rho} = \rho_{aa}(t)\left|a\right\rangle\left\langle a\right| + \rho_{bb}(t)\left|b\right\rangle\left\langle b\right| + \rho_{ab}(t)\left|a\right\rangle\left\langle b\right| + \rho_{ba}(t)\left|b\right\rangle\left\langle a\right|. \tag{2.26}$$

Equations (2.25) and (2.26) in matrix representation will take the form

$$\tilde{H} = \begin{pmatrix} E_a & V_{ab} \\ V_{ba} & E_b \end{pmatrix}, \tag{2.27}$$

$$\tilde{\rho}(t) = \begin{pmatrix} \rho_{aa}(t) & \rho_{ab}(t) \\ \rho_{ba}(t) & \rho_{bb}(t) \end{pmatrix}. \tag{2.28}$$

We can further proceed and derive the time evolution of the density matrix (eq. (2.28)) using the Liouville equation, $\frac{d\hat{\rho}(t)}{dt} = -\frac{i}{\hbar}\left[\hat{H}, \hat{\rho}(t)\right]$. This results in four coupled equations for the density matrix elements [2],

$$
\begin{aligned}
\dot{\rho}_{aa} &= -\frac{i}{\hbar}\left(V_{ab}\rho_{ba} - V_{ba}\rho_{ab}\right), \\
\dot{\rho}_{bb} &= -\frac{i}{\hbar}\left(V_{ba}\rho_{ab} - V_{ab}\rho_{ba}\right), \\
\dot{\rho}_{ab} &= -\frac{i}{\hbar}\left(E_a - E_b\right)\rho_{ab} - \frac{i}{\hbar}V_{ab}\left(\rho_{bb} - \rho_{aa}\right), \\
\dot{\rho}_{ba} &= -\frac{i}{\hbar}\left(E_b - E_a\right)\rho_{ba} - \frac{i}{\hbar}V_{ba}\left(\rho_{aa} - \rho_{bb}\right).
\end{aligned}
\tag{2.29}
$$

We rewrite these equations in a matrix form in order to obtain the respective Liouville space representation of the Liouvillian superoperator $\hat{L}$ and the equation $\frac{d\hat{\rho}(t)}{dt} = -\frac{i}{\hbar}\hat{L}\hat{\rho}(t)$ in the unperturbed $|a\rangle$, $|b\rangle$ basis. In addition we rewrite the 2×2 density matrix in Hilbert space (eq. (2.28)) as a vector with four components in Liouville space,

$$
\tilde{\rho}(t) = \begin{pmatrix} \rho_{aa}(t) & \rho_{ab}(t) \\ \rho_{ba}(t) & \rho_{bb}(t) \end{pmatrix} \rightarrow \vec{\rho}(t) = \begin{pmatrix} \rho_{aa}(t) \\ \rho_{bb}(t) \\ \rho_{ab}(t) \\ \rho_{ba}(t) \end{pmatrix}. \tag{2.30}
$$

Therefore, the above equations for the density matrix elements may be written as [2]

$$
\frac{d}{dt}\underbrace{\begin{pmatrix} \rho_{aa} \\ \rho_{bb} \\ \rho_{ab} \\ \rho_{ba} \end{pmatrix}}_{\vec{\rho}} = -\frac{i}{\hbar}\underbrace{\begin{pmatrix} 0 & 0 & -V_{ba} & V_{ab} \\ 0 & 0 & V_{ba} & -V_{ab} \\ -V_{ab} & V_{ab} & \left(E_a - E_b\right) & 0 \\ V_{ba} & -V_{ba} & 0 & \left(E_b - E_a\right) \end{pmatrix}}_{\tilde{L}}\begin{pmatrix} \rho_{aa} \\ \rho_{bb} \\ \rho_{ab} \\ \rho_{ba} \end{pmatrix}. \tag{2.31}
$$

The representation of the Liouvillian superoperator in Liouville space is given by a 4×4 matrix

$$
\tilde{L} = \begin{pmatrix} 0 & 0 & -V_{ba} & V_{ab} \\ 0 & 0 & V_{ba} & -V_{ab} \\ -V_{ab} & V_{ab} & \left(E_a - E_b\right) & 0 \\ V_{ba} & -V_{ba} & 0 & \left(E_b - E_a\right) \end{pmatrix}. \tag{2.32}
$$

This form is not limited to the current two-level system but is widely general.

2.1.5 N-level system in Hilbert space and its representation in Liouville space

If we consider a *N*-level Hilbert space system characterized by a Hamiltonian $\hat{H}$ and a complete basis set of functions $\left(|j\rangle,|k\rangle,...\right)$, the Liouville equation jk matrix element will be

$$\frac{d\rho_{jk}}{dt}=-\frac{i}{\hbar}\left[\left(\tilde{H}\tilde{\rho}\right)_{jk}-\left(\tilde{\rho}\tilde{H}\right)_{jk}\right]=-\frac{i}{\hbar}\sum_{m}\left[H_{jm}\rho_{mk}-\rho_{jm}H_{mk}\right]\ ,\ \left(j,k,m=1-N\right). \quad (2.33)$$

The above equation may be rewritten as

$$\frac{d\rho_{jk}}{dt}=-\frac{i}{\hbar}\sum_{m,n}L_{jk,mn}\rho_{mn} \quad (2.34)$$

where,

$$L_{jk,mn}=H_{jm}\delta_{kn}-H_{kn}^{*}\delta_{jm}\,. \quad (2.35)$$

Expressing now the $N\times N$ density matrix as $N^2\times 1$ vector [2]

$$\vec{\rho}\left(t\right)=\begin{pmatrix}\vdots\\ \rho_{jk}\left(t\right)\\ \vdots\\ \rho_{mn}\left(t\right)\\ \vdots\end{pmatrix}, \quad (2.36)$$

we obtain the representation of $\frac{d\hat{\rho}(t)}{dt}=-\frac{i}{\hbar}\hat{L}\hat{\rho}(t)$ in Liouville space, $\frac{d\vec{\rho}}{dt}=-\frac{i}{\hbar}\tilde{L}\vec{\rho}$, where the $N^2\times N^2$ Liouvillian superoperator matrix elements will be $L_{jk,mn}=H_{jm}\delta_{kn}-H_{kn}^{*}\delta_{jm}$. Since each element ρ_{mn} is labeled by two indices, the matrix elements of $\tilde{L}$ are labeled by four indices (tetradic matrix representation of a superoperator).

2.2 The Reduced Density Operator

Most of the experiments in physics perform measurements over a system which is a small fraction of an infinitely larger system, that often describes the environment (thermal bath) and with which the system consistently interacts. The measurements provide detailed information about the dynamics of the system of interest under the influence of its

environment. The theoretical analog of these experimental measurements is the reduced description of the density operator that focuses on the system's degrees of freedom and that traces over the respective environmental degrees of freedom.

Let us denote with S the quantum system of interest and with B the surrounding bath that describes the environment (also a quantum system). The Hamiltonian that describes the total quantum system is [1-4]

$$\hat{H} = \hat{H}^0 + \hat{V}^{SB}, \tag{2.37a}$$

$$\hat{H}^0 = \hat{H}^S + \hat{H}^B, \tag{2.37b}$$

where the zeroth order Hamiltonian $\hat{H}^0$ describes uncoupled system and thermal bath, and $\hat{V}^{SB}$ is the system-bath interaction. We further denote as $\{|s\rangle\}, \{|b\rangle\}$ the orthonormal sets of eigenstates of $\hat{H}^S$ and $\hat{H}^B$, respectively. The density operator $\hat{\rho}$ of the total system (system–bath) may be expressed in the $|sb\rangle = |s\rangle|b\rangle$ representation as

$$\hat{\rho} = \sum_{s,b}\sum_{s',b'} \rho_{sb,s'b'} |sb\rangle\langle s'b'| \quad , \quad \rho_{sb,s'b'} = \langle sb|\hat{\rho}|s'b'\rangle . \tag{2.38}$$

The reduced description of the system S will give a density operator

$$\hat{\sigma} = \sum_{s,s'} \sigma_{s,s'} |s\rangle\langle s'| \quad , \quad \sigma_{s,s'} = \langle s|\hat{\sigma}|s'\rangle \tag{2.39}$$

in the system space.

Physical measurements of the system S can be described by operators that solely act on system states

$$\hat{A}^S = \sum_{s,s'} A_{s,s'} |s\rangle\langle s'| . \tag{2.40}$$

The reduced density operator has the property that the average of any system operator $\hat{A}^S$ is given by

$$\left\langle \hat{A}^S \right\rangle = \sum_s \langle s|\hat{\sigma}\hat{A}^S|s\rangle = Tr_S\left[\hat{\sigma}\hat{A}^S\right]. \tag{2.41}$$

We can also obtain the same average from the total quantum system

$$\left\langle \hat{A}^S \right\rangle = Tr_{S+B}\left[\hat{\rho}\hat{A}^S\right] = \sum_{sb}\langle sb|\hat{\rho}\hat{A}^S|sb\rangle = \sum_{sb}\sum_{s'b'}\langle sb|\hat{\rho}|s'b'\rangle\langle s'b'|\hat{A}^S|sb\rangle . \tag{2.42}$$

Since, $\hat{A}^S$ is a system's operator it satisfies

$$\langle s'b'|\hat{A}^S|sb\rangle = A_{s,s'}\delta_{b,b'} \tag{2.43}$$

then,

$$\langle \hat{A}^S \rangle = \sum_{s,s'}\sum_{b}\langle sb|\hat{\rho}|s'b\rangle\langle s'|\hat{A}^S|s\rangle = Tr_S\left[\left(Tr_B\hat{\rho}\right)\hat{A}^S\right]. \tag{2.44}$$

Comparing eq. (2.41) with eq. (2.44) for the average value of the operator $\hat{A}^S$ we conclude that

$$\hat{\sigma} = Tr_B\left[\hat{\rho}\right]. \tag{2.45}$$

The time evolution of the density operator for the total system is

$$\frac{d\hat{\rho}}{dt} = -\frac{i}{\hbar}\left[\hat{H},\hat{\rho}\right] = -\frac{i}{\hbar}\left[\hat{H}^S,\hat{\rho}\right] - \frac{i}{\hbar}\left[\hat{H}^B,\hat{\rho}\right] - \frac{i}{\hbar}\left[\hat{V}^{SB},\hat{\rho}\right]. \tag{2.46}$$

To determine the corresponding differential equation that describes the time evolution of the reduced density operator of the system we trace over the bath degrees of freedom $\left(Tr_B\right)$ on both sides of $d\hat{\rho}/dt$ (eq. 2.46). We observe that [1]

$$Tr_B\left[\hat{H}^S,\hat{\rho}\right] = \left[\hat{H}^S, Tr_B\hat{\rho}\right] = \left[\hat{H}^S,\hat{\sigma}\right] \text{ and } Tr_B\left[\hat{H}^B,\hat{\rho}\right] = \sum_b\left[E_b,\hat{\rho}\right] = 0, \tag{2.47}$$

this leads to:

$$\frac{d\hat{\sigma}}{dt} = -\frac{i}{\hbar}\left[\hat{H}^S,\hat{\sigma}\right] - \frac{i}{\hbar}Tr_B\left(\left[\hat{V}^{SB},\hat{\rho}\right]\right). \tag{2.48}$$

The differential equation for the time evolution of the reduced density operator differs from the corresponding differential equation for the total density operator and can be only solved approximately because it contains the calculation of Tr_B. Usually the eigenstates of the thermal bath are infinite in number and their exact form is unknown.

2.3 The Operator-Sum Representation

Suppose, that initially the system and the environment are completely uncorrelated and the respective total density matrix is given by a product state of the form

$$\hat{\rho}(0) = \hat{\sigma}(0) \otimes \hat{\rho}^{B}(0), \tag{2.49a}$$

$$\hat{\rho}^{B}(0) = |0_B\rangle\langle 0_B|, \tag{2.49b}$$

where $\hat{\rho}^{B}(0) = Tr_S\left[\hat{\rho}(0)\right]$ is the initial density matrix of the environment, assumed to be in a pure state.

The time evolution of the density matrix is given by a time evolution operator $\hat{U}_{SB}(t)$ (eqs. (2.19), (2.20)), that acts both on the system and the environment

$$\hat{\rho}(t) = \hat{U}_{SB}(t)\left(\hat{\sigma}(0) \otimes |0_B\rangle\langle 0_B|\right)\hat{U}_{SB}^{\dagger}(t). \tag{2.50}$$

To obtain the time evolution of the reduced density matrix of the system we perform a trace over the environmental degrees of freedom (e.g., eq. (2.45))

$$\begin{aligned}\hat{\sigma}(t) = Tr_B\left[\hat{\rho}(t)\right] &= \sum_{\mu}\langle\mu_b|\hat{U}_{SB}(t)\left(\hat{\sigma}(0)\otimes|0_B\rangle\langle 0_B|\right)\hat{U}_{SB}^{\dagger}(t)|\mu_b\rangle \\ &= \sum_{\mu}\langle\mu_b|\hat{U}_{SB}(t)|0_B\rangle\hat{\sigma}(0)\langle 0_B|\hat{U}_{SB}^{\dagger}(t)|\mu_b\rangle \\ &= \sum_{\mu}\hat{M}_{\mu}(t)\hat{\sigma}(0)\hat{M}_{\mu}^{\dagger}(t),\end{aligned} \tag{2.51}$$

where, $\{|\mu_b\rangle\}$ is an orthonormal basis set for the environment and the partial matrix elements $\hat{M}_{\mu}(t) = \langle\mu_b|\hat{U}_{SB}(t)|0_B\rangle$ are the Kraus operators [5-7] that act on system space. The Kraus operators describe the effect of the environment on the reduced density matrix of the system, as their definition contains information about the initial state of the environment and the combined system-environment dynamics. Further, Kraus operators satisfy the completeness property

$$\sum_{\mu}\hat{M}_{\mu}^{\dagger}(t)\hat{M}_{\mu}(t) = \hat{I}. \tag{2.52}$$

The introduced operator-sum representation (or Kraus representation) [5-7] defines a dynamical quantum map $\hat{\Lambda}$. The dynamical map $\hat{\Lambda}$ generates the time evolution of the reduced density matrix of the system. The map $\hat{\Lambda}$ is usually termed as a superoperator, since it represents an operator that acts on some other operator. $\hat{\Lambda}$ can be regarded as an input-output map that takes an input state $\hat{\sigma}(0)$ to an output state $\hat{\sigma}(t)$. Equation (2.51) is the Kraus decomposition of this map for the density operator which, in terms of Kraus operators, is given by

$$\hat{\sigma}(t)=\sum_{\mu}\hat{M}_{\mu}(t)\hat{\sigma}(0)\hat{M}_{\mu}^{\dagger}(t)=\hat{\Lambda}(t)\left[\hat{\sigma}(0)\right]. \tag{2.53}$$

Every set of Kraus operators (which are not unique) that satisfy the completeness condition (eq. (2.52)) can be realized by a map of eq. (2.53) form. A superoperator (or Kraus) map $\hat{\Lambda}$ must fulfill the following properties in order to efficiently describe a physical process:

i. $\hat{\Lambda}$ is a linear map on operators, e.g., $\hat{\Lambda}\left[a\hat{\rho}_a+b\hat{\rho}_b\right]=a\hat{\Lambda}\left[\hat{\rho}_a\right]+b\hat{\Lambda}\left[\hat{\rho}_b\right]$.

ii. It is trace preserving or decreasing, e.g., $Tr\left[\hat{\Lambda}\left[\hat{\rho}\right]\right]\le Tr\left[\hat{\rho}\right]$ for any state $\hat{\rho}$.

iii. It preserves positivity and gives non-negative eigenvalues e.g., $\hat{\rho}\ge 0\Rightarrow\hat{\Lambda}\left[\hat{\rho}\right]\ge 0$.

iv. $\hat{\Lambda}$ is a completely positive map. Suppose, there is another system S' apart from the system S. Further, suppose that $\hat{\Lambda}_S$ is a positive map for S (i.e., property iii). The map $\hat{\Lambda}_S$ is completely positive if $\hat{\Lambda}_S\otimes\hat{I}_{S'}$, acting on $S\otimes S'$ is also positive ($\hat{I}_{S'}$ is the identity operator for S').

Any map that satisfies the aforementioned properties is a Kraus map and corresponds to a physical process.

2.3.1 Generalization of the Map's Time Evolution

We will try to generalize the dynamical map $\hat{\Lambda}$ expression eq. (2.53), starting our discussion by propagating the total density matrix of eq. (2.50) forward in time. From time t to $t+dt$

$$\hat{\rho}(t+dt)=\hat{U}_{SB}(t+dt;t)\,\hat{\rho}(t)\hat{U}_{SB}^{\dagger}(t+dt;t), \tag{2.54}$$

where $\hat{U}_{SB}(t+dt;t)$ is the time evolution operator that evolves the total system from time t to $t+dt$. To first order in dt,

$$\hat{U}_{SB}(t+dt;t)=\hat{1}-\frac{i}{\hbar}\hat{H}(t)dt\,. \tag{2.55}$$

Substituting eq. (2.55) into eq. (2.54) and keeping only terms of order dt gives

$$\begin{aligned}\hat{\rho}(t+dt) &= \hat{\rho}(t) - \frac{i}{\hbar}\left[\hat{H}(t), \hat{\rho}(t)\right]dt \\ &= \hat{\rho}(t) - \frac{i}{\hbar}\left[\hat{H}^{S}(t), \hat{\rho}(t)\right]dt - \frac{i}{\hbar}\left[\hat{H}^{B}(t) + \hat{V}^{SB}(t), \hat{\rho}(t)\right]dt,\end{aligned} \tag{2.56}$$

which can be described by a map of the form in eq. (2.53) that takes the system from time t to $t+dt$,

$$\hat{\sigma}(t+dt) = Tr_{B}\left[\hat{\rho}(t+dt)\right] = \hat{\Lambda}(t+dt;t)\left[\hat{\sigma}(t)\right]. \tag{2.57}$$

In terms of Kraus operators

$$\hat{\Lambda}(t+dt;t)\left[\hat{\sigma}(t)\right] = \sum_{\mu}\hat{M}_{\mu}(t+dt;t)\hat{\sigma}(t)\hat{M}_{\mu}^{\dagger}(t+dt;t). \tag{2.58}$$

We will restrict our attention to master equations, that can be expressed under some approximations, as first order differential equations that are local in time, e.g.,

$$\frac{d}{dt}\hat{\sigma}(t) = \hat{\mathcal{L}}(t)\left[\hat{\sigma}(t)\right], \tag{2.59}$$

where $\hat{\mathcal{L}}$ is a superoperator or dynamical map that acts on $\hat{\sigma}(t)$. This equation is local in time, in the sense that the time evolution of $\hat{\sigma}$ at time t depends only on $\hat{\sigma}$ evaluated exclusively at time t and not from any previous times. In other words, we are interested in Markovian open system dynamics, in which the environment does not retain any history, neither keeps memory, of the earlier states of the system of interest.

Let's return to eqs. (2.57) to (2.59) and express them as

$$\begin{aligned}\hat{\sigma}(t+dt) = \hat{\Lambda}(t+dt;t)\left[\hat{\sigma}(t)\right] &= \hat{\sigma}(t) + \hat{\mathcal{L}}(t)\left[\hat{\sigma}(t)\right]dt \\ &= \sum_{\mu}\hat{M}_{\mu}(t+dt;t)\hat{\sigma}(t)\hat{M}_{\mu}^{\dagger}(t+dt;t),\end{aligned} \tag{2.60}$$

where $\hat{\mathcal{L}}$, the generator of dynamics that only depends on state $\hat{\sigma}$ at time t and not on the whole previous history, is commonly called the Lindbladian. Equation (2.58) shows that $\hat{\mathcal{L}}$ can be expressed in terms of Kraus operators.

We now need to find the explicit form of Kraus operators that give Markovian dynamics. There must be one Kraus operator that becomes the identity operator when $dt \to 0$. We thus define this operator as

$$\hat{M}_{\mu=0}(t+dt;t)=\hat{I}+\hat{G}(t)dt\,, \tag{2.61}$$

where $\hat{I}$ is the identity operator and $\hat{G}$ is an arbitrary operator that could depend on t. The Kraus decomposition of $\hat{M}_{\mu=0}$ will be

$$\hat{M}_{\mu=0}(t+dt;t)\hat{\sigma}(t)\hat{M}^{\dagger}_{\mu=0}(t+dt;t)=\hat{\sigma}(t)+\left(\hat{G}(t)\hat{\sigma}(t)+\hat{\sigma}(t)\hat{G}^{\dagger}(t)\right)dt \tag{2.62}$$

(keeping only terms of order dt). From eq. (2.60) we see that all other Kraus operators with $\mu\neq 0$ must be of the form

$$\hat{M}_{\mu}(t+dt;t)=\hat{\mathcal{L}}_{\mu}(t)\sqrt{dt}\,, \tag{2.63}$$

since their Kraus decomposition $\hat{M}_{\mu}\hat{\sigma}\hat{M}^{\dagger}_{\mu}$ has to be proportional to dt, i.e.,

$$\hat{M}_{\mu}(t+dt;t)\hat{\sigma}(t)\hat{M}^{\dagger}_{\mu}(t+dt;t)=\hat{\mathcal{L}}_{\mu}(t)\hat{\sigma}(t)\hat{\mathcal{L}}^{\dagger}_{\mu}(t)dt\,. \tag{2.64}$$

Operator $\hat{\mathcal{L}}_{\mu}(t)$ is sometimes called the μth Lindblad operator.

The overall map must be trace preserving, $\sum_{\mu}\hat{M}^{\dagger}_{\mu}\hat{M}_{\mu}=\hat{I}$, and keeping only order dt terms we get

$$\hat{G}(t)+\hat{G}^{\dagger}(t)=-\sum_{\mu=1}\hat{\mathcal{L}}^{\dagger}_{\mu}(t)\hat{\mathcal{L}}_{\mu}(t)\,. \tag{2.65}$$

Thus we can define the $\hat{G}$ operator as

$$\hat{G}(t)=-\frac{1}{2}\sum_{\mu=1}\hat{\mathcal{L}}^{\dagger}_{\mu}(t)\hat{\mathcal{L}}_{\mu}(t)+i\,\hat{A}(t)\,, \tag{2.66}$$

where $\hat{A}$ is an arbitrary operator. We see from eq. (2.56), after taking the trace over the bath degrees of freedom, that $\hat{A}$ is proportional to the system Hamiltonian, i.e.,

$$\hat{A}(t)=-\frac{1}{\hbar}\hat{H}^{S}(t)\,. \tag{2.67}$$

Therefore, the time evolution of the density operator eqs. (2.57) and (2.58) becomes

$$\begin{aligned}\hat{\sigma}(t+dt) &= \sum_{\mu}\hat{M}_{\mu}(t+dt;t)\hat{\sigma}(t)\hat{M}_{\mu}^{\dagger}(t+dt;t)\\ &= \hat{\sigma}(t)-\frac{i}{\hbar}\left[\hat{H}^{S}(t),\hat{\sigma}(t)\right]dt\\ &+\sum_{\mu}\left[\hat{\mathcal{L}}_{\mu}(t)\hat{\sigma}(t)\hat{\mathcal{L}}_{\mu}^{\dagger}(t)-\frac{1}{2}\left(\hat{\mathcal{L}}_{\mu}^{\dagger}(t)\hat{\mathcal{L}}_{\mu}(t)\hat{\sigma}(t)+\hat{\sigma}(t)\hat{\mathcal{L}}_{\mu}^{\dagger}(t)\hat{\mathcal{L}}_{\mu}(t)\right)\right]dt,\end{aligned} \tag{2.68}$$

and the respective time evolution of the differential equation of the reduced density operator of the system $\hat{\sigma}=Tr_{B}\left[\hat{\rho}\right]$ consistent with eq. (2.56) will be

$$\begin{aligned}\frac{d}{dt}\hat{\sigma}(t) &= -\frac{i}{\hbar}\left[\hat{H}^{S}(t),\hat{\sigma}(t)\right]\\ &+\sum_{\mu}\left[\hat{\mathcal{L}}_{\mu}(t)\hat{\sigma}(t)\hat{\mathcal{L}}_{\mu}^{\dagger}(t)-\frac{1}{2}\left(\hat{\mathcal{L}}_{\mu}^{\dagger}(t)\hat{\mathcal{L}}_{\mu}(t)\hat{\sigma}(t)+\hat{\sigma}(t)\hat{\mathcal{L}}_{\mu}^{\dagger}(t)\hat{\mathcal{L}}_{\mu}(t)\right)\right].\end{aligned} \tag{2.69}$$

This is the Lindblad form of Master equation, and is the most general form for the density matrix differential equation that describes Markovian dynamics.

2.4 Deriving the Master Equation from First Principles

In this Section, we adopt the Born-Markov approximations and further derive a master equation expression that describes Markovian dynamics, e.g., first order differential equations that are local in time.

2.4.1 Interaction Picture Description of the Density Operator

Consider again the composite system-environment Hamiltonian of eq. (2.37a)

$$\hat{H}=\hat{H}^{0}+\hat{V}^{SB}, \tag{2.70}$$

where $\hat{H}^{0}=\hat{H}^{S}+\hat{H}^{B}$ (eq. (2.37b)) describes the system and thermal bath uncorrelated to each other, and $\hat{V}^{SB}$ describes the interaction between them. The interaction representation for the density operator of the system and the bath is given by

$$\hat{\rho}^{(I)}(t)=e^{i\hat{H}^{0}t/\hbar}\hat{\rho}(t)\;e^{-i\hat{H}^{0}t/\hbar}. \tag{2.71}$$

The equation of motion for the density matrix in the interaction representation is

$$\frac{d}{dt}\hat{\rho}^{(I)}(t) = -\frac{i}{\hbar}\left[\hat{V}^{SB(I)}(t), \hat{\rho}^{(I)}(t)\right] \tag{2.72}$$

where,

$$\hat{V}^{SB(I)}(t) = e^{i\hat{H}^0 t/\hbar}\ \hat{V}^{SB}(t)\ e^{-i\hat{H}^0 t/\hbar}. \tag{2.73}$$

The respective reduced density matrices in the interaction picture, for the system and the thermal bath can be defined as

$$\hat{\sigma}^{(I)}(t) = Tr_B\left[\hat{\rho}^{(I)}(t)\right] \quad , \quad \hat{\rho}^{B(I)}(t) = Tr_S\left[\hat{\rho}^{(I)}(t)\right]. \tag{2.74}$$

2.4.2 Iterative Solution by Integration

Integrating now eq. (2.72) we obtain

$$\hat{\rho}^{(I)}(t) = \hat{\rho}^{(I)}(0) - \frac{i}{\hbar}\int_0^t dt'\left[\hat{V}^{SB(I)}(t'), \hat{\rho}^{(I)}(t')\right]. \tag{2.75}$$

Substituting eq. (2.75) for $\hat{\rho}^{(I)}(t)$ in the right-hand side of eq. (2.72) gives

$$\begin{aligned}\frac{d}{dt}\hat{\rho}^{(I)}(t) &= -\frac{i}{\hbar}\left[\hat{V}^{SB(I)}(t), \left\{\hat{\rho}^{(I)}(0) - \frac{i}{\hbar}\int_0^t dt'\left[\hat{V}^{SB(I)}(t'), \hat{\rho}^{(I)}(t')\right]\right\}\right] \\ &= -\frac{i}{\hbar}\left[\hat{V}^{SB(I)}(t), \hat{\rho}^{(I)}(0)\right] - \frac{1}{\hbar^2}\int_0^t dt'\left[\hat{V}^{SB(I)}(t), \left[\hat{V}^{SB(I)}(t'), \hat{\rho}^{(I)}(t')\right]\right].\end{aligned} \tag{2.76}$$

Tracing over the bath degrees of freedom (Tr_B) in eq. (2.76) we derive the reduced density matrix of the system

$$\begin{aligned}\frac{d}{dt}\hat{\sigma}^{(I)}(t) = &-\frac{i}{\hbar}Tr_B\left\{\left[\hat{V}^{SB(I)}(t), \hat{\rho}^{(I)}(0)\right]\right\} \\ &-\frac{1}{\hbar^2}\int_0^t dt' Tr_B\left\{\left[\hat{V}^{SB(I)}(t), \left[\hat{V}^{SB(I)}(t'), \hat{\rho}^{(I)}(t')\right]\right]\right\}.\end{aligned} \tag{2.77}$$

Until this point of the discussion we did not adopt any approximation and eq. (2.77) is an exact description of the time evolution of the system's reduced density operator. In the forthcoming considerations we will briefly describe the successive approximations implemented in eq. (2.77) to derive the Lindblad form of the Master equation.

2.4.3 Born-Markov Approximation

The Born approximation states that the system-bath coupling $\hat{V}^{SB}$ is a sufficiently weak interaction, such that the influence of the system on the bath is negligible for a large bath (large compared to the size of the system) [7,8]. Within the Born approximation we can treat the bath density matrix as time-independent $\left(\rho^{B(I)}(t) \approx \rho^{B}\right)$ and express the total density operator of the (system-bath) system as a product state for all times

$$\hat{\rho}^{(I)}(t) = \hat{\sigma}^{(I)}(t) \otimes \rho^{B}. \tag{2.78}$$

We can further express the total system-bath density operator as a function of two contributions

$$\hat{\rho}^{(I)}(t) = \hat{\sigma}^{(I)}(t) \otimes \rho^{B} + \hat{\rho}^{corr(I)}(t). \tag{2.79}$$

The first term in the right-hand site of eq. (2.79) is the total density operator in the absence of system-bath correlations. The second term describes the influence of the correlations among the dynamics of the system and the dynamics of the bath in the time evolution of the total density operator. We define τ_c to be the time after which the correlations between system and bath disappear or, in other words, the characteristic timescale in which the thermal-bath loses the information (energy) obtained from the system. We further assume that τ_c is extremely small compared to the propagation time (Δt), such that the environment has no memory about the earlier states of the interacting system, defining this way a Markovian process.

Due to weak system-bath interaction for a large environment (Born approximation) and because $\tau_c \ll \Delta t$, the correlations contributions to the time evolution of the density matrix are negligible. Therefore, we can safely assume the absence of system-bath correlations at initial times and that the total density operator is well described by a product state of eq. (2.78) form. The initial density matrix can be written as $\hat{\rho}^{(I)}(0) = \hat{\sigma}^{(I)}(0) \otimes \rho^{B}$, and the commutator of eq. (2.77), without loss of generality, can be assumed to be zero, i.e.,

$$\left[\hat{V}^{SB(I)}(t), \hat{\rho}^{(I)}(0)\right] = 0. \tag{2.80}$$

Substituting eqs. (2.78) and (2.80) into eq. (2.77) the reduced density matrix of the system becomes

$$\frac{d}{dt}\hat{\sigma}^{(I)}(t) = -\frac{1}{\hbar^2}\int_0^t dt' Tr_B\left\{\left[\hat{V}^{SB(I)}(t),\left[\hat{V}^{SB(I)}(t'),\hat{\sigma}^{(I)}(t')\otimes\rho^B\right]\right]\right\}. \quad (2.81)$$

This is an integro-differential equation since the differential change of the system reduced density operator $\hat{\sigma}^{(I)}$ at time t, depends on an integral of $\hat{\sigma}^{(I)}$ over all previous times $t' < t$. This can be further simplified using the Markov approximation, which transforms eq. (2.81) into a time-local differential equation.

We first assume slow variations of the density matrix with respect to the propagation time (Δt) and replace $\hat{\sigma}^{(I)}(t')$ in the right-hand site of eq. (2.81) by the density matrix at the present time $\hat{\sigma}^{(I)}(t') \to \hat{\sigma}^{(I)}(t)$

$$\frac{d}{dt}\hat{\sigma}^{(I)}(t) = -\frac{1}{\hbar^2}\int_0^t dt' Tr_B\left\{\left[\hat{V}^{SB(I)}(t),\left[\hat{V}^{SB(I)}(t'),\hat{\sigma}^{(I)}(t)\otimes\rho^B\right]\right]\right\}. \quad (2.82)$$

The above substitution $\left(\hat{\sigma}^{(I)}(t') \to \hat{\sigma}^{(I)}(t)\right)$ implies that we assume that the propagation time Δt is too small relative to the characteristic time of evolution of the total density operator. Since the dynamics of the total density operator is determined primarily by the thermal-bath, the characteristic time of evolution of the density operator is expressed as Δt_B. Consequently we assume that $\Delta t << \Delta t_B$ and equivalently that the system-bath interaction $\hat{V}^{SB}$ is too weak.

In contrast to eq. (2.81), eq. (2.82) is the time-local Born-Markov master equation for the reduced density matrix of the system, described by a differential equation of the form of eq. (2.59), i.e.,

$$\frac{d}{dt}\hat{\sigma}^{(I)}(t) = \hat{\mathcal{L}}^{(I)}(t)\left[\hat{\sigma}^{(I)}(t)\right], \quad (2.83)$$

that determines the time evolution of $\hat{\sigma}^{(I)}$ at time t exclusively by terms of $\hat{\sigma}^{(I)}$ evaluated at time t and not from earlier times. $\hat{\mathcal{L}}^{(I)}$ is a superoperator or dynamical map that acts on $\hat{\sigma}^{(I)}(t)$. The most general form of $\hat{\mathcal{L}}^{(I)}$, consistent with a completely positive and trace preserving map is the Lindblad form (eq. 2.69). The time-local Born-Markov master equation for the reduced density matrix in the interaction representation (eqs. (2.82) and (2.83)), when transformed to the Schrödinger picture must be consistent with eq. (2.69), i.e.,

$$\frac{d}{dt}\hat{\sigma}(t) = -\frac{i}{\hbar}\left[\hat{H}^S(t), \hat{\sigma}(t)\right] + \sum_{\mu}\left[\hat{\mathcal{L}}_{\mu}(t)\hat{\sigma}(t)\hat{\mathcal{L}}_{\mu}^{\dagger}(t) - \frac{1}{2}\left(\hat{\mathcal{L}}_{\mu}^{\dagger}(t)\hat{\mathcal{L}}_{\mu}(t)\hat{\sigma}(t) + \hat{\sigma}(t)\hat{\mathcal{L}}_{\mu}^{\dagger}(t)\hat{\mathcal{L}}_{\mu}(t)\right)\right]. \quad (2.84)$$

This is the Lindblad form of master equation, and it is the most general form for the density matrix differential equation that describes Markovian dynamics.

Equation (2.84) can be written as

$$i\hbar\frac{d}{dt}\hat{\sigma}(t) = \hat{L}^{coh}(t)\hat{\sigma}(t) + \hat{L}^{diss}(t)\hat{\sigma}(t), \quad (2.85)$$

where $\hat{L}^{coh}(t)\hat{\sigma}(t) = \left[\hat{H}^S(t), \hat{\sigma}(t)\right]$ is the coherent part and $\hat{L}^{diss}(t)\hat{\sigma}(t)$ is the dissipative part of the Liouvilian for the system,

$$\hat{L}^{diss}(t)\hat{\sigma}(t) = i\hbar\sum_{\mu}\left[\hat{\mathcal{L}}_{\mu}(t)\hat{\sigma}(t)\hat{\mathcal{L}}_{\mu}^{\dagger}(t) - \frac{1}{2}\left(\hat{\mathcal{L}}_{\mu}^{\dagger}(t)\hat{\mathcal{L}}_{\mu}(t)\hat{\sigma}(t) + \hat{\sigma}(t)\hat{\mathcal{L}}_{\mu}^{\dagger}(t)\hat{\mathcal{L}}_{\mu}(t)\right)\right]. \quad (2.86)$$

The above term contains dissipation effects between the system of interest and its environment, such as population relaxation decay rates between different states of the system. Further, it often contains decay rates that do not involve any energy exchange between the system and its environment, e.g., pure dephasing rates associated with relative phase decay between the system's states, describing fluctuations in the energy gap between system's states due to their coupling to the bath (see following Section).

2.4.4 Lindblad Forms of the Master Equation in Liouville Space

Consider a two-level system Hamiltonian

$$\hat{H}^S = E_a|a\rangle\langle a| + E_b|b\rangle\langle b| + V_{ab}|a\rangle\langle b| + V_{ba}|b\rangle\langle a|, \quad (2.87)$$

where $|a\rangle$, $|b\rangle$ are the eigenstates and E_a, E_b are the eigenvalues of the unperturbed Hamiltonian, respectively. V_{ab}, V_{ba} are external perturbations that directly couple eigenstates $|a\rangle$ and $|b\rangle$.

Expressing eq. (2.85) using Liouville space we get

$$\underbrace{\frac{d}{dt}\begin{pmatrix}\sigma_{aa}\\ \sigma_{bb}\\ \sigma_{ab}\\ \sigma_{ba}\end{pmatrix}}_{\frac{d}{dt}\bar{\sigma}} = \underbrace{-\frac{i}{\hbar}\begin{pmatrix}L_{aa,aa} & L_{aa,bb} & L_{aa,ab} & L_{aa,ba}\\ L_{bb,aa} & L_{bb,bb} & L_{bb,ab} & L_{bb,ba}\\ L_{ab,aa} & L_{ab,bb} & L_{ab,ab} & L_{ab,ba}\\ L_{ba,aa} & L_{ba,bb} & L_{ba,ab} & L_{ba,ba}\end{pmatrix}}_{-\frac{i}{\hbar}\tilde{L}}\underbrace{\begin{pmatrix}\sigma_{aa}\\ \sigma_{bb}\\ \sigma_{ab}\\ \sigma_{ba}\end{pmatrix}}_{\bar{\sigma}}, \tag{2.88}$$

where $\tilde{L}$ is the matrix representation of the total Liouvilian composed by the coherent and the dissipative parts (eqs. (2.85) and (2.86))

$$\hat{L} = \hat{L}^{coh} + \hat{L}^{diss}. \tag{2.89}$$

The matrix representation of the coherent part $\tilde{L}^{coh}$ corresponds to the real part of the total Liouvilian and its representation in terms of the system's $|a\rangle$, $|b\rangle$ states has the form (eq. (2.32))

$$\tilde{L}^{coh} = \begin{pmatrix} 0 & 0 & -V_{ba} & V_{ab}\\ 0 & 0 & V_{ba} & -V_{ab}\\ -V_{ab} & V_{ab} & (E_a - E_b) & 0\\ V_{ba} & -V_{ba} & 0 & (E_b - E_a)\end{pmatrix}, \tag{2.90}$$

which is also given by eq. (2.35)

$$L^{coh}_{jk,mn} = H^{S}_{jm}\,\delta_{kn} - H^{S*}_{kn}\,\delta_{jm}. \tag{2.91}$$

The second part of the total Liouvilian eq. (2.89), the dissipative part $\left(\hat{L}^{diss}\right)$, is often taken to consist of two components, the population relaxation $\left(\hat{L}^{rel}\right)$ and the pure dephasing $\left(\hat{L}^{pd}\right)$ components

$$\hat{L}^{diss} = \hat{L}^{rel} + \hat{L}^{pd}. \tag{2.92}$$

As discussed previously, the dissipative Liouvilian (both population relaxation and pure dephasing parts), for closed quantum systems with respect to energy (population) exchange with the surrounding environment (thermal bath) must have the Lindblad form that preserve the total probability $\sum_a \sigma_{aa}(t)$. Thus, the population relaxation part is often taken to be

$$\hat{L}^{rel} = \hat{L}_a^{rel} + \hat{L}_b^{rel}\,, \tag{2.93a}$$

$$\hat{L}_k^{rel}\,\hat{\sigma} = i\hbar\left[\hat{\mathcal{L}}_k^{rel}\,\hat{\sigma}\left(\hat{\mathcal{L}}_k^{rel}\right)^{\dagger} - \frac{1}{2}\left(\left(\hat{\mathcal{L}}_k^{rel}\right)^{\dagger}\hat{\mathcal{L}}_k^{rel}\,\hat{\sigma} + \hat{\sigma}\left(\hat{\mathcal{L}}_k^{rel}\right)^{\dagger}\hat{\mathcal{L}}_k^{rel}\right)\right]\,,\ k = a,b\,, \tag{2.93b}$$

$$\hat{\mathcal{L}}_a^{rel} = \sqrt{\Gamma_{a\to b}^{rel}}\,|b\rangle\langle a|\quad,\quad \hat{\mathcal{L}}_b^{rel} = \sqrt{\Gamma_{b\to a}^{rel}}\,|a\rangle\langle b|\,, \tag{2.93c}$$

where $\hat{L}_k^{rel}$ are the population relaxation Liouvilians and $\hat{\mathcal{L}}_k^{rel}$ are the respective population relaxation Lindblad operators. The population relaxation Liouvilians in the matrix representation is

$$\tilde{L}_a^{rel} = i\hbar\begin{pmatrix} -\Gamma_{a\to b}^{rel} & 0 & 0 & 0 \\ \Gamma_{a\to b}^{rel} & 0 & 0 & 0 \\ 0 & 0 & -\frac{1}{2}\Gamma_{a\to b}^{rel} & 0 \\ 0 & 0 & 0 & -\frac{1}{2}\Gamma_{a\to b}^{rel} \end{pmatrix},\ \tilde{L}_b^{rel} = i\hbar\begin{pmatrix} 0 & \Gamma_{b\to a}^{rel} & 0 & 0 \\ 0 & -\Gamma_{b\to a}^{rel} & 0 & 0 \\ 0 & 0 & -\frac{1}{2}\Gamma_{b\to a}^{rel} & 0 \\ 0 & 0 & 0 & -\frac{1}{2}\Gamma_{b\to a}^{rel} \end{pmatrix}. \tag{2.94}$$

The pure dephasing part is usually of the form

$$\hat{L}^{pd}\,\hat{\sigma} = i\hbar\sum_{k=a}^{b}\left[\hat{\mathcal{L}}_k^{pd}\,\hat{\sigma}\left(\hat{\mathcal{L}}_k^{pd}\right)^{\dagger} - \frac{1}{2}\left(\left(\hat{\mathcal{L}}_k^{pd}\right)^{\dagger}\hat{\mathcal{L}}_k^{pd}\,\hat{\sigma} + \hat{\sigma}\left(\hat{\mathcal{L}}_k^{pd}\right)^{\dagger}\hat{\mathcal{L}}_k^{pd}\right)\right], \tag{2.95a}$$

$$\hat{\mathcal{L}}_k^{pd} = \sqrt{\Gamma_{a,b}^{pd}}\,|k\rangle\langle k|\ ;\ k = a,b\,, \tag{2.95b}$$

where $\hat{\mathcal{L}}_k^{pd}$ are the pure dephasing Lindblad operators. The pure dephasing Liouvilian in matrix representation is

$$\tilde{L}^{pd} = i\hbar\begin{pmatrix} 0 & 0 & 0 & 0 \\ 0 & 0 & 0 & 0 \\ 0 & 0 & -\Gamma_{a,b}^{pd} & 0 \\ 0 & 0 & 0 & -\Gamma_{a,b}^{pd} \end{pmatrix}. \tag{2.96}$$

The total Liouvilian composed by the coherent and the dissipative part eq. (2.89), becomes

$$\tilde{L} = \begin{pmatrix} -i\hbar\Gamma_{a\to b}^{relax} & i\hbar\Gamma_{b\to a}^{relax} & -V_{ba} & V_{ab} \\ i\hbar\Gamma_{a\to b}^{relax} & -i\hbar\Gamma_{b\to a}^{relax} & V_{ba} & -V_{ab} \\ -V_{ab} & V_{ab} & \left(E_a - E_b\right) - i\hbar\left[\frac{1}{2}\left(\Gamma_{a\to b}^{relax} + \Gamma_{b\to a}^{relax}\right) + \Gamma_{a,b}^{pure}\right] & 0 \\ V_{ba} & -V_{ba} & 0 & \left(E_b - E_a\right) - i\hbar\left[\frac{1}{2}\left(\Gamma_{a\to b}^{relax} + \Gamma_{b\to a}^{relax}\right) + \Gamma_{a,b}^{pure}\right] \end{pmatrix}. \tag{2.97}$$

Equation (2.97) shows that the perturbation directly couples populations to coherences but the coherences are not directly coupled to each other, demonstrating an exponential decay of the off-diagonal elements of the reduced density matrix over time

$$\sigma_{ab}(t) \approx e^{-i(E_a - E_b)t/\hbar} e^{-\left[\left(\Gamma^{relax}_{a\to b} + \Gamma^{relax}_{b\to a}\right)/2 + \Gamma^{pure}_{a,b}\right]t/\hbar}, \tag{2.98a}$$

$$\sigma_{ba}(t) \approx e^{-i(E_b - E_a)t/\hbar} e^{-\left[\left(\Gamma^{relax}_{a\to b} + \Gamma^{relax}_{b\to a}\right)/2 + \Gamma^{pure}_{a,b}\right]t/\hbar}. \tag{2.98b}$$

For open quantum systems with respect to population exchange with the environment, the total probability is not conserved and the population relaxation Liouvilians are replaced by

$$\tilde{L}^{rel}_a = i\hbar \begin{pmatrix} -\Gamma^{rel}_{a\to b} & 0 & 0 & 0 \\ 0 & 0 & 0 & 0 \\ 0 & 0 & -\frac{1}{2}\Gamma^{rel}_{a\to b} & 0 \\ 0 & 0 & 0 & -\frac{1}{2}\Gamma^{rel}_{a\to b} \end{pmatrix}, \quad \tilde{L}^{rel}_b = i\hbar \begin{pmatrix} 0 & 0 & 0 & 0 \\ 0 & -\Gamma^{rel}_{b\to a} & 0 & 0 \\ 0 & 0 & -\frac{1}{2}\Gamma^{rel}_{b\to a} & 0 \\ 0 & 0 & 0 & -\frac{1}{2}\Gamma^{rel}_{b\to a} \end{pmatrix}. \tag{2.99}$$

In comparison to eq. (2.94), the positive population relaxation rates are eliminated, so that energy (population) exchange can occur between the system and the environment.

2.5 References

[1] A. Nitzan, Chemical Dynamics in Condensed Phases, Oxford Univ. Press, Oxford, 2006.

[2] S. Mukamel, Principles of Nonlinear Optical Spectroscopy, Oxford Univ. Press, Oxford, 1999.

[3] V. May and O. Kühn, Charge and Energy Transfer Dynamics in Molecular Systems, Wiley-VCH, Weinheim, Germany, 2004.

[4] C. Cohen-Tannoudji, J. Dupont-Roc and G. Grynberg, Atom-Photon Interactions: Basic Processes and Applications, Wiley-VCH, 1998.

[5] K. Kraus, States, Effects and Operations, Springer-Verlag, Berlin, 1983.

[6] P. Kaye, R. Laflamme and M. Mosca, An Introduction to Quantum Computing, Oxford: NY, 2007.

[7] M. Schlosshauer, Decoherence and the Quantum-to-Classical Transition, Springer-Verlag Berlin Heidelberg NY, 2007.

[8] H. M. Wiseman and G. J. Milburn, Quantum Measurement and Control, Cambridge Univ. Press, 2010.

Chapter 3: Computational Methodologies

The major aim of most approaches of quantum-chemical computational methods is to determine molecular electronic and vibrational structure. The leading approximation used in most methods is the Born-Oppenheimer approximation discussed in Section 1.1.2. Due to the complex and relatively large molecular structures, electronic and vibrational structure computations are routinely solved using existing quantum chemistry computer programs. In this Chapter I give a brief description of the basic concepts of computational techniques that are used in the following Chapters. I mainly performed *ab initio* electronic structure calculations using the ADF and the Gaussian 09 package programs. The Latin term *ab initio* means "from the beginning" and describes computational methods that are derived from exact theoretical quantum mechanical principles, not relying on empirical or experimental parameters. The basic idea is that the Schrödinger equation is solved using approximate electronic wavefunctions, with only input the values of fundamental constants and the atomic numbers of the nuclei.

3.1 Hartree-Fock Theory

The Hartree-Fock (HF) method is conceptually the starting point for a variety of electronic structure calculations [1-4]. The key approximation of HF method is to model the N_{el} electron ground state wave function Ψ_0 as a single Slater determinant [5], which is approximated as an antisymmetrized product of N_{el} orthonormal spin orbitals $\chi(\vec{x})$, each a product of a spatial orbital $\psi(\vec{r})$ and a spin function, one corresponding to spin up $\alpha(\omega)$ and the other to spin down $\beta(\omega)$

$$\Psi_0 = \frac{1}{\sqrt{N_{el}!}} \begin{vmatrix} \chi_i(\vec{x}_1) & \chi_j(\vec{x}_1) & \cdots & \chi_k(\vec{x}_1) \\ \chi_i(\vec{x}_2) & \chi_j(\vec{x}_2) & \cdots & \chi_k(\vec{x}_2) \\ \vdots & \vdots & & \vdots \\ \chi_i(\vec{x}_{N_e}) & \chi_j(\vec{x}_{N_e}) & \cdots & \chi_k(\vec{x}_{N_e}) \end{vmatrix}. \tag{3.1}$$

In the equation above $\vec{x}_i$ indicates both space and spin coordinates and the factor $(N_{el}!)^{-1/2}$ is a normalization factor. The above Slater determinant consists of N_{el} spin orbitals $\chi(\vec{x})$ occupied by N_{el} electrons, but it does not explicitly define which electron occupies any of the individual spatial orbitals. Most importantly, the wavefunction is antisymmetric with respect to an interchange of any two electrons coordinates and further fulfills the Pauli Exclusion Principle.

Within the Born-Oppenheimer approximation the molecular Hamiltonian is given (eq. 1.6) by

$$\hat{H}^{BO} = \hat{H}^{el} + \hat{V}_{nuc-nuc}, \tag{3.2a}$$

$$\hat{H}^{el} = \hat{T}_{el} + \hat{V}_{el-nuc} + \hat{V}_{el-el}. \tag{3.2b}$$

The essence of the HF method is that the electron-electron Coulomb repulsion interactions $\hat{V}_{el-el}$ are treated in an "average" way, such that each individual electron is considered to be embedded in the average electrostatic field of the nuclei and the remaining $N_{el}-1$ electrons [1,2]. Further, the nuclear-nuclear Coulomb repulsion interactions $\hat{V}_{nuc-nuc}$ are considered constant and initially they are ignored (but added at the end of the calculation in order to compute Born-Oppenheimer energies, see Chapter 1).

The computational methodology of the HF method is based on the variational principle. The principle states that the best wave function of the form in eq. (3.1) is the one that gives the lowest possible expectation value for the ground state energy E_0

$$E_0 = \langle \Psi_0 | \hat{H}^{el} | \Psi_0 \rangle \geq \mathcal{E}, \tag{3.3}$$

(which is always greater or equal to the true ground state energy $\mathcal{E}$ of a given Hamiltonian). As a result, the variational principle obtains an upper bound to the true ground state energy. This minimization/optimization process of the energy E_0 with respect to variations of spin orbitals, leads to the Hartree-Fock equation [1,2]

$$\hat{f}(\vec{x}_1)\chi_i(\vec{x}_1) = \varepsilon_i \chi_i(\vec{x}_1), \tag{3.4}$$

where ε_i is the energy of spin orbital χ_i and $\hat{f}$ is the Fock operator. $\hat{f}$ is an effective one-electron operator, defined as the sum of the core-Hamiltonian $\hat{H}^c$, the Coulomb operator $\hat{J}$, and the exchange operator $\hat{K}$, i.e.,

$$\hat{f}(\vec{x}_1) = \hat{H}^c(\vec{x}_1) + \sum_a \left[\hat{J}_a(\vec{x}_1) - \hat{K}_a(\vec{x}_1) \right]. \tag{3.5}$$

The sum in eq. (3.5) is over the occupied orbitals. The core-Hamiltonian $\hat{H}^c(\vec{x}_1)$ of a single-electron, e.g., chosen to be electron one $(\vec{x}_1)$, consists of the electron kinetic energy operator and the corresponding attractive Coulomb interaction between the electron and the nuclei

$$\hat{H}^c(\vec{x}_1) = \hat{T}_{el}(\vec{x}_1) + \hat{V}_{el-nuc}(\vec{x}_1). \tag{3.6}$$

The Coulomb operator $\hat{J}_a$ acting on spin orbital χ_i represents the average potential that an electron in spin orbital χ_i at position $\vec{x}_1$ experiences due to the charge distribution from an electron in spin orbital χ_a. It is defined as

$$\hat{J}_a(\vec{x}_1)\,\chi_i(\vec{x}_1) = \left[\int d\vec{x}_2\, \chi_a^*(\vec{x}_2) r_{12}^{-1} \chi_a(\vec{x}_2) \right] \chi_i(\vec{x}_1). \tag{3.7}$$

The exchange operator $\hat{K}_a$ acting on spin orbital χ_i, arises from the antisymmetric nature of the determinantal wave function and does not have a simple classical interpretation like the Coulomb term. It is defined as

$$\hat{K}_a(\vec{x}_1)\,\chi_i(\vec{x}_1)=\left[\int d\vec{x}_2\,\chi_a^*(\vec{x}_2)\,r_{12}^{-1}\,\chi_i(\vec{x}_2)\right]\chi_a(\vec{x}_1). \tag{3.8}$$

In the following discussion we will briefly describe Roothan's [6] method for solving computationally the HF equations.

Roothan introduces a set of known spatial basis functions, which convert the complex HF equations into a problem that can be solved by standard matrix manipulation techniques. We will limit our discussion to the restricted closed-shell Hartree-Fock (RHF) method, because this is the method we used in our computations in Chapter 5. The RHF method assumes that each spin orbital $\chi(\vec{x})$ for the N_{el} electron ground state wavefunction Ψ_0^{RHF} is constrained to have the same spatial function $\psi(\vec{r})$ for $\alpha(\omega)$ (spin up) and $\beta(\omega)$ (spin down) spin functions. In other words, every spatial orbital $\psi(\vec{r})$ is doubly occupied by electrons with opposite spins.

A restricted set of N_{el} spin orbitals $\chi_i(\vec{x})$ has the following form [1]

$$\chi_i(\vec{x})=\begin{cases}\psi_j(\vec{r})\alpha(\omega)\\ \psi_j(\vec{r})\beta(\omega)\end{cases},\quad j=1,\ldots,N_{el}/2 \tag{3.9}$$

and the corresponding RHF N_{el} electron ground state wavefunction is

$$\Psi_0^{RHF}=\frac{1}{\sqrt{N_{el}!}}\times$$

$$\begin{vmatrix}
\psi_1(\vec{r}_1)\alpha(\omega_1) & \psi_1(\vec{r}_1)\beta(\omega_1) & \cdots & \psi_{N_{el}/2}(\vec{r}_1)\alpha(\omega_1) & \psi_{N_{el}/2}(\vec{r}_1)\beta(\omega_1)\\
\psi_1(\vec{r}_2)\alpha(\omega_2) & \psi_1(\vec{r}_2)\beta(\omega_2) & & \psi_{N_{el}/2}(\vec{r}_2)\alpha(\omega_2) & \psi_{N_{el}/2}(\vec{r}_2)\beta(\omega_2)\\
\vdots & \vdots & \cdots & \vdots & \vdots\\
\psi_1(\vec{r}_{N_{el}})\alpha(\omega_{N_{el}}) & \psi_1(\vec{r}_{N_{el}})\beta(\omega_{N_{el}}) & \cdots & \psi_{N_{el}/2}(\vec{r}_{N_{el}})\alpha(\omega_{N_{el}}) & \psi_{N_{el}/2}(\vec{r}_{N_{el}})\beta(\omega_{N_{el}})
\end{vmatrix}. \tag{3.10}$$

In order to obtain the Roothan equations we need to convert the general spin orbital HF equation (eq. (3.4)) to a spatial orbital equation. For closed-shell systems with doubly occupied spatial orbitals, the HF equations for the individual spatial orbital wavefunctions are

$$\hat{f}(\vec{r}_1)\psi_i(\vec{r}_1)=\varepsilon_i\psi_i(\vec{r}_1). \tag{3.11}$$

Similar to eq. (3.4) $\hat{f}$ is the Fock operator, which is defined as the sum of the core-Hamiltonian $\hat{H}^c$, the Coulomb operator $\hat{J}$, and the exchange operator $\hat{K}$,

$$\hat{f}(\vec{r}_1) = \hat{H}^c(\vec{r}_1) + \sum_a^{N_{el}/2} \left[2\hat{J}_a(\vec{r}_1) - \hat{K}_a(\vec{r}_1) \right], \tag{3.12a}$$

$$\hat{H}^c(\vec{r}_1) = \hat{T}_{el}(\vec{r}_1) + \hat{V}_{el-nuc}(\vec{r}_1), \tag{3.12b}$$

$$\hat{J}_a(\vec{r}_1)\,\psi_i(\vec{r}_1) = \left[\int d\vec{r}_2\, \psi_a^*(\vec{r}_2)\, r_{12}^{-1}\, \psi_a(\vec{r}_2) \right] \psi_i(\vec{r}_1), \tag{3.12c}$$

$$\hat{K}_a(\vec{r}_1)\,\psi_i(\vec{r}_1) = \left[\int d\vec{r}_2\, \psi_a^*(\vec{r}_2)\, r_{12}^{-1}\, \psi_i(\vec{r}_2) \right] \psi_a(\vec{r}_1). \tag{3.12d}$$

These equations are analogous to eqs. (3.4)–(3.8) for spin orbitals, with the only difference being the factor of two present for the Coulomb operator. Also, the sum in eq. (3.12a) is over the $N_{el}/2$ occupied spatial orbitals $\{\psi_a(\vec{r})\}$.

As we have eliminated spin functions from the HF equations we can express molecular orbitals as a linear combination of atomic orbitals (LCAO-MO procedure) using known spatial basis functions, which describe atomic orbitals (localized on individual atoms). For a finite set of K atomic orbital basis functions $\phi_\mu(\vec{r})$, ($\mu = 1, 2, \ldots, K$) we express each unknown spatial molecular orbital wavefunction ψ_i as a linear combination of these basis functions, i.e.,

$$\psi_i = \sum_{\mu=1}^{K} C_{\mu i} \phi_\mu \quad , \quad i = 1, 2, \ldots, K, \tag{3.13}$$

where $C_{\mu i}$ are unknown expansion coefficients. Using now eq. (3.13) the problem of calculating the molecular orbitals has been transformed to the problem of computing the expansion coefficients $C_{\mu i}$. Substituting eq. (3.13) to the HF equation (eq. (3.11)) gives

$$\hat{f}(\vec{r}_1) \sum_\nu C_{\nu i}\, \phi_\nu(\vec{r}_1) = \varepsilon_i \sum_\nu C_{\nu i}\, \phi_\nu(\vec{r}_1). \tag{3.14}$$

Multiplication of both sides of eq. (3.14) by $\phi_\mu^*(\vec{r}_1)$ and integration over all space, yields a matrix equation of the following form

$$\sum_\nu C_{\nu i} \int d\vec{r}_1\, \phi_\mu^*(\vec{r}_1)\, \hat{f}(\vec{r}_1) \phi_\nu(\vec{r}_1) = \varepsilon_i \sum_\nu C_{\nu i} \int d\vec{r}_1\, \phi_\mu^*(\vec{r}_1) \phi_\nu(\vec{r}_1). \tag{3.15}$$

We can now define two matrices, the overlap matrix $\tilde{S}$ and the Fock matrix $\tilde{F}$ with elements

$$S_{\mu\nu} = \int d\vec{r}_1 \, \phi_\mu^*(\vec{r}_1)\phi_\nu(\vec{r}_1), \tag{3.16}$$

$$F_{\mu\nu} = \int d\vec{r}_1 \, \phi_\mu^*(\vec{r}_1)\, \hat{f}(\vec{r}_1)\phi_\nu(\vec{r}_1) \tag{3.17}$$

(both of them are $K \times K$ Hermitian matrices). With the above definitions of $\tilde{S}$ and $\tilde{F}$ eq. (3.15) becomes

$$\sum_\nu F_{\mu\nu} C_{\nu i} = \varepsilon_i \sum_\nu S_{\mu\nu} C_{\nu i} \quad i = 1, 2, \ldots, K. \tag{3.18}$$

These are the Roothan equations, which in a more compact notation can be written as a single matrix equation

$$\tilde{F}\tilde{C} = \tilde{S}\tilde{C}\tilde{\varepsilon}, \tag{3.19}$$

where $\tilde{C}$ is a $K \times K$ matrix composed of the expansion coefficients $C_{\mu i}$ and $\tilde{\varepsilon}$ is an $K \times K$ diagonal matrix of the orbitals energies ε_i.

To further proceed and to determine the molecular orbitals ψ_i and orbital energies ε_i we need to solve the matrix eq. (3.19). Unfortunately, the solution of this matrix equation is not as simple as might be expected and cannot be solved directly because the Fock matrix elements involve integrals over the Coulomb and exchange operators. To obtain the explicit form of the Fock matrix elements we substitute eq. (3.12a) into eq. (3.17)

$$\begin{aligned} F_{\mu\nu} &= \int d\vec{r}_1 \, \phi_\mu^*(\vec{r}_1)\, \hat{f}(\vec{r}_1)\phi_\nu(\vec{r}_1) \\ &= \int d\vec{r}_1 \, \phi_\mu^*(\vec{r}_1)\hat{H}^c(\vec{r}_1)\phi_\nu(\vec{r}_1) + \sum_a^{N_{el}/2} \int d\vec{r}_1 \, \phi_\mu^*(\vec{r}_1)\left[2\hat{J}_a(\vec{r}_1) - \hat{K}_a(\vec{r}_1)\right]\phi_\nu(\vec{r}_1). \end{aligned} \tag{3.20}$$

From the first term of the right hand side of eq. (3.20) we can define a core-Hamiltonian matrix, whose elements are composed by one-electron integrals describing the kinetic energy and nuclear attraction of an electron

$$H_{\mu\nu}^c = \int d\vec{r}_1 \, \phi_\mu^*(\vec{r}_1)\hat{H}^c(\vec{r}_1)\phi_\nu(\vec{r}_1) = T_{\mu\nu}^{el} + V_{\mu\nu}^{el-nuc}, \tag{3.21a}$$

$$T_{\mu\nu}^{el} = \int d\vec{r}_1 \, \phi_\mu^*(\vec{r}_1)\hat{T}_{el}(\vec{r}_1)\phi_\nu(\vec{r}_1), \tag{3.21b}$$

$$V_{\mu\nu}^{el-nuc} = \int d\vec{r}_1 \, \phi_\mu^*(\vec{r}_1)\hat{V}_{el-nuc}(\vec{r}_1)\phi_\nu(\vec{r}_1). \tag{3.21c}$$

Substituting eq. (3.13) into the two-electron terms of eq. (3.20) we get

$$\begin{aligned} F_{\mu\nu} &= H^c_{\mu\nu} + \sum_{\alpha}^{N_{el}/2} \sum_{\lambda\sigma} C_{\lambda\alpha} C^*_{\sigma\alpha} \left[2\left(\mu\nu|\sigma\lambda\right) - \left(\mu\lambda|\sigma\nu\right) \right] \\ &= H^c_{\mu\nu} + \sum_{\lambda\sigma} P_{\lambda\sigma} \left[\left(\mu\nu|\sigma\lambda\right) - \left(\mu\lambda|\sigma\nu\right)/2 \right], \end{aligned} \tag{3.22}$$

where $P_{\lambda\sigma} = 2\sum_{\alpha}^{N_{el}/2} C_{\lambda\alpha} C^*_{\sigma\alpha}$ is the charge density matrix. The Fock matrix elements eq. (3.22) involve a one-electron part ($H^c_{\mu\nu}$) and a two-electron part that depends on the density matrix $P_{\lambda\sigma}$ and on a set of two-electron integrals of the form

$$\left(\mu\nu|\lambda\sigma\right) = \frac{e^2}{4\pi\varepsilon_0} \int d\vec{r}_1\, d\vec{r}_2\; \phi^*_\mu\left(\vec{r}_1\right) \phi_\nu\left(\vec{r}_1\right) r_{12}^{-1}\, \phi^*_\lambda\left(\vec{r}_2\right) \phi_\sigma\left(\vec{r}_2\right). \tag{3.23}$$

Because the number of two-electron integrals to evaluate is large, their efficient calculation poses a difficulty in a HF calculation. For a set of K basis functions ϕ_μ the number of two-electron integrals to evaluate is of order K^4. This number often approaches several millions of two-electron integrals.

Having now demonstrated the basic mathematical formulation of the HF method it is clear that the HF equations are really nonlinear equations and cannot be solved by a single diagonalization. Thus the HF equations need to be solved iteratively or self-consistently and the respective computational solution procedure is known as the self-consistent-field (SCF) method. The basic idea of the SCF method is simple. We initially choose a set of spatial basis functions $\{\phi_\mu\}$ and subsequently guess a set of trial expansion coefficients $\{C_{\mu i}\}$. We therefore construct the trial molecular orbital wavefunctions $\{\psi_i\}$ (e.g., eq. (3.13)). We then calculate all the required molecular integrals, such as the overlap matrix elements $S_{\mu\nu}$, the one-electron core-Hamiltonian elements $H^c_{\mu\nu}$, and the two-electron integrals $\left(\mu\nu|\lambda\sigma\right)$ and then solve eq. (3.19) for a new set of expansion coefficients $\{C_{\mu i}\}$ (which correspond to a new set of molecular orbitals $\{\psi_i\}$). Using these new molecular orbitals we can obtain updated matrix elements $S_{\mu\nu}$, $H^c_{\mu\nu}$, and $\left(\mu\nu|\lambda\sigma\right)$ and repeat the procedure until self-consistency is reached (e.g., until a convergence criterion for the ground state energy has been satisfied).

3.2 Configuration Interaction

The HF ground state wavefunction is an approximation and definitely does not represent the exact wavefunction. HF theory treats the interactions among electrons in an average way: each electron is exposed to an average potential arising from all the other electrons. This deficiency of the HF theory is simply summarized by stating that the HF method ignores electron correlation. In this Section we will consider the method of configuration interaction [1,2] as a means for: i) improving the HF method's approximations with respect to electron correlation, ii) for computing excited states.

In the configuration interaction (CI) method the exact N_{el}-electron ground state wavefunction may be expressed as a linear combination of all possible N_{el}-electron determinants (developed using a complete basis set). These determinants are described by reference to the RHF N_{el}-electron ground state wavefunction Ψ_0^{RHF} (eq. (3.10). The exact electronic wavefunction Φ is of the following form

$$\left|\Phi\right\rangle = c_0\left|\Psi_0^{RHF}\right\rangle + \sum_{ix} c_i^x\left|\Psi_i^x\right\rangle + \sum_{\substack{i<j\\x<y}} c_{ij}^{xy}\left|\Psi_{ij}^{xy}\right\rangle + \sum_{\substack{i<j<k\\x<y<z}} c_{ijk}^{xyz}\left|\Psi_{ijk}^{xyz}\right\rangle + \cdots \tag{3.24}$$

which is also known as the full CI wave function. $\left|\Psi_0^{RHF}\right\rangle$ is the RHF best Slater determinant describing the ground electronic state, also called the "reference" state. $\left|\Psi_i^x\right\rangle$ is a singly excited determinant, in which an electron in an occupied spin orbital χ_i in the reference state, has been promoted to an unoccupied (virtual) spin orbital χ_x. $\left|\Psi_{ij}^{xy}\right\rangle$ is a doubly excited determinant in which two electrons have been promoted, compared to the reference state, one from χ_i to χ_x and one from χ_j to χ_y. $\left|\Psi_{ijk}^{xyz}\right\rangle$ is the triply excited determinant, etc., up to and including N_{el}-tuply excited determinants. The c's are expansion coefficients and the limits in the summations, e.g., $i<j$ ($x<y$), ensure that we sum every individual excited determinant only once.

The energy obtained from the exact wave function eq. (3.24) is the exact ground state energy $\mathcal{E}_0$ ($\mathcal{E}_0 = \left\langle\Phi\left|\hat{H}\right|\Phi\right\rangle$) of the system. The difference between this exact energy $\mathcal{E}_0$ and the HF-limit energy E_0^{RHF} ($E_0^{RHF} = \left\langle\Psi_0^{RHF}\left|\hat{H}\right|\Psi_0^{RHF}\right\rangle$), is called the correlation energy

defined as $E_{corr} = \mathcal{E}_0 - E_0^{RHF}$ (when the basis functions used to represent the molecular orbitals are of infinite number and compose a complete basis set).

3.3 Configuration Interaction Singles

In this Section we will consider CI calculations of excited state energies, namely the configuration interaction singles (CIS) method that gives accurate excitation energies only for transitions that are dominated by single excitations [1,7,8]. To obtain singly excited state energies within the CIS method one must truncate the full CI wave function (eq. (3. 24)) to include only single excitations, described by the singly excited determinants $\left|\Psi_i^x\right\rangle$ with respect to the RHF ground state wavefunction $\left|\Psi_0^{RHF}\right\rangle$. The CIS wavefunction can be expanded as

$$\left|\Phi_{CIS}\right\rangle = c_0\left|\Psi_0^{RHF}\right\rangle + \sum_{ix} c_i^x \left|\Psi_i^x\right\rangle. \tag{3.25}$$

In the CIS approach both spin singlet and spin triplet states can be generated, and the Hamiltonian matrix elements among CIS basis states for spin singlet states are

$$\left\langle {}^1\Psi_i^x \left| \hat{H} \right| {}^1\Psi_j^y \right\rangle = E_0^{RHF}\delta_{ij}\delta_{xy} + \delta_{ij}F_{xy} - \delta_{xy}F_{ij} + 2\left(ix\middle|jy\right) - \left(ij\middle|xy\right). \tag{3.26}$$

For spin triplet states the Hamiltonian matrix elements are

$$\left\langle {}^3\Psi_i^x \left| \hat{H} \right| {}^3\Psi_j^y \right\rangle = E_0^{RHF}\delta_{ij}\delta_{xy} + \delta_{ij}F_{xy} - \delta_{xy}F_{ij} - \left(ij\middle|xy\right). \tag{3.27}$$

E_0^{RHF} is the RHF ground state energy, the F_{xy} and F_{ij} are Fock matrix elements from the HF theory, and the two-electron integrals present in eqs. (3.26) and (3.27) describe the Coulomb $(ix|jy)$ and exchange $(ij|xy)$ two-electron interactions. In the CIS method the Hamiltonian is diagonalized to obtain many-electron excited eigenstates and the corresponding excited state eigenenergies. Each CIS excitation energy is the difference between the CIS excited state energy given by an eigenvalue of eqs. (3.26) and (3.27) and the RHF ground state energy E_0^{RHF}. The CIS computational method is commonly used to predict absorption and fluorescence emission spectra of molecules.

3.4 Density Functional Theory

Density functional theory (DFT) is presently one of the most successful computational approaches for molecular electronic structure calculations [2-4]. DFT is an alternative to wavefunction-based electronic structure methods, e.g., the HF method discussed in Section 3.1. The basic idea of DFT is that the properties of an electronic system, more often the ground state energy of the system, are expressed in terms of functionals (i.e., functions of another function) of the total electron probability density. Hence, the abbreviation DFT describes the use of functionals of the electron density.

The DFT method has its roots in the 1920s, where independently L.H. Thomas and E. Fermi [9,10] developed an entirely new approach to the calculation of the electronic structures of atoms, namely the Thomas-Fermi model, based on the uniform electron gas. Thomas and Fermi managed to demonstrate that the kinetic energy of electrons is directly related to the electron density. A more solid theoretical framework of the DFT method was given by P. Hohenberg and W. Kohn in the 1960s [11]. The Hohenberg-Kohn existence theorem demonstrates that the electron density uniquely determines all the electronic properties of the ground state of a molecular system. This powerful statement reduces the many-electron problem of solving a N_{el}-wavefunction in $3N_{el}$ dimensional space to solving electron density functionals in 3 dimensional space.

The ground-state electron density $\rho(\vec{r})$ is the central quantity in DFT and it is defined as the total electron density at a particular point $\vec{r}$ in space, for a system of N_{el} electrons. $\rho(\vec{r})$ further determines the total number of electrons as $N_{el} = \int d\vec{r}\,\rho(\vec{r})$. Within the Born-Oppenheimer approximation the electronic Hamiltonian of the system given by eq. (3.2b) is reproduced here in a modified notation in order to clearly indicate the crucial term of the external potential

$$\hat{H}^{el} = \hat{T}_{el} + \hat{V}_{ext} + \hat{V}_{el-el}. \tag{3.28}$$

In eq. (3.28) the interaction between electrons and nuclei $\left(\hat{V}_{el-nuc}\right)$ are included in the external potential ($\hat{V}_{ext}$).

The aforementioned Hohenberg-Kohn existence theorem states that the external potential $\hat{V}_{ext}$, and hence the total ground state energy of a molecule is a unique functional of the ground state electron density, i.e.,

$$E[\rho] = \langle \Psi | \hat{H}^{el} | \Psi \rangle = \underbrace{T_{el}[\rho] + V_{el-el}[\rho]}_{E_{HK}[\rho]} + \int d\vec{r}\, \rho(\vec{r}) V_{ext}(\vec{r}). \tag{3.29}$$

The second theorem, the variational theorem of Hohenberg-Kohn [2,11], states that any new trial density function $\rho'(\vec{r})$ results in a new external potential and thus a new wavefunction Ψ'. In that way the ground state energy can be obtained variationally. More precisely, using this new wavefunction Ψ' as a trial function for the molecular system with Hamiltonian of eq. (3.28), and using the variation theorem gives

$$E[\rho'] = \langle \Psi' | \hat{H}^{el} | \Psi' \rangle \geq E[\rho]. \tag{3.30}$$

Equation (3.30) clearly shows that for a trial density function $\rho'(\vec{r})$, the obtained energy functional $E[\rho']$ is always greater than the true ground state energy $E[\rho]$ of the molecular system. The variation principle further implies that the desired ground-state electron density corresponds to a minimum of the energy functional (eq. (3.29)) under the restriction that the total number of electrons $N_{el} = \int d\vec{r}\, \rho(\vec{r})$ in the system is kept constant as $\rho(\vec{r})$ is varied.

P. Hohenberg and W. Kohn [11], proved the above theorem. W. Kohn and L. J. Sham [12] demonstrated how such a calculation actually can be carried out. Specifically, they managed to transform the many-electron problem of N_{el} interacting electrons in a static average potential to a problem of N_{el} non-interacting electrons embedded in an effective external potential. They further showed that the electron density of the reference non-interacting system $\rho_{ref}(\vec{r})$ is identical to the true electron density $\rho(\vec{r})$.

The total energy functional of the molecular system (eq. (3.29)) can be written in terms of the reference system and some complementary correction terms [2,3]

$$\begin{aligned} E[\rho] &= T_{el}[\rho] + V_{el-el}[\rho] + \int d\vec{r}\, \rho(\vec{r}) V_{ext}(\vec{r}) \\ &= T_{ref}[\rho] + J[\rho] + \int d\vec{r}\, \rho(\vec{r}) V_{ext}(\vec{r}) + \left\{ \left(T_{el}[\rho] - T_{ref}[\rho] \right) + \left(V_{el-el}[\rho] - J[\rho] \right) \right\}. \end{aligned} \tag{3.31}$$

$T_{ref}[\rho]$ is the kinetic energy of the electrons and $J[\rho]$ is the classical Coulombic interaction between electrons of the reference system the non-interacting electrons. The total energy functional (eq. (3.31)) of the molecular system can be written as

$$E[\rho] = T_{ref}[\rho] + J[\rho] + \int d\vec{r}\, \rho(\vec{r}) V_{ext}(\vec{r}) + E_{XC}[\rho] \tag{3.32}$$

where,

$$E_{XC}[\rho] = T_{el}[\rho] - T_{ref}[\rho] + V_{el-el}[\rho] - J[\rho]. \tag{3.33}$$

$E_{XC}[\rho]$ is the exchange-correlation energy functional. $E_{XC}[\rho]$ contains the difference in the kinetic energy of the true system, $T_{el}[\rho]$, and of the non-interacting reference system, $T_{ref}[\rho]$. $E_{XC}[\rho]$ also contains the difference between the true electron-electron interactions, $V_{el-el}[\rho]$, and the non-interacting system Coulomb interaction $J[\rho]$.

To find the ground state energy of the molecular system we need to minimize the system's energy functional eq. (3.32) with respect to the density,

$$\frac{\delta E[\rho]}{\delta \rho(\vec{r})} = V_{eff}(\vec{r}) + \frac{\delta T_{reff}[\rho]}{\delta \rho(\vec{r})}. \tag{3.34}$$

The effective potential is defined as

$$V_{eff}(\vec{r}) = V_{ext}(\vec{r}) + \frac{\delta J[\rho]}{\delta \rho(\vec{r})} + \frac{\delta E_{XC}[\rho]}{\delta \rho(\vec{r})}. \tag{3.35}$$

The derivative of the Coulombic contribution functional $J[\rho]$ is

$$\frac{\delta J[\rho]}{\delta \rho(\vec{r})} = \frac{e^2}{4\pi\varepsilon_0} \int d\vec{r}' \frac{\rho(\vec{r}')}{|\vec{r} - \vec{r}'|}, \tag{3.36}$$

and we further define the exchange-correlation potential to be the derivative of the exchange-correlation energy functional $E_{XC}[\rho]$

$$V_{XC}(\vec{r}) = \frac{\delta E_{XC}[\rho]}{\delta \rho(\vec{r})}. \tag{3.37}$$

To find the electron density that minimizes the energy functional (eq. (3.32)) Kohn and Sham introduced the concept of one-electron Kohn-Sham orbitals ϕ_i^{KS}. The electron density of the N_{el}-electron non-interacting system is expressed as a function of the Kohn-Sham orbitals

$$\rho(\vec{r}) = \sum_{i=1}^{N_{el}} \left| \phi_i^{KS}(\vec{r}) \right|^2 . \tag{3.38}$$

$E[\rho]$ in eq. (3.32) is written in terms of the Kohn-Sham orbitals which are varied in order to compute $\delta E[\rho]/\delta\rho$. The resulting equation for the Kohn-Sham orbitals that minimize $E[\rho]$ is

$$\underbrace{\left(-\frac{\hbar^2}{2m_e}\nabla_i^2 + V_{eff}(\vec{r}) \right)}_{\hat{H}^{KS}} \phi_i^{KS}(\vec{r}) = \varepsilon_i^{KS}\, \phi_i^{KS}(\vec{r}) . \tag{3.39}$$

$\hat{H}^{KS}$ is the one-electron Kohn-Sham Hamiltonian, ε_i^{KS} is the corresponding energy of the Kohn-Sham orbital ϕ_i^{KS}, and $V_{eff}(\vec{r})$ is the effective potential defined in eq. (3.35).

In conclusion, to obtain the electron density of a molecular system, the Kohn-Sham equations (eq. (3.39)) are solved with the insertion of the effective potential eq. (3.35). Since the effective potential contains functionals of the electron density, the solution of the Kohn-Sham equations needs to be found in a self-consistent (e.g., iterative) way, starting with an initial guess for the electron density. Then the effective potential is calculated and eq. (3.39) is solved to obtain the Kohn-Sham equations for the ϕ_i^{KS}. From the obtained orbitals ϕ_i^{KS} a new electron density is calculated using eq. (3.38) and the previous calculations are repeated until convergence is reached.

It must be emphasized that DFT would be an exact theory and the Kohn-Sham formulation would lead to the exact energy of the system if the exchange-correlation functional $E_{XC}[\rho]$ were known. The main challenge in DFT is to develop approximate forms of high accuracy for the exchange-correlation energy functional $E_{XC}[\rho]$, which most often is the main source of error in DFT calculations due to the approximate nature of $E_{XC}[\rho]$. Even though the exact form of $E_{XC}[\rho]$ is not known there are many ways to approximate this functional, which is generally divided into two separate terms,

$$E_{XC}[\rho] = E_X[\rho] + E_C[\rho]. \tag{3.40}$$

The first term is the exchange functional $E_X[\rho]$ describing exchange energy and the second term is the correlation functional $E_C[\rho]$ that describes correlation energy, respectively. In terms of contributions, the exchange functional $E_X[\rho]$ is the dominant term in the exchange-correlation functional $E_{XC}[\rho]$.

In most electronic structure calculations $E_{XC}[\rho]$ is commonly approximated within the local density approximation (LDA), which only depends on the electron density at each point in space, or within the generalized-gradient approximation (GGA) that depends not only on the electron density at a point but also on its gradient there. There also exist hybrid functionals in which the $E_{XC}[\rho]$ is developed as a linear combination of a Hartree-Fock exchange contribution with a density-functional exchange contribution.

3.5 Time-dependent Density Functional Theory

Time-dependent density functional theory (TDDFT) is an extension of DFT used to investigate the properties and dynamics of multi-electron molecular systems under the influence of time-dependent external potentials (perturbations), i.e., electromagnetic fields. TDDFT is commonly used to extract excited states features such as excitation energies and photo-absorption spectra.

TDDFT is a more recent development compared to DFT. It is based on the Runge-Gross theorem [13] which can be considered as the time-dependent equivalent of the Hohenberg-Kohn theorem [11] introduced in the foregoing Section. The Runge-Gross theorem states that for a given initial state, there is a unique one-to-one mapping between the time-dependent external potential, under which the system time-evolves, and its time-dependent electron density $\rho(\vec{r},t)$. That is, for the same initial state, two (or even more) different external potentials cannot give the same electronic probability density $\rho(\vec{r},t)$.

Given the Runge-Gross theorem, the major challenge is to develop an effective potential of N_{el}-electrons non-interacting system that gives the same electron density that would be obtained by a physical N_{el}-electrons interacting system. This is the time-dependent

analogue of Kohn-Sham approach discussed in the previous Section. In the time-dependent Kohn-Sham approach, the Kohn-Sham orbitals $\phi_i^{KS}(\vec{r},t)$ obey the time-dependent Schrödinger equation

$$\left(-\frac{\hbar^2}{2m_e}\nabla_i^2 + V_{eff}(\vec{r},t)\right)\phi_i^{KS}(\vec{r},t) = i\hbar\frac{\partial}{\partial t}\phi_i^{KS}(\vec{r},t). \tag{3.41}$$

The effective potential of a non-interacting system is defined as

$$V_{eff}(\vec{r},t) = V_{ext}(\vec{r},t) + V_J\left[\rho(\vec{r},t)\right] + V_{XC}\left[\rho(\vec{r},t)\right], \tag{3.42}$$

where $V_{ext}(\vec{r},t)$ is the external potential, $V_J\left[\rho(\vec{r},t)\right]$ is the Coulombic potential contribution, and $V_{XC}\left[\rho(\vec{r},t)\right]$ is the exchange correlation potential.

The time-dependent electronic density is obtained from the Kohn-Sham orbitals as

$$\rho(\vec{r},t) = \sum_{i=1}^{N_{el}} \left|\phi_i^{KS}(\vec{r},t)\right|^2. \tag{3.43}$$

The time-dependent Kohn-Sham equations (eq. (3.41)) are solved in a self-consistent way, starting with the solution of a set of static Kohn-Sham equations (as in eq. (3.39)) in order to obtain a set of N_{el} ground state orbitals $\phi_i^{KS(0)}(\vec{r})$,

$$\left(-\frac{\hbar^2}{2m_e}\nabla_i^2 + V_{eff}(\vec{r},t_0)\right)\phi_i^{KS(0)}(\vec{r}) = \varepsilon_i^{KS}\phi_i^{KS(0)}(\vec{r}). \tag{3.44}$$

The N_{el} static ground-state Kohn-Sham orbitals $\phi_i^{KS(0)}(\vec{r})$ are taken as initial orbitals

$$\phi_i^{KS}(\vec{r},t_0) = \phi_i^{KS(0)}(\vec{r}) \quad , \quad i = 1,\ldots,N_{el} \tag{3.45}$$

and propagated in a time window $[t_0,T]$ using eq. (3.41). Then the electron density (eq. (3.43)) is calculated and used to estimate the Kohn-Sham effective potential (eq. (3.42)) for the propagated time window. For this calculated effective potential eq. (3.41) is further propagated in the same time window $[t_0,T]$ and a new set of orbitals $\phi_i^{KS}(\vec{r},t)$ are obtained. Using these new orbitals one can calculate a new electron density and subsequently a new effective potential. This procedure is repeated until self-consistency is

reached, that is, convergence has been met within a predefined tolerance criterion (among the final and the previously calculated effective potential for the same time window).

In the case of a weak time-dependent external perturbation (i.e., a weak electromagnetic field) we do not need to solve the full time-dependent Kohn-Sham equations (eq. (3.41). Consider for instance, that for times before the application of the external perturbation the system is its ground state, described by the ground state electron density $\rho(\vec{r})$. When the external perturbation V_I is turned on, it induces changes to the electron density. Thus, we can express electron density in a perturbative series, i.e.,

$$\rho(\vec{r},t) = \rho(\vec{r}) + \rho_1(\vec{r},t) + \rho_2(\vec{r},t) + \ldots, \tag{3.46}$$

where $\rho_1(\vec{r},t)$ is the linear (first-order), $\rho_2(\vec{r},t)$ is the quadratic (second-order), etc., response of the electron density to the perturbation V_I.

Since we consider a weak perturbation, we take into account only linear response of the density to the perturbation V_I (i.e., $\rho_1(\vec{r},t)$). The linear term of the density response to the perturbation in frequency domain is [14-16]

$$\rho_1(\vec{r},\omega) = \int d\vec{r}'\, \chi(\vec{r},\vec{r}';\omega) V_I(\vec{r}',\omega), \tag{3.47}$$

where $\chi(\vec{r},\vec{r}',\omega')$ is the linear density-density response function of the system.

Using perturbation theory, the computation of the $\chi(\vec{r},\vec{r}',\omega')$ for the full N_{el}-electron interacting system is a very difficult task. To evaluate $\chi(\vec{r},\vec{r}',\omega')$ we adopt the time-dependent Kohn-Sham methodology that uses a reference non-interacting N_{el}-electron system. The respective $\rho_1(\vec{r},\omega)$ in the Kohn-Sham formulation will be

$$\rho_1(\vec{r},\omega) = \int d\vec{r}'\, \chi_{KS}(\vec{r},\vec{r}';\omega) V_I^{KS}(\vec{r}',\omega) \tag{3.48}$$

where, V_I^{KS} is the linear change of the effective Kohn-Sham potential V_{eff}. χ_{KS} is the linear density-density response function of a non-interacting N_{el}-electron system, which in terms of the unperturbed stationary (ground-state) Kohn-Sham orbitals can be written as [14-16]

$$\chi_{KS}\left(\vec{r},\vec{r}';\omega\right)\approx\lim_{n\to 0^{+}}\sum_{j,k}^{\infty}\left(f_k-f_j\right)\frac{\phi_k^{KS*}\left(\vec{r}\right)\phi_j^{KS}\left(\vec{r}\right)\phi_j^{KS*}\left(\vec{r}'\right)\phi_k^{KS}\left(\vec{r}'\right)}{\omega-\omega_{jk}+in} \tag{3.49}$$

where, f_k, f_j are the Fermi occupation factors (one or zero). χ_{KS} has poles at frequencies ω_{jk} that correspond to the excitations energies of the non-interacting system. The respective true excitations energies of the interacting system are given by [14-16]

$$\Omega=\omega_{jk}+K\left(\omega_{jk}\right) \tag{3.50}$$

where, ω_{jk} is the energy difference between the Kohn-Sham eigenvalues of the unoccupied orbital j and the occupied orbital k. $K\left(\omega_{jk}\right)$ is a correction term that arises from the external-perturbation-induced variations on the V_J and V_{XC} potentials (eq. (3.42)).

The linear response of the electron density to the external perturbation, provide us formulas (eqs. (3.49) and (3.50)) to calculate the excitation energies and the respective absorption spectrum.

3.6 Gradient Methods and Molecular Properties

In the previous Sections we gave a brief description of computational methodologies, such as the HF and DFT methods, whose primary goal is to determine the electronic structure of a molecular system. As long as the electronic eigenstates and eigenenergies are computed, several other molecular properties can immediately be determined. A most significant computation is finding the equilibrium molecular geometry for a ground or excited electronic state, by computing the minimum of the corresponding Born-Oppenheimer energy surface.

We will initiate this discussion with a description of the geometry optimization procedure [2,17], which is essential for a variety of other computations that require the optimized equilibrium molecular structure. Geometry optimization is the process of finding an atomic arrangement that minimizes the molecular Born-Oppenheimer potential energy surface. To find the Born-Oppenheimer potential surface minimum we need to compute first order

energy gradients with respect to nuclear coordinates (R_i) that represent the forces exerted on a nucleus by electrons and other nuclei, i.e.,

$$F_i^{BO} = -\frac{\partial E^{BO}}{\partial R_i} = 0 \,. \tag{3.51}$$

The optimized equilibrium geometry in principle is the molecular geometry for which all of the computed forces (eq. (3.51)) are close to zero, within a predefined tolerance. These zero net forces actually only characterize a stationary point on the potential surface. To further distinguish if this stationary point is the desirable minimum of the potential and not a maximum or a saddle point, we need to compute second energy derivatives with respect to nuclear coordinates $\partial^2 E^{BO} / \partial R_i \partial R_j$, and to obtain the so-called Hessian matrix. We now diagonalize the Hessian matrix, and if the obtained eigenvalues of the Hessian matrix are all positive, the computed stationary point of the potential surface defines the equilibrium molecular structure.

Furthermore, second energy derivatives of the optimized equilibrium molecular structure with respect to nuclear coordinates determine force constants for harmonic vibrational normal mode frequencies [2,17]. Within the assumption of small displacements of the nuclei from their equilibrium positions we obtain the matrix of force constants, which we further express in mass-weighted Cartesian coordinates $q_i = \sqrt{m}\, R_i$, i.e.,

$$K_{ij} = \frac{\partial^2 E^{BO}}{\partial q_i \partial q_j} \,. \tag{3.52}$$

Diagonalization of the force constant K_{ij}, gives the normal modes as eigenvectors and the respective eigenvalues (λ_K) are directly related to the harmonic vibrational normal mode frequencies as

$$\omega_K = \sqrt{\lambda_K} \,. \tag{3.53}$$

In addition to second order derivatives, higher order derivatives with respect to nuclear coordinates, describe anharmonic corrections to the vibrational frequencies. Finally, mixed second energy derivatives with respect to a nuclear normal mode coordinate Q_i and an electric field component produces dipole moment derivatives ($\partial \mu_{IR} / \partial Q_i$) that determine infrared intensities of the ith fundamental vibrational band [17-19]

$$A_i = \frac{1}{4\pi\varepsilon_0}\frac{N_A \pi g_i}{3c^2}\left(\frac{\partial \mu_{IR}}{\partial Q_i}\right)^2, \tag{3.54}$$

where N_A, c and g_i are Avogadro's number, the velocity of light and the degeneracy of the ith band, respectively.

3.7 Electronic Couplings – Charge Transfer Integrals

As we have seen in Chapter 1, one of the most crucial factors of charge transfer (electron or hole) theoretical models is the electronic coupling, which is also referred to as the charge transfer integral. To calculate electronic couplings for our models (see Chapter 4) we used the DFT Kohn-Sham approach implemented in ADF program [17,19] and further exploited ADF's unique feature for calculating electronic couplings using the fragment approach.

In several charge transport theoretical models, the whole system is divided into fragments (e.g., D, B, A). In ADF transport computations [20-22], the total system can be split up into smaller interacting subsystems in which a charge (electron or hole) is localized on an individual fragment and can thus transfer from one fragment to another. The electron or hole orbital is approximated with a fragment molecular orbital. To compute the charge transfer coupling between initial and final electron (hole) fragment molecular orbitals, ADF builds a Hamiltonian

$$\hat{H} = \varepsilon_i |\phi_i\rangle\langle\phi_i| + \varepsilon_f |\phi_f\rangle\langle\phi_f| + V_{if}\left(|\phi_i\rangle\langle\phi_f| + |\phi_f\rangle\langle\phi_i|\right), \tag{3.55}$$

where $|\phi_i\rangle$, $|\phi_f\rangle$ denotes (initial and final) fragment molecular orbitals, ε_i (ε_f) is the energy of the orbital i (f), and V_{if} is the electronic coupling (also known as effective generalized transfer integral) between the orbitals.

This tight-binding model (eq. (3.55)) requires accurate values of site energies and electronic couplings. These parameters are calculated from the matrix elements of the molecular Kohn-Sham Hamiltonian in the basis of fragment orbitals (a unique feature of the ADF program that allows one to use molecular orbitals on individual molecules as a basis set in calculations on a system composed of two or more molecules [19,21,22]).

The electronic coupling (effective generalized transfer integral) between the fragment molecular orbitals is defined to be [21,22]

$$V_{if} = \frac{J_{if} - S_{if}\left(\varepsilon_i + \varepsilon_f\right)/2}{1 - S_{if}^2}. \tag{3.56}$$

$J_{if} = \left\langle \phi_i \middle| \hat{H}^{KS} \middle| \phi_f \right\rangle$ and $\varepsilon_{i/f} = \left\langle \phi_{i/f} \middle| \hat{H}^{KS} \middle| \phi_{i/f} \right\rangle$, where $\hat{H}^{KS}$ is the Kohn-Sham Hamiltonian. S_{if} are the spatial overlap integrals between fragment orbitals defined as $S_{if} = \left\langle \phi_i \middle| \phi_f \right\rangle$.

In ADF the fragment LUMO's are used for electron-transfer calculations and the corresponding fragment HOMO's are used for hole-transfer calculations [19,21,22].

3.8 Electron-Phonon Couplings

To calculate the electron-phonon coupling parameters of the effective models in Chapter 4 (also known as electron-vibrational coupling parameters) we used the ADF FCF module [23-25]. FCF denotes Franck-Condon factors, already introduced in Chapter 1. These are the squares of the overlap integrals of vibrational wave functions (e.g., eq. (1.32)), and they enter the formulas for the initial and final vibronic states.

ADF's FCF module, computes the Franck-Condon factors for the transition between a pair of electronic states and also computes all other parameters, which characterize the vibronic transition (such as reorganization energies and electron-phonon couplings). The specific module computes normal modes and normal-mode reorganization energies for electron and hole insertion at the DFT level, using geometry optimization for the neutral and the charged molecules.

When a molecule undergoes an electronic transition from an initial to a final electronic state, in addition to the change of the electronic state, the equilibrium positions of the nuclei also change, and the normal modes are modified and displaced. This phenomenon was first considered by Duschinsky and is abbreviated as the Duschinsky effect [26]. In the ADF FCF implementation the displacement of the nuclei in the normal modes is given by [19,24]

$$\vec{k} = \tilde{L}'^{T} \tilde{m}^{1/2} \left(\tilde{B}_0 \, \vec{x}_0 - \vec{x}_0' \right), \tag{3.57}$$

where $\vec{k}$ is the normal coordinate displacement vector. $\vec{k}$ gives the displacements between the initial and final state equilibrium geometries, in terms of initial state normal coordinates. $\tilde{L}$ is the normal coordinate mode matrix, which transforms the mass-weighted displacement coordinates into normal coordinates. $\tilde{m}$ is a matrix with the mass of the nuclei on the diagonal, $\tilde{B}_0$ is the zero-order axis-switching matrix and $\vec{x}_0$ and $\vec{x}_0'$ are equilibrium position vectors of the nuclei. The primed terms refer to the initial electronic state and the unprimed terms refer to the final electronic state. The equilibrium geometries of both states must be oriented with respect to each other around the center of mass in order to obtain maximum possible symmetry elements in common. To remove the six translational and rotational degrees of freedom ADF further rotates one of the states succeeding in that way maximum overlap between the states. This is implemented through the zero-order axis-switching $\tilde{B}_0$ [24].

If the displacement vector $\vec{k}$ eq. (3.57) is known, it is straightforward to further calculate the dimensionless electron-phonon couplings defined as [19]

$$\vec{\lambda}_{ADF} = \left(\frac{\vec{\Gamma}}{2}\right)^{1/2} \vec{k} \tag{3.58}$$

where $\vec{\Gamma} = \vec{\omega}/\hbar$ is the reduced frequencies vector [25].

The reorganization energy per mode i is given by

$$\lambda_i = \hbar\omega_i \left(\lambda_{ADF}^2\right)_i . \tag{3.59}$$

We extract the desirable electron-phonon couplings using ADF's FCF module, in order to incorporate them in the electron-vibrational Hamiltonian of eq. (1.28),

$$\hat{H}^{el-vi} = \left(|el\rangle\langle el|\right) \otimes \left[-\Delta F_{el}\, \hat{R}\right]. \tag{3.60}$$

ΔF_{el} is the force exerted by the electron on the normal-mode oscillator and $\hat{R}$ is the displacement of the normal-mode oscillator. Using a dimensionless displacement for the oscillator in eq. (3.60), i.e., $\hat{s} = \hat{R}/\sqrt{\hbar/2m\omega_i}$, the electron-vibrational coupling term becomes $\left(|el\rangle\langle el|\right) \otimes a_{el}\, \hat{s}$ where $a_{el} = -\Delta F_{el}\sqrt{\hbar/2m\omega_i}$. Combining now the reorganization energy definition of eq. (1.30), that is $\lambda_i = \Delta F_{el}^2 / 2m\omega_i^2$, with the reorganization energy as

obtained by the ADF's FCF module ((eq. (3.59)), leads to the definition of the electron-phonon coupling which is directly related to ADF's dimensionless electron-phonon coupling λ_{ADF}.

$$a_{el} = -\Delta F_{el}\sqrt{\frac{\hbar}{2m\omega_i}} = -\sqrt{\hbar\omega_i\,\lambda_i} = -\hbar\omega_i\left(\lambda_{ADF}\right)_i, \tag{3.61}$$

for a specific normal mode i.

3.9 References

[1] A. Szabo and N. S. Ostlund, Modern Quantum Chemistry, Dover, Mineola, NY, 1996.

[2] P. Atkins and R. Friedman, Molecular Quantum Mechanics, fifth edition, Oxford Univ. Press, New York, 2011.

[3] C. J. Cramer, Essentials of Computational Chemistry, Wiley, 2002.

[4] A. Hinchliffe, Molecular Modelling for Beginners, Wiley, 2003.

[5] J. C. Slater, Phys. Rev., 1951, 81, 385-390.

[6] C. C. J. Roothaan, Rev. Mod. Phys., 1951, 23, 69-89.

[7] J. B. Foresman, M. Head-Gordon, J. A. Pople, and M. J. Frisch, J. Phys. Chem., 1992, 96, 135.

[8] D. Maurice and M. Head-Gordon, Int. J. Quantum Chem. Symp., 1995, 29, 361.

[9] E. Fermi, Rend. Accad. Lincei, 1927, 602-607.

[10] L. H. Thomas, Math. Proc. of the Cambridge Phil. Soc., 1927, 23(5), 542-548.

[11] P. Hohenberg and W. Kohn, Phys. Rev., 1964, 136, B864- B871.

[12] W. Kohn and L. J. Sham, Phys. Rev., 1965, 140, A1133–A1138.

[13] E. Runge and E. K. U. Gross, Phys. Rev. Lett., 1984, 52 (12), 997–1000.

[14] M. Petersilka, U. J. Gossmann, and E. K. U. Gross, Phys. Rev. Lett., 1996, 76, 1212.

[15] C. A. Ullrich, Time-Dependent Density-Functional Theory: Concepts and Applications, Oxford Univ. Press, New York, 2012.

[16] M. A. L. Marques and E .K. U. Gross, Ann. Rev. Phys. Chem., 2004, 55, 427-455.

[17] G. T. Velde, F. M. Bickelhaupt, E. J. Baerends, C. F. Guerra, S. J. A. Van Gisbergen, J. G. Snijders and T. Ziegler, J. Comput. Chem., 2001, 9(22), 931–967.

[18] W. B. Person and G. Zerbi, Vibrational Intensities in Infrared and Raman Spectroscopy, Elsevier, 1982.

[19] ADF Manual, ADF Program System 2013.

[20] M.D. Newton, Chem. Rev., 1991, 91, 767.

[21] K. Senthilkumar, F. C. Grozema, F. M. Bickelhaupt, and L. D. A. Siebbeles, J. Chem. Phys., 2003, 119, 9809.

[22] K. Senthilkumar, F.C. Grozema and C. Fonseca Guerra, et al., J. Am. Chem. Soc., 2005, 127, 14894.

[23] J. S. Seldenthuis, H. S. J. van der Zant, M. A. Ratner and J. M. Thijssen, ACS Nano, 2008, 2(7), 1445–1451.

[24] G. M. Sando and K. G. Spears, J. Phys. Chem. A, 2001, 105, 5326–5333.

[25] P. T. Ruhoff and M. A. Ratner, Int. J. Quantum Chem., 2000, 77, 383–392.

[26] F. Duschinsky, Acta Physicochim. URSS, 1937, 7, 551.

Chapter 4: Vibrational Control of Electron Transfer Reactions

Molecular vibrations and electron-vibrational interactions are central to the control of biomolecular electron and energy-transfer rates. The vibrational control of molecular electron-transfer reactions by infrared pulses may enable the precise probing of electronic-vibrational interactions and of their roles in determining electron-transfer mechanisms. This type of electron-transfer rate control is advantageous because it does not alter the electronic state of the molecular electron-transfer system or irreversibly change its molecular structure. For bridge-mediated electron-transfer reactions, infrared (vibrational) excitation of the bridge linking the electron donor to the electron acceptor was suggested as being capable of influencing the electron-transfer rate by modulating the bridge-mediated donor-to-acceptor electronic coupling. This kind of electron-transfer experiment has been realized, demonstrating that bridge-mediated electron-transfer rates can be changed by exciting vibrational modes of the bridge. Here, we use simple models and ab initio computations to explore the physical constraints on one's ability to vibrationally perturb electron-transfer rates using infrared excitation. These constraints stem from the nature of molecular vibrational spectra, the strengths of the electron-vibrational coupling, and the interaction between molecular vibrations and infrared radiation. With these constraints in mind, we suggest parameter regimes and molecular architectures that may enhance the vibrational control of electron transfer for fast coherent electron-transfer reactions.

Biomolecular electron-transfer and energy-transfer reactions are central to bioenergetics and to cellular function [1-13]. Molecular motions are critical in determining the electron-transfer (ET) rates for long-distance biological electron-transfer reactions mediated by through-bridge tunneling. Such biomolecular ET systems have weak bridge-mediated electron-donor to electron-acceptor couplings (tunneling matrix elements), so their ET rates are nonadiabatic and relatively slow (time scales longer than ns). Low frequency molecular motions influence these nonadiabatic ET rates by modulating the donor-acceptor electronic energy gap and the donor-acceptor couplings.

Recently, it was recognized that biomolecular electron and energy-transfer reactions in the nearly-adiabatic or adiabatic regimes may also depend critically on bridge molecular motions that cause fluctuations in electronic site-energies and inter-site electronic couplings, or that serve as electronic energy sinks (e.g., ref. [14-16] and references

therein). In such transport systems, fast and partially coherent transport is possible over relatively large distances (greater than nm), often with high transport efficiency [16,17]. Questions that are of central interest in this strong coupling regime is how molecular motion tunes the transport mechanism and how the motion influences electronic coherences [15,16,18]. Similar questions apply to transport in molecular junction systems, e.g., ref. [19,20].

Recently, two-dimensional spectroscopy experiments provided evidence that vibrational (in addition to electronic) coherences may improve the efficiency of the primary charge separation events in photosynthesis (ref. [21,22] and references therein). A natural approach to probing the vibrational control of electron-transfer and energy-transfer rates experimentally is to identify vibrational modes that influence the transport rate and to perturb these modes selectively by IR-excitation [10,23-27]. Since these biomolecular transport systems often have complex electronic and vibrational spectra, it is productive to use simpler and smaller molecular model systems in both experiment and theory. Further, small molecules may be used as building blocks for transport devices whose transport rates and yields may be controlled by IR excitation.

Consider a donor (D) – bridge (B) – acceptor (A) molecule that undergoes photoinduced nonadiabatic electron transfer (ET) mediated by the electronic states of the intervening bridge [7-12]. Exciting the B vibrational modes before or after the electronic excitation could make it possible to control the D-A ET rate by modulating the B state energies and the D-B (A-B) electronic couplings [23-26]. This idea was initially discussed in the context of molecular architectures that offer parallel D-B-A tunneling pathways [23-25]. In systems where the bridge connecting D to A provides two different interfering electron tunneling pathways (i.e., involving different groups of atoms), the selective excitation of B vibrational modes localized in one pathway may lead to the exchange of the excess vibrational energy of the B modes with the tunneling electron. This energy exchange leaves an inelastic-tunneling marker of the route taken by the electron and thus "labels" the path of the electron. As such, one can built a molecular double slit experiment or a which-way interferometer based upon molecular ET [23-26].

Several challenges are faced in accomplishing the vibrational control of electron tunneling pathway interferences, as the interferences are sensitive to thermal structural fluctuations and to dephasing [10,25,28]. A more modest goal is to perturb the D-B-A ET rate by modulating the elastic bridge-mediated D-A tunneling interaction [9,10]. The first

experiment that performed this modulation was reported in ref. [27] using mid-IR pulses with UV-pump/mid-IR/VIS-probe spectroscopy. The ET system has an anthracene-derived acceptor connected to a dimethylaniline-containing donor linked by guanosine-cytidine (GC) hydrogen bonds. Mid-IR excitation was targeted to drive bridge G-C H-bond motion that influences the D-A coupling. The reported fractional changes in charge separation and recombination rates were approximately 60%. More recently, ET rate modulation by IR excitation was demonstrated in ref. [29] for an electronically excited covalent trans-acetylide platinum(II) D-B-A system. Excitation of the high-frequency bridge carbon-carbon triple-bond vibrations leads to the switching off of ET. In addition, ref. [30] reported IR-induced ET rate modulations of 28% in Re(I) D-A complexes. In spite of the theoretical [23-26] and recent experimental progress [29-36], it remains challenging to explain the rate modulations in these systems and to design structures that enable enhanced control of the ET rates by IR excitation.

ET rate control is an example of quantum transport driven by external fields [37,38]. The aims of this study are to further explore the feasibility of perturbing bridge-mediated ET rates by exciting selected B vibrations with infrared (IR) pulses and to suggest experimental observables and molecular architectures to enable the measurement of IR-induced ET rate perturbations. The advantage of using B vibrations (rather than D or A vibrations) to perturb bridge-mediated ET rates is derived from the possibility of manipulating ET pathways – and thus kinetics – selectively, without perturbing the donor and acceptor electronic states.

4.1 Kinetic Rate Models

What experimental observables can be used to probe the effects of IR excitation on the ET rate? What are that D-B-A rate-network architectures that enable effective control of ET rates by IR excitation? We first examine simple examples using simple kinetic rate models that suggest answers to these questions.

4.1.1 Populations *vs*. Yields in a single D single A molecular architecture

We consider a linear DBA system and a pump-probe experiment where a UV (VIS) pulse excites the D electronic state to initiate ET, and an IR pulse excites selected B vibrational

modes (Fig. 4.1). The final D and/or A state population is probed directly by UV (VIS) pulses. We assume that the D-to-A ET rate is much faster than the back rate (both with and without the IR pulse), and we ignore the back rate (this assumption does not change the generic conclusions, but it gives simple analytical expressions). In the absence of the IR pulse, the ET rate is k. The IR pulse changes k for a period of time (related to the width of the pulse and to the time scale of vibrational relaxation), i.e., $k \to k(t)$. The changes in this rate may be due to the quantum interference effects linked to the IR-pulse, to changes in the conformational energy landscape, or to other sources.

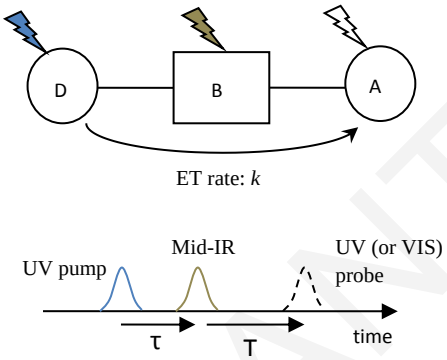

Figure 4.1: DBA ET where a UV (VIS) pulse excites the D electronic state initiating ET to the A state, and an IR pulse excites selected B vibrational modes. The final A state population is either probed by another UV (VIS) pulse or indirectly if A is involved in a chemical reaction whose rate is measurable.

In the absence of IR excitation, the rate equations are $dP_D(t)/dt = -kP_D(t)$ and $dP_A(t)/dt = kP_D(t)$, and the A state population is given by $P_A(t) = P_D(0)\left[1-\exp(-kt)\right]$ with $P_A(\infty) = P_D(0)$. With IR excitation, the rate is changed as $k \to k^{(IR)}(t) = k + \delta k^{(IR)}(t)$, where $\delta k^{(IR)}(t) = \delta k^{(IR)} \times f(t-t_0)$. $f(t-t_0)$ is a normalized function with width σ_t and $\delta k^{(IR)}$ is generally a small perturbation (assuming that the influence of the IR excitation on the molecule is nondestructive and reversible). The final A state population is given by $P_A(t) = P_D(0)\left\{1-\exp\left(-\int_0^t dt' k^{(IR)}(t')\right)\right\}$ with $P_A(\infty) = P_D(0)$. Thus, the pulse does not change the final A population. The population changes induced by IR excitation are transient and disappear at some time after the application of the pulse.

Figure 4.2 shows an example where the D electronic state participates in an irreversible chemical reaction that produces the product X, i.e., $dP_X(t)/dt = k_{D\to X} P_D(t)$. The infinite time yield of the product X is $Y_X(\infty) = k_{D\to X}\int_0^\infty dt\, P_D(t)$. We assume that $k_{D\to X} \ll k$ so that the time evolution of the D population is determined predominantly by ET to A. For $t >> t_0 + \sigma_t$, the D survival probability is $P_D^{(IR)}(t) \approx P_D(0)\exp\left(-\left(k+\delta k^{(IR)}\right)t\right)$. The fractional change in the $D\to X$ reaction yield upon application of the IR pulse is

$$I = \frac{Y_x^{(IR)}(\infty) - Y_x(\infty)}{Y_x(\infty)} = \frac{\int_0^\infty dt\left(P_D^{(IR)}(t) - P_D(t)\right)}{\int_0^\infty dt P_D(t)} \approx -\frac{\delta k^{(IR)}}{\left(k+\delta k^{(IR)}\right)} \approx -\frac{\delta k^{(IR)}}{k}. \qquad (4.1)$$

Therefore, we can measure time-dependent changes in the ET rates induced by application of an IR pulse by measuring the yield of a competing reaction from the photochemically prepared D state.

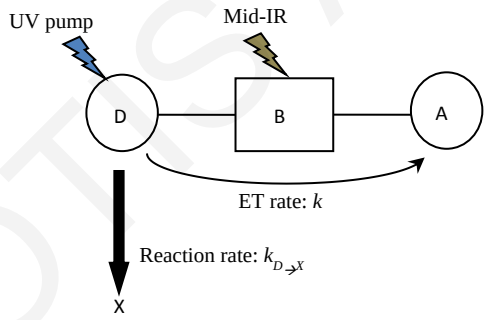

Figure 4.2: DBA ET where a UV (VIS) pulse excites the D electronic state that initiates ET to the A state, and an IR pulse excites selected B vibrational modes. The D state is involved in a competing chemical reaction that produces the product X. By measuring the fractional change upon IR excitation of the infinite time yield of this reaction it is possible to deduce the fractional change in the ET rate induced by IR (eq. (4.1)).

4.1.2 Populations *vs*. Yields in a single D multiple A molecular architecture

The above examples considered a linear DBA architecture. For more complex architectures, perturbations of the ET rates by finite IR pulses change both the long-time populations and yields. For example, consider a donor D connected to left and right B units

(B_L, B_R), each with independent A moieties (A_L, A_R), (Fig. 4.3). Photoinduced ET may proceed to A_L and to A_R with rates k_L and k_R, respectively. The rate equations are $dP_D(t)/dt = -(k_L + k_R)P_D(t)$, $dP_{A_L}(t)/dt = k_L P_D(t)$ and $dP_{A_R}(t)/dt = k_R P_D(t)$. Therefore,

$$\frac{P_{A_L}(\infty)}{P_{A_R}(\infty)} = \frac{k_L}{k_R}, \tag{4.2a}$$

$$\frac{P_{A_L}(\infty) - P_{A_R}(\infty)}{P_{A_L}(\infty) + P_{A_R}(\infty)} = \frac{k_L - k_R}{k_L + k_R}. \tag{4.2b}$$

For a symmetric system with $k_L = k_R = k$, (e.g., $B_L = B_R$ and $A_L = A_R$), selective excitation of IR vibrational modes on one of the B units, (e.g., B_L) may be accessible if isotopic substitutions are made to one of the units [23-25]. If D is prepared in its electronic excited state and B_L is excited by the IR pulse, then $k_L^{(IR)}(t) = k + \delta k^{(IR)}(t)$. The ratios in eq. (4.2) become

$$\frac{P_{A_L}^{(IR)}(\infty)}{P_{A_R}^{(IR)}(\infty)} \approx \frac{k + \delta k^{(IR)}}{k}, \tag{4.3a}$$

$$\frac{P_{A_L}^{(IR)}(\infty) - P_{A_R}^{(IR)}(\infty)}{P_{A_L}^{(IR)}(\infty) + P_{A_R}^{(IR)}(\infty)} \approx \frac{\delta k^{(IR)}}{2k} \tag{4.3b}$$

(assuming weak perturbation, $\delta k^{(IR)}(t) = \delta k^{(IR)} \times f(t - t_0)$). The asymmetry in the L/R A populations following the IR pulse (eq. (4.3b)) is a direct measure of $\delta k^{(IR)}$. Further, if A_L and A_R participate in separate reactions that produce the products X_L and X_R i.e., $dP_{X_{L(R)}}(t)/dt = k_{A_{L(R)} \to X_{L(R)}} P_{A_{L(R)}}(t)$, then

$$\frac{Y_{A_L}^{(IR)}(\infty)}{Y_{A_R}^{(IR)}(\infty)} \approx \frac{k + \delta k^{(IR)}}{k}, \tag{4.4a}$$

$$\frac{Y_{A_L}^{(IR)}(\infty) - Y_{A_R}^{(IR)}(\infty)}{Y_{A_L}^{(IR)}(\infty) + Y_{A_R}^{(IR)}(\infty)} \approx \frac{\delta k^{(IR)}}{2k}, \tag{4.4b}$$

assuming $k_{A_L \to X_L} \approx k_{A_R \to X_R} \gg k$.

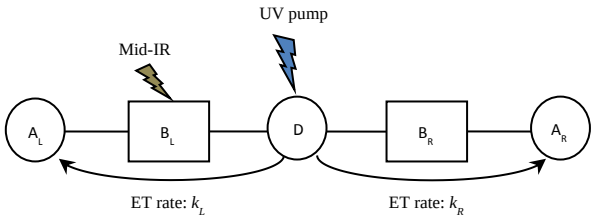

Figure 4.3: A D moiety is connected *via* left and right B units (B_L , B_R) to A moieties (A_L , A_R). Upon photo-excitation of D, irreversible ET is initiated simultaneously to A_L and to A_R (with ET rates k_L and k_R). For this system architecture, the IR excitation of one B unit can irreversibly affect the directionality of ET. In addition, the asymmetry in the infinite-time yield of the A_L and A_R can give a direct measure of the IR perturbation of the ET rate.

In summary, the influence of time-dependent IR perturbations on ET rates can be measured using time-independent observables (e.g., long-time populations and reaction yields) if secondary reactions compete with ET. ET systems with a single D and multiple A units (connected by independent links) are good candidates for directly measuring the influence of IR pulses on ET rates. Importantly, in such systems, pulsed-IR excitation can change the relative populations and yields of the charge-separated states, and may influence the directionality of ET without causing irreversible photochemical changes to the ET structures. The ability to change the yields of competing reactions using small external fields is familiar in the context of magnetic sensing by molecular and biomolecular compasses, where a weak external magnetic field affects the yield ratio of singlet and triplet reaction products produced by ET [39].

4.2 The IR perturbation of ET rates: low *vs*. high frequency ET-active vibrations

Now, we switch to a quantum mechanical (rather than a kinetic) formulation to study how molecular B vibrations perturb ET rates through their excitation. Given a candidate DBA molecule for vibrational control of the ET rate, the first step is to identify the B vibrations that influence ET by modulating the B electronic state energies and/or D-B (A-B) electronic couplings. These "ET-active" modes may be of low and/or high frequency. Since vibrational energy relaxation time scales are usually in the range of hundreds fs to a

few ps [40-42], there are different strategies to perturb bridge-mediated ET by IR excitation of bridge modes. These strategies depend on the time scale of ET and on the nature of the ET-active modes.

We first consider the case of high-frequency IR-active/ET-active bridge vibrational modes ($\hbar\omega >> K_B T$). Modes of this kind are targets for IR control of ET because they can be selectively excited and they remain in an excited state for a relatively long time, as they are not embedded in a mode continuum that produces very rapid intramolecular vibrational redistribution (IVR). If the ET timescale is of the order of the mode lifetime, then an experiment with ET triggering followed by IR excitation (Fig. 4.1) could modulate the ET rate "as the electron transfers" and possibly while the electronic motion is coherent.

4.3 Vibronic Hamiltonian Models

In previous studies [23-26], IR-modulation of ET was introduced in the context of simple quantum Hamiltonian models. Here, we use a more involved vibronic-state quantum-mechanical density matrix formulation that takes into account the effects of vibrational relaxation. Vibrational relaxation effects are critical since the de-excitation of the IR-vibrations that are selected for ET rate modulation influence the magnitude of the modulation. Further, in this study we aim to explore a realistic ET system and experimental parameter regimes that are likely to be optimal for the IR perturbation of ET (e.g., electronic structure, vibrational and electron-phonon coupling parameters, IR-molecule coupling and IR-pulse characteristics).

Our simple model D-B-A ET system (Fig. 4.1) incorporates vibrational relaxation and IR perturbation. The DBA system (S) Hamiltonian is

$$\hat{H}_S = \hat{H}_D + \hat{H}_B + \hat{H}_A + \hat{V}_{DB} + \hat{V}_{AB}, \tag{4.5}$$

where $\hat{H}_D$, $\hat{H}_B$ and $\hat{H}_A$ are vibronic D, B and A Hamiltonians and $\hat{V}_{DB}$ and $\hat{V}_{AB}$ are D-B and A-B electronic interaction Hamiltonians. Each of the D, B and A Hamiltonians are of the form

$$\hat{H}_K = \hat{H}_K^{el} + \hat{H}_K^{vi} + \hat{H}_K^{el-vi} \quad (K = D, B, A), \tag{4.6}$$

where "el" denotes electronic, "vi" vibrational and "el-vi" electronic-vibrational-couplings. $\hat{H}_K^{el}$ describe site energies for the relaxed D, B and A electron (or hole) states (the energies are denoted as E_D^0, E_B^0 and E_A^0, respectively). $\hat{H}_K^{vi}$ describe the high-frequency modes that are perturbed by ET and that may also be excited by IR. For $\hat{H}_K^{el-vi}$, we assume linear electron-vibrational coupling. The $\hat{V}_{DB}$ and $\hat{V}_{AB}$ Hamiltonians contain the D-B and A-B electronic couplings. We consider a system that is coupled to two high-frequency vibrational modes. The first oscillator (frequency ω_B) is perturbed when the electron occupies the B state and the second oscillator (frequency ω_A) is perturbed when the electron occupies the A state (Fig. 4.4a). For each of the oscillators, we denote the oscillator eigenstates in the absence of the electron-vibrational coupling as "unrelaxed" and use the symbol $|n^u\rangle$. With the electron-vibrational coupling turned on, we denote the oscillator eigenstates as "relaxed" and we use the symbol $|n^R\rangle$. In summary, the system electronic Hamiltonian is

$$\begin{aligned}\hat{H}^{el} &= E_D^0|D\rangle\langle D| + E_B^0|B\rangle\langle B| + E_A^0|A\rangle\langle A| \\ &+ V_{DB}^{el}\left(|D\rangle\langle B| + |B\rangle\langle D|\right) + V_{AB}^{el}\left(|B\rangle\langle A| + |A\rangle\langle B|\right).\end{aligned} \tag{4.7}$$

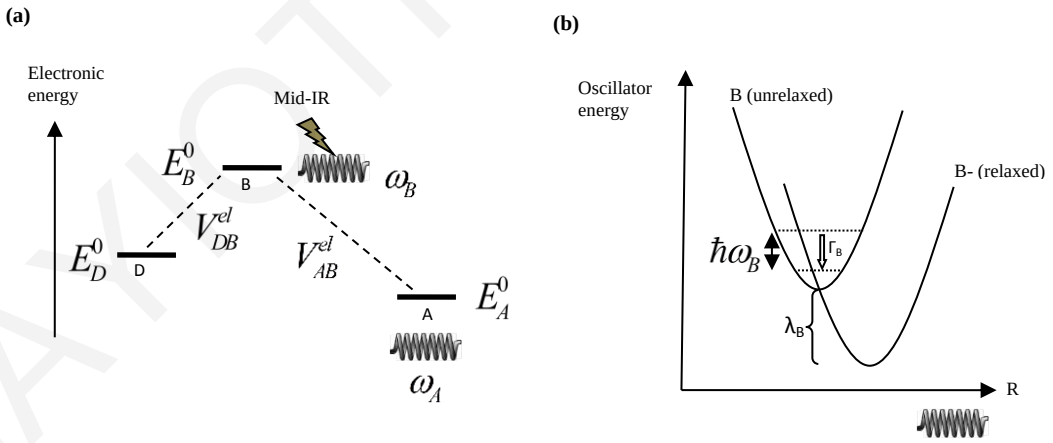

Figure 4.4: (a) Schematic diagram of the model system in eqs. (4.7)-(4.13). The system is comprised of a D, B and A electronic state and two oscillators, one coupled to the B state and the other to A state. (b) Diagram showing that the oscillator-electronic state coupling is linear. The oscillator state dynamics is dissipative with vibrational relaxation rates $\Gamma_{v\to v'}^{rel}$. In this work we focus on fast coherent ET, where the ET rate is of the order of the vibrational relaxation rates.

In the unrelaxed oscillator representation, the vibrational Hamiltonian is

$$\hat{H}^{vi} = \sum_{n_B^u} \hbar\omega_B \left(n_B^u + \frac{1}{2} \right) \left| n_B^u \right\rangle \left\langle n_B^u \right| + \sum_{n_A^u} \hbar\omega_A \left(n_A^u + \frac{1}{2} \right) \left| n_A^u \right\rangle \left\langle n_A^u \right|, \tag{4.8}$$

and the electron-vibrational interaction Hamiltonian is

$$\hat{H}^{el-vi} = \left(|B\rangle\langle B| \right) \otimes \left[-\Delta F_B \, \hat{R} \right] + \left(|A\rangle\langle A| \right) \otimes \left[-\Delta F_A \, \hat{R}' \right], \tag{4.9}$$

where $\hat{R}$ and $\hat{R}'$ are the displacements of the B and A oscillators and ΔF_B and ΔF_A are the forces exerted by the electron on the B and A oscillators. The vibronic states of the system are product states. For example, in the unrelaxed representation, $\left| el; vi, vi' \right\rangle = \left| el \right\rangle \left| n_B^u \right\rangle \left| n_A^u \right\rangle$, where $el = D$, B or A. Using dimensionless displacements for the oscillators in eq. (4.9), i.e., $\hat{s} = \hat{R} \big/ \sqrt{\hbar / 2m_B\omega_B}$, $\hat{s}' = \hat{R}' \big/ \sqrt{\hbar / 2m_A\omega_A}$, the electron-vibrational coupling terms are $\left(|B\rangle\langle B| \right) \otimes a_B \, \hat{s}$ and $\left(|A\rangle\langle A| \right) \otimes a_A \, \hat{s}'$, where $a_B = -\Delta F_B \sqrt{\hbar / 2m_B\omega_B}$ and $a_A = -\Delta F_A \sqrt{\hbar / 2m_A\omega_A}$ are in units of energy (Fig. 4.4b).

The interaction of the B oscillator with the IR field is described by the Hamiltonian

$$\hat{V}_{B,IR}(t) = -\frac{\partial \hat{\mu}_{B,IR}}{\partial R} \hat{R} \, E(t-\tau, \Omega_{IR}, \sigma_{IR}) = -\frac{\partial \hat{\mu}_{B,IR}}{\partial R} \hat{R} \, E_0 \, e^{-(t-\tau)^2 / 2\sigma_{IR}^2} \cos\left(\Omega_{IR} \, t \right), \tag{4.10}$$

where E_0 is the field intensity. $\hat{\mu}_{B,IR}$ is the vibronic dipole operator, and $E(t-\tau, \Omega_{IR}, \sigma_{IR})$ represents a Gaussian electric field pulse of frequency Ω_{IR} centered at time τ with width σ_{IR}. The IR frequency is assumed to be resonant with a vibrational transition of the B oscillator. Setting $\hat{s} = \hat{R} \big/ \sqrt{\hbar / 2m\omega}$ gives $\hat{V}_{B,IR}(t) = -a_{IR} \, e^{-(t-\tau)^2 / 2\sigma_{IR}^2} \cos\left(\Omega_{IR} \, t \right)$, where the IR field-to-mode coupling strength is $a_{IR} = E_0 \left(\partial \mu_{B,IR} / \partial R \right) \sqrt{\left(\hbar / 2m_B\omega_B \right)}$ (in units of energy).

The effect of vibrational energy transfer and relaxation of the two oscillators, due to interactions with the remaining vibrational degrees of freedom, are included in the dissipative relaxation terms. The time evolution of vibronic populations and coherences of the system is described by a stochastic Liouville equation for the system density matrix $\hat{\sigma}(t)$, given by

$$i\hbar\frac{d\hat{\sigma}(t)}{dt}=\hat{L}^{coh}(t)\hat{\sigma}(t)+\hat{L}^{diss}\hat{\sigma}(t), \tag{4.11}$$

where $\hat{L}^{coh}(t)\hat{\sigma}(t)=\left[\hat{H}_S+\hat{V}_{B,IR}(t),\hat{\sigma}(t)\right]$ is the coherent part and $\hat{L}^{diss}\hat{\sigma}(t)$ is the dissipative part, chosen to have the Lindblad form that preserves the total probability. The dissipative part contains decay rates $\Gamma^{rel}_{\nu\to\nu'}$ between vibrational states ν and ν' of the system modes, i.e.,

$$\hat{L}^{rel}\hat{\sigma}=i\hbar\sum_{\nu,\nu'}\hat{\mathcal{L}}^{rel}_{\nu\to\nu'}\hat{\sigma}\hat{\mathcal{L}}^{rel\,\dagger}_{\nu\to\nu'}-\frac{1}{2}\left(\hat{\mathcal{L}}^{rel\,\dagger}_{\nu\to\nu'}\hat{\mathcal{L}}^{rel}_{\nu\to\nu'}\hat{\sigma}+\hat{\sigma}\hat{\mathcal{L}}^{rel\,\dagger}_{\nu\to\nu'}\hat{\mathcal{L}}^{rel}_{\nu\to\nu'}\right), \tag{4.12}$$

where $\hat{\mathcal{L}}^{rel}_{\nu\to\nu'}=\sqrt{\Gamma^{rel}_{\nu\to\nu'}}\left|\nu'\right\rangle\left\langle\nu\right|$ (Fig. 4.4b). On the basis of vibronic states in the unrelaxed representation, eqs. (4.11) and (4.12) become

$$\begin{aligned}
i\hbar\frac{\partial\sigma_{el;n_i,n_i';el';n_j,n_j'}(t)}{\partial t}&=\left[\hat{H}_S+\hat{V}_{B,IR}(t),\hat{\sigma}(t)\right]_{el;n_i,n_i';el';n_j,n_j'}\\
&+i\hbar\Gamma^{rel}_{B}\left[\sqrt{n_i+1}\sqrt{n_j+1}\left\langle el;n_i+1,n_i'\right|\hat{\sigma}\left|el';n_j+1,n_j'\right\rangle-\frac{1}{2}\left(n_i+n_j\right)\left\langle el;n_i,n_i'\right|\hat{\sigma}\left|el';n_j,n_j'\right\rangle\right]\\
&+i\hbar\Gamma^{rel}_{A}\left[\sqrt{n_i'+1}\sqrt{n_j'+1}\left\langle el;n_i,n_i'+1\right|\hat{\sigma}\left|el';n_j,n_j'+1\right\rangle-\frac{1}{2}\left(n_i'+n_j'\right)\left\langle el;n_i,n_i'\right|\hat{\sigma}\left|el';n_j,n_j'\right\rangle\right],
\end{aligned} \tag{4.13}$$

where the $\Gamma^{rel}_{\nu\to\nu'}$ for $K=B,A$ are given by $\Gamma^{rel}_{n+1\to n}=(n+1)\Gamma^{rel}_{K}$ [43]. The above Liouville equation is solved with and without the intermediate IR excitation, since at time $t=0$ the electronic state is the donor D, and the high frequency oscillators vibrations are in their ground unrelaxed states. To connect with the observables in eqs. (4.1)-(4.4), we compute the time evolution of the D and A probabilities with and without the IR perturbation ($P_D(t)$, $P_D^{(IR)}(t)$ and $P_A(t)$, $P_A^{(IR)}(t)$, respectively).

To perform the necessary calculations we have developed an extensive numerical code (see Appendix) that solves the Liouville equation (eq. (4.13)). The code is written in MATLAB and its present form is optimized for speed and computational memory usage. Importantly, the code is readily expandable, and allows one to increase the number of electronic and vibrational states of the system. This gives us the flexibility to adjust the complexity of the D-B-A system model.

4.4 Parameter Search

Equations (4.7)-(4.13) contain a large number of parameters: the electronic energies and couplings (eq. (4.7)), the frequencies of the oscillators (eq. (4.8)), the electron-phonon coupling constants (eq. (4.9)), the molecule-IR pulse coupling (eq. (4.10)), and the vibrational decay rates (eq. (4.13)). This parameter space can be partially reduced because many of the parameters have restricted ranges for typical molecular structures.

In the following, we will often compare the electron-vibrational coupling energy, $a_K = -\Delta F_K \sqrt{\hbar/2m_K\omega_K}$ (K=B,A), to the vibrational energy level spacing $\hbar\omega_K$. In particular, $|a_K|/\hbar\omega_K = \sqrt{\lambda_K/\hbar\omega_K} = \sqrt{S_K}$ where λ_K is the reorganization energy for charging and S_K is the Huang-Rhys factor for the mode K [44] (Fig. 4.4b). For high-frequency modes, $|a_K|/\hbar\omega_K < 1$, for typical organic species (see below).

For the IR field-to-mode coupling strength, $a_{IR} = E_0\left(\partial\mu_{B,IR}/\partial R\right)\sqrt{\left(\hbar/2m_B\omega_B\right)}$, we vary the ratio $|a_{IR}|/\hbar\omega_B$, which is the ratio of the IR field-to-mode coupling strength to the energy-level spacing between vibrational levels of the mode involved in an IR-induced transition. We can partially constrain a_{IR} by using typical values of $\partial\mu_{B,IR}/\partial R$ for IR-active high-frequency normal modes of organic molecules.

Several parameters of the model are largely system dependent (the electronic site-energies and couplings in eq. (4.7) and the phonon and electron-phonon parameters in eqs. (4.8) and (4.9), respectively). These parameters determine the ET mechanism (e.g., deep tunneling, resonant tunneling, or thermally-activated hopping). However, their values must be such that the D-to-A ET timescale is of the order of or less than the lifetime of the excited ET-active IR-active mode, otherwise the excited mode energy will be lost before ET takes place. To associate the parameter exploration with ET systems that support fast ET, we consider the rigid D-B_n-A pi-stacked structures of Therien and co-workers [45] as an example. In these systems, the electron donor is a Zn porphyrin, the acceptor is a quinone, and the bridge is comprised of a variable number of phenyl rings connected by naphthalene pillars (Fig. 4.5a). These structures are chosen because the photo-induced D-to-A electron transfer time scale for the single-bridge structure (2a-Zn) and double-bridge structure (3a-Zn) are 600 fs and 3 ps, respectively [45] (of the order of typical lifetimes of high-frequency modes). Further, since we are seeking reversible effects of IR excitation, it is

natural to consider rigid systems with high frequency modes that, when excited, do not change the structure of the molecule irreversibly. This condition is also satisfied by the chosen molecular systems. Thus, we imagine introducing IR-active oscillators (e.g., CN groups) to the phenyl of the bridge (Fig. 4.5b) so that one may perform the experiment indicated in Fig. 4.1. We intend to use these CN-modified molecules to derive some of the parameters for the model indicated in eqs. (4.7)-(4.10).

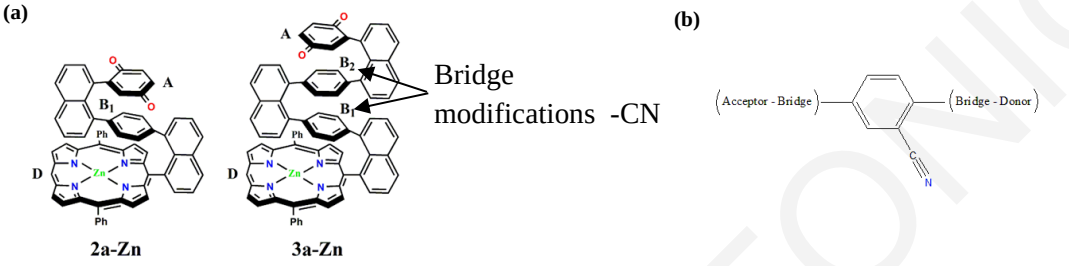

Figure 4.5: (a) The pi-stacked D-B-A systems that are used as a case study for photo-induced ET. The Zinc-porphyrin is the D, the B is comprised of phenyl rings connected by naphthalene units and the A is quinone [45]. Photo-induced ET rates are 600 fs for 2a-Zn and 3 ps for 3a-Zn. We envisaged adding IR active groups to the B units such as CN in order to probe for IR perturbed ET (e.g., as in Fig. 4.1). (b) A CN group substitution to the phenyl of the B.

We briefly describe the computation of model parameters for the CN-modified 2a-Zn system (denoted 2a-Zn-CN) in Fig. 4.5, using DFT implemented in the ADF program [46]. We used the GGA PBE functional with TZ2P basis sets and the frozen core approximation to obtain the energies of the virtual orbitals for the isolated D (porphyrin), B ((naphthalene-phenyl/CN)–naphthalene) and A (quinone) fragments of the 2a-Zn-CN molecule. We also used ADF's charge-transfer-integral module to compute the electronic couplings between the virtual orbitals. The energies obtained for the fragment LUMO orbitals and for the electronic couplings between them are shown in Fig. 4.6 (the fragment LUMO orbitals are shown in Fig. 4.7). For excited state ET, these LUMO orbitals represent D, and possible B and A orbitals for ET. Fig. 4.6 shows that in these pi-stacked systems, $V_{DB}^{el} \approx V_{AB}^{el} \approx 0.2eV$ and $V_{DB}^{el} / \Delta E_{DB} < 1$ ($V_{AB}^{el} / \Delta E_{AB} < 1$).

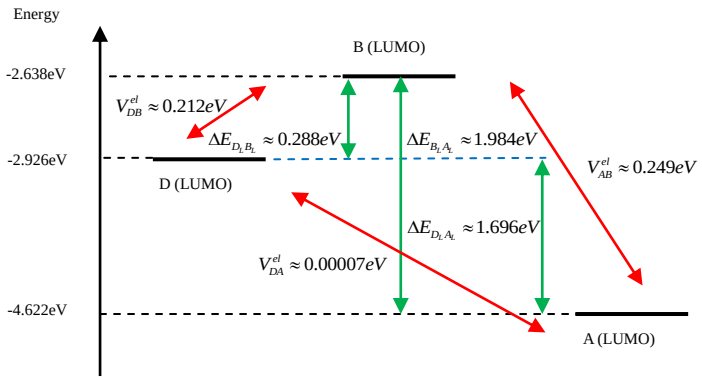

Figure 4.6: Energies of LUMO molecular orbitals of the D, B and A fragments of 2a-Zn-CN (Fig. 4.5). The red lines represent the charge transfer integrals between these states. All computations were performed using the ADF program [46].

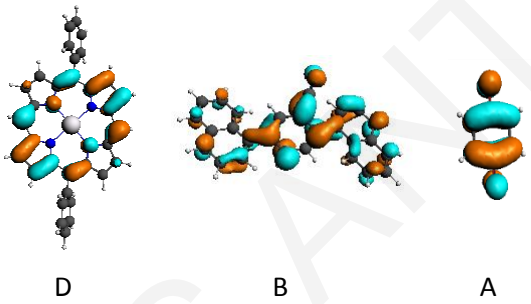

Figure 4.7: The LUMO orbitals of the isolated D, B and A fragments of the 2a-Zn-CN (Fig. 4.5). The B LUMO (middle) is delocalized over the phenyl ring and the connecting naphthalenes.

To make contact with the experiments in ref. [45], we also computed the 2a-Zn-CN molecule's absorption spectrum using TDDFT and compared to the experiment using ADF with the same methods as described above. The experimental absorption spectrum for 2a-Zn has a peak centered at $\sim 550nm$, and the excitation that initiates photo-induced ET is centered near this wavelength [45]. The ADF computed spectrum for 2a-Zn-CN contains a band at about $585nm$ and the corresponding excited states contains HOMO-1/HOMO to LUMO+1/LUMO+2 $\pi \to \pi^*$ excitations localized on the porphyrin subunit of 2a-Zn-CN. These $\pi \to \pi^*$ states resemble the corresponding excited states computed for the isolated porphyrin fragment (Fig. 4.7, left), and the π and π^* orbitals involved are very close to the HOMO-1/HOMO and LUMO/LUMO+1 orbitals of the fragment (LUMO and LUMO+1 are energetically very close). Further, the computed minimum energy HOMO to LUMO transition for 2a-Zn-CN involves a π orbital HOMO localized on the porphyrin D

subunit (very close to the HOMO of the isolated porphyrin fragment), and a LUMO that is localized on the quinone subunit and that approximates the LUMO of the isolated quinone fragment (Fig. 4.7 right). Therefore the D, and A orbitals and their energies for 2a-Zn-CN ET are well represented by the values computed for the isolated fragments shown in Fig. 4.6. The D state is energetically higher than the A state ($E_D^0 > E_A^0$ in Fig. 4.4), and the B electronic states present a tunneling barrier for ET.

The electron-phonon coupling parameters of our effective model (eq. (4.9)) depend on the delocalization of the bridge orbitals occupied by the electron during ET. Although the bridge LUMO shown in Fig. 4.7 is delocalized over the phenyl ring and the connecting naphthalenes, there are higher-energy bridge virtual orbitals that are more localized on the phenyl ring. To obtain representative values for the electron-phonon coupling parameters for bridge virtual orbitals with different extents of delocalization, we use the ADF FCF module [47-49]. The module computes normal modes and normal-mode reorganization energies for electron and hole insertion at the DFT level (using geometry optimization for the neutral and the charged molecules).

In our computations of bridge electron-phonon coupling parameters, we use either a bridge fragment that incorporates the central phenyl ring with a CN group and the naphthalene units, or a fragment with just the central phenyl ring with a CN group (all capped with hydrogens). The high frequency normal modes involving CN group vibrations are the same for both bridge fragments and partially delocalize on the phenyl near the CN bond. However, the lowest energy virtual orbital that is occupied by the electron in the anionic bridge fragment of the ADF computation (the LUMO of the fragment), has different localizations for the two bridge types. For the larger bridge structure, the LUMO is delocalized over the phenyl ring and the naphthalene units (as in Fig. 4.7). For the smallest bridge structure, the LUMO is localized on the phenyl ring (mimicking virtual orbitals of the phenyl ring – naphthalene bridge with energies higher than the LUMO bridge of Fig. 4.7). This methodology allows us to access a range of electron-phonon parameter values typical of electron insertion in delocalized and localized bridge virtual orbitals. We find that for a bridge virtual orbital delocalized over the phenyl and naphthalene rings (Fig. 4.7, middle), the highest $a_B/\hbar\omega_B$ ratio for a CN localized normal mode is $a_B/\hbar\omega_B \approx 10^{-2}$ (where $\hbar\omega_B \approx 0.28eV$, $a_B \approx 0.002eV$, $\lambda_B \approx 2\times10^{-5}eV$). For bridge virtual orbitals that are mostly localized on the phenyl ring, the highest $a_B/\hbar\omega_B$ ratio is $a_B/\hbar\omega_B \approx 0.4$ ($\hbar\omega_B \approx 0.28eV$, $a_B \approx 0.11eV$, $\lambda_B \approx 0.04eV$). We use this range of parameters in our model.

To obtain electron-phonon coupling parameters for the acceptor, we use the ADF FCF module using the A (quinone) fragment. We choose the quinone mode with the highest value of the $a_A/\hbar\omega_A$ ratio ($\hbar\omega_A \approx 0.2eV$, $a_A \approx 0.15eV$ and $\lambda_A = 0.11eV$).

The IR field-to-mode coupling strength $a_{IR} = E_0\left(\partial\mu_{B,IR}/\partial R\right)\sqrt{\left(\hbar/2m_B\omega_B\right)}$ (eq. (4.10)) depends on the electric field strength E_0. We consider a typical mid-IR pulsed laser with a repetition rate of $\sim 1KHz$, an energy per pulse of about $10\mu J$, a pulse duration of $\sigma_{IR} = 100$ fs and a pulse diameter of about $\sim 50\mu m$. From the power of one pulse and the pulse diameter, we can compute the intensity I of the laser beam and calculate E_0 (using $I = 0.5\varepsilon_0 cE_0^2$, where ε_0 is the electric permittivity of vacuum and c is the velocity of light). By relating $\partial\mu_{B,IR}/\partial R$ to the integrated absorption intensity A of the IR-exited mode, we find $a_{IR} = 1.464\times10^{-11}E_0\sqrt{A/\hbar\omega_B}$ (see Supplement), where a_{IR} and $\hbar\omega_B$ are in units of eV, E_0 is in units of V/cm and A in units of km/mole. Both A and ω_B are computed for the CN localized mode using ADF. The result is $|a_{IR}|/\hbar\omega_B \approx 3\times10^{-2}$, which is quite small, as expected for high frequency modes.

However, if we consider the case where the molecular structure is adsorbed and/or located in close proximity to rough metal surfaces, metal island films, or metal particles, the molecular IR absorption intensities may be significantly enhanced. This phenomenon of IR absorption enhancement is called "surface-enhanced infrared absorption" (SEIRA) (for reviews see ref. [50-52]), and the SEIRA absorption intensity is often expressed as $A_{SEIRA} = A \times f_{SEIRA}$, where $f_{SEIRA} = 10-1000$. Therefore, the SEIRA effect may allow greater flexibility upon varying the magnitude of a_{IR} in an experiment, $a_{IR} = 1.464\times10^{-11}E_0\sqrt{f_{SEIRA}A/\hbar\omega_B}$. We use a conservative value of $f_{SEIRA} \approx 40$ to bring a_{IR} up to magnitudes that could be accessible by SEIRA experiments. For high-frequency CN modes, this enhancement gives $|a_{IR}|/\hbar\omega_B \approx 0.2$. Since we are considering SEIRA experiments, we have to allow the possibility of fast vibrational relaxation of the IR-excited mode in the simulations. Therefore, we vary $1/\Gamma_B^{rel}$ from sub-ps (100 fs) to ps values.

To summarize, we have obtained a set of model parameter values for a class of DBA ET systems that perform fast (sub-ps to ps) photo-induced ET. These values will be used as a starting point in our numerical exploration of IR-perturbed ET. Using our model (eqs. (4.7)-(4.11)), we compute $P_K(t)$, $P_K^{(IR)}(t)$ (K=D,B,A), and the integrals $\int_0^T dt P_K(t)$ and $\int_0^T dt P_K^{(IR)}(t)$ (K=D,A) that are necessary for computing yields. The time T in the integrals is the time required for the IR-perturbed D, B, and A probabilities to return to their unperturbed values (this is always the case since the IR pulse is of finite width). In the examples shown in the figures, we report the fractional changes in D and A yields computed over finite times T,

$$I_D = \frac{\int_0^T dt\, P_D^{(IR)}(t) - \int_0^T dt\, P_D(t)}{\int_0^T dt\, P_D(t)}, \tag{4.14a}$$

$$I_A = \frac{\int_0^T dt\, P_A^{(IR)}(t) - \int_0^T dt\, P_A(t)}{\int_0^T dt\, P_A(t)}. \tag{4.14b}$$

The large values of I_K suggest that the IR perturbations of the ET rates can be observed *via* yield measurements of reactions that involve either D or A. The IR pulse is always applied during the ET event. We choose the initial state with electron on D and the oscillators in their unrelaxed ground states ($|D\rangle|0_B^u\rangle|0_A^u\rangle$). For the final state, the electron is transferred fully to A, the bridge oscillator is in an unrelaxed state, and the acceptor oscillator in a relaxed state ($|A\rangle|n_B^u\rangle|n_A^R\rangle$). In all computations we maintain initial state to final state resonance which ensures that the unperturbed (no IR) ET rate is ~ps timescale. Further, in eq. (4.10), the pulse width σ_{IR} is ~100 fs and $|a_{IR}|/\hbar\omega_B$ can vary between $3\text{x}10^{-2}$ and ~0.2 (the minimum value mimics a solution-phase experiment and the maximum value, a SEIRA experiment with ~40 times enhancement, see Supplement). $|a_B|/\hbar\omega_B$ can vary between ~10^{-2} and ~0.5 (delocalized *versus* localized bridge orbitals).

4.5 Results

Our simulations show that the effect of IR on the D, B and A probabilities and on the ET yields (eq. (4.14)) is negligible for the parameters derived for 2a-Zn-CN, even for high $|a_{IR}|$ values compatible with SEIRA experiments and for the largest $|a_B|$. This is because the B LUMO is off-resonant with the D LUMO, thus creating a high tunneling barrier for the electron as it transfers from D to A (Fig. 4.6). Therefore, the transferring electron does not occupy the bridge with high probability, and the IR excitation of the B oscillator (eq. (4.10)) cannot perturb ET even with very strong surface-enhanced fields. A design solution to produce stronger IR perturbations of ET is to change the D, B or A moieties so that the B LUMO energy lies between the D and A LUMO energies in order to obtain energetic resonance ($E_D^0 > E_B^0 > E_A^0$). In this case, the transferring electron may occupy the bridge with high probability. Several examples of this regime are discussed below.

Figure 4.8 shows the time evolution of the D, B and A probabilities with and without IR for the parameters derived from the computations on 2a-Zn-CN (Fig. 4.5 and 4.6) and with a large $|a_{IR}|/\hbar\omega_B \approx 0.2$. In the simulation we have set $E_D^0 > E_B^0 > E_A^0$ to mimic the regime of ET where the bridge electronic states can be occupied by the transferring electron with high probability. The vibrational relaxation time is 1 ps and $V^{el}/\hbar\Gamma_B^{rel} >> 1$ ($V_{DB}^{el}/\hbar\Gamma_B^{rel} \approx 333$ and $V_{AB}^{el}/\hbar\Gamma_B^{rel} \approx 338$). The effect of the IR pulse on the yields is 10-65% (Table 4.1). Therefore, if the B orbital energy is brought within the D-A energy gap, ($E_D^0 > E_B^0 > E_A^0$), the IR-perturbation of the D and A yields can be substantial. This energy shift can be achieved in our model compound by adding substituents to the porphyrin ring or to the bridge. For example, we performed ADF computations using the GGA PBE functional with TZ2P basis to confirm that the bridge LUMO energy can be tuned between the D and A LUMO energies by substituting electron-withdrawing groups (e.g., -NO_2, -CHO, -CN, -CF_3) on the phenyl ring. Similarly, the D LUMO can be lifted above the B LUMO by substituting electron-donating groups on the porphyrin (e.g., -NH_2, -CH_3, -OCH_3) [53].

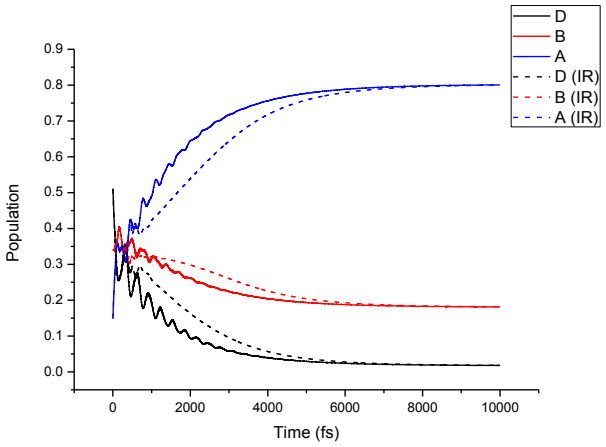

Figure 4.8: Time evolution of D, B and A probabilities with and without the IR pulse for the model in eqs. (4.7) and (4.8) using some of the parameters computed for the 2a-Zn-CN molecule (Figs. 4.5 and 4.6). The electronic Hamiltonian parameters are: $E_D^0 = 0eV$, $E_B^0 = -0.24eV$, $E_A^0 = -0.57eV$ and $V_{DB}^{el} = 0.233eV$, $V_{AB}^{el} = 0.237eV$. E_B^0 is brought to a value between E_D^0 and E_A^0 while maintaining initial-to-final vibronic state resonance. The vibrational and electronic-vibrational Hamiltonian parameters are: $\hbar\omega_B = 0.28eV$, $\hbar\omega_A = 0.2eV$, $a_B = 0.11eV$ and $a_A = 0.15eV$. The vibrational relaxation time scales are ps, $\hbar\Gamma_B^{rel} = \hbar\Gamma_A^{rel} = 0.0007eV$. For the IR-perturbation, $a_{IR} = 0.06eV$, $t_0 = 500$ fs and $\sigma_{IR} = 100$ fs. The effect of IR-excitation is significant, giving $I_D \approx 0.35$ and $I_A \approx 0.1$ (eq. (4.14) with $T = 6$ ps). Observe that in this system $V_{DB}^{el} / \hbar\Gamma_B^{rel} \approx 333$ and $V_{AB}^{el} / \hbar\Gamma_B^{rel} \approx 338$. Defining the ET time scale τ_{ET} to be approximately the time when the unperturbed acceptor probability passes through ~50% ($P_A \approx 0.5$), and $\tau_B^{rel} \approx 1/\Gamma_B^{rel}$, we have $\tau_B^{rel} \approx 1000$ fs and $\tau_{ET} \approx 1000$ fs.

t_0 (fs)	I_D	I_A
500	0.344	-0.077
700	0.399	-0.093
1000	0.462	-0.096
1500	0.549	-0.105
2000	0.604	-0.118
3000	0.654	-0.118
4000	0.668	-0.112
5000	0.671	-0.113

Table 4.1: D and A fractional yields (eq. (4.14)) as a function of IR pulse delay t_0 for the system of Fig. 4.8 (vibrational relaxation time of ps, $V^{el} / \hbar\Gamma_B^{rel} > 1$). The effect of the IR-pulse is larger for the D yield and it is maximized for the longer time delays.

To demonstrate the robustness of the above result to changes in system parameters, Figs. 4.9 and 4.10 show the same system as in Fig. 4.8 with a vibrational relaxation time of 1 ps, but with different values for the electronic couplings that lower the ratios of $V^{el}/\hbar\Gamma_B^{rel}$ while maintaining $V^{el}/\hbar\Gamma_B^{rel} > 1$. We see that the ET-perturbation effect is relatively robust to changes in V^{el} in the regime $V^{el}/\hbar\Gamma_B^{rel} > 1$, especially with respect to I_D. Further, if the electronic couplings are not symmetric ($V_{DB}^{el} \neq V_{AB}^{el}$) the IR-perturbation to the D yield can be enhanced by up to 40% for short IR-pulse delay times t_0 (Table 4.3).

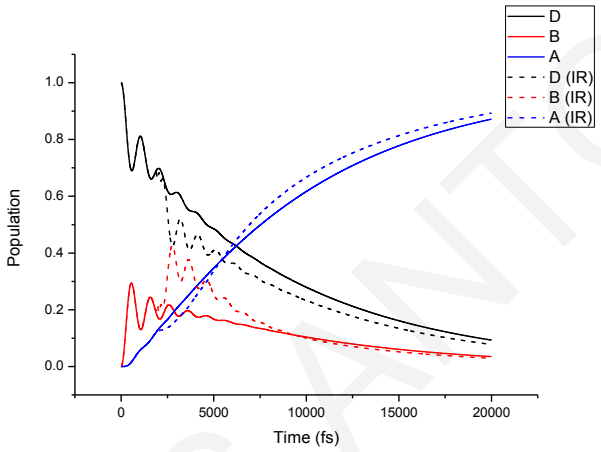

Figure 4.9: As in Fig. 4.8 but with weaker couplings ($V_{DB}^{el} = 0.003eV$, $V_{AB}^{el} = 0.002eV$), such that the ratios $V^{el}/\hbar\Gamma_B^{rel}$ are lowered ($V_{DB}^{el}/\hbar\Gamma_B^{rel} \approx 4$, $V_{AB}^{el}/\hbar\Gamma_B^{rel} \approx 3$). The pulse is applied at $t_0 = 2000$ fs, and the other parameters are the same as in Fig. 4.8. The effect of IR-excitation is not very different from Fig. 4.8 for the D fractional yield, $I_D \approx -0.13$, but it is reduced for the A fractional yield, $I_A \approx 0.04$. For this system $\tau_B^{rel} \approx 1000$ fs, and $\tau_{ET} \approx 7600$ fs.

t_0 (fs)	I_D	I_A
200	-0.147	0.045
2000	-0.130	0.040
4000	-0.098	0.025
6000	-0.073	0.015
8000	-0.053	0.008

Table 4.2: D and A fractional yields (eq. (4.14)) as a function of IR pulse delay t_0 for the system of Fig. 4.9 (vibrational relaxation time of ps, $V^{el}/\hbar\Gamma_B^{rel} > 1$). The effect of the IR-pulse is reduced compared to the case of Table 4.1.

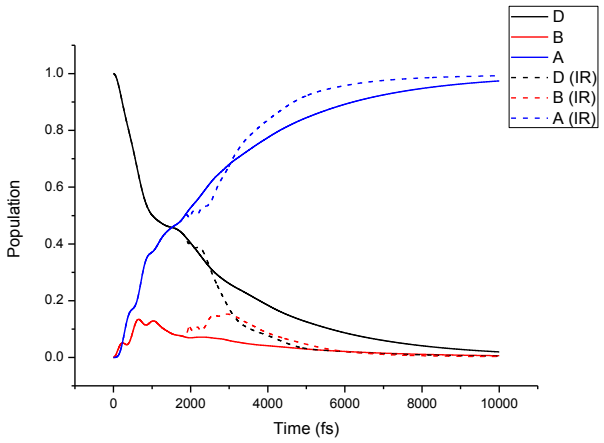

Figure 4.10: As in Fig. 4.9 but with very asymmetric inter-site coupling ($V_{DB}^{el} = 0.003eV$, $V_{AB}^{el} = 0.02eV$, $V_{DB}^{el} / \hbar\Gamma_B^{rel} \approx 4$, $V_{AB}^{el} / \hbar\Gamma_B^{rel} \approx 30$). The pulse is applied at $t_0 = 2000$ fs and the other parameters are the same as in Fig. 4.9. The effect of IR-excitation is comparable to Fig. 4.9, with $I_D \approx -0.21$ and $I_A \approx 0.04$. For this system $\tau_B^{rel} \approx 1000$ fs and $\tau_{ET} \approx 1870$ fs.

t_0 (fs)	I_D	I_A
200	-0.404	0.083
1000	-0.343	0.078
2000	-0.216	0.032
4000	-0.080	0.008

Table 4.3: D and A fractional yields (eq. (4.14)) as a function of IR pulse delay t_0 for the system of Fig. 4.10 (vibrational relaxation time of ps, $V^{el} / \hbar\Gamma_B^{rel} > 1$). The effect of the IR-pulse is larger for the D yield and it is maximized for the shorter time delays (35-40%).

Figure 4.11 shows the influence of faster-than-ps vibrational relaxation of the B oscillator ($1/\Gamma_B^{rel} = 164$ fs), keeping the other parameters of the system as in Fig. 4.8. In this case, the electronic couplings are symmetric and $V_{DB}^{el} / \hbar\Gamma_B^{rel} \approx 60$, $V_{AB}^{el} / \hbar\Gamma_B^{rel} \approx 60$. The effect of increasing the vibrational relaxation rate while keeping $V^{el} / \hbar\Gamma_B^{rel} > 1$ is to enhance the IR perturbation for the D yield to values close to 70% ($I_D \approx 0.7$, $I_A \approx -0.1$). This enhancement is robust with as the IR-pulse delay time changes (Table 4.4). Figure 4.12 shows the same system as in Fig. 4.11 where the A-B coupling is reduced to introduce a coupling asymmetry ($V_{DB}^{el} / \hbar\Gamma_B^{rel} \approx 60$ and $V_{AB}^{el} / \hbar\Gamma_B^{rel} \approx 5$). The asymmetry, as in the case

of Fig. 4.10 (Table 4.3), enhances the yields with $I_D \approx 0.93$ and $I_A \approx -0.19$. The IR perturbations are largely independent of the IR-pulse delay times (Table 4.5).

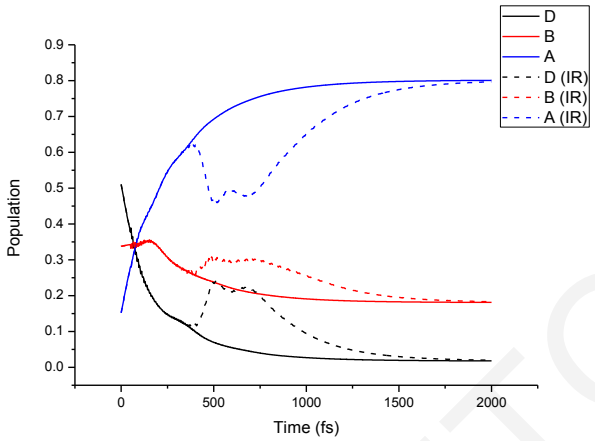

Figure 4.11: As in Fig. 4.8 but with faster vibrational relaxation time scales of 164 fs ($\hbar\Gamma_B^{rel} = \hbar\Gamma_A^{rel} = 0.004eV$), giving $V_{DB}^{el} / \hbar\Gamma_B^{rel} \approx 60$ and $V_{AB}^{el} / \hbar\Gamma_B^{rel} \approx 60$. The pulse is applied at $t_0 = 500$ fs and the other parameters are the same as in Fig. 4.8. The effect of IR-excitation on the D yield is large, $I_D \approx 0.7$ ($I_A \approx -0.1$). For this system $\tau_B^{rel} \approx 164$ fs and $\tau_{ET} \approx 207$ fs.

t_0 (fs)	I_D	I_A
200	0.598	-0.106
500	0.698	-0.112
700	0.739	-0.122
1000	0.751	-0.126

Table 4.4: D and A fractional yields (eq. (4.14)) as a function of IR pulse delay t_0 for the system of Fig. 4.11 where the vibrational relaxation time is reduced to 164 fs and $V^{el} / \hbar\Gamma_B^{rel} > 1$. The effect of the IR-pulse is enhanced for the D yield compared to the case of Table 4.3 and it remains relatively constant as a function of the delay time. The yield perturbation is of the order of 70 % for D and 10% for A.

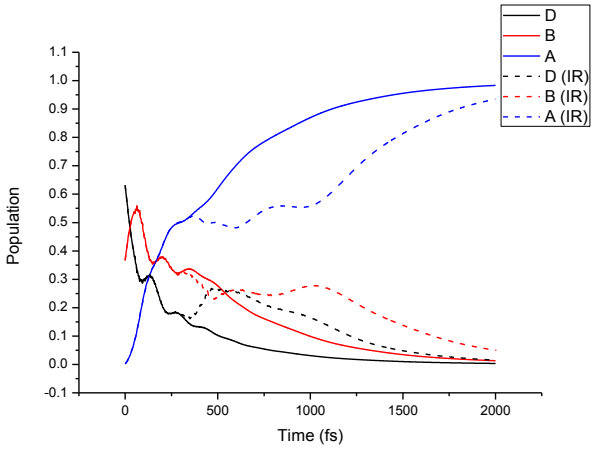

Figure 4.12: As in Fig. 4.11 (164 fs vibrational relaxation) with asymmetry in the electronic couplings giving $V_{DB}^{el}/\hbar\Gamma_B^{rel} \approx 60$ and $V_{AB}^{el}/\hbar\Gamma_B^{rel} \approx 5$. The pulse is applied at $t_0 = 500$ fs. For this system $\tau_B^{rel} \approx 164$ fs and $\tau_{ET} \approx 292$ fs and $I_D \approx 0.93$ and $I_A \approx -0.19$.

t_0 (fs)	I_D	I_A
200	0.954	-0.171
300	0.818	-0.150
500	0.931	-0.189
700	0.963	-0.216
1000	0.883	-0.206

Table 4.5: D and A fractional yields (eq. (4.14)) as a function of IR pulse delay t_0 for the system of Fig. 4.12 with unsymmetric electronic couplings and $V^{el}/\hbar\Gamma_B^{rel} > 1$ (vibrational relaxation time of 164 fs). The effects of the IR-pulse remain relatively constant as a function of the delay time. The yield perturbation is of the order of 100% for D and 20% for A.

In the above simulations, $V_{DB}^{el}/\hbar\Gamma_B^{rel}$ and $V_{AB}^{el}/\hbar\Gamma_B^{rel}$ are greater than unity. This is due to the relatively high coupling values (imposed by the pi-stacking DBA arrangements in the molecules used as an example), and the sub-ps to ps lifetime of the bridge CN vibrational mode excited by IR. If these ratios are reduced, the effect of the IR on the D and A yields is also reduced. In Fig. 4.13, we show the effect of reducing $V^{el}/\hbar\Gamma_B^{rel}$ to values less than 1 (the other parameters are the same, as in Figs. 4.11 and 4.12). The IR-perturbation to the ET yields drops to 10% and 4% for D and A, respectively (eq. (4.14)). Table 4.6 shows that the 10% perturbation persists for all time delays of the IR pulse.

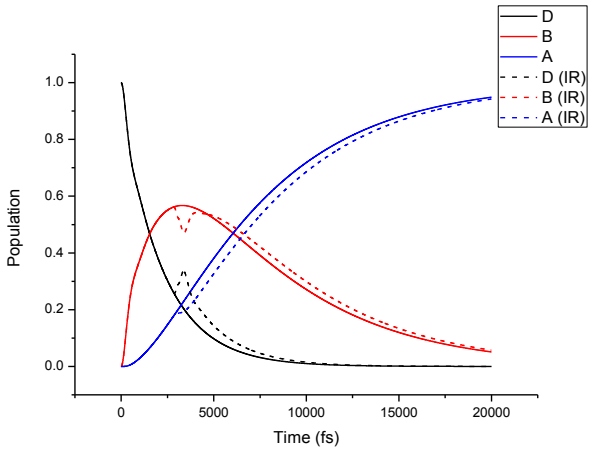

Figure 4.13: As in Figs. 4.11 and 4.12 (vibrational relaxation time scales of 164 fs), but with reduced couplings giving $V_{DB}^{el}/\hbar\Gamma_B^{rel} \approx 0.75$ and $V_{AB}^{el}/\hbar\Gamma_B^{rel} \approx 0.5$. The pulse is applied at $t_0 = 3000$ fs, and the other parameters are the same as in Fig. 4.12. The effect of IR-excitation is greatly diminished, $I_D \approx 0.1$ and $I_A \approx -0.04$ because the ratios $V^{el}/\hbar\Gamma_B^{rel}$ are below unity. For this system $\tau_B^{rel} \approx 164$ fs and $\tau_{ET} \approx 6326$ fs.

t_0 (fs)	I_D	I_A
200	-0.079	0.015
1000	-0.012	-0.037
3000	0.122	-0.039
5000	0.139	-0.038
6000	0.132	-0.035

Table 4.6: D and A fractional yields (eq. (4.14)) as a function of IR pulse delay t_0 for the system of Fig. 4.13 (vibrational relaxation time of 164 fs). The effects of the IR-pulse on the yields are reduced compared to Tables 4.4 and 4.5 because $V^{el}/\hbar\Gamma_B^{rel} < 1$.

A general trend is observed in Figs. 4.8-4.13 if we define the ET time scale τ_{ET} to be approximately the time when the unperturbed acceptor probability passes through ~50% ($P_A \approx 0.5$), and we compare this time to the vibrational relaxation time of the IR-perturbed B mode, $\tau_B^{rel} \approx 1/\Gamma_B^{rel}$. For Figs. 4.8 and 4.10-4.12, $\tau_B^{rel} \approx \tau_{ET}$ (the time scales of ET and vibrational relaxation are of the same order), and for Figs. 4.9 and 4.13, $\tau_B^{rel} < \tau_{ET}$ (the vibrational relaxation of the B mode is faster than ET). In Figs. 4.8 and 4.10-4.12 the application of the IR perturbation targeting the B mode leads to a significant

IR effect on the D, A populations and the yields ($I_D \sim 0.1-0.96$, $I_A \sim 0.01-0.22$). In contrast, in Figs. 4.9 and 4.13, the IR-perturbation effect is much smaller ($I_D \sim 0.01-0.15$, $I_A \sim 0.01-0.05$).

Our simulations indicate that IR perturbations of ET yields can be substantial if the electron-vibrational coupling is significant (up to the realistic value of $|a_B|/\hbar\omega_B \approx 0.5$) and if the transport mechanism is resonant through-bridge tunneling with $V^{el}/\hbar\Gamma_B^{rel} > 1$, provided that the IR-perturbation is strong (e.g., $|a_{IR}|/\hbar\omega_B \approx 0.2$). Such strong IR perturbation is readily achievable *via* SEIRA experiments. The $|a_B|/\hbar\omega_B$ ratio is never taken to be much greater than unity because this would give unrealistic electron-vibrational coupling constants a_B given that $\hbar\omega_B$ is always a few tenths of eV (as we are considering high frequency ET-active modes that lie above the mode continuum).

In summary, we have shown that in D-B-A systems where the ET mechanism is coherent resonant tunneling, the ET rate can be perturbed during electron transfer by IR excitation of a high-frequency B ET-active mode. The ET rate perturbation is enhanced if the ET system's D-B and A-B electronic couplings are sufficiently large such that the overall ET time is of the order of the vibrational relaxation time of the system's IR-perturbed mode. These conditions are valid for systems with realistic electron-vibrational coupling values ($|a_B|/\hbar\omega_B \leq 1$), and they can give up to 100% changes in the ET yields if the IR-pulse perturbation is strong, within the limits that can be achieved by SEIRA experiments.

4.6 IR perturbation of slow ET rates with low-frequency ET-active vibrations

The typical vibrational-relaxation and energy-redistribution times of excited vibrational modes in molecules are sub-ps to a few ps. Most bridge-mediated ET time scales are much longer than ps. In this regime of slow ET (slow with respect to vibrational relaxation), bridge ET-active modes (modulating B electronic state energies and/or D-B (A-B) electronic couplings) may have periods much longer than ps. Such "low frequency" ET-active modes lie deep in the mode continuum of the molecule and are very difficult to excite directly and selectively by IR. Even if these modes could be excited, they would be likely to lose their excess energy to the mode continuum on a very fast time scale (sub-ps). Therefore, to perturb the ET rate using the low-frequency ET-active modes, the latter must

serve as a sink of excess energy supplied to the system *via* other high-frequency modes that can be selectively excited by IR. ET must be initiated when the excess vibrational energy has reached the ET-active modes, such that the ET reaction will take place in a nonequilibrium ensemble of these modes. Further, the ET-active modes should be able to retain the excess energy for a sufficiently long time to sustain the nonequilibrium ET ensemble.

To illustrate this point, consider bridge-mediated ET where the ET mechanism is through-bridge elastic tunneling and the ET timescales are much longer than ps [1,2,11]. Often, the bridge-mediated D-A coupling is very sensitive to bridge vibrations [54,55], e.g., when the relevant electron-tunneling pathways contain through-space or hydrogen bond steps (i.e., soft vibrations) [9-12,56,57]. In this case, where access to a wide range of structures is possible and the time scale of interchange is rapid, the rate is given by $k_{D\to A} = (2\pi/\hbar)\langle T_{DA}^2\rangle_{eq}\,\rho_{FC}$, where ρ_{FC} is the Franck-Condon factor and $\langle T_{DA}^2\rangle_{eq}$ is the thermal equilibrium average of T_{DA}^2. Consider high-frequency IR-active modes that transfer excess energy to the ET-active modes that modulate T_{DA} (when the former are excited by IR) on a time scale of τ_{IVR} (Fig. 4.14a). If ET is initiated at a time τ_{IVR} after IR excitation, the ET rate is $k_{D\to A}^{(IR)} = (2\pi/\hbar)\langle T_{DA}^2\rangle_{neq}\,\rho_{FC}$, where $\langle T_{DA}^2\rangle_{neq}$ is an average over a nonequilibrium ensemble (with respect to the ET-active modes) which modulates the D-A coupling (Fig. 4.14b).

Therefore, the ET system must have vibrations that modulate ET pathways, and these vibrations must also be sinks for the excess energy supplied to the system by the excitation of high-frequency IR-active modes. It is thus essential to have computational tools that can identify the molecular electron tunneling pathways, the ET-active modes that modulate them, the IVR pathways that deactivate the ET-active modes, and the corresponding IVR timescales, τ_{IVR}. The computation of time-dependent tunneling pathways and $\langle T_{DA}^2\rangle_{eq}$ is quite familiar [10], but the computation of IVR pathways and IVR time scales remains a challenging task [40-42]. Combining electron tunneling and IVR pathway design in order to maximize $\langle T_{DA}^2\rangle_{neq}$ is possible in the context of classical nonequilibrium molecular dynamics simulations (that model the effect of IR excitation) coupled to electronic structure computations on DBA structures derived from the nonequilibrium ensemble (the subject of a future paper [58]).

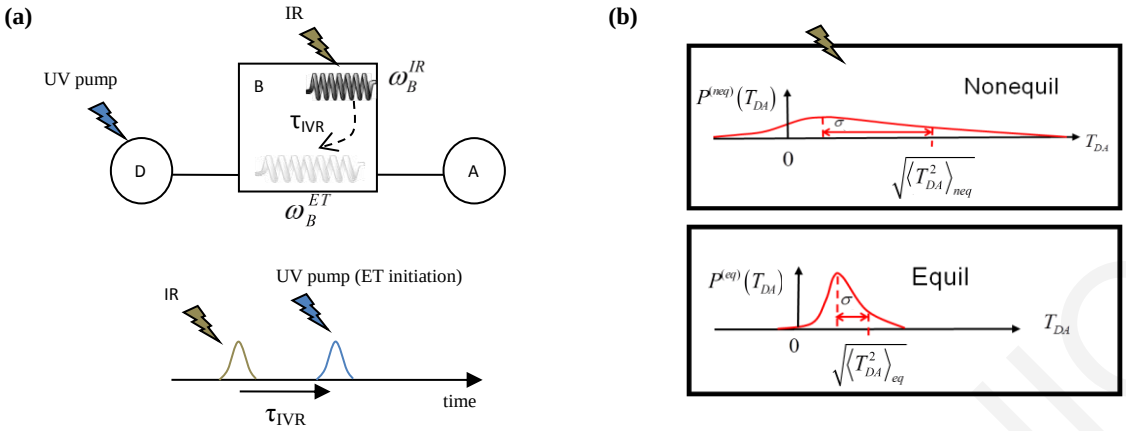

Figure 4.14: The nonadiabatic ET time scales are much slower than vibrational energy redistribution time scales. Due to the long distance between D and A, low-frequency bridge modes modulate the bridge-mediated D-A tunneling matrix element. Low frequency modes cannot be selectively excited by IR and lose their excitation energy very fast to the continuum. In this situation a design principle for perturbing the ET rate with IR is to use high-frequency IR-active modes that dump their energy to the low-frequency ET-active modes (a). If this energy transfer is of a time scale τ_{IVR}, the IR excitation must be applied at time τ_{IVR} prior to the UV (VIS) excitation that initiates ET. This strategy will create a nonequilibrium bridge structural ensemble and a corresponding non-equilibrium T_{DA} ensemble described by a probability density $P^{neq}\left(T_{DA}\right)$ (Fig. 4.14b, upper). If $P^{neq}\left(T_{DA}\right)$ is sufficiently different from the thermal (equilibrium) probability density $P^{eq}\left(T_{DA}\right)$ (Fig. 4.14b, lower), the nonadiabatic ET rate will change upon excitation with IR.

4.7 Conclusions

Previous theoretical studies of IR-pulse control of ET rates [23-26] motivated experiments on small D-B-A systems that demonstrate that ET rate modulation is possible by targeting specific bridge ET-active modes [27,29]. These experiments showed different levels of IR-induced modulation and the challenges now are to understand the parameter regimes that enhance the magnitude of the effect and to suggest ET systems and experimental designs that optimize ET rate control. Another central challenge is to understand the influence of vibrational energy redistribution (and dephasing) that is likely to decrease the influence of vibrational excitation of ET-active modes on ET rates and yields. To this end, we have explored the feasibility of perturbing bridge-mediated ET by exciting ET-active bridge

vibrations with a single IR pulse using a density matrix (Lindblad-type) model that takes into account vibrational relaxation. We also presented experimental observables, pulse sequences and molecular architectures that may enable measurement of IR-pulse perturbations to bridge-mediated ET rates. The suggested molecular architectures may also allow control of ET pathways in D-B-A systems *via* selective IR excitations of bridge modes.

In this work, we explored two scenarios for IR control, one for slow nonadiabatic ET rates (slower than vibrational relaxation times) and the other for fast ET rates (of the order of vibrational relaxation times). The main focus of our study was the fast ET rate regime (~ps) where the aim was to perturb ET "as the electron transfers" by directly exciting an IR-active ET-active bridge mode with a subpsec period and a frequency above the mode continuum. In this fast ET regime, vibronic coherences are likely to influence ET as long as the solvent environment does not destroy such coherences on time scales faster than the ET time scale. The IR perturbation changes the ET rate by directly affecting these coherences.

We find that two important generic conditions need to be satisfied to have a measurable IR-perturbing effect on the ET rate "as the electron transfers". First, the B electronic state must be occupied with substantial probability during ET. Since the IR pulse weakly perturbs the bridge oscillator, and the bridge oscillator interacts with the occupied B electronic state, the state should have large occupation during ET in order to perturb ET sufficiently with IR. This means that the B state cannot create a very deep tunneling barrier for the transferring electron. The second condition relates to the competition between vibrational relaxation and ET. If the timescale of ET into B (from D) and out of B (to A) is slower than typical vibrational relaxation times of the B oscillator excited state, effects of the IR pulse on ET as the electron transfers will be diminished. By the time ET to (and from) the bridge takes place, the IR-excited oscillator will have relaxed to the ground state and the IR pulse will not influence ET.

This timescale-competition condition can be roughly described as follows: if the D-B system is isolated by turning off the B-A electronic coupling then the D-to-B ET timescale should be comparable to or shorter than the B oscillator vibrational relaxation timescale. The same should hold for the B-to-A ET time scale if the B-A system is isolated by turning off the D-B electronic coupling. It must be emphasized that in this work we are not analyzing a simple activation (heating) effect of the IR pulse. That is, if B vibrational

relaxation is fast and it takes place before ET from B-to-A, then IR excitation of B after vibrational relaxation could activate ET to A. The regime studied here is different; it is the IR-pulse perturbation (disturbance) of coherent ET prior to or during vibrational relaxation.

For typical and moderate bridge electron-vibrational couplings, the IR-perturbation effect is substantial only for relatively strong IR fields that are accessible *via* surface enhanced infrared absorption settings. An alternative to surface enhanced IR for augmenting the vibrational excitation of the bridge (albeit less specifically) is to attach heat source molecules to the bridge [59]. These molecules (e.g., azobenzene) undergo rapid internal conversion when excited electronically, damping the excess electronic energy to neighboring vibrations.

For the slow ET rate regime modulated by low-frequency ET-active bridge modes, IR-excitation of high frequency bridge modes should be designed to change the thermal ET ensemble to a nonequilibrium ensemble of the ET-active modes. This is possible only if the ET-active modes serve as a sink for the excess vibrational energy supplied by the IR-pulse. Alternatively it is interesting to explore whether THz pulses that directly excite the low frequency ET active modes can be used to perturb ET. Designing ET systems with such characteristics requires realistic simulations of IVR pathways coupled to ET pathways, and such simulation protocols are the subject of a follow up paper.

4.8 Supplement

An ultrafast pulsed laser periodically emits pulses of energy, with a specific repetition rate [60] (Fig. 4.15). Typical mid-IR pulses of interest can be generated with a repetition rate of $\sim 1KHz$ (a pulse every $1ms$, Fig. 4.15), with energy per pulse of about $1-10\mu J$ and pulse duration $\sigma_{IR} = 100\,\text{fs}$ and with pulse diameter of about $\sim 50\mu m$. In the D-B-A systems under study the ET time scale is of order ps. After ET initiation, and within a ps time interval, we assume that one IR pulse can be applied, centered at t_0 (where $t_0 = \tau$ in eq. (4.10)). In order to calculate the power of one pulse, we divide the generated pulse energy with the pulse duration, which is described by its width σ_{IR}. From the power of one pulse and the pulse diameter we can compute the intensity I of the laser beam (power per unit area). The intensity is then set equal to $I = 0.5\varepsilon_0 c E_0^2$, where ε_0 is the electric permittivity of vacuum, c the velocity of light and E_0 is an average of the electric field strength. Using

this latter equation and the previously computed value of I we can derive a value for E_0 in units V/cm that corresponds to the pulse characteristics.

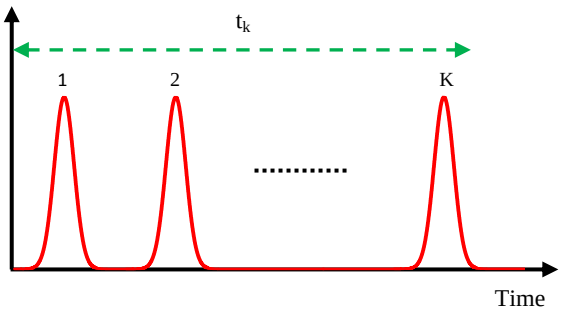

Figure 4.15: Representation of the generated pulses. K : number of pulses in the time interval t_k .

If we assume Beer's law ($I = I_0 e^{-aC\ell}$), the integrated absorption intensity of an infrared transition is defined as [61]

$$A = \int_{band} a(\nu)\, d\nu = \frac{1}{C\ell} \int_{band} \ln\left(\frac{I_0}{I}\right) d\nu \tag{4.15}$$

where I_0 is the intensity of radiation incident on the sample at wavenumber ν, I is the transmitted intensity, a is the absorptivity, C is the sample concentration and ℓ the path length. The range of integration is over a spectral region of interest.

The integrated absorption intensity of the ith fundamental vibrational band, A_i in $km/mole$, is related to the dipole moment derivative with respect to the ith mass-weighted normal mode coordinate, Q_i by [46,61,62]

$$A_i = \frac{1}{4\pi\varepsilon_0} \frac{N_A \pi g_i}{3c^2} \left(\frac{\partial \mu_{IR}}{\partial Q_i}\right)^2 \tag{4.16}$$

where N_A, c and g_i are Avogadro's number, the velocity of light and the degeneracy of the ith band, respectively, and $4\pi\varepsilon_0$ permits use of SI units.

In our models we defined the IR pulse perturbation as (eq. (4.10)) $a_{IR} = E_0 \left|\partial\mu_{B,IR}/\partial R\right| \sqrt{(\hbar/2m_B\omega_B)}$. Using eq. (4.16) where $Q_i = \sqrt{m_B} R$ to solve for $\left|\partial\mu_{B,IR}/\partial Q_i\right|$, and substituting into a_{IR}, gives

$$a_{IR} = 1.464\times10^{-11} E_0 \sqrt{A_i / \hbar\omega_B} \tag{4.17}$$

in units of eV.

We use this equation to compute a_{IR} with the value of E_0 as derived from the pulse characteristics above, and with A_i and $\hbar\omega_B$ values computed for the CN normal mode of interest using the ADF normal mode module. This gives the lowest limit of $a_{IR} / \hbar\omega_B \approx 3\times10^{-2}$.

To obtain upper limits for $a_{IR} / \hbar\omega_B$ we consider the surface enhancement infrared absorption (SEIRA) effect. This effect is described by introducing an enhancement factor for the molecule's specific absorption intensity ($A_i^{SEIRA} = A_i f_{SEIRA}$), where $f_{SEIRA} \approx 10-1000$. Therefore, taking into account the SEIRA effect,

$$a_{IR} = 1.464\times10^{-11} E_0 \sqrt{(f_{SEIRA} \times A_i) / \hbar\omega_B} \tag{4.18}$$

where a_{IR} and $\hbar\omega_B$ are in units of eV, E_0 is in units of V/cm and A_i in units of km/mole. We use $f_{SEIRA} \approx 40$ (a conservative value) to obtain the upper limit of $a_{IR} / \hbar\omega_B \approx 0.2$.

4.9 References

[1] R. A. Marcus and N. Sutin, Biochim. Biophys. Acta, 1985, 811, 265–322.

[2] J. R. Winkler and H. B. Gray, Biochim. Biophys. Acta, 2010, 1797, 1563–1572.

[3] J. Jortner and M. Bixon, Electron Transfer: From Isolated Molecules to Biomolecules, Adv. Chem. Phys. Ser., Wiley Intersci, New York, 1999, vols. 106–107.

[4] V. Balzani, P. Piotrowiak, M. A. J. Rodgers, J. Mattay and D. Astruc, et al., Electron Transfer in Chemistry, Wiley-VCH, Weinheim, vol. IV, 2001.

[5] A. Nitzan, Chemical Dynamics in Condensed Phases, Oxford Univ. Press, Oxford, 2006.

[6] V. May and O. Kuhn, Charge and Energy Transfer Dynamics in Molecular Systems, Wiley-VCH, Berlin, 2000.

[7] D. N. Beratan and S. S. Skourtis, Curr. Opin. Chem. Biol., 1998, 2, 235–243.

[8] S. S. Skourtis and D. N. Beratan, Adv. Chem. Phys., 1999, 106, 377–452.

[9] S. S. Skourtis, J. Lin and D. N. Beratan, in Modern Methods for Theoretical Physical Chemistry of Biopolymers, ed. E. B. Starikov, J. P. Lewis and S. Tanaka, Elsevier, Boston, MA, 2006.

[10] D. N. Beratan, S. S. Skourtis, I. A. Balabin and A. Balaeff, et al., Acc. Chem. Res., 2009, 42, 1669–1678.

[11] S. S. Skourtis, D. H. Waldeck and D. N. Beratan, Annu. Rev. Phys. Chem., 2010, 61, 461–485.

[12] S. S. Skourtis, Biopolymers, 2012, 100, 82–92.

[13] D. N. Beratan, C. Liu, A. Migliore, N. F. Polizzi, S. S. Skourtis, P. Zhang and Y. Zhang, Acc. Chem. Res., 2015, 48, 474–481.

[14] Y. Zhang, C. Liu, A. Balaeff, S. S. Skourtis and D. N. Beratan, Proc. Natl. Acad. Sci. U. S. A., 2014, 111(28), 10049–10054.

[15] F. Fassiolo, R. Dinshaw, P. C. Arpin and G. D. Scholes, J. R. Soc., Interface, 2013, 11, 20130901.

[16] M. Mohseni, Y. Omar, G. Engel and M. Plenio, Quantum Effects in Biology, Cambridge University Press, 2014.

[17] I. Gideon, G. I. Livshits, A. Stern and D. Rotem, et al., Nat. Nanotechnol., 2014, 9, 1040 1046.

[18] A. de la Lande, J. Rezac, B. Levy, B. C. Sanders and D. R. Salahub, J. Am. Chem. Soc., 2011, 133(11), 3883–3894.

[19] R. Volkovich, R. Härtle, M. Thoss and U. Peskin, Phys. Chem. Chem. Phys., 2011, 13, 14333–14349.

[20] J. C. Cuevas and E. Sheer, Molecular Electronics: An Introduction to Theory and Experiment, World Scientific Publishing, 2010.

[21] E. Romero, R. Augulis, V. I. Novoderezhkin, M. Ferretti, J. Thieme, D. Zigmantas and R. van Grondelle, Nat. Phys., 2014, 10, 676–682.

[22] F. D. Fuller, J. Pan, A. Gelzinis, V. Butkus, S. Seckin Senlik, D. E. Wilcox, C. F. Yocum, L. Valkunas, D. Abramavicius and J. P. Ogilvie, Nat. Chem., 2014, 6, 706–711.

[23] S. S. Skourtis, D. H. Waldeck and D. N. Beratan, J. Phys. Chem. B, 2004, 108, 15511–15518.

[24] S. S. Skourtis and D. N. Beratan, AIP Conf. Proc., 2007, 963, 809–812.

[25] D. Xiao, S. S. Skourtis, I. V. Rubtsov and D. N. Beratan, Nano Lett., 2009, 9, 1818–1823.
[26] H. Carias, D. N. Beratan and S. S. Skourtis, J. Phys. Chem. B, 2011, 115, 5510–5518.
[27] Z. Lin, C. M. Lawrence, D. Xiao and V. V. Kireev, et al., J. Am. Chem. Soc., 2009, 131, 18060–18062.
[28] R. A. Goldsmith, M. R. Wasielewski and M. A. Ratner, J. Phys. Chem., 2006, 110, 20258-20262.
[29] M. Delor, P. A. Scattergood, I. V. Sazanovich, A. W. Parker, G. M. Greetham, A. J. H. M. Meijer, M. Towrie and J. A. Weinstein, Science, 2014, 346(6216), 1492–1495.
[30] Y. Yue, T. Grusenmeyer, Z. Ma, P. Zhang, R. H. Schmehl, D. N. Beratan and I. V. Rubtsov, Dalton Trans., 2015, DOI: 10.1039/C4DT02145B.
[31] M. Fedoseeva, M. Delor, S. C. Parker, I. V. Sazanovich, M. Towrie, A. W. Parker and J. A. Weinstein, Phys. Chem. Chem. Phys., 2015, 17, 1688–1696.
[32] M. Delor, I. V. Sazanovich, M. Towrie, S. J. Spall, T. Keane, A. J. Blake, C. Wilson, A. J. Meijer and J. A. Weinstein, J. Phys. Chem. B, 2014, 118, 11781–11791.
[33] M. Delor, I. V. Sazanovich, M. Towrie and J. A. Weinstein, Acc. Chem. Res., 2015, DOI: 10.1021/ar500420c.
[34] A. Vlcek, Jr., H. Kvapilova, M. Towrie and S. Zalis, Acc. Chem. Res., 2015, 48, 868–876.
[35] T. A. A. Oliver, N. H. C. Lewis and G. R. Fleming, Proc. Natl. Acad. Sci. U. S. A., 2014, 111, 10061–10066.
[36] J. L. Miller, Phys. Today, 2015, 68, 10–11.
[37] D. G. Evans, R. D. Coalson and Y. J. Dakhnovski, Chem. Phys., 1996, 104, 2287–2296.
[38] S. Kohler, J. Lehmann and P. Hanggi, Phys. Rep., 2005, 406, 379–443.
[39] I. A. Solov'yov, T. Ritz, K. Schulten and P. J. Hore, in Quantum effects in biology, ed. M. Mohseni, Y. Omar, G. Engel and M. Plenio, Cambridge University Press, 2014.
[40] H. Fujisaki and J. E. Straub, Proc. Natl. Acad. Sci. U. S. A., 2005, 102, 6726–6731.
[41] G. Stock, Phys. Rev. Lett., 2009, 102, 118301.
[42] D. M. Leiner, Annu. Rev. Phys. Chem., 2008, 59, 233–259.
[43] G. Li, B. Movaghar, A. Nitzan and M. A. Ratner, J. Chem. Phys., 2013, 138, 044112.
[44] P. F. Barbara, T. J. Meyer and M. A. Ratner, J. Phys. Chem., 1996, 100, 13148–13168.
[45] Y. K. Kang, P. M. Iovine and M. J. Therien, Coord. Chem. Rev., 2011, 255, 804–824.

[46] G. T. Velde, F. M. Bickelhaupt, E. J. Baerends, C. F. Guerra, S. J. A. Van Gisbergen, J. G. Snijders and T. Ziegler, J. Comput. Chem., 2001, 9(22), 931–967.

[47] J. S. Seldenthuis, H. S. J. van der Zant, M. A. Ratner and J. M. Thijssen, ACS Nano, 2008, 2(7), 1445–1451.

[48] G. M. Sando and K. G. Spears, J. Phys. Chem. A, 2001, 105, 5326–5333.

[49] P. T. Ruhoff and M. A. Ratner, Int. J. Quantum Chem., 2000, 77, 383–392.

[50] M. Osawa, in Near-Field Optics and Surface Plasmon Polaritons, ed. S. Kawata, Top. Appl. Phys.,Springer-Verlag Berlin Heidelberg, 2001, vol. 81, pp.163–187.

[51] F. Siebert and P. Hildebrandt, Vibrational Spectroscopy in Life Science, Wiley-VCH, 2008.

[52] R. Aroca, Surface-Enhanced Vibrational Spectroscopy,Wiley, 2006.

[53] W. A. Goddard, D. W. Brenner, S. E. Lyshevski and G. J. Iafrate, Handbook of Nanoscience, Engineering, and Technology, CRC Press, 2003.

[54] S. S. Skourtis, Q. Xie and G. Archontis, J. Chem. Phys., 2001, 115, 9444–9462.

[55] A. Teklos and S. S. Skourtis, Chem. Phys., 2005, 319, 52–68.

[56] S. S. Skourtis, I. A. Balabin, T. Kawatsu and D. N. Beratan, Proc. Natl. Acad. Sci. U. S. A., 2005, 102, 3552–3557.

[57] I. A. Balabin, D. N. Beratan and S. S. Skourtis, Phys. Rev. Lett., 2008, 101, 158102.

[58] Z. Ma, P. Antoniou, P. Zhang, S. S. Skourtis and D. N. Beratan, Vibrational Control of Electron Transfer Reactions II: A Non- Equilibrium Molecular Dynamics Study. To be submitted.

[59] W. J. Schreier, T. Aumuller, K. Haiser, F. O. Koller, M. Loweneck, H.-J. Musiol, T. E. Schrader, T. Kiefhaber, L. Moroder and W. Zinth, Biopolymers, 2013, 100, 38–50.

[60] C. Rulliere, Femtosecond Laser Pulses Principles and Experiments, 2nd edn, Springer, 2005.

[61] W. B. Person and G. Zerbi, Vibrational Intensities in Infrared and Raman Spectroscopy, Elsevier, 1982.

[62] ADF Manual, ADF Program System 2013.

Chapter 5: Dexter Energy Transfer Pathways

Energy transfer with an associated spin change of the donor and acceptor, Dexter energy transfer, is critically important in solar energy harvesting assemblies, damage protection schemes of photobiology, and organometallic opto-electronic materials. Dexter transfer between chemically linked donors and acceptors is bridge mediated, presenting an enticing analogy with bridge-mediated electron and hole transfer. However, Dexter coupling pathways must convey both an electron and a hole from donor to acceptor, and this adds considerable richness to the mediation process. We dissect the bridge-mediated Dexter coupling mechanisms and formulate a theory for triplet energy transfer coupling pathways. Virtual donor–acceptor charge-transfer exciton intermediates dominate at shorter distances or higher tunneling energy gaps, whereas virtual intermediates with an electron and a hole both on the bridge (virtual bridge excitons) dominate for longer distances or lower energy gaps. The effects of virtual bridge excitons were neglected in earlier treatments. The two-particle pathway framework developed here shows how Dexter energy-transfer rates depend on donor, bridge, and acceptor energetics, as well as on orbital symmetry and quantum interference among pathways.

A compelling challenge in supramolecular chemistry is to direct the flow, fission, and fusion of excitons in molecular assemblies [1–4]. When donor or acceptor species undergo a spin change during energy transfer, a two-particle or Dexter interaction enables the energy transfer because the Förster (dipole–dipole) coupling is spin forbidden [5]. Developing design principles for Dexter energy transfer is a considerable challenge compared with that of single-electron (hole) transfer because of the combinatorial growth in the number of mediating (virtual) two-particle states with system size [6–9]. As with single-particle (electron or hole) transfer, Dexter energy transfer arises from donor–acceptor coupling mediated by molecular species [10]. Here, we develop a coupling pathway theory for bridge-mediated Dexter energy transfer and explore the relative contributions of bridge and donor–acceptor charge-transfer excitons to the transport.

A wide variety of critical chemical systems rely on bridge-mediated Dexter transfer of triplet excitons. The lowest-energy electronic excited states of transition metal complexes used for solar-energy harvesting are often high spin, and the excitation energy usually flows to a low-spin ground state acceptor [3]. In the electro-optics underpinning light-

emitting diodes based on metal-containing chromophores, the exchange of energy between low- and high-spin excited states is crucial for device efficiency [11]. As well, protection of biological light-harvesting machinery from damage induced by sensitized singlet oxygen formation relies on a Dexter energy transfer quenching mechanism [12]. The strong dependence of the Dexter coupling on the bridge structure indicates that triplet energy-transfer materials offer additional control (compared with the case for Förster energy transfer) through the manipulation of the bridge-mediated coupling.

Dexter's 1953 analysis of spin-forbidden excitation energy transfer between donor (D) and acceptor (A) moieties in contact invoked coupling *via* the electron–electron Coulomb operator [5]. However, most Dexter systems of interest today involve chemically bridged species. In addition to the two-electron interaction identified by Dexter, one-electron interactions (applied to second or higher order) also couple D to A. The term "Dexter coupling" is now understood to arise from both one- and two-electron interactions that may be mediated by a bridge (see Section 5.1), and two-state approximations to the Dexter coupling that include both contributions are well known [13]. Pioneering kinetic studies of bridge-mediated Dexter energy transport in molecules have been reported by Closs et al. [14], Albinsson et al. [15], Harriman et al. [16], and Spieser [10]; and considerable recent attention has turned to Dexter energy transfer at nanoparticle–molecule junctions [4]. Despite the crucial role played by bridge-mediated Dexter energy transfer, a general framework to assess coupling pathway-mediated Dexter interactions and their interferences is lacking. We formulate a theory for bridge-mediated Dexter coupling pathways that allows the appraisal of specific coupling mechanisms.

Our description of Dexter coupling pathways relies on a configuration-interaction single-excitations (CIS) framework, motivated by schemes used to assess bridge-mediated interactions for single-electron/hole transfer [6,7], adapted here to track the coupled motion of two particles. Pathway decompositions allow molecular-level understanding of energy, orbital symmetry, and interference effects on energy-transfer rates. The framework developed here allows analysis of Dexter-pathway coupling mechanisms in the language of virtual exciton pathways mediated by the bridge. We find that Dexter pathways through short bridges with high tunneling-energy gaps are dominated by charge-transfer virtual exciton intermediates (donor–acceptor charge-transfer excitons (DAE)) with one particle (electron or hole) on D and the other on A. The coupling in this short-distance high-barrier regime is consistent with an early conjecture of Closs et al. [14] and with the picture of Harcourt et al. [13]. At longer distances or lower bridge energy gaps, however, bridge-

localized virtual excitons (without DAE intermediates) dominate the Dexter coupling. These virtual excited states of the bridge, or bridge excitons (BE), are characterized by electron-hole pairs localized on the bridge. We provide formulas to assess the BE contribution to the Dexter coupling, because the earlier theories did not account for these BE intermediates.

We denote the donor, bridge, and acceptor chemical fragments in the energy transfer (EnT) system as D, B, and A, respectively. To describe the electron/hole charge distributions in these regions we use a $+$, $-$ notation. For an exciton with both the hole and the electron localized in a single D, B, or A region, we use $R^{\mp}$ (R=D, B, or A, where the plus sign indicates a hole, and the minus sign indicates an electron). For an exciton with electron and hole localized in separate regions R and R', we use $R^{+}R'^{-}$. A specific exciton state (configuration) with hole in orbital i and excited electron in orbital x is denoted $|i,x\rangle$. Specific excited-electron orbitals x, y are denoted with the * notation.

5.1 Two-State Energy Transfer Kinetics

Nonadiabatic triplet-to-triplet (tr) EnT is well described in the golden-rule approximation when the (resonant) donor and acceptor electronic transitions are at much lower energies than all other electronic transitions. The golden rule rate is

$$k = \frac{2\pi}{\hbar}|V_{tr}|^2 \rho_{FC}, \tag{5.1}$$

where V_{tr} is the bridge-mediated donor–acceptor coupling and ρ_{FC} is the Franck–Condon factor associated with molecular and medium polarization that brings the donor and acceptor excitation energies into coincidence [17,18].

A commonly used expression for the bridge-mediated Dexter coupling is given in eq. (5.2) [19]. We find that eq. (5.2) does not capture these crucial BE contributions to the Dexter coupling, and we provide more general formulas that account for the BE contributions. The approximate Dexter coupling between D-centered $\left(|D,D^*\rangle\right)$ and A-centered $\left(|A,A^*\rangle\right)$ triplet excited states is

$$V_{tr} \simeq 2\frac{\langle D|\hat{V}^h|A\rangle\langle D^*|\hat{V}^e|A^*\rangle}{\Delta E_{CT}} - \left(DA|D^*A^*\right). \quad (5.2)$$

$|D\rangle$, $|D^*\rangle$, (and $|A\rangle$, $|A^*\rangle$) denote hole-occupied and electron-occupied diabatic orbitals that are mostly localized on the D (and A) fragments with tails on B. These orbitals can be written in a basis of zeroth-order hole or electron orbitals that are fully localized on D, B, or A fragments; i.e., $|D\rangle \simeq |d\rangle + |\delta_D^{br}\rangle$, $|D^*\rangle \simeq |d^*\rangle + |\delta_{D^*}^{br}\rangle$, $|A\rangle \simeq |a\rangle + |\delta_A^{br}\rangle$ and $|A^*\rangle \simeq |a^*\rangle + |\delta_{A^*}^{br}\rangle$, where $|d\rangle$ $\left(|d^*\rangle\right)$ and $|a\rangle$ $\left(|a^*\rangle\right)$ are the zeroth-order D-localized and A-localized basis orbitals and $|\delta^{br}\rangle$ are the bridge tails.

In equation (5.2), $\langle D|\hat{V}^h|A\rangle$ is the bridge-mediated hole-tunneling matrix element between $|D\rangle$ and $|A\rangle$, and $\langle D^*|\hat{V}^e|A^*\rangle$ is the bridge-mediated electron-tunneling matrix element between $|D^*\rangle$ and $|A^*\rangle$ ($\hat{V}^h$ and $\hat{V}^e$ denote the hole- and electron-tunneling operators of the one-electron Hamiltonian). ΔE_{CT} is the energy difference between the triplet donor–acceptor charge-transfer exciton state $|D, A^*\rangle$ (or $|A, D^*\rangle$) and the triplet donor state $|D, D^*\rangle$. In the CT states, a hole occupies the $|D\rangle$ $\left(|A\rangle\right)$ orbital and an electron the $|A^*\rangle$ $\left(|D^*\rangle\right)$ orbital. $\left(DA|D^*A^*\right)$ is the Coulomb exchange integral $\left(DA|D^*A^*\right) = k\int d^3r_1 d^3r_2 \Psi_D(\vec{r}_1)\Psi_A(\vec{r}_1) r_{12}^{-1} \Psi_{D^*}(\vec{r}_2)\Psi_{A^*}(\vec{r}_2)$ ($k = e^2/4\pi\varepsilon_0$) [5,19]. Equation (5.2) indicates that $|D, D^*\rangle$ and $|A, A^*\rangle$ are coupled by both a one-electron/hole Hamiltonian operator (to second order) and a two-electron Coulomb Hamiltonian operator (to first order) [5,19].

In eq. (5.2), $\langle D|\hat{V}^h|A\rangle$ and $\langle D^*|\hat{V}^e|A^*\rangle$ are the couplings that cause hole or electron D-to-A CT reactions mediated by through-bridge tunneling [7]. There are numerous approaches to compute these couplings [6,17,18,20]. Diabatization approaches compute the diabatic orbitals $|D\rangle$ $\left(|D^*\rangle\right)$, and $|A\rangle$ $\left(|A^*\rangle\right)$ and then obtain the matrix elements of $\hat{V}^h$ and $\hat{V}^e$ [14,21–23]. Green's function (GF) strategies based on the Löwdin projection technique [7] express $\langle D|\hat{V}^h|A\rangle$ and $\langle D^*|\hat{V}^e|A^*\rangle$ in terms of the zero-order $|d\rangle$, $|d^*\rangle$ and $|a\rangle$, $|a^*\rangle$ orbitals mentioned above, i.e., $\langle D|\hat{V}^h|A\rangle = \langle d|\hat{V}^h\hat{G}_B\hat{V}^h|a\rangle$ and $\langle D^*|\hat{V}^e|A^*\rangle =$

$\left\langle d^* \left| \hat{V}^e \hat{G}_B \hat{V}^e \right| a^* \right\rangle$, where $\hat{G}_B = \left(E_t \hat{I}_B - \hat{H}_B \right)^{-1}$ is the single-particle bridge GF ($\hat{H}_B$ is the bridge Hamiltonian and E_t is the electron- or hole-tunneling energy).

The GF approach is useful to interpret $\langle D|\hat{V}^h|A\rangle$ $\left(\left\langle D^* \left| \hat{V}^e \right| A^* \right\rangle\right)$ as a sum of through-bridge hole (electron)-coupling pathways [7], symbolized by $D^{\mp}BA \rightarrow D^- B^+ A \rightarrow D^- BA^+$ ($D^{\mp}BA \rightarrow D^+ B^- A \rightarrow D^+ BA^-$). Thus, the first term in eq. (5.2) describes the contribution of single-particle transfer (SPT) pathways to the triplet-EnT coupling V_{tr} ($D^{\mp}BA \rightarrow D^+ B^- A \rightarrow D^+ BA^- \rightarrow DB^+ A^- \rightarrow DBA^{\mp}$ and $D^{\mp}BA \rightarrow D^- B^+ A \rightarrow D^- BA^+ \rightarrow DB^- A^+ \rightarrow DBA^{\mp}$). Equation (5.2) suggests that this contribution always involves DAE virtual intermediates with charge distributions $D^+ BA^-$ or $D^- BA^+$. We formulate a general GF approach to analyze V_{tr} in terms of more general triplet exciton tunneling pathways. We show that eq. (5.2) excludes an important class of triplet BE virtual mediating states ($DB^{\mp}A$). For long bridges or low bridge tunneling barriers, these BE pathways dominate the Dexter coupling.

5.2 Characteristics of the Dexter Coupling

Experimental and theoretical studies of Dexter transport have been carried out in rigid and flexible molecules, in polymers, in polymer assemblies, and in metal–organic frameworks [3,24,25]. Dexter rates drop approximately exponentially with distance [10], and eq. (5.2) suggests a distance decay constant equal to the sum of the electron and hole superexchange decay constants [14]. Experimental studies of Harriman found that some Dexter rates decay with exponential decay constants as small as 0.1 $Å^{-1}$ for Ru(II)–Os(II) terpyridyl complexes linked by 1,4-diethynylene-2,5-dialkoxy-benzene bridges [16]. Albinsson et al. found exponential decay constants of 0.45 $Å^{-1}$ for phenylene ethynelene linked porphyrins [15]. For alkane linkers, Closs et al. found large decay exponents, 2.8 $Å^{-1}$ [14]. Computed decay constants as large as 3.4–3.8 $Å^{-1}$ were reported by Curutchet and Voityuk for through-solvent Dexter transport [26]. Experimental and theoretical studies clearly indicate that Dexter couplings depend on the structure and energetics of the bridge.

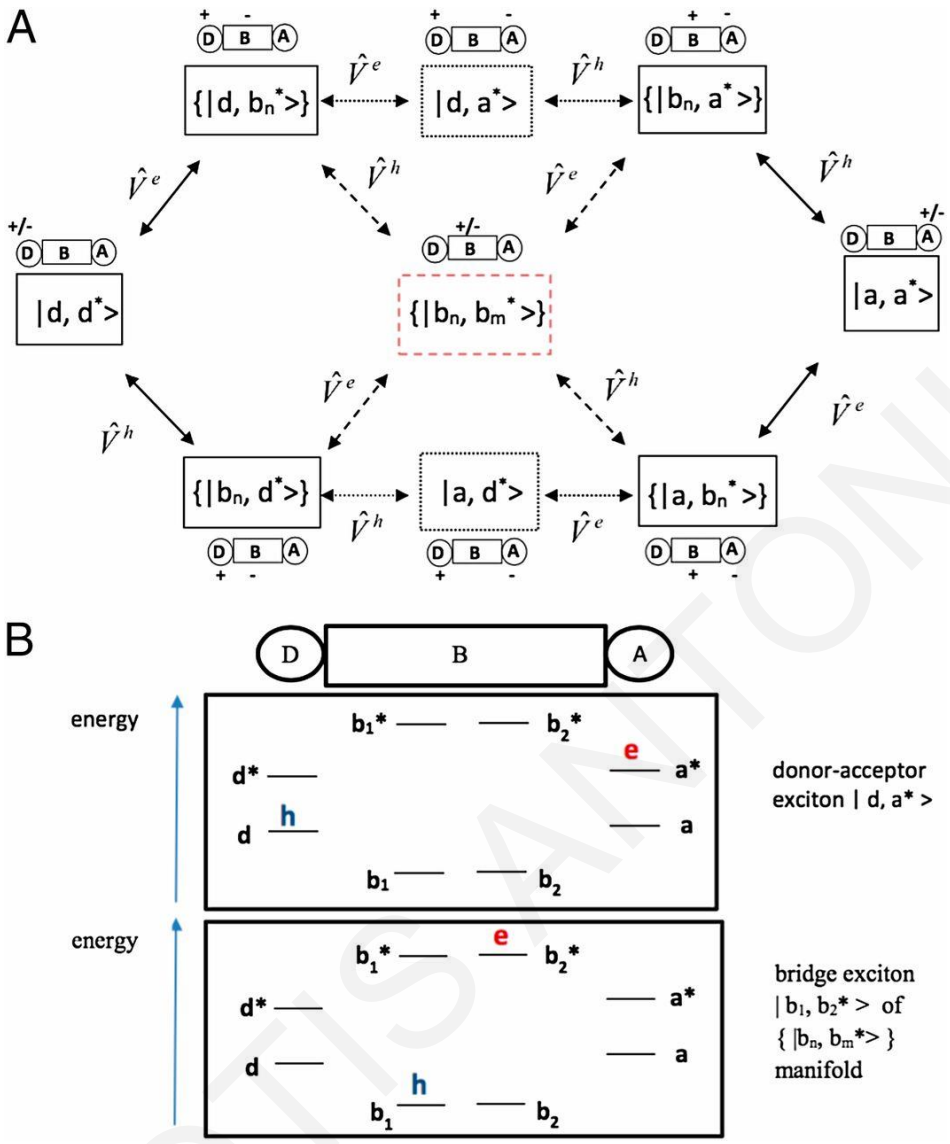

Figure 5.1: (A) Schematic view of the electron-then-hole DAE pathways (upper route via $|d,a^*\rangle$), hole-then-electron DAE pathways (lower route via $|a,d^*\rangle$), and mixed electron/hole bridge-exciton BE pathways (routes through the center block of the bridge-exciton states $\{|b_n,b_m^*\rangle\}$). The DAE pathways (upper and lower routes, dotted lines) avoid the BE manifold $\{|b_n,b_m^*\rangle\}$. The BE pathways (dashed lines to and from the center block) avoid $|d,a^*\rangle$ and $|a,d^*\rangle$. (B) Schematic diagrams of hole- and electron-occupied orbitals in the DAE state $|d,a^*\rangle$ and in a BE state $|b_1,b_2^*\rangle$. For example, NLMO orbitals $|b_1\rangle$ and $|b_2^*\rangle$ could correspond to the first σ bond and the second σ^* antibond of the alkane bridge in Fig. 5.2A.

5.3 CIS Model in a Localized Basis

We use a CIS approach [27] to describe the tr Dexter coupling. CIS methods were found to describe tr EnT couplings accurately in earlier studies [21–23]. We use an orthogonal basis of natural localized molecular orbitals (NLMOs) that are mostly two-center bonding (e.g., σ and π) and two-center antibonding orbitals (e.g., σ^* and π^*) with occupations of two and zero, respectively [28]. A triplet CIS configuration is defined as $|i,x\rangle \equiv \hat{\psi}^{\dagger}_{x\uparrow}\hat{\psi}_{i\downarrow}|\Phi_0\rangle$, where $\hat{\psi}_{i\downarrow}$ destroys a spin-down electron (creates a hole) in occupied NLMO spatial orbital i $(\varphi_i(\vec{r}))$, and $\hat{\psi}^{\dagger}_{x\uparrow}$ creates a spin-up electron in virtual NLMO spatial orbital x $(\varphi_x(\vec{r}))$. $|\Phi_0\rangle$ is a ground-state restricted Hartree–Fock Slater determinant (linear combinations of $|i,x\rangle$ must be used for triplet states [29]).

The NLMO representation for i and x produces an intuitive interpretation of a triplet basis state $|i,x\rangle$ as an exciton with hole and electron localized on different (D, B, A) molecular segments. The $|i,x\rangle$ basis set can be divided into different groups (Fig. 5.1). $|d,d^*\rangle$ and $|a,a^*\rangle$ describe triplet exciton states with the electron and hole entirely localized in D and A regions, respectively. $|d,a^*\rangle$ and $|a,d^*\rangle$ describe DAE states with a hole on D (orbital $|d\rangle$) and an electron on A (orbital $|a^*\rangle$) or the reverse (an electron on $|d^*\rangle$ and a hole on $|a\rangle$). There is a set of states $\{|d,b_n^*\rangle\}$ with an electron on B (one of the $\{|b_n^*\rangle\}$ NLMOs) and a hole on D, as well as a set $\{|a,b_n^*\rangle\}$ with an electron on B and a hole on A. (In Fig. 5.1, braces { } denote multiple $|i,x\rangle$). The $\{|b_n,d^*\rangle\}$ and $\{|b_n,a^*\rangle\}$ sets contain all states with a hole on B and an electron on either D or A. Finally, $\{|b_n,b_m^*\rangle\}$ contains all BE basis states with both an electron and a hole on B. We establish a framework to understand how these sets of configurations mediate the Dexter coupling (Fig. 5.1).

The Hamiltonian elements among CIS basis states are [29]

$$H_{ix,jy} = \langle i,x|\hat{H}|j,y\rangle = \delta_{i,j}F_{x,y} - \delta_{x,y}F_{i,j} - (ij|xy), \tag{5.3}$$

where $F_{i,j}$ and $F_{x,y}$ are Fock matrix elements that arise from the (mean field) Hartree–Fock theory. Each diagonal Fock matrix element $F_{i,i}$ ($F_{x,x}$) corresponds to the energy of the NLMO i (x); each off-diagonal Fock matrix element $F_{i,j}$ ($F_{x,y}$) corresponds to the electronic interaction between orbital i and orbital j (orbital x and orbital y) [28,29]

$$\left(ij\middle|xy\right) = k\int d^3r_1\, d^3r_2\, \varphi_i\left(\vec{r}_1\right)\varphi_j\left(\vec{r}_1\right) r_{12}^{-1}\, \varphi_x\left(\vec{r}_2\right)\varphi_y\left(\vec{r}_2\right), \tag{5.4}$$

($k = e^2/4\pi\varepsilon_0$) are Coulomb matrix elements. It is useful to separate the CIS Hamiltonian matrix elements (eq. (5.3)) into diagonal $\hat{h}^{(di)}$ and off-diagonal $\hat{V}$ parts

$$h_{ix,ix}^{(di)} \equiv \left\langle i,x\middle|\hat{h}^{(di)}\middle|i,x\right\rangle = F_{x,x} - F_{i,i} - \left(ii\middle|xx\right), \tag{5.5}$$

and

$$V_{ix,jy} \equiv \left\langle i,x\middle|\hat{V}\middle|j,y\right\rangle = V_{ix,jy}^{(1p)} + V_{ix,jy}^{(2p)}. \tag{5.6}$$

$\hat{h}^{(di)}$ (eq. (5.5)) contains the electron and hole NLMO orbital energies ($F_{x,x}$ and $-F_{i,i}$, respectively) and the electron–hole Coulomb attraction energy, $-\left(ii\middle|xx\right)$. The off-diagonal interaction (eq. (5.6)) contains one-particle $\left(V_{ix,jy}^{(1p)}\right)$ and two-particle $\left(V_{ix,jy}^{(2p)}\right)$ components. $V_{ix,jy}^{(1p)} = \delta_{i,j}F_{x,y} - \delta_{x,y}F_{i,j}$ (Fig. 5.1). These Fock matrix elements $F_{i,j}$ and $F_{x,y}$ describe, e.g., the through-bond (or through-anti-bond) interactions familiar in electron-transfer theory. $V_{ix,jy}^{(2p)} = -\left(ij\middle|xy\right)$ is the two-electron pure exchange interaction.

The term BE used for the $\left\{\left|b_n,b_m^*\right\rangle\right\}$ CIS basis states does not imply that a physical BE state in a molecular system corresponds to a single $\left|b_n,b_m^*\right\rangle$. Physical BE states are eigenstates of the Hamiltonian submatrix involving the BE basis states, i.e., the submatrix with elements $\left\langle b_n,b_m^*\middle|\hat{H}\middle|b_k,b_l^*\right\rangle$. These eigenstates, which are linear combinations of the $\left|b_n,b_m^*\right\rangle$, are denoted $\left|\psi_\ell^{bb^*}\right\rangle$ (eigenenergies $E_\ell^{bb^*}$).

5.4 Exact Energy Transfer Splittings in Model Compounds

We focus on a simple set of n-alkyl–bridged dienes and norbornanes (Fig. 5.2) to study bridge-mediated EnT couplings, including their distance, energy-gap, molecular-conformation, and coupling-pathway dependence. For all of the molecules in Fig. 5.2 we choose the donor and acceptor segments to be the left (L) and right (R) $C=C$ bonds, and we set $|d,d^*\rangle=|\pi_L,\pi_L^*\rangle$ and $|a,a^*\rangle=|\pi_R,\pi_R^*\rangle$. These states are quasi-resonant with each other and are off-resonance with the other $|i,x\rangle$, ensuring that the $|d,d^*\rangle$ to $|a,a^*\rangle$ Dexter coupling is an entirely virtual process. We then scan the energy difference $\langle d,d^*|\hat{H}|d,d^*\rangle-\langle a,a^*|\hat{H}|a,a^*\rangle$ until we find two eigenstates $|\Psi_\pm\rangle$ of $\hat{H}$ (eq. (5.3)) given by $|\Psi_\pm\rangle\simeq(1/\sqrt{2})[|d,d^*\rangle\pm|a,a^*\rangle]+|\delta_\pm\rangle$, where $|\delta_\pm\rangle$ is small, and it contains the contribution to $|\Psi_\pm\rangle$ of all $|i,x\rangle$ other than $|d,d^*\rangle$ and $|a,a^*\rangle$.

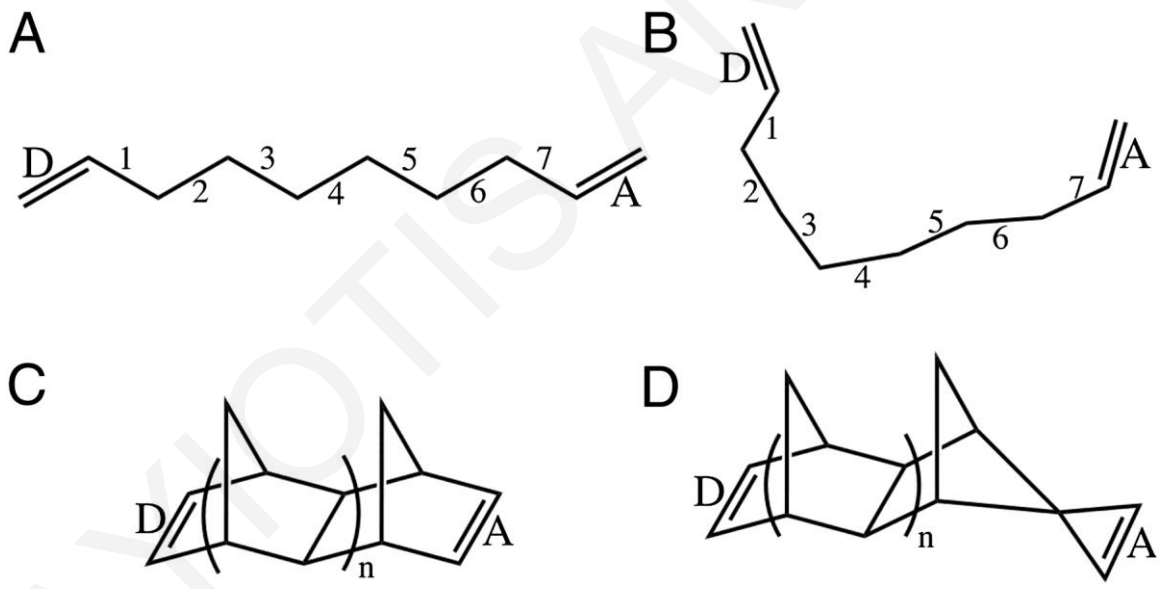

Figure 5.2: (A) Alkyl-bridged diene model compound with seven bridging σ bonds. The alkane bridge is planar, and the left and right $C=C$ bonds are twisted approximately 60^o in opposite directions out of the CC-bonded bridge plane. These double bonds are taken to be the D and A. In our computations (Fig. 5.3), the number of bridge σ bonds is varied from 4 to 13. (B) Example of disordered alkyl-bridged diene model compound with seven bridging σ bonds used in the computations of Tables 5.1 and 5.2. (C) Norbornyl bridged diene model compound with two parallel $C=C$ bonds (D and A). These compounds with n = 1, 2 are used in the computations shown in Tables 5.3 and 5.4. (D) Norbornyl bridged diene model compound with orthogonal $C=C$ bonds (D and A) with symmetry-forbidden triplet EnT.

In this virtual coupling (tunneling) regime, the energy eigenvalues $E_{\pm}$ of $|\Psi_{\pm}\rangle$ are near each other and are separated from the other energy eigenvalues. This setup provides a definition of an "exact" coupling V_{tr} between $|d,d^*\rangle$ and $|a,a^*\rangle$ as one-half of the splitting computed by diagonalizing the full Hamiltonian matrix $\tilde{H}$ in eq. (5.3)

$$V_{tr} \equiv \frac{(E_+ - E_-)}{2}. \tag{5.7}$$

Figure 5.1 shows that the bridge-mediated $|d,d^*\rangle$ to $|a,a^*\rangle$ EnT coupling can be mediated by the virtual states $|d,a^*\rangle$ and $|a,d^*\rangle$ (DAE) or the virtual-state manifold $\{|b_n,b_m^*\rangle\}$ (BE). We therefore define the exact tr EnT coupling mediated by DAE as $V_{tr}^{(dae)} \equiv \left(E_+^{(dae)} - E_-^{(dae)}\right)/2$, where $E_{\pm}^{(dae)}$ are obtained by diagonalizing the $\tilde{H}$ matrix (eq. (5.3)) with all elements containing the $|b_n,b_m^*\rangle$ states in Fig. 5.1 set to zero. By construction, $V_{tr}^{(dae)}$ is thus mediated by DAE rather than by BE. Similarly, we define the exact tr EnT coupling mediated by BE as $V_{tr}^{(be)} \equiv \left(E_+^{(be)} - E_-^{(be)}\right)/2$, where $E_{\pm}^{(be)}$ are obtained by diagonalizing the $\tilde{H}$ matrix with all elements containing the $|d,a^*\rangle$ and $|a,d^*\rangle$ states in Fig. 5.1 set to zero.

5.5 Contributions of DAE and BE Virtual Intermediates to the Dexter Coupling

In our quantum computations, we used restricted Hartree–Fock methods implemented in Gaussian 09 [30] with a 6–31G basis. Figure 5.3A shows V_{tr}, $V_{tr}^{(dae)}$, and $V_{tr}^{(be)}$ as a function of bridge length for the extended alkane systems of Fig. 5.2A. Figure 5.3A, *Inset* indicates the relative magnitude of the DAE and BE contributions $(V_{tr}^{(dae)}/\left(V_{tr}^{(dae)} + V_{tr}^{(be)}\right)$, as well as the contribution of $V_{tr}^{(be)}/\left(V_{tr}^{(dae)} + V_{tr}^{(be)}\right)$, respectively) as a function of bridge length. Figures 5.2A and 5.3A show that the BE contribution in extended alkane bridges with more than seven to eight CC bonds is larger than the DAE contribution. The relative BE contribution is larger for bridges with smaller tunneling barriers. To explore this switching effect, we shift the energies of all bridge NLMO diagonal Fock matrix elements,

$F_{x,x} = F_{b_n^*,b_n^*}$ and $F_{i,i} = F_{b_n,b_n}$ in eq. (5.5), so that the energy gaps $aver\,(F_{b_n^*,b_n^*}) - F_{d^*,d^*}$ and $F_{d,d} - aver\,(F_{b_n,b_n})$ are reduced (*aver* indicates the average value). We ensure that the energy-shifted systems remain in the tunneling regime. That is, we can still find two eigenstates $|\Psi_{\pm}\rangle$ of $\tilde{H}$ (eq. (5.3)) equally delocalized over $|d,d^*\rangle$ and $|a,a^*\rangle$ with small amplitude on the bridge. Then, we compute V_{tr}, $V_{tr}^{(dae)}$, and $V_{tr}^{(be)}$, using the new CIS Hamiltonian.

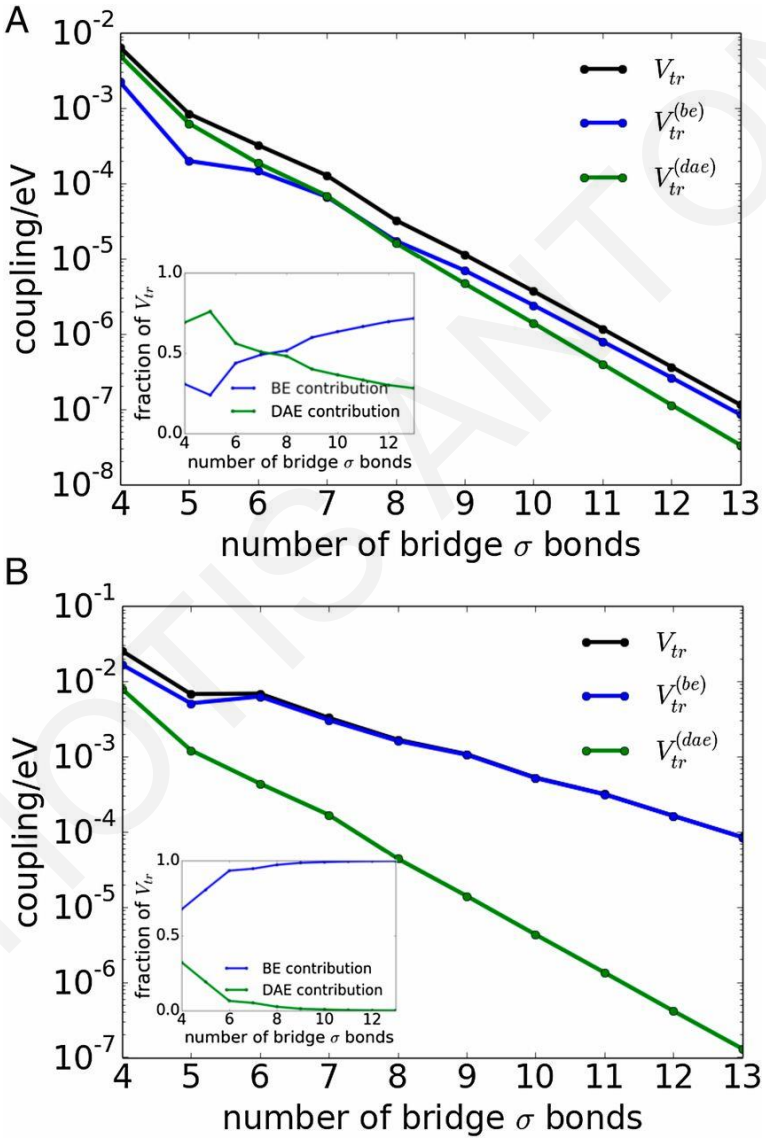

Figure 5.3: (A) Dexter coupling and the BE and DAE contributions to the couplings for linear alkanes (Fig. 5.2A) as a function of bridge length. (B) Same structures as in A, where the average energy gaps $aver\,(F_{b_n^*,b_n^*}) - F_{d^*,d^*}$ and $F_{d,d} - aver\,(F_{b_n,b_n})$ are lowered.

Figure 5.3B shows V_{tr}, $V_{tr}^{(dae)}$, and $V_{tr}^{(be)}$ as a function of bridge length for the extended alkane structures used in Fig. 5.2A, where we have set the $aver(F_{b_n^*,b_n^*}) - F_{d^*,d^*} = 6.15\,\text{eV}$ and $F_{d,d} - aver(F_{b_n,b_n}) = 6.35\,\text{eV}$ (compared with the original values $aver(F_{b_n^*,b_n^*}) - F_{d^*,d^*} = 11.32\,\text{eV}$ and $F_{d,d} - aver(F_{b_n,b_n}) = 11.52\,\text{eV}$ in Fig. 5.3A). For the seven-bond bridge in Fig. 5.3B, the lowest BE eigenstate $\left|\psi_{\ell_{\min}}^{bb^*}\right\rangle$ is 2.2 eV above $\left|d,d^*\right\rangle$, whereas the DAE state $\left|d,a^*\right\rangle$ is 10.8 eV above $\left|d,d^*\right\rangle$ (as opposed to values of 12.4 eV and 10.8 eV, respectively for the seven-bond bridge in Fig. 5.3A). Therefore, for the lower barrier systems in Fig. 5.3B, the BE contribution dominates the coupling for all bridge lengths, becoming more than two orders of magnitude larger than the DAE contribution for longer bridges. Figure 5.3B shows that the BE contribution produces large V_{tr} matrix elements of the order 10^{-2}–10^{-3} eV.

To investigate the effects of molecular conformations on the alkane systems, we sampled structures by choosing random torsional angles and optimizing these conformations with restricted Hartree–Fock methods using a 6–31G basis set (RHF/6–31G). The folded structures thus generated (Fig. 5.2B) were used to compute V_{tr} values and the DAE and BE coupling contributions as a function of energy gap. In Table 5.1, we show V_{tr}, $V_{tr}^{(dae)}$, and $V_{tr}^{(be)}$ for five folded alkanes with seven CC bonds that have $aver(F_{b_n^*,b_n^*}) - F_{d^*,d^*} = 11.32\,\text{eV}$ and $F_{d,d} - aver(F_{b_n,b_n}) = 11.52\,\text{eV}$. Table 5.2 shows V_{tr}, $V_{tr}^{(dae)}$, and $V_{tr}^{(be)}$ for the structures in Table 5.1 with lowered the energy gaps to $aver(F_{b_n^*,b_n^*}) - F_{d^*,d^*} = 6.15\,\text{eV}$ and $F_{d,d} - aver(F_{b_n,b_n}) = 6.35\,\text{eV}$ (the same energy gap as in Fig. 5.3B). In most cases, the BE contribution is greater than or approximately equal to the DAE contribution. The Dexter couplings for the conformationally sampled alkane bridges are smaller compared with the couplings for the extended alkane bridges (for the seven-CC bond bridge, $V_{tr} = 1.27\times10^{-4}\,\text{eV}$ in Fig. 5.3A, and for the partially folded seven-CC bond bridges in Table 5.1, $\langle V_{tr}\rangle = 1.67\times10^{-5}$ eV).

Conformation	$V_{tr}(eV)$	$V_{tr}^{(be)}(eV)$	$V_{tr}^{(dae)}(eV)$
Conf1	5.07×10^{-7}	1.10×10^{-6}	1.25×10^{-6}
Conf2	8.90×10^{-7}	9.36×10^{-7}	1.48×10^{-7}
Conf3	1.66×10^{-5}	1.42×10^{-6}	1.46×10^{-5}
Conf4	2.06×10^{-5}	9.77×10^{-6}	1.38×10^{-5}
Conf5	4.47×10^{-5}	1.27×10^{-5}	2.89×10^{-5}

Table 5.1: Total Dexter coupling and BE and DAE contributions of seven-bond folded alkanes (Fig. 5.2B).

Conformation	$V_{tr}(eV)$	$V_{tr}^{(be)}(eV)$	$V_{tr}^{(dae)}(eV)$
Conf1	2.14×10^{-4}	2.17×10^{-4}	1.33×10^{-6}
Conf2	4.67×10^{-5}	4.68×10^{-5}	1.58×10^{-7}
Conf3	2.34×10^{-5}	4.26×10^{-5}	1.58×10^{-5}
Conf4	2.68×10^{-4}	2.43×10^{-4}	2.46×10^{-5}
Conf5	1.60×10^{-4}	1.12×10^{-4}	3.41×10^{-5}

Table 5.2: Total Dexter coupling and BE and DAE contributions of seven-bond folded alkanes (Fig. 5.2B) with lowered average energy gaps compared with the values for Table 5.1.

The trends in the coupling mechanism apply to more complex bridged structures. Tables 5.3 and 5.4 show V_{tr}, $V_{tr}^{(dae)}$, and $V_{tr}^{(be)}$ for norbonyl bridged systems (Fig. 5.2C) where, as with the linear alkanes, we choose the donor and acceptor segments to be the L and R $C=C$ bonds, and we set $|d,d^*\rangle = |\pi_L,\pi_L^*\rangle$ and $|a,a^*\rangle = |\pi_R,\pi_R^*\rangle$. In Table 5.3, we examine two bridge lengths with n=1,2 (Fig. 5.2C). In Table 5.4, we use the same structures as in Table 5.3 with lowered energy gaps. The $aver(F_{b_n,b_n})$ values are increased by 4.90 eV and the $aver(F_{b_n^*,b_n^*})$ values are lowered by 4.90 eV. The splittings shown in Tables 5.3 and 5.4 indicate that the BE contribution dominates the Dexter coupling as the chain length grows and the tunneling barrier drops. As a final example, we consider a norbonyl system with orthogonal donor/acceptor $C=C$ bonds (Fig. 5.2D). In this structure, the Dexter coupling is symmetry forbidden ($V_{tr}=2.10\times10^{-13}$ eV) and both BE and DAE contributions are symmetry forbidden ($V_{tr}^{(dae)}=3.70\times10^{-13}$ eV and $V_{tr}^{(be)}=1.53\times10^{-13}$ eV, within the numerical noise).

To summarize, the splitting computations find that the Dexter coupling is mediated by BE virtual states, rather than by DAE virtual states; i.e., $V_{tr} \simeq V_{tr}^{(be)}$ and $V_{tr}^{(be)} > V_{tr}^{(dae)}$ for low tunneling energy gaps and/or long bridges. The distance at which the transition from DAE to BE dominance occurs is structure and energy gap dependent.

Number of bridge units	$V_{tr}(eV)$	$V_{tr}^{(be)}(eV)$	$V_{tr}^{(dae)}(eV)$
n=1	4.00×10^{-2}	9.86×10^{-3}	2.91×10^{-2}
n=2	2.42×10^{-3}	8.65×10^{-4}	1.48×10^{-3}

Table 5.3: V_{tr}, $V_{tr}^{(be)}$, and $V_{tr}^{(dae)}$ for the polynorbornyl bridged model compounds with n = 1, 2 (see Fig. 5.2C for the molecular structures). The edge D, A C=C bonds are parallel.

Number of bridge units	$V_{tr}(eV)$	$V_{tr}^{(be)}(eV)$	$V_{tr}^{(dae)}(eV)$
n=1	1.13×10^{-1}	5.89×10^{-2}	4.36×10^{-2}
n=2	2.39×10^{-2}	2.01×10^{-2}	2.70×10^{-3}

Table 5.4: V_{tr}, $V_{tr}^{(be)}$, and $V_{tr}^{(dae)}$ for the polynorbornyl bridged model compounds with n=1, 2 (see Fig. 5.2C for the molecular structures) with parallel D, A C=C bond fragments. For these computations the energy gaps were lowered compared to their values in Table 5.3.

5.6 Triplet Energy Transfer Pathways

Having established the importance of BE contributions to the Dexter coupling V_{tr}, we return to our consideration of eq. (5.2). Our focus is the first single-particle transfer (SPT) term, which is a product of D-to-A electron transfer (ET) and hole transfer (HT) couplings. To understand the contributions of this term to V_{tr}, we develop a general GF pathway description of V_{tr}, $V_{tr}^{(dae)}$, and $V_{tr}^{(be)}$, using Löwdin (effective Hamiltonian) projection methods that are applicable to tunneling matrix element computations. Below, T_{tr}, $T_{tr}^{(dae)}$, and $T_{tr}^{(be)}$ denote the Löwdin projection (GF) expressions for V_{tr}, $V_{tr}^{(dae)}$, and $V_{tr}^{(be)}$, respectively. The Löwdin projection expression for V_{tr} is given by

$$T_{tr} \equiv \left\langle d,d^* \middle| \hat{H}^{ef}\left(E_t\right) \middle| a,a^* \right\rangle,$$
$$\hat{H}^{ef}\left(E_t\right) = \hat{P}\hat{H}\hat{P} + \hat{P}\hat{H}\hat{Q}\hat{G}\left(E_t\right)\hat{Q}\hat{H}\hat{P}, \tag{5.8}$$

where $\hat{P} = \left|d,d^*\right\rangle\left\langle d,d^*\right| + \left|a,a^*\right\rangle\left\langle a,a^*\right|$ is the projection operator for the DAE subspace and $\hat{Q} = \hat{I} - \left(\left|d,d^*\right\rangle\left\langle d,d^*\right| + \left|a,a^*\right\rangle\left\langle a,a^*\right|\right)$ is the projection operator for the complementary subspace containing all exciton states $\left|i,x\right\rangle$ other than $\left|d,d^*\right\rangle$ and $\left|a,a^*\right\rangle$. Given the subspace grouping of Fig. 5.1

$$\hat{Q} = \hat{Q}_{db^*} + \hat{Q}_{bd^*} + \hat{Q}_{ba^*} + \hat{Q}_{ab^*} + \hat{Q}_{da^*} + \hat{Q}_{ad^*} + \hat{Q}_{bb^*}, \tag{5.9}$$

where $\hat{Q}_{db^*} = \sum_n \left|d,b_n^*\right\rangle\left\langle d,b_n^*\right|$, $\hat{Q}_{da^*} = \left|d,a^*\right\rangle\left\langle d,a^*\right|$, etc. $\hat{Q}_{bb^*} = \sum_{n,m}\left|b_n,b_m^*\right\rangle\left\langle b_n,b_m^*\right|$ is the projection operator for the BE subspace, etc. $\hat{G}\left(E\right) = \left[E\hat{Q} - \hat{Q}\hat{H}\hat{Q}\right]^{-1}$ is the exact GF for the CIS Hamiltonian (eq. (5.3)) in the $\hat{Q}$ subspace ($\hat{Q}\hat{H}\hat{Q}$). E_t is the tunneling energy that can be adjusted so that T_{tr} is infinite order in perturbation theory so that $T_{tr} = V_{tr}$ (e.g., refs. [7,31] and Section 5.10). We also define $T_{tr}^{(dae)}$ and $T_{tr}^{(be)}$ in the same way that we defined $V_{tr}^{(dae)}$ and $V_{tr}^{(be)}$ (eqs. (5.18) and (5.19)). That is, we use equations identical to eq. (5.8) where we zero out all $\hat{H}$ matrix elements that contain $\left|d,a^*\right\rangle$ and $\left|a,d^*\right\rangle$ states (for $T_{tr}^{(be)}$) or all $\hat{H}$ matrix elements containing $\left|b_n,b_m^*\right\rangle$ (for $T_{tr}^{(dae)}$). The important conclusion is that for all systems in Fig. 5.2 and all tunneling energy gaps, we can reproduce the splitting-derived V_{tr}, $V_{tr}^{(dae)}$, and $V_{tr}^{(be)}$ values, using the Löwdin GF expressions for T_{tr}, $T_{tr}^{(dae)}$, and $T_{tr}^{(be)}$, respectively, thus confirming that the Löwdin projection method is applicable (Tables 5.5–5.7).

$\Delta E_1\left(eV\right)$	$\Delta E_2\left(eV\right)$	$T_{tr}\left(eV\right)$	$V_{tr}\left(eV\right)$
6.32	6.52	2.60×10^{-3}	2.52×10^{-3}
11.32	11.52	1.22×10^{-4}	1.27×10^{-4}

Table 5.5: Couplings for a linear alkane system with a bridge of seven CC bonds (Fig. 5.2A) as a function of energy gap ΔE. $\Delta E_1 = aver\left(F_{b_n^*,b_n^*}\right) - F_{d^*,d^*}$, $\Delta E_2 = F_{d,d} - aver\left(F_{b_n,b_n}\right)$.

$\Delta E_1(eV)$	$\Delta E_2(eV)$	$T_{tr}(eV)$	$V_{tr}(eV)$
6.32	6.52	2.93×10^{-3}	2.32×10^{-3}
11.32	11.52	6.04×10^{-5}	6.59×10^{-5}

Table 5.6: BE contribution to the Dexter couplings as a function of energy gap for the linear alkane systems in Table 5.5.

$\Delta E_1(eV)$	$\Delta E_2(eV)$	$T_{tr}(eV)$	$V_{tr}(eV)$
6.32	6.52	1.65×10^{-4}	1.72×10^{-4}
11.32	11.52	6.27×10^{-5}	6.81×10^{-5}

Table 5.7: DAE contribution to the Dexter coupling as a function of energy gap for the linear alkane systems in Table 5.5.

5.7 Donor-Acceptor Exciton *vs*. Bridge-Exciton Triplet Energy Transfer Pathways

We derive a generalized GF expression for the first (SPT) term of eq. (5.2). This term contains electron-transfer $\hat{V}^e$ and hole-transfer $\hat{V}^h$ off-diagonal operators. Therefore, in eq. (5.8), we replace the total CIS Hamiltonian $\hat{H}$ (eq. (5.3)) with a Hamiltonian $\hat{H}^{(ne)}$ where the pure exchange terms $(ij|xy)$ in the off-diagonal elements $V_{ix,jy}$ of eq. (5.6) are ignored (*ne* means no exchange). Therefore, $\hat{H}^{(ne)}=\hat{h}^{(di)}+\hat{V}^e+\hat{V}^h$, where $\hat{h}^{(di)}$ is the diagonal part of the CIS Hamiltonian (eq. (5.5)) (containing the Coulomb attraction terms $-(ii|xx)$), and $\langle i,x|\hat{V}^e|j,y\rangle=\delta_{i,j}F_{x,y}$, $\langle i,x|\hat{V}^h|j,y\rangle=-\delta_{x,y}F_{i,j}$. Replacing $\hat{H}$ by $\hat{H}^{(ne)}$ in T_{tr} (eq. (5.8)), we obtain pathway expressions for the SPT components of the total Dexter coupling (Table 5.8), of the DAE mediated coupling, and of the BE-mediated coupling. These expressions (eqs. (5.27), (5.31), and (5.33)) are denoted $T_{tr(ne)}$, $T_{tr(ne)}^{(dae)}$, and $T_{tr(ne)}^{(be)}$, respectively, to emphasize that they do not include the effects of pure-exchange interactions in transferring electrons and holes. The final result is

$$T_{tr(ne)}=T_{tr(ne)}^{(dae)}+T_{tr(ne)}^{(be)}, \tag{5.10}$$

where $T_{tr(ne)}^{(dae)}$ in eq. (5.10) describes DAE pathways and is given by

$$T_{tr(ne)}^{(dae)} \simeq \frac{\left\langle d,d^* \middle| \hat{V}^e \hat{G}_{db^*} \hat{V}^e \middle| d,a^* \right\rangle \left\langle d,a^* \middle| \hat{V}^h \hat{G}_{ba^*} \hat{V}^h \middle| a,a^* \right\rangle}{E_t - E_{da^*}} + \frac{\left\langle d,d^* \middle| \hat{V}^h \hat{G}_{bd^*} \hat{V}^h \middle| a,d^* \right\rangle \left\langle a,d^* \middle| \hat{V}^e \hat{G}_{ab^*} \hat{V}^e \middle| a,a^* \right\rangle}{E_t - E_{ad^*}} \tag{5.11}$$

(eq. (5.37)). $T_{tr(ne)}^{(be)}$ in eq. (5.10) describes BE pathways

$$\begin{aligned} T_{tr(ne)}^{(be)} \simeq & \left\langle d,d^* \middle| \hat{V}^e \hat{G}_{db^*} \hat{V}^h \hat{G}_{bb^*} \hat{V}^e \hat{G}_{ba^*} \hat{V}^h \middle| a,a^* \right\rangle \\ & + \left\langle d,d^* \middle| \hat{V}^h \hat{G}_{bd^*} \hat{V}^e \hat{G}_{bb^*} \hat{V}^h \hat{G}_{ab^*} \hat{V}^e \middle| a,a^* \right\rangle \\ & + \left\langle d,d^* \middle| \hat{V}^e \hat{G}_{db^*} \hat{V}^h \hat{G}_{bb^*} \hat{V}^h \hat{G}_{ab^*} \hat{V}^e \middle| a,a^* \right\rangle \\ & + \left\langle d,d^* \middle| \hat{V}^h \hat{G}_{bd^*} \hat{V}^e \hat{G}_{bb^*} \hat{V}^e \hat{G}_{ba^*} \hat{V}^h \middle| a,a^* \right\rangle \end{aligned} \tag{5.12}$$

(eq. (5.38)). E_t is the exciton tunneling energy. The $\hat{G}_K$ are $\hat{H}^{(ne)}$ GFs for the individual subspaces K of virtual intermediate states shown in Fig. 5.1. $\hat{G}_K(E_t) = \left[E_t \hat{Q}_K - \hat{Q}_K \hat{H}^{(ne)} \hat{Q}_K \right]^{-1}$, where the $\hat{Q}_K$ are the projection operator components of eq. (5.9).

The DAE contribution $T_{tr(ne)}^{(dae)}$ in eq. (5.11) is the generalized GF pathway expression for the first (SPT) component of eq. (5.2). It describes EnT as a sequence of two complete D-to-A electron and hole tunneling steps (first term, $D^{\mp}BA \rightarrow D^+B^-A \rightarrow D^+BA^- \rightarrow DB^+A^- \rightarrow DBA^{\mp}$; second term $D^{\mp}BA \rightarrow D^-B^+A \rightarrow D^-BA^+ \rightarrow DB^-A^+ \rightarrow DBA^{\mp}$). In the framework of Fig. 5.1, eq. (5.11) contains all of the upper and lower tunneling paths connecting $\left| d,d^* \right\rangle$ to $\left| a,a^* \right\rangle$ *via* virtual DAE states $\left| a,d^* \right\rangle$ and $\left| d,a^* \right\rangle$, respectively (avoiding the BE manifold $\left| b_n,b_m^* \right\rangle$. $\left\langle d,d^* \middle| \hat{V}^e \hat{G}_{db^*} \hat{V}^e \middle| d,a^* \right\rangle$ and $\left\langle a,d^* \middle| \hat{V}^e \hat{G}_{ab^*} \hat{V}^e \middle| a,a^* \right\rangle$ are the bridge-mediated electron tunneling matrix elements for photo-excited electron transfer from $\left| d^* \right\rangle$ to $\left| a^* \right\rangle$. Similarly, $\left\langle d,a^* \middle| \hat{V}^h \hat{G}_{ba^*} \hat{V}^h \middle| a,a^* \right\rangle$ and $\left\langle d,d^* \middle| \hat{V}^h \hat{G}_{bd^*} \hat{V}^h \middle| a,d^* \right\rangle$ are the bridge-mediated hole tunneling matrix elements for photo-excited hole transfer from $\left| a \right\rangle$ to $\left| d \right\rangle$. These matrix elements include the influence of electron-hole Coulomb attraction.

The bridge exciton contribution, $T_{tr(ne)}^{(be)}$ (eq. (5.12)), describes all tunneling pathways from $\left| d,d^* \right\rangle$ to $\left| a,a^* \right\rangle$ through the virtual BE manifold $\left| b_n,b_m^* \right\rangle$ in Fig. 5.1 (avoiding the

DAE states) (first two terms, $D^{\mp}BA \to D^{+}B^{-}A \to DB^{\mp}A \to DB^{+}A^{-} \to DBA^{\mp}$ and $D^{\mp}BA \to D^{-}B^{+}A \to DB^{\mp}A \to DB^{-}A^{+} \to DBA^{\mp}$; last two terms, $D^{\mp}BA \to D^{+}B^{-}A \to DB^{\mp}A \to DB^{-}A^{+} \to DBA^{\mp}$ and $D^{\mp}BA \to D^{-}B^{+}A \to DB^{\mp}A \to DB^{+}A^{-} \to DBA^{\mp}$).

$\Delta E_1(eV)$	$\Delta E_2(eV)$	$T_{tr(ne)}(eV)$	$V_{tr(ne)}(eV)$
6.32	6.52	5.59×10^{-3}	5.41×10^{-3}
11.32	11.52	1.55×10^{-4}	1.53×10^{-4}

Table 5.8: Single-particle component to the Dexter couplings (i.e., using a CIS Hamiltonian with no pure exchange) as a function of energy gap for the linear alkane systems in Table 5.5.

5.8 Rapid Growth in the Number of Bridge-Exciton Intermediate States with Chain Length

Ignoring pure exchange when computing the Dexter coupling is not generally sound. For the systems studied in Fig. 5.2A, the average exchange contribution to the Dexter coupling in the long chain limit (Fig. 5.2A) is about 25% of V_{tr}. The analysis above finds that the SPT component of the Dexter coupling contains DAE and BE pathway terms that are of the same order in $\hat{V}^{e}$ and $\hat{V}^{h}$. Therefore, DAE and BE pathways must both be considered; it is not appropriate to retain only $T_{tr(ne)}^{(dae)}$ (which is analogous to the first term in eq. (5.2)) without keeping the $T_{tr(ne)}^{(be)}$ term as well. For bridges with N bonding/antibonding orbitals ($|b_n\rangle, |b_m^*\rangle$), the number of BE CIS configurations $|b_n, b_m^*\rangle$ is at least N^2. Therefore, the number of BE eigenstates $|\psi_{\ell}^{bb^*}\rangle$ of the submatrix $\langle b_n, b_m^*|\hat{H}|b_k, b_l^*\rangle$ (or $\langle b_n, b_m^*|\hat{H}^{(ne)}|b_k, b_l^*\rangle$) is also N^2. In eq. (5.12) for $T_{tr(ne)}^{(be)}$, $\hat{G}_{bb^*} = \sum_{L=1}^{N^2}\left(|\psi_{\ell}^{bb^*}\rangle\langle\psi_{\ell}^{bb^*}|\right)/\left(E_t - E_{\ell}^{bb^*}\right)$ (where $E_{\ell}^{bb^*}$ is the eigenvalue of BE eigenstate $|\psi_{\ell}^{bb^*}\rangle$). As the bridge length N grows, the number of possible BE virtual intermediates $|\psi_{\ell}^{bb^*}\rangle$ grows as N^2 (as opposed to the two DAE intermediates $|d, a^*\rangle$ and $|a, d^*\rangle$ in eq. (5.11)). Thus, BE pathways are important for long bridge lengths or low energy gaps, where omitting the BE contribution to the Dexter coupling may introduce errors of one to two orders of magnitude.

5.9 Conclusions

We have found that bridge-exciton tunneling pathways dominate triplet energy transfer mediation in the long-distance/small tunneling gap regime accessed in many molecular structures of current interest. As well, we have developed a coupling pathway description for bridge-mediated triplet Dexter coupling. The Dexter coupling is exponentially sensitive to donor-acceptor distance and to bridge structure, suggesting that these EnT rates and their directionality may be manipulated by the bridge structure. As with bridge-mediated electron and hole transfer, control can be realized by using pathway interference effects, bridge energetics, and through-bond/through space coupling trade-offs. The theory enables an atomic-level description for the origins of Dexter coupling, a necessary step toward controlling Dexter coupling interactions in a wide range of systems of current interest in energy science and molecular biophysics.

The most significant result of the Dexter pathway analysis is the demonstration that virtual bridge-exciton intermediate states (Fig. 5.1, center) can dominate the EnT coupling for long bridges and low tunneling-energy bridges. This BE-mediated coupling, and thus the Dexter coupling, cannot be expressed as a simple product of electron and hole donor-to-acceptor tunneling steps. Indeed, Curutchet and Voityuk's studies of Dexter couplings through solvent found Dexter decay exponents to be smaller than the sum of the electron- and hole-mediated superexchange coupling decay exponents [26]. The coupling pathway dissections introduced here are sufficiently general to enable the further development of structure–function relations for Dexter energy-transfer interactions.

5.10 Supplement

Pathway Analysis

The full CIS Hamiltonian $\hat{H}$ of the system in the local NLMO representation is

$$\langle i,x|\hat{H}|j,y\rangle = \delta_{i,j}F_{x,y} - \delta_{x,y}F_{i,j} - (ij|xy). \tag{5.13}$$

To proceed with the Löwdin projection method we write the identity operator in the $|i,x\rangle$ basis as a sum of projection operators, $\hat{I} = \hat{P} + \hat{Q}$, where

$$\hat{P} = \left|d,d^*\right\rangle\left\langle d,d^*\right| + \left|a,a^*\right\rangle\left\langle a,a^*\right| \tag{5.14}$$

and $\hat{Q} = \hat{Q}_1 + \hat{Q}_2$, with

$$\hat{Q}_1 = \hat{Q}_{db^*} + \hat{Q}_{bd^*} + \hat{Q}_{ba^*} + \hat{Q}_{ab^*}, \tag{5.15}$$

$$\hat{Q}_2 = \hat{Q}_{da^*} + \hat{Q}_{ad^*} + \hat{Q}_{bb^*}. \tag{5.16}$$

In the equation above the $\hat{Q}_K$ are projection operators for the bridging subspaces of Fig. 5.1 e.g., $\hat{Q}_{db^*} = \sum_n \left|d,b_n^*\right\rangle\left\langle d,b_n^*\right|$, $\hat{Q}_{bb^*} = \sum_{n,m}\left|b_n,b_m^*\right\rangle\left\langle b_n,b_m^*\right|$, etc.

From the above definitions, and using the projection technique, we can obtain a GF expression (T_{tr}) for the splitting-derived total EnT coupling (V_{tr}). This is done by deriving an effective two-state Hamiltonian $\hat{H}^{ef}$ defined on the subspace $\hat{P}$ of $\left|d,d^*\right\rangle$ with $\left|a,a^*\right\rangle$. The off-diagonal matrix element ($\left|d,d^*\right\rangle$ to $\left|a,a^*\right\rangle$) of $\hat{H}^{ef}$ is T_{tr}; i.e.,

$$\begin{gathered} T_{tr} = \left\langle d,d^*\right|\hat{H}^{ef}\left(E_t\right)\left|a,a^*\right\rangle; \\ \hat{P}\hat{H}^{ef}\left(E_t\right)\hat{P} = \hat{P}\hat{H}\hat{P} + \hat{P}\hat{H}\hat{Q}\hat{G}\left(E_t\right)\hat{Q}\hat{H}\hat{P}, \end{gathered} \tag{5.17}$$

where the GF $\hat{G}\left(E_t\right) = \left[E_t\hat{Q} - \hat{Q}\hat{H}\hat{Q}\right]^{-1}$ is infinite order in all matrix elements of $\hat{Q}\hat{H}\hat{Q}$. Here E_t is the tunneling energy; i.e., $E_t = E_t^{(0)}$, where $E_t^{(0)} = \left\langle d,d^*\right|\hat{H}\left|d,d^*\right\rangle = \left\langle a,a^*\right|\hat{H}\left|a,a^*\right\rangle$ as a first approximation. E_t can be improved iteratively, e.g., $E_t^{(1)} = \left(\left\langle d,d^*\right|\hat{H}^{ef}\left(E_t^{(0)}\right)\left|d,d^*\right\rangle + \left\langle a,a^*\right|\hat{H}^{ef}\left(E_t^{(0)}\right)\left|a,a^*\right\rangle\right)/2$ [7,31], in which case the above expression for T_{tr} also becomes infinite order in all matrix elements of $\hat{Q}\hat{H}\hat{Q}$. With the iterative readjustment of E_t, eq. (5.17) can reproduce the value of V_{tr} in the tunneling limit.

The Löwdin projection expression $T_{tr}^{(be)}$ for the splitting-derived $V_{tr}^{(be)}$ is obtained by an equation similar to eq. (5.17) where $\hat{H}$ is replaced by $\hat{H}^{(be)}$, the CIS Hamiltonian in the $\left|i,x\right\rangle$ representation with DAE states $\left|d,a^*\right\rangle$ and $\left|a,d^*\right\rangle$ deleted. Therefore

$$T_{tr}^{(be)} = \left\langle d,d^*\right|\hat{H}_{be}^{ef}\left(E_t\right)\left|a,a^*\right\rangle; \tag{5.18}$$

$$\hat{P}\hat{H}^{ef}_{be}\left(E_t\right)\hat{P} = \hat{P}\hat{H}^{(be)}\hat{P} + \hat{P}\hat{H}^{(be)}\hat{Q}\left[E_t\hat{Q} - \hat{Q}\hat{H}^{(be)}\hat{Q}\right]^{-1}\hat{Q}\hat{H}^{(be)}\hat{P}\,.$$

Similarly, the Löwdin projection expression $T^{(dae)}_{tr}$ for the splitting-derived $V^{(dae)}_{tr}$ is

$$\begin{aligned} T^{(dae)}_{tr} &= \left\langle d, d^* \middle| \hat{H}^{ef}_{dae}\left(E_t\right) \middle| a, a^* \right\rangle; \\ \hat{P}\hat{H}^{ef}_{dae}\left(E_t\right)\hat{P} &= \hat{P}\hat{H}^{(dae)}\hat{P} + \hat{P}\hat{H}^{(dae)}\hat{Q}\left[E_t\hat{Q} - \hat{Q}\hat{H}^{(dae)}\hat{Q}\right]^{-1}\hat{Q}\hat{H}^{(dae)}\hat{P}\,, \end{aligned} \tag{5.19}$$

where $\hat{H}^{(dae)}$ is the CIS Hamiltonian in the $\left|i, x\right\rangle$ representation with all BE states $\left|b_n, b^*_m\right\rangle$ deleted.

To derive single particle pathway contributions to the EnT coupling, we define a Hamiltonian operator without pure exchange ($ij \,|\, xy$) interactions as

$$\hat{H}^{(ne)} = \hat{h}^{(di)} + \hat{V}^{(1p)}, \tag{5.20}$$

where $\hat{h}^{(di)}$ is the diagonal part and $\hat{V}^{(1p)} = \hat{V}^e + \hat{V}^h$ is the off-diagonal part. The matrix elements of the diagonal Hamiltonian are given by (eq. (5.5))

$$\left\langle i, x \middle| \hat{h}^{(di)} \middle| i, x \right\rangle = F_{x,x} - F_{i,i} - \left(ii \middle| xx\right). \tag{5.21}$$

The matrix elements of the off-diagonal Hamiltonian $\hat{V}^{(1p)}$ are given by the electron or hole transfer terms

$$\left\langle i, x \middle| \hat{V}^e \middle| j, y \right\rangle = \delta_{i,j}F_{x,y} \quad , \quad \left\langle i, x \middle| \hat{V}^h \middle| j, y \right\rangle = -\delta_{x,y}F_{i,j}\,. \tag{5.22}$$

The exact (spitting-derived) $V_{tr(ne)}$, $V^{(dae)}_{tr(ne)}$, and $V^{(be)}_{tr(ne)}$ are computed from diagonalization of $\hat{H}^{(ne)}$ (by analogy to V_{tr}, $V^{(dae)}_{tr}$, and $V^{(be)}_{tr}$). We obtain GF expressions $T_{tr(ne)}$, $T^{(dae)}_{tr(ne)}$, and $T^{(be)}_{tr(ne)}$ for $V_{tr(ne)}$, $V^{(dae)}_{tr(ne)}$, and $V^{(be)}_{tr(ne)}$.

Replacing $\hat{H}$ by $\hat{H}^{(ne)}$ in eq. (5.17) gives

$$T_{tr(ne)}\left(E_t\right) = \left\langle d, d^* \middle| \hat{H}^{(ne)} \middle| a, a^* \right\rangle + \left\langle d, d^* \middle| \hat{H}^{(ne)}\hat{Q}\hat{G}^{(ne)}\left(E_t\right)\hat{Q}\hat{H}^{(ne)} \middle| a, a^* \right\rangle, \tag{5.23}$$

where the GF $\hat{G}^{(ne)}(E_t)=\left[E_t\hat{Q}-\hat{Q}\hat{H}^{(ne)}\hat{Q}\right]^{-1}$. To proceed further, we ignore the direct matrix element $\left\langle d,d^*\left|\hat{H}^{(ne)}\right|a,a^*\right\rangle$, which is zero for long-distance EnT. We then get

$$T_{tr(ne)}(E_t)=\left\langle d,d^*\left|\hat{V}^{(1p)}\hat{Q}\hat{G}^{(ne)}(E_t)\hat{Q}\hat{V}^{(1p)}\right|a,a^*\right\rangle. \tag{5.24}$$

Using again the projection technique for $\hat{Q}_1\hat{G}^{(ne)}(E_t)\hat{Q}_1$ in eq. (5.24),

$$\hat{Q}_1\hat{G}(E_t)\hat{Q}_1=\left[E\hat{Q}_1-\hat{Q}_1\hat{H}^{(ne)}\hat{Q}_1-\hat{Q}_1\hat{R}(E_t)\hat{Q}_1\right]^{-1}. \tag{5.25}$$

In the equation above $\hat{Q}_1\hat{H}^{(ne)}\hat{Q}_1=\hat{H}^{(ne)}_{db^*}+\hat{H}^{(ne)}_{bd^*}+\hat{H}^{(ne)}_{ba^*}+\hat{H}^{(ne)}_{ab^*}$, where $\hat{H}^{(ne)}_K=\hat{Q}_K\hat{H}^{(ne)}\hat{Q}_K$ denotes the full Hamiltonians for these subspaces ($\hat{H}^{(ne)}$ is given in eq. (5.20)). $\hat{Q}_1\hat{R}(E_t)\hat{Q}_1$ is a resolvent operator given

$$\hat{Q}_1\hat{R}(E_t)\hat{Q}_1=\hat{Q}_1\hat{V}^{(1p)}\hat{Q}_2\left[E\hat{Q}_2-\hat{Q}_2\hat{H}^{(ne)}\hat{Q}_2\right]^{-1}\hat{Q}_2\hat{V}^{(1p)}\hat{Q}_1 \tag{5.26}$$

that can be written as a sum of two resolvent operators $\hat{R}^{(dae)}$ and $\hat{R}^{(be)}$ describing effective couplings between the $\left\{\left|d,b_n^*\right\rangle\right\}$ $\left(\left\{\left|b_n,d^*\right\rangle\right\}\right)$ and $\left\{\left|b_n,a^*\right\rangle\right\}$ $\left(\left\{\left|a,b_n^*\right\rangle\right\}\right)$ subspaces mediated by the DAE (dae) and BE (be), respectively

In summary, the GF expression $T_{tr(ne)}$ for the splitting-derived EnT coupling $V_{tr(ne)}$ is

$$T_{tr(ne)}(E_t)=\left\langle d,d^*\left|\left(\hat{V}^e\hat{Q}_{db^*}+\hat{V}^h\hat{Q}_{bd^*}\right)\hat{G}^{(ne)}(E_t)\left(\hat{Q}_{ab^*}\hat{V}^e+\hat{Q}_{ba^*}\hat{V}^h\right)\right|a,a^*\right\rangle, \tag{5.27}$$

where $\langle i,x|\hat{V}^e|j,y\rangle=\delta_{i,j}F_{x,y}$, $\langle i,x|\hat{V}^h|j,y\rangle=-\delta_{x,y}F_{i,j}$, E_t is the tunneling energy, and

$$\hat{G}^{(ne)}(E_t)=\left[E_t\left(\hat{Q}_{db^*}+\hat{Q}_{bd^*}+\hat{Q}_{ba^*}+\hat{Q}_{ab^*}\right)-\left(\hat{H}^{(ne)}_{db^*}+\hat{H}^{(ne)}_{bd^*}+\hat{H}^{(ne)}_{ba^*}+\hat{H}^{(ne)}_{ab^*}+\hat{R}^{(dae)}+\hat{R}^{(be)}\right)\right]^{-1}. \tag{5.28}$$

$\hat{R}^{(dae)}$ and $\hat{R}^{(be)}$ are resolvent operators that describe effective couplings between the $\left\{\left|d,b_n^*\right\rangle\right\}$ $\left(\left\{\left|b_n,d^*\right\rangle\right\}\right)$ and $\left\{\left|b_n,a^*\right\rangle\right\}$ $\left(\left\{\left|a,b_n^*\right\rangle\right\}\right)$ subspaces mediated by the DAE (dae: $\left|d,a^*\right\rangle$ and $\left|a,d^*\right\rangle$) and BE (be: $\left\{\left|b_n,b_m^*\right\rangle\right\}$), respectively. The resolvents are

$$\hat{R}^{(dae)}(E_t)=\hat{Q}_{db^*}\hat{V}^e\hat{Q}_{da^*}\hat{G}_{da^*}(E_t)\hat{Q}_{da^*}\hat{V}^h\hat{Q}_{ba^*}+\hat{Q}_{bd^*}\hat{V}^h\hat{Q}_{ad^*}\hat{G}_{ad^*}(E_t)\hat{Q}_{ad^*}\hat{V}^e\hat{Q}_{ab^*}, \tag{5.29}$$

and

$$\begin{aligned}\hat{R}^{(be)}\left(E_t\right)=&\hat{Q}_{db^*}\hat{V}^h\hat{Q}_{bb^*}\hat{G}_{bb^*}\left(E_t\right)\hat{Q}_{bb^*}\hat{V}^e\hat{Q}_{ba^*}\\&+\hat{Q}_{bd^*}\hat{V}^e\hat{Q}_{bb^*}\hat{G}_{bb^*}\left(E_t\right)\hat{Q}_{bb^*}\hat{V}^h\hat{Q}_{ab^*}\\&+\hat{Q}_{db^*}\hat{V}^h\hat{Q}_{bb^*}\hat{G}_{bb^*}\left(E_t\right)\hat{Q}_{bb^*}\hat{V}^h\hat{Q}_{ab^*}\\&+\hat{Q}_{bd^*}\hat{V}^e\hat{Q}_{bb^*}\hat{G}_{bb^*}\left(E_t\right)\hat{Q}_{bb^*}\hat{V}^e\hat{Q}_{ba^*},\end{aligned}\tag{5.30}$$

where $\hat{G}_K\left(E_t\right)=\left[E_t\hat{Q}_K-\hat{Q}_K H^{(ne)}\hat{Q}_K\right]^{-1}$ are the GFs for the subspaces $\hat{Q}_K$.

From eq. (5.27), we can obtain an exact expression for the effective EnT coupling mediated by the DAE (and not the BE) denoted $T_{tr(ne)}^{(dae)}$ if we remove $\hat{R}^{(be)}$ (the bridge-exciton contribution) from $\hat{G}^{(ne)}$ in eq. (5.28). Namely,

$$T_{tr(ne)}^{(dae)}\equiv\left\langle d,d^*\middle|\left(\hat{V}^e\hat{Q}_{db^*}+\hat{V}^h\hat{Q}_{bd^*}\right)\hat{G}^{(dae)}\left(E_t\right)\left(\hat{Q}_{ab^*}\hat{V}^e+\hat{Q}_{ba^*}\hat{V}^h\right)\middle|a,a^*\right\rangle,\tag{5.31}$$

where

$$\hat{G}^{(dae)}\left(E_t\right)=\left[E_t\left(\hat{Q}_{db^*}+\hat{Q}_{bd^*}+\hat{Q}_{ba^*}+\hat{Q}_{ab^*}\right)-\left(\hat{H}_{db^*}^{(ne)}+\hat{H}_{bd^*}^{(ne)}+\hat{H}_{ba^*}^{(ne)}+\hat{H}_{ab^*}^{(ne)}+\hat{R}^{(dae)}\right)\right]^{-1}.\tag{5.32}$$

Similarly, we can obtain an exact expression for the EnT coupling mediated by BE (and not DAE) denoted $T_{tr(ne)}^{(be)}$ if we remove the DAE contribution ($\hat{R}^{(dae)}$) from $\hat{G}^{(ne)}$ in eq. (5.28); i.e.,

$$T_{tr(ne)}^{(be)}\equiv\left\langle d,d^*\middle|\left(\hat{V}^e\hat{Q}_{db^*}+\hat{V}^h\hat{Q}_{bd^*}\right)\hat{G}^{(be)}\left(E_t\right)\left(\hat{Q}_{ab^*}\hat{V}^e+\hat{Q}_{ba^*}\hat{V}^h\right)\middle|a,a^*\right\rangle,\tag{5.33}$$

where

$$\hat{G}^{(be)}\left(E_t\right)=\left[E_t\left(\hat{Q}_{db^*}+\hat{Q}_{bd^*}+\hat{Q}_{ba^*}+\hat{Q}_{ab^*}\right)-\left(\hat{H}_{db^*}^{(ne)}+\hat{H}_{bd^*}^{(ne)}+\hat{H}_{ba^*}^{(ne)}+\hat{H}_{ab^*}^{(ne)}+\hat{R}^{(be)}\right)\right]^{-1}.\tag{5.34}$$

To simplify the expression for $T_{tr(ne)}$ we write $\hat{G}^{(ne)}$ in eq. (5.28) as

$$\begin{aligned}\hat{G}^{(ne)}\left(E_t\right)&=\left[\hat{G}^{-1}\left(E_t\right)-\left(\hat{R}^{(dae)}+\hat{R}^{(be)}\right)\right]^{-1},\\\hat{G}^{-1}\left(E_t\right)&=\hat{G}_{db^*}^{-1}\left(E_t\right)+\hat{G}_{bd^*}^{-1}\left(E_t\right)+\hat{G}_{ba^*}^{-1}\left(E_t\right)+\hat{G}_{ab^*}^{-1}\left(E_t\right),\end{aligned}\tag{5.35}$$

where $\hat{G}_K\left(E_t\right)=\left[E_t\hat{Q}_K-\hat{Q}_K H^{(ne)}\hat{Q}_K\right]^{-1}$ are the GFs for the subspaces $\hat{Q}_K$. To first order in $\hat{R}^{(dae)}+\hat{R}^{(be)}$, $\hat{G}^{(ne)}\left(E_t\right)\simeq\hat{G}\left(E_t\right)+\hat{G}\left(E_t\right)\left(\hat{R}^{(dae)}+\hat{R}^{(be)}\right)\hat{G}\left(E_t\right)$. Substituting this approximate equation into eq. (5.27) gives

$$T_{tr(ne)}\simeq T_{tr(ne)}^{(dae)}+T_{tr(ne)}^{(be)}, \tag{5.36}$$

where

$$\begin{aligned}T_{tr(ne)}^{(dae)}\simeq&\frac{\left\langle d,d^*\left|\hat{V}^e\hat{G}_{db^*}\hat{V}^e\right|d,a^*\right\rangle\left\langle d,a^*\left|\hat{V}^h\hat{G}_{ba^*}\hat{V}^h\right|a,a^*\right\rangle}{E_t-E_{da^*}}\\&+\frac{\left\langle d,d^*\left|\hat{V}^h\hat{G}_{bd^*}\hat{V}^h\right|a,d^*\right\rangle\left\langle a,d^*\left|\hat{V}^e\hat{G}_{ab^*}\hat{V}^e\right|a,a^*\right\rangle}{E_t-E_{ad^*}}\end{aligned} \tag{5.37}$$

is the lowest-order (in $\hat{R}^{(dae)}$) expression for the D-A exciton contribution to $T_{tr(ne)}$ and

$$\begin{aligned}T_{tr(ne)}^{(be)}\simeq&\left\langle d,d^*\left|\hat{V}^e\hat{G}_{db^*}\hat{V}^h\hat{G}_{bb^*}\hat{V}^e\hat{G}_{ba^*}\hat{V}^h\right|a,a^*\right\rangle\\&+\left\langle d,d^*\left|\hat{V}^h\hat{G}_{bd^*}\hat{V}^e\hat{G}_{bb^*}\hat{V}^h\hat{G}_{ab^*}\hat{V}^e\right|a,a^*\right\rangle\\&+\left\langle d,d^*\left|\hat{V}^e\hat{G}_{db^*}\hat{V}^h\hat{G}_{bb^*}\hat{V}^h\hat{G}_{ab^*}\hat{V}^e\right|a,a^*\right\rangle\\&+\left\langle d,d^*\left|\hat{V}^h\hat{G}_{bd^*}\hat{V}^e\hat{G}_{bb^*}\hat{V}^e\hat{G}_{ba^*}\hat{V}^h\right|a,a^*\right\rangle\end{aligned} \tag{5.38}$$

is the lowest-order (in $\hat{R}^{(be)}$) expression for the bridge exciton contribution to $T_{tr(ne)}$.

The terms $\left\langle d,d^*\left|\hat{V}^e\hat{G}_{db^*}\hat{V}^e\right|d,a^*\right\rangle$ and $\left\langle a,d^*\left|\hat{V}^e\hat{G}_{ab^*}\hat{V}^e\right|a,a^*\right\rangle$ in the expression for $T_{tr(ne)}^{(dae)}$ are the bridge-mediated electron tunneling matrix elements. Similarly, $\left\langle d,a^*\left|\hat{V}^h\hat{G}_{ba^*}\hat{V}^h\right|a,a^*\right\rangle$ and $\left\langle d,d^*\left|\hat{V}^h\hat{G}_{bd^*}\hat{V}^h\right|a,d^*\right\rangle$ are the bridge-mediated hole tunneling matrix elements. Strictly speaking, these matrix elements describe excited-state bridge-mediated electron and hole transfer DA couplings, rather than electron- or hole-shift DA couplings

For the compounds under study and for all energy gaps mentioned in the main text (Fig. 5.2 and 5.3), we find that T_{tr}, $T_{tr}^{(dae)}$, and $T_{tr}^{(be)}$ approximate well the splitting-derived V_{tr}, $V_{tr}^{(dae)}$, and $V_{tr}^{(be)}$ even within one iteration with $E_t=E_t^{(0)}$ or $E_t^{(1)}=$

$\left(\left\langle d,d^{*}\left|\hat{H}^{ef}\left(E_{t}^{(0)}\right)\right|d,d^{*}\right\rangle+\left\langle a,a^{*}\left|\hat{H}^{ef}\left(E_{t}^{(0)}\right)\right|a,a^{*}\right\rangle\right)\Big/2$. This also holds for the $T_{tr(ne)}$, $T_{tr(ne)}^{(dae)}$, and $T_{tr(ne)}^{(be)}$ to the splitting-derived $V_{tr(ne)}$, $V_{tr(ne)}^{(dae)}$, and $V_{tr(ne)}^{(be)}$ values. Examples are given in Tables 5.5–5.8.

5.11 References

[1] M. B. Smith and J. Michl, Annu. Rev. Phys. Chem., 2013, 64(1), 361–386.

[2] T. N. Singh-Rachford and F. N. Castellano, Coord. Chem. Rev., 2010, 254(21), 2560–2573.

[3] J. Lin, et al., J. Phys. Chem. C, 2013, 117(43), 22250–22259.

[4] C. Mongin, S. Garakyaraghi, N. Razgoniaeva, M. Zamkov and F. N. Castellano, Science, 2016, 351(6271), 369–372.

[5] D. L. Dexter, J. Chem. Phys., 1953, 21(5), 836 850.

[6] J. Jortner and M. Ratner, Molecular Electronics, Blackwell, Oxford, 1997.

[7] S. S. Skourtis and D. N. Beratan, Adv. Chem. Phys., 1999, 106, 377–452.

[8] J. Lin, D. Balamurugan, P. Zhang, S. S. Skourtis and D. N. Beratan, J. Phys. Chem. B, 2015, 119(24), 7589–7597.

[9] G. D. Scholes, ACS Nano, 2008, 2(3), 523–537.

[10] S. Speiser, Chem. Rev., 1996, 96(6), 1953–1976.

[11] M. A. Baldo, et al., Nature, 1998, 395(6698), 151–154.

[12] R. J. Cogdell and H. A. Frank HA, Biochim. Biophys. Acta, 1987, 895(2), 63–79.

[13] R. D. Harcourt, G. D. Scholes and K. P. Ghiggino, J. Chem. Phys., 1994, 101(12), 10521.

[14] G. L. Closs, M. D. Johnson, J. R. Miller and P. Piotrowiak, J. Am. Chem. Soc., 1989, 111(10), 3751–3753.

[15] B. Albinsson, M. P. Eng, K. Pettersson and M. U. Winters, Phys. Chem. Chem. Phys., 2007, 9(44),5847–5864.

[16] A. Harriman, A. Khatyr, R. Ziessel and A. C. Benniston, Angew. Chem. Int. Ed., 2000, 39(23), 4287–4290.

[17] V. Balzani, et al., Electron Transfer in Chemistry, Wiley-VCH, Weinheim, Germany, vols. 1–4, 2001.

[18] V. May and O. Kühn, Charge and Energy Transfer Dynamics in Molecular Systems, Wiley-VCH, Weinheim, Germany, 2004.

[19] G. D. Scholes, Annu. Rev. Phys. Chem., 2003, 54(18), 57–87.

[20] A. Migliore, N. F. Polizzi, M. J. Therien and D. N. Beratan, Chem. Rev., 2014, 114(7), 3381–3465.

[21] C. P. Hsu, G. R. Fleming, M. Head-Gordon and T. Head-Gordon, J. Chem. Phys., 2001, 114(7), 3065–3072.

[22] Z. Q. You, C. P. Hsu and G. R. Fleming, J. Chem. Phys., 2006, 124(4), 044506.

[23] J. E. Subotnik, J. Vura-Weis, A. J. Sodt and M. A. Ratner, J. Phys. Chem. A, 2010, 114(33), 8665–8675.

[24] L. Zaikowski, et al., J. Phys. Chem. B, 2015, 119(24), 7231–7241.

[25] Z. Chen, H. Y. Hsu, M. Arca and K. S. Schanze, J. Phys. Chem. B, 2015, 119(24), 7198–7209.

[26] C. Curutchet and A. A. Voityuk, J. Phys. Chem. C, 2012, 116(42), 22179–22185.

[27] J. B. Foresman, M. Head-Gordon, J. A. Pople and M. J. Frisch, J. Phys. Chem., 1992, 96(1), 135–149.

[28] A. E. Reed and F. Weinhold, J. Chem. Phys., 1985, 83(4), 1736–1740.

[29] A. Szabo and N. S. Ostlund, Modern Quantum Chemistry, Dover, Mineola, NY, 1996.

[30] M. J. Frisch, et al., Gaussian09 Revision D.01, Gaussian Inc., Wallingford, CT, 2009.

[31] S. S. Skourtis, S. Mukamel S, Chem. Phys., 1995, 197(3), 367–388.

Chapter 6: Dexter Energy Transfer Pathways Analysis in Eigenstate and Local Basis

Energy transfer (EnT) pathway analysis provides a molecular-level understanding of EnT couplings. The framework developed in the previous Chapter (eqs. (5.11) and (5.12)) allows the analysis of bridge-mediated triplet-EnT coupling pathways. In the previous Chapter we demonstrated the importance of bridge exciton contributions to the overall Dexter coupling and provided formulas that assess these contributions (which are ignored by previous theories). This Chapter is devoted to further pathway analysis of the single-particle (SPT) contributions (eqs. (5.11) and (5.12)) and the two-particle exchange contribution (eq. (5.2)) to the triplet EnT coupling.

Specifically, in Section 6.1 we further analyze the bridge-mediated SPT component of the coupling (eq. (5.12)) in the bridge-eigenstate-basis. This method allows the decomposition of eq. (5.12) in terms of individual bridge-exciton-eigenstate pathways. Using the alkane molecules we find the virtual bridge-exciton eigenstates that contribute in the SPT coupling. In Section 6.2 we develop simple D-B-A models to illustrate SPT EnT pathways (using eqs. (5.11) and (5.12)) and to derive analytically the bridge-exciton dominance of the triplet EnT coupling as the bridge length increases. Equations (5.11) and (5.12) ignore pure exchange contributions to the EnT couplings. These exchange contributions are reconsidered in Section 6.3 where we develop D-B-A models to illustrate exchange EnT pathways and we formulate an intuitive framework that demonstrates strong analogies to electron transfer pathways.

6.1 Dexter Energy Transfer Pathways Analysis in Eigenstate Basis

In this Section we derive a bridge-eigenstate-basis formulation for $T_{tr(ne)}^{(be)}$ (eq. (5.12)). We use this formulation to decompose $T_{tr(ne)}^{(be)}$ into the individual pathway components for some of the alkane systems studied in the previous Chapter.

6.1.1 CIS Hamiltonian in Eigenstate Basis

The CIS Hamiltonian without pure exchange $(ij|xy)$ interactions in the NLMO representation is defined as (eq. (5.20))

$$\hat{H}^{(ne)} = \hat{h}^{(di)} + \hat{V}^{(1p)}, \tag{6.1}$$

where $\hat{h}^{(di)}$ is the diagonal part given by $\langle i,x|\hat{h}^{(di)}|i,x\rangle = F_{x,x} - F_{i,i} - (ii|xx)$ (eqs. (5.5) and (5.21)), and $\hat{V}^{(1p)} = \hat{V}^{e} + \hat{V}^{h}$ is the off-diagonal part, given by the matrix elements $\langle i,x|\hat{V}^{e}|j,y\rangle = \delta_{i,j}F_{x,y}$ and $\langle i,x|\hat{V}^{h}|j,y\rangle = -\delta_{x,y}F_{i,j}$ (eq. (5.22)). The term (ne) means no exchange.

To express $\hat{H}^{(ne)}$ in an eigenstate basis representation we write the identity operator in the CIS NLMO basis $(|i,x\rangle)$ as a sum of projection operators $\hat{I} = \hat{P} + \hat{Q}$,

$$\hat{P} = |d,d^*\rangle\langle d,d^*| + |d,a^*\rangle\langle d,a^*| + |a,d^*\rangle\langle a,d^*| + |a,a^*\rangle\langle a,a^*|. \tag{6.2}$$

$\hat{P}$ is the projection operator containing the donor $(|d,d^*\rangle)$ and acceptor $(|a,a^*\rangle)$ exciton states, and the donor-acceptor (DAE) charge transfer (CT) exciton states $(|d,a^*\rangle, |a,d^*\rangle)$. $\hat{Q}$ is the projection operator for the complementary subspace containing all other NLMO exciton states $|i,x\rangle$, i.e.,

$$\hat{Q} = \hat{Q}_{db^*} + \hat{Q}_{bd^*} + \hat{Q}_{ba^*} + \hat{Q}_{ab^*} + \hat{Q}_{bb^*}, \tag{6.3}$$

where $\hat{Q}_{db^*} = \sum_n |d,b_n^*\rangle\langle d,b_n^*|$, $\hat{Q}_{ab^*} = \sum_n |a,b_n^*\rangle\langle a,b_n^*|$, $\hat{Q}_{bb^*} = \sum_{n,m} |b_n,b_m^*\rangle\langle b_n,b_m^*|$, etc.

In the following, for the subspaces $\hat{Q}_{db^*}, \hat{Q}_{bd^*}$, $\hat{Q}_{ba^*}, \hat{Q}_{ab^*}$ and $\hat{Q}_{bb^*}$ we will use eigenstate representations. For example, for the bridge exciton (BE) projection operator $\hat{Q}_{bb^*}$ we use the basis of BE eigenstates $\left\{\left|\psi_\ell^{bb^*}\right\rangle\right\}$. These BE eigenstates satisfy the following equation

$$\left(\hat{Q}_{bb^*}\hat{H}^{(ne)}\hat{Q}_{bb^*}\right)\left|\psi_\ell^{bb^*}\right\rangle = E_\ell^{bb^*}\left|\psi_\ell^{bb^*}\right\rangle, \tag{6.4}$$

where $E_\ell^{bb^*}$ are the BE eigenvalues. Similarly, for $\hat{Q}_{db^*}$ we use the eigenstates $\left\{\left|\psi_m^{db^*}\right\rangle\right\}$ of $\hat{Q}_{db^*}\hat{H}^{(ne)}\hat{Q}_{db^*}$, etc. Therefore, in eq. (6.3) the projection operators are $\hat{Q}_{db^*} = \sum_m \left|\psi_m^{db^*}\right\rangle\left\langle\psi_m^{db^*}\right|, \hat{Q}_{bb^*} = \sum_\ell \left|\psi_\ell^{bb^*}\right\rangle\left\langle\psi_\ell^{bb^*}\right|$, etc.

The reason for this change of basis is two-fold. First it simplifies the perturbation theory analysis of the triplet EnT coupling $\left(T_{tr(ne)}^{(be)}\right)$ which leads to the pathway picture. Second, the eigenstates $\left\{\left|\psi_\ell^{bb^*}\right\rangle\right\}$ describe physical bridge-excitons (i.e., eigenstates with both electron and hole in the bridge).

6.1.2 Pathways Analysis in Eigenstate Basis

Our starting point is eq. (5.12)

$$\begin{aligned} T_{tr(ne)}^{(be)} \simeq & \left\langle d, d^* \left| \hat{V}^e \hat{G}_{db^*} \hat{V}^h \hat{G}_{bb^*} \hat{V}^e \hat{G}_{ba^*} \hat{V}^h \right| a, a^* \right\rangle \\ & + \left\langle d, d^* \left| \hat{V}^h \hat{G}_{bd^*} \hat{V}^e \hat{G}_{bb^*} \hat{V}^h \hat{G}_{ab^*} \hat{V}^e \right| a, a^* \right\rangle \\ & + \left\langle d, d^* \left| \hat{V}^e \hat{G}_{db^*} \hat{V}^h \hat{G}_{bb^*} \hat{V}^h \hat{G}_{ab^*} \hat{V}^e \right| a, a^* \right\rangle \\ & + \left\langle d, d^* \left| \hat{V}^h \hat{G}_{bd^*} \hat{V}^e \hat{G}_{bb^*} \hat{V}^e \hat{G}_{ba^*} \hat{V}^h \right| a, a^* \right\rangle. \end{aligned} \tag{6.5}$$

The $\hat{G}_K$ are $\hat{H}^{(ne)}$ Green functions for the individual subspaces K of virtual intermediate eigenstates, i.e., $\hat{G}_K = \left[E\hat{Q}_K - \hat{Q}_K \hat{H}^{(ne)} \hat{Q}_K\right]^{-1}$. In the new "eigenstate" representation the $\hat{G}_K$ simplify, e.g., $\hat{G}_{bb^*} = \sum_{\ell=1}^{N^2} \left(\left|\psi_\ell^{bb^*}\right\rangle\left\langle\psi_\ell^{bb^*}\right|\right) \Big/ \left(E_t - E_\ell^{bb^*}\right)$, where E_t is the exciton

tunneling energy. For bridges with N bonding/antibonding NLMO orbitals $\left(\left|b_n\right\rangle,\left|b_m^*\right\rangle\right)$, the number of BE eigenstates/eigenvalues is N^2.

To express the bridge-exciton contribution, $T_{tr(ne)}^{(be)}$ (eq. (6.5)), in the eigenstate representation we dissect eq. (6.5) into four independent terms, as anticipated by the four independent terms present in $T_{tr(ne)}^{(be)}$ eq. (6.5)

$$A=\left\langle d,d^*\left|\hat{V}^e\hat{G}_{db^*}\hat{V}^h\hat{G}_{bb^*}\hat{V}^e\hat{G}_{ba^*}\hat{V}^h\right|a,a^*\right\rangle, \tag{6.6a}$$

$$B=\left\langle d,d^*\left|\hat{V}^h\hat{G}_{bd^*}\hat{V}^e\hat{G}_{bb^*}\hat{V}^h\hat{G}_{ab^*}\hat{V}^e\right|a,a^*\right\rangle, \tag{6.6b}$$

$$C=\left\langle d,d^*\left|\hat{V}^e\hat{G}_{db^*}\hat{V}^h\hat{G}_{bb^*}\hat{V}^h\hat{G}_{ab^*}\hat{V}^e\right|a,a^*\right\rangle, \tag{6.6c}$$

$$D=\left\langle d,d^*\left|\hat{V}^h\hat{G}_{bd^*}\hat{V}^e\hat{G}_{bb^*}\hat{V}^e\hat{G}_{ba^*}\hat{V}^h\right|a,a^*\right\rangle. \tag{6.6d}$$

For instance, let's consider only the first term of $T_{tr(ne)}^{(be)}$ (eq. (6.6a)), and insert into eq. (6.6a) the BE Green function $\hat{G}_{bb^*}=\sum_{\ell=1}^{N^2}\left(\left|\psi_\ell^{bb^*}\right\rangle\left\langle\psi_\ell^{bb^*}\right|\right)\Big/\left(E_t-E_\ell^{bb^*}\right)$. The $\hat{G}_{bb^*}$ insertion leads to the division of eq. (6.6a) into two parts

$$A_1^{(\ell)}=\left\langle d,d^*\left|\hat{V}^e\hat{G}_{db^*}\hat{V}^h\right|\psi_\ell^{bb^*}\right\rangle, \tag{6.7a}$$

$$A_2^{(\ell)}=\left\langle\psi_\ell^{bb^*}\left|\hat{V}^e\hat{G}_{ba^*}\hat{V}^h\right|a,a^*\right\rangle, \tag{6.7b}$$

and eq. (6.6a) may be expressed as a sum over the BE eigenstates of the product of $A_1^{(\ell)}$ and $A_2^{(\ell)}$

$$A=\sum_\ell^{N^2}\frac{A_1^{(\ell)}A_2^{(\ell)}}{E_t-E_\ell^{bb^*}}. \tag{6.8}$$

Inserting the respective Green functions $\hat{G}_{db^*}=\sum_{m=1}^{N}\left(\left|\psi_m^{db^*}\right\rangle\left\langle\psi_m^{db^*}\right|\right)\Big/\left(E_t-E_m^{db^*}\right)$ and $\hat{G}_{ba^*}=\sum_{n=1}^{N}\left(\left|\psi_n^{ba^*}\right\rangle\left\langle\psi_n^{ba^*}\right|\right)\Big/\left(E_t-E_n^{ba^*}\right)$ in eqs. (6.7a) and (6.7b) we get

$$A_1^{(\ell)}=\sum_m^N\frac{\left\langle d,d^*\left|\hat{V}^e\right|\psi_m^{db^*}\right\rangle\left\langle\psi_m^{db^*}\left|\hat{V}^h\right|\psi_\ell^{bb^*}\right\rangle}{E_t-E_m^{db^*}}, \tag{6.9a}$$

$$A_2^{(\ell)} = \sum_n^N \frac{\left\langle \psi_\ell^{bb^*} \middle| \hat{V}^e \middle| \psi_n^{ba^*} \right\rangle \left\langle \psi_n^{ba^*} \middle| \hat{V}^h \middle| a, a^* \right\rangle}{E_t - E_n^{ba^*}} \,. \tag{6.9b}$$

Thus, the first term of $T_{tr(ne)}^{(be)}$ (eq. (6.6a)), becomes

$$A = \sum_\ell^{N^2} \sum_m^N \sum_n^N \frac{\left\langle d, d^* \middle| \hat{V}^e \middle| \psi_m^{db^*} \right\rangle \left\langle \psi_m^{db^*} \middle| \hat{V}^h \middle| \psi_\ell^{bb^*} \right\rangle}{E_t - E_m^{db^*}} \left(\frac{1}{E_t - E_\ell^{bb^*}} \right) \frac{\left\langle \psi_\ell^{bb^*} \middle| \hat{V}^e \middle| \psi_n^{ba^*} \right\rangle \left\langle \psi_n^{ba^*} \middle| \hat{V}^h \middle| a, a^* \right\rangle}{E_t - E_n^{ba^*}}. \tag{6.10}$$

Equation (6.10) describes the total contribution of the first "A" pathway (see Figs. 6.2 and 6.3) to the $T_{tr(ne)}^{(be)}$.

This expression (eq. (6.10)) does not provide detailed information about the individual pathway contributions through the bridge-eigenstate manifold $\left| \psi_\ell^{bb^*} \right\rangle$. To further analyze the total "A" pathway contribution into its $\left| \psi_\ell^{bb^*} \right\rangle$ components, we restrict the summations in eq. (6.10) over specific eigenstates. In particular, the BE eigenstates $\left| \psi_\ell^{bb^*} \right\rangle$ summation is reduced to a smaller fragment ℓ' of the total N^2 BE eigenstates, and the summations over the $\left| \psi_m^{db^*} \right\rangle$ and $\left| \psi_n^{ba^*} \right\rangle$ eigenstates are modified in order to exclusively select only a specific eigenstate $\left| \psi_{m'}^{db^*} \right\rangle$ and $\left| \psi_{n'}^{ba^*} \right\rangle$. Thus, if we sum over specific $\left| \psi_{m'}^{db^*} \right\rangle$, $\left| \psi_{n'}^{ba^*} \right\rangle$ and $\left| \psi_{\ell'}^{bb^*} \right\rangle$ eigenstates, eq. (6.10) becomes

$$A_{m',n',\ell'} = \sum_{\ell=1}^{\ell'} \frac{\left\langle d, d^* \middle| \hat{V}^e \middle| \psi_{m'}^{db^*} \right\rangle \left\langle \psi_{m'}^{db^*} \middle| \hat{V}^h \middle| \psi_\ell^{bb^*} \right\rangle}{E_t - E_{m'}^{db^*}} \left(\frac{1}{E_t - E_\ell^{bb^*}} \right) \frac{\left\langle \psi_\ell^{bb^*} \middle| \hat{V}^e \middle| \psi_{n'}^{ba^*} \right\rangle \left\langle \psi_{n'}^{ba^*} \middle| \hat{V}^h \middle| a, a^* \right\rangle}{E_t - E_{n'}^{ba^*}}. \tag{6.11}$$

Using eq. (6.11) we can perform a detailed inspection of the individual pathway contributions through the respective $\left| \psi_\ell^{bb^*} \right\rangle$ BE components. Similar analysis may be carried out for the remaining three terms of eq. (6.5) (eqs. (6.6b)-(6.6d)) such that

$$B_{m',n',\ell'}=\sum_{\ell=1}^{\ell'}\frac{\left\langle d,d^{*}\left|\hat{V}^{h}\right|\psi_{m'}^{bd^{*}}\right\rangle\left\langle\psi_{m'}^{bd^{*}}\left|\hat{V}^{e}\right|\psi_{\ell}^{bb^{*}}\right\rangle}{E_t-E_{m'}^{bd^{*}}}\left(\frac{1}{E_t-E_{\ell}^{bb^{*}}}\right)\frac{\left\langle\psi_{\ell}^{bb^{*}}\left|\hat{V}^{h}\right|\psi_{n'}^{ab^{*}}\right\rangle\left\langle\psi_{n'}^{ab^{*}}\left|\hat{V}^{e}\right|a,a^{*}\right\rangle}{E_t-E_{n'}^{ab^{*}}},\quad(6.12a)$$

$$C_{m',n',\ell'}=\sum_{\ell=1}^{\ell'}\frac{\left\langle d,d^{*}\left|\hat{V}^{e}\right|\psi_{m'}^{db^{*}}\right\rangle\left\langle\psi_{m'}^{db^{*}}\left|\hat{V}^{h}\right|\psi_{\ell}^{bb^{*}}\right\rangle}{E_t-E_{m'}^{db^{*}}}\left(\frac{1}{E_t-E_{\ell}^{bb^{*}}}\right)\frac{\left\langle\psi_{\ell}^{bb^{*}}\left|\hat{V}^{h}\right|\psi_{n'}^{ab^{*}}\right\rangle\left\langle\psi_{n'}^{ab^{*}}\left|\hat{V}^{e}\right|a,a^{*}\right\rangle}{E_t-E_{n'}^{ab^{*}}},\quad(6.12b)$$

$$D_{m',n',\ell'}=\sum_{\ell=1}^{\ell'}\frac{\left\langle d,d^{*}\left|\hat{V}^{h}\right|\psi_{m'}^{bd^{*}}\right\rangle\left\langle\psi_{m'}^{bd^{*}}\left|\hat{V}^{e}\right|\psi_{\ell}^{bb^{*}}\right\rangle}{E_t-E_{m'}^{bd^{*}}}\left(\frac{1}{E_t-E_{\ell}^{bb^{*}}}\right)\frac{\left\langle\psi_{\ell}^{bb^{*}}\left|\hat{V}^{e}\right|\psi_{n'}^{ba^{*}}\right\rangle\left\langle\psi_{n'}^{ba^{*}}\left|\hat{V}^{h}\right|a,a^{*}\right\rangle}{E_t-E_{n'}^{ba^{*}}}.\quad(6.12c)$$

The total BE pathway contribution $T_{tr(ne)}^{(be)}$ over specific $\left|\psi_{m'}^{db^{*}}\right\rangle$, $\left|\psi_{n'}^{ba^{*}}\right\rangle$ and $\left|\psi_{\ell'}^{bb^{*}}\right\rangle$ eigenstates will be

$$\left(T_{tr(ne)}^{(be)}\right)_{m',n',\ell'}=A_{m',n',\ell'}+B_{m',n',\ell'}+C_{m',n',\ell'}+D_{m',n',\ell'}.\quad(6.13)$$

6.1.3 Pathway Topology of the Most Important Bridge-Exciton Pathways in Extended Alkane Systems

In our numerical investigation we used the *ab*-initio data, obtained by RHF methods implemented in Gaussian 09 with 6-31G basis, for the seven-CC bond bridge of the extended alkane system of Fig. 6.1. Keeping everything else the same we shift the energies of all bridge NLMO diagonal Fock matrix elements, $F_{x,x}=F_{b_n^{*},b_n^{*}}$ and $F_{i,i}=F_{b_n,b_n}$ in eq. (6.1), so that the energy gaps $\Delta E_1=aver\,(F_{b_n^{*},b_n^{*}})-F_{d^{*},d^{*}}$ and $\Delta E_2=F_{d,d}-aver\,(F_{b_n,b_n})$ are reduced (*aver* indicates the average value) with respect to the original system energy gaps ($\Delta E_1=11.32eV$, $\Delta E_2=11.52eV$). We further ensure that the energy-shifted systems remain in the tunneling regime. That is, we can still find two eigenstates $\left|\Psi_{\pm}\right\rangle$ of $\tilde{H}^{(ne)}$ (eq. (6.1)) equally delocalized over $\left|d,d^{*}\right\rangle$ and $\left|a,a^{*}\right\rangle$ with small amplitude on the bridge.

Reducing the energy gaps ΔE_1 and ΔE_2, while retaining the tunneling limit (see previous Chapter), increases the BE contribution up to ~50 times. Pathways analysis demonstrates that BE transfer can be described by 5 intermediate BE eigenstates (with the lowest energies) each creating 4 pathways (Fig. 6.2) and their sum (Fig. 6.3). Thus overall, we

obtain 20 distinct dominant pathways in the bridge-exciton eigenstates basis. Table 6.1 summarizes the obtained results, e.g., for the original system energy gaps ($\Delta E_1 = 11.32eV$, $\Delta E_2 = 11.52eV$) 72.3% of $V_{tr(ne)}^{(be)}$ or 79.4% of $T_{tr(ne)}^{(be)}$ can be described by the first 5 lowest bridge eigenvalues. For these 5 lowest bridge eigenvalues, the main pathways contributions are: 20.9% for pathways $A_{2,1,5}$ and $B_{1,2,5}$, 4.6% for pathway $C_{2,2,5}$ and 53.6% for pathway $D_{1,1,5}$. The table clearly demonstrates that the dominant through bridge pathway is the $D_{1,1,5}$ pathway.

Figure 6.1: Alkyl-bridged diene model compound with seven bridging σ bonds. The alkane bridge is planar, and the left and right $C=C$ bonds are taken to be the D and A.

Pathway $A_{2,1,5}$

$$\left|dd^*\right\rangle - \left|\psi_2^{db^*}\right\rangle$$
$$\Big|$$
$$\left|\psi_\ell^{bb^*}\right\rangle - \left|\psi_1^{ba^*}\right\rangle$$
$$\Big|$$
$$\left|aa^*\right\rangle$$

Pathway $B_{1,2,5}$

$$\left|dd^*\right\rangle$$
$$\Big|$$
$$\left|\psi_1^{bd^*}\right\rangle - \left|\psi_\ell^{bb^*}\right\rangle$$
$$\Big|$$
$$\left|\psi_2^{ab^*}\right\rangle - \left|aa^*\right\rangle$$

Pathway $C_{2,2,5}$

$$\left|dd^*\right\rangle - \left|\psi_2^{db^*}\right\rangle$$
$$\Big|$$
$$\left|\psi_\ell^{bb^*}\right\rangle$$
$$\Big|$$
$$\left|\psi_2^{ab^*}\right\rangle - \left|aa^*\right\rangle$$

Pathway $D_{1,1,5}$

$$\left|dd^*\right\rangle$$
$$\Big|$$
$$\left|\psi_1^{bd^*}\right\rangle - \left|\psi_\ell^{bb^*}\right\rangle - \left|\psi_1^{ba^*}\right\rangle$$
$$\Big|$$
$$\left|aa^*\right\rangle$$

Figure 6.2: Pathway topology of most important pathways in the BE eigenstate basis. The DA CT intermediates do not contribute.

$\Delta E_1(eV)$	$\Delta E_2(eV)$	$V_{tr(ne)}^{(be)}$	$T_{tr(ne)}^{(be)}(eV)$	$A_{m',n',\ell'}$	$B_{m',n',\ell'}$	$C_{m',n',\ell'}$	$D_{m',n',\ell'}$
6.32	6.52	88.9	83.9	16.5	16.5	3.3	63.7
7.32	7.52	77.1	75.1	-0.2	21.5	4.1	74.6
8.32	8.52	93.7	93.7	18.7	18.7	3.7	58.9
11.32	11.52	72.3	79.4	20.9	20.9	4.6	53.6

Table 6.1: Pathway analysis using eqs. (6.11) and (6.12) for $A_{m',n',\ell'}$, $B_{m',n',\ell'}$, $C_{m',n',\ell'}$, and $D_{m',n',\ell'}$ pathway contributions (Figs. 6.2 and 6.3) over specific m', n' and ℓ' eigenvalues as a function of energy gaps $\Delta E_1 = aver(F_{b_n^*,b_n^*}) - F_{d^*,d^*}$, and $\Delta E_2 = F_{d,d} - aver(F_{b_n,b_n})$. $V_{tr(ne)}^{(be)}$ is the exact splitting-derived BE coupling, and $T_{tr(ne)}^{(be)}$ is the total BE coupling contribution using eq. (6.5).

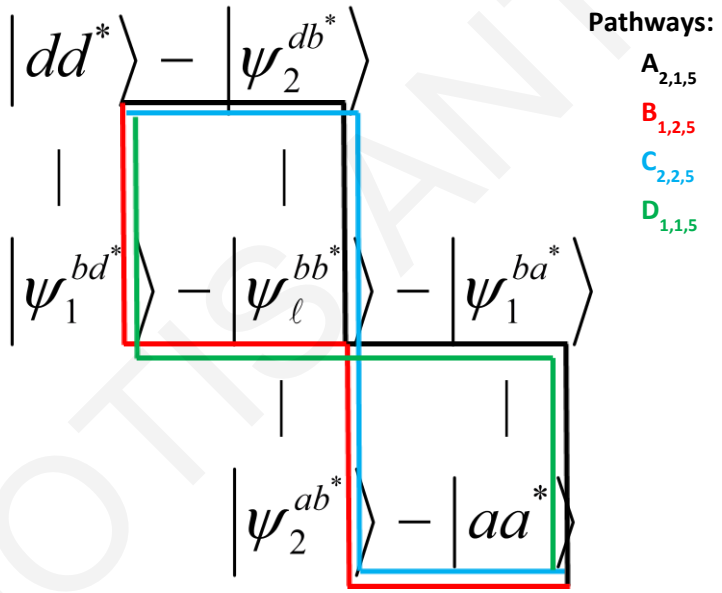

Figure 6.3: The scheme demonstrates the sum of the dominant pathways from $|d,d^*\rangle$ to $|a,a^*\rangle$ through the BE eigenstate basis manifold. The first pathway $A_{2,1,5}$ is $|d,d^*\rangle \rightarrow |\psi_2^{db^*}\rangle \rightarrow |\psi_\ell^{bb^*}\rangle \rightarrow |\psi_1^{ba^*}\rangle \rightarrow |a,a^*\rangle$, the second pathway $B_{1,2,5}$ is $|d,d^*\rangle \rightarrow |\psi_1^{bd^*}\rangle \rightarrow |\psi_\ell^{bb^*}\rangle \rightarrow |\psi_2^{ab^*}\rangle \rightarrow |a,a^*\rangle$, the third pathway $C_{2,2,5}$ is $|d,d^*\rangle \rightarrow |\psi_2^{db^*}\rangle \rightarrow |\psi_\ell^{bb^*}\rangle \rightarrow |\psi_2^{ab^*}\rangle \rightarrow |a,a^*\rangle$, and the fourth pathway $D_{1,1,5}$ is $|d,d^*\rangle \rightarrow |\psi_1^{bd^*}\rangle \rightarrow |\psi_\ell^{bb^*}\rangle \rightarrow |\psi_1^{ba^*}\rangle \rightarrow |a,a^*\rangle$.

6.2 Single-Particle Dexter Energy Transfer Pathways Analysis in a Local Basis

In this section we develop simple D-B-A models to illustrate analytically single-particle Dexter energy transfer pathways. Through this analysis we intend to obtain an intuition for the single-particle pathway expressions of the total Dexter coupling and, further, to demonstrate the bridge-exciton pathways dominance in the coupling as the bridge length increases. In the following we will use the formulation developed in the previous Chapter for the single-particle DAE-mediated $\left(T_{tr(ne)}^{(dae)}\right)$ and BE-mediated $\left(T_{tr(ne)}^{(be)}\right)$ couplings, where the pure exchange interactions are ignored (given by eqs. (5.11) and (5.12)). Further, we will use the localized (NLMO) representation for the bridge electron and hole orbitals (i.e., the $\left|d,b_n^*\right\rangle$, $\left|b_n,b_m^*\right\rangle$ exciton representation, etc.), and lowest order perturbation theory in the off-diagonal matrix elements between localized orbitals.

6.2.1 One-Site Bridge

For a one-site bridge (Fig. 6.4) all $\hat{Q}_K$ are one-state projection operators, i.e.,

$$\hat{Q}_{db^*}=\left|d,b^*\right\rangle\left\langle d,b^*\right| \quad , \quad \hat{Q}_{bb^*}=\left|b,b^*\right\rangle\left\langle b,b^*\right|. \tag{6.14}$$

Therefore, $\hat{G}_{ix}\left(E_t\right)=\left(E_t-E_{ix}\right)^{-1}\left|i,x\right\rangle\left\langle i,x\right|$ and eqs. (5.11) and (5.12) simplify to

$$T_{tr(ne)}^{(dae)}\approx\frac{1}{\left(E_t-E_{da^*}\right)}\left[\frac{V_{d^*b^*}^{e}V_{a^*b^*}^{e}}{E_t-E_{db^*}}\right]\left[\frac{V_{db}^{h}V_{ab}^{h}}{E_t-E_{ba^*}}\right]+\frac{1}{\left(E_t-E_{ad^*}\right)}\left[\frac{V_{db}^{h}V_{ab}^{h}}{E_t-E_{bd^*}}\right]\left[\frac{V_{d^*b^*}^{e}V_{a^*b^*}^{e}}{E_t-E_{ab^*}}\right], \tag{6.15}$$

and

$$\begin{aligned}T_{tr(ne)}^{(be)}\approx&\frac{1}{\left(E_t-E_{bb^*}\right)}\left[\frac{V_{d^*b^*}^{e}V_{db}^{h}}{E_t-E_{db^*}}\right]\left[\frac{V_{a^*b^*}^{e}V_{ab}^{h}}{E_t-E_{ba^*}}\right]+\frac{1}{\left(E_t-E_{bb^*}\right)}\left[\frac{V_{db}^{h}V_{d^*b^*}^{e}}{E_t-E_{bd^*}}\right]\left[\frac{V_{ab}^{h}V_{a^*b^*}^{e}}{E_t-E_{ab^*}}\right]\\&+\frac{1}{\left(E_t-E_{bb^*}\right)}\left[\frac{V_{d^*b^*}^{e}V_{db}^{h}}{E_t-E_{db^*}}\right]\left[\frac{V_{ab}^{h}V_{a^*b^*}^{e}}{E_t-E_{ab^*}}\right]+\frac{1}{\left(E_t-E_{bb^*}\right)}\left[\frac{V_{db}^{h}V_{d^*b^*}^{e}}{E_t-E_{bd^*}}\right]\left[\frac{V_{a^*b^*}^{e}V_{ab}^{h}}{E_t-E_{ba^*}}\right].\end{aligned} \tag{6.16}$$

It should be noted that the energy gaps $E_t - E_{ix}$ in the equations above contain both one-particle (electron and hole) and two-particle (electron-hole Coulomb attraction) contributions since $E_{ix} = \langle i,x|\hat{h}^{(di)}|i,x\rangle = F_{x,x} - F_{i,i} - (ii|xx)$.

Equations (6.15) and (6.16) show the lowest-order DA-CT and BE pathways contributions to the $|d,d^*\rangle$-to-$|a,a^*\rangle$ coupling. In this model there is one bridge exciton state $|b,b^*\rangle$ and two DA CT exciton states, $|d,a^*\rangle$ and $|a,d^*\rangle$. However, the number of pathways that visit the DA CT exciton states are less than the pathways that avoid these states and visit the BE state.

(a)

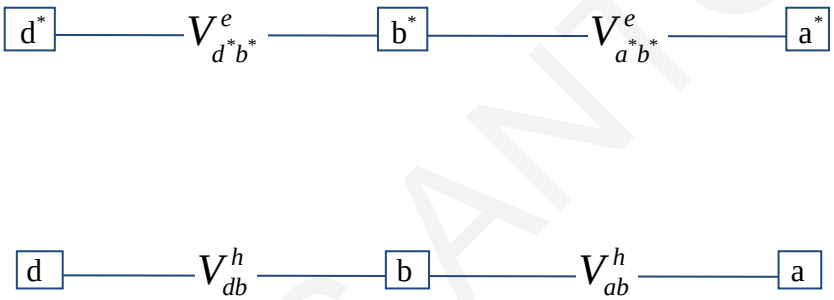

(b)

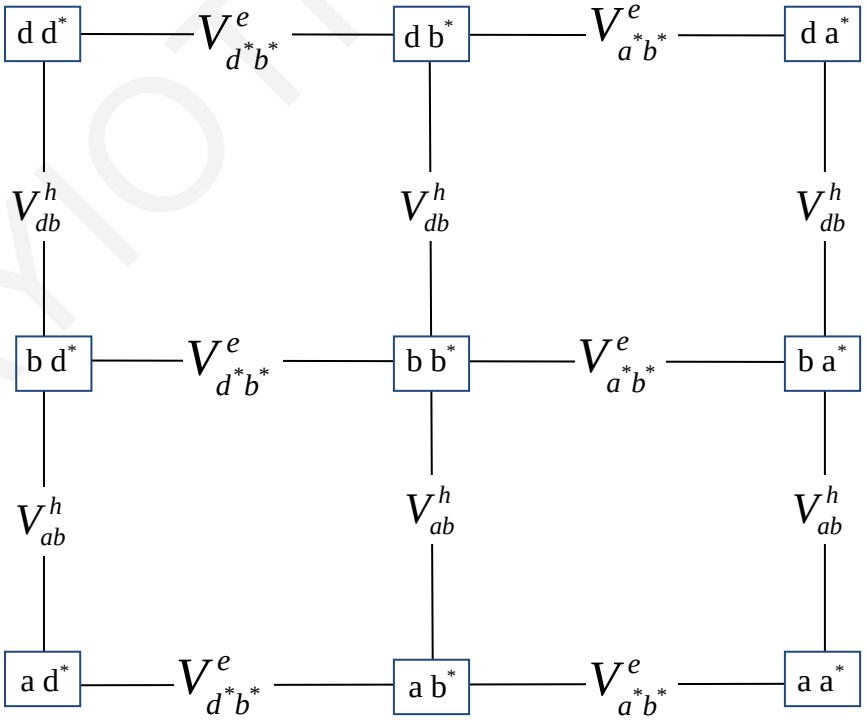

Figure 6.4: (a) Electron and hole transfer couplings for a linear one-site bridge system. (b) Exciton subspaces in local basis (NLMOs) and the coupling topology between the subspaces.

To simplify the expressions, we define $\Delta E_{CT} = E_t - E_{da^*} = E_t - E_{ad^*}$, where $E_t = E_{dd^*} = E_{aa^*}$ and replace individual state energy gaps by average ones, i.e., we assume that $\Delta E_{ET} = E_t - E_{db^*} = E_t - E_{ab^*}$, $\Delta E_{HT} = E_t - E_{ba^*} = E_t - E_{bd^*}$ and $\Delta E_{BE} = E_t - E_{bb^*}$ and eqs. (6.15) and (6.16) become

$$T_{tr(ne)}^{(dae)} \approx \frac{2}{\Delta E_{CT}} \left[\frac{V_{d^*b^*}^e V_{a^*b^*}^e}{\Delta E_{ET}} \right] \left[\frac{V_{db}^h V_{ab}^h}{\Delta E_{HT}} \right], \tag{6.17}$$

and

$$T_{tr(ne)}^{(be)} \approx \frac{2}{\Delta E_{BE}} \left[\frac{V_{d^*b^*}^e V_{a^*b^*}^e V_{db}^h V_{ab}^h}{\Delta E_{ET}\, \Delta E_{HT}} \right] + \frac{1}{\Delta E_{BE}} \left[\frac{V_{d^*b^*}^e V_{a^*b^*}^e V_{db}^h V_{ab}^h}{\Delta E_{ET}\, \Delta E_{ET}} \right] + \frac{1}{\Delta E_{BE}} \left[\frac{V_{d^*b^*}^e V_{a^*b^*}^e V_{db}^h V_{ab}^h}{\Delta E_{HT}\, \Delta E_{HT}} \right]. \tag{6.18}$$

Assuming $\Delta E_{HT} \approx \Delta E_{ET}$, we find that $T_{tr(ne)}^{(be)} \approx T_{tr(ne)}^{(dae)}$ if $\Delta E_{BE} \approx 2\Delta E_{CT}$. Therefore, the BE pathways and the DA CT exciton pathways can be of similar magnitude even for a single bridge unit. The DA CT exciton pathway coupling (eq. 6.17) is proportional to the product of electron and hole couplings, or the lowest-order perturbation theory couplings of electron- and hole-mediated ET theory [1-7]. However, the BE coupling (eq. 6.18) contains mixed electron and hole energy denominators, so the Dexter coupling is not always simply proportional to the product of the electron and hole couplings. We show below that the relative dominance of these competing terms is bridge-length dependent.

6.2.2 Linear Two-Site Bridge with Nearest Neighbor Couplings

We now examine a linear two-site bridge with nearest-neighbor couplings indicated in Fig. 6.5. From eqs. (5.11) and (5.12) we compute $T_{tr(ne)}^{(dae)}$ and $T_{tr(ne)}^{(be)}$ to lowest-order in $V^{(1p)}$ by writing $\hat{G}_K(E_t) = \left[E_t \hat{Q}_K - \hat{Q}_K \hat{H}^{(ne)} \hat{Q}_K \right]^{-1}$ as $\hat{G}_K(E_t) = \left[\hat{g}_K^{-1}(E_t) - \hat{Q}_K \hat{V}^{(1p)} \hat{Q}_K \right]^{-1}$, where $\hat{g}_K(E_t) = \left[E_t \hat{Q}_K - \hat{Q}_K \hat{h}^{(di)} \hat{Q}_K \right]^{-1}$ is the *K*-subspace Green's function corresponding to the diagonal part of the subspace Hamiltonian, eq. (5.5). Substituting into eqs. (5.11) and (5.12) the perturbative expansion $\hat{G}_K(E_t) \approx \hat{g}_K(E_t) + \hat{g}_K(E_t) \hat{Q}_K \hat{V}^{(1p)} \hat{Q}_K \hat{g}_K(E_t) + \ldots$ we find

$$T_{tr(ne)}^{(dae)} \approx \frac{2}{\Delta E_{CT}}\left[\frac{V_{d^*b_1^*}^e V_{b_1^*b_2^*}^e V_{a^*b_2^*}^e V_{db_1}^h V_{b_1b_2}^h V_{ab_2}^h}{\Delta E_{ET}^2\,\Delta E_{HT}^2}\right], \tag{6.19}$$

i.e., two lowest-order DA exciton pathways, and

$$\begin{aligned}
T_{tr(ne)}^{(be)} \approx & \left[\frac{V_{d^*b_1^*}^e V_{db_1}^h}{\Delta E_{ET}} + \frac{V_{d^*b_1^*}^e V_{db_1}^h}{\Delta E_{HT}}\right]\left[\frac{2V_{b_1^*b_2^*}^e V_{b_1b_2}^h}{\Delta E_{BE}^3}\right]\left[\frac{V_{a^*b_2^*}^e V_{ab_2}^h}{\Delta E_{ET}} + \frac{V_{a^*b_2^*}^e V_{ab_2}^h}{\Delta E_{HT}}\right] \\
& + \left[\frac{V_{d^*b_1^*}^e V_{db_1}^h}{\Delta E_{ET}} + \frac{V_{d^*b_1^*}^e V_{db_1}^h}{\Delta E_{HT}}\right]\left[\frac{V_{b_1^*b_2^*}^e}{\Delta E_{BE}^2}\right]\left[\frac{V_{a^*b_2^*}^e V_{b_1b_2}^h V_{ab_2}^h}{\Delta E_{HT}^2}\right] \\
& + \left[\frac{V_{d^*b_1^*}^e V_{db_1}^h}{\Delta E_{ET}} + \frac{V_{d^*b_1^*}^e V_{db_1}^h}{\Delta E_{HT}}\right]\left[\frac{V_{b_1b_2}^h}{\Delta E_{BE}^2}\right]\left[\frac{V_{ab_2}^h V_{b_1^*b_2^*}^e V_{a^*b_2^*}^e}{\Delta E_{ET}^2}\right] \\
& + \left[\frac{V_{db_1}^h V_{b_1b_2}^h V_{d^*b_1^*}^e}{\Delta E_{HT}^2}\right]\left[\frac{V_{b_1^*b_2^*}^e}{\Delta E_{BE}^2}\right]\left[\frac{V_{a^*b_2^*}^e V_{ab_2}^h}{\Delta E_{ET}} + \frac{V_{a^*b_2^*}^e V_{ab_2}^h}{\Delta E_{HT}}\right] \\
& + \left[\frac{V_{d^*b_1^*}^e V_{b_1^*b_2^*}^e V_{db_1}^h}{\Delta E_{ET}^2}\right]\left[\frac{V_{b_1b_2}^h}{\Delta E_{BE}^2}\right]\left[\frac{V_{a^*b_2^*}^e V_{ab_2}^h}{\Delta E_{ET}} + \frac{V_{a^*b_2^*}^e V_{ab_2}^h}{\Delta E_{HT}}\right] \\
& + \left[\frac{V_{db_1}^h V_{b_1b_2}^h V_{d^*b_1^*}^e}{\Delta E_{HT}^2}\right]\left[\frac{1}{\Delta E_{BE}}\right]\left[\frac{V_{ab_2}^h V_{b_1^*b_2^*}^e V_{a^*b_2^*}^e}{\Delta E_{ET}^2}\right] \\
& + \left[\frac{V_{d^*b_1^*}^e V_{b_1^*b_2^*}^e V_{db_1}^h}{\Delta E_{ET}^2}\right]\left[\frac{1}{\Delta E_{BE}}\right]\left[\frac{V_{a^*b_2^*}^e V_{b_1b_2}^h V_{ab_2}^h}{\Delta E_{HT}^2}\right],
\end{aligned} \tag{6.20}$$

i.e., eighteen lowest-order BE pathways that involve at least one bridge-exciton state and no DA excitons. Here, $\Delta E_{CT} = E_t - E_{da^*} = E_t - E_{ad^*}$, where $E_t = E_{dd^*} = E_{aa^*}$. To further simplify the expressions we replace individual state energy gaps by average ones, i.e., we assume that $\Delta E_{ET} = E_t - E_{db_i^*} = E_t - E_{ab_i^*}$, $\Delta E_{HT} = E_t - E_{b_ia^*} = E_t - E_{b_id^*}$ and $\Delta E_{BE} = E_t - E_{b_ib_j^*}$. The rapid growth of the number of bridge exciton pathways compared to the DA exciton pathways is reflected in the distance-dependence of the coupling.

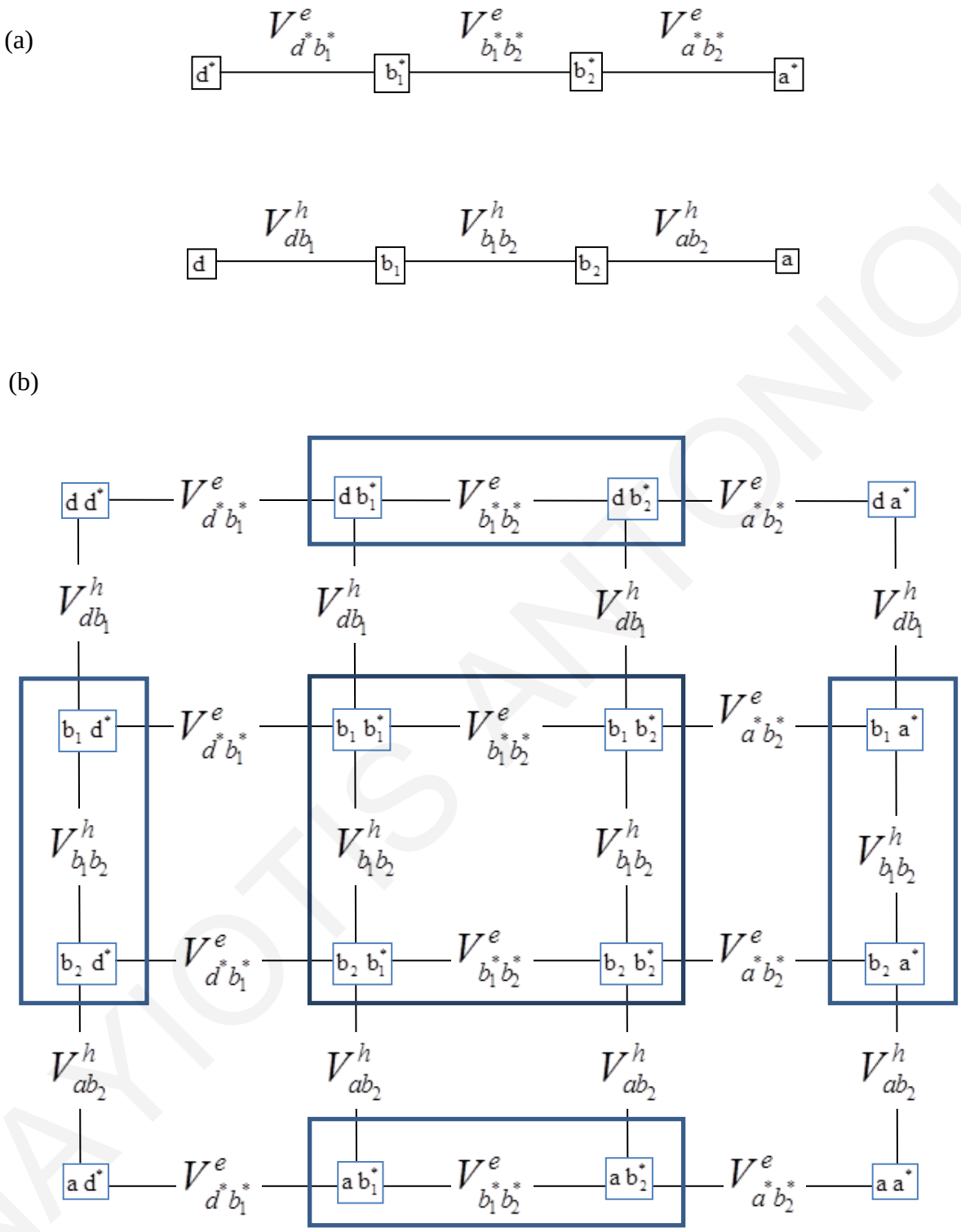

Figure 6.5: (a) Electron and hole transfer couplings for a linear two-site bridge system. (b) Exciton subspaces in local basis (NLMOs) and the coupling topology between the subspaces.

6.2.3 Parallel Two-Site Bridge with Nearest Neighbor Couplings and no cross-talk

Chemical bridges consist of multiple coupling pathways that generate constructive and destructive interferences. Searching for correlations between ET pathway and EnT pathway interferences is promising, since the structural basis of pathway interference effects in single-particle transfer (SPT) is well understood [8-15]. A popular model for SPT pathway interferences (ET or HT) is the double-slit parallel bridge with two-bridge units and no cross-talk [15,16] (e.g., Fig. 6.6). For example, if in this model system with parallel SPT ET pathway amplitudes of opposite signs and parallel SPT HT pathway amplitudes of the same signs, the ET pathways interfere destructively while the HT pathways interfere constructively. As a result, the effective SPT couplings $\left\langle d^* \left| \hat{V}^e \hat{G}_B \hat{V}^e \right| a^* \right\rangle \approx T^e_{d^* a^*} = 0$ and $\left\langle d \left| \hat{V}^h \hat{G}_B \hat{V}^h \right| a \right\rangle \approx T^h_{da} \neq 0$, where $\hat{G}_B = \left(E_t \hat{I}_B - \hat{H}_B \right)^{-1}$ is the single-particle bridge GF ($\hat{H}_B$ is the bridge Hamiltonian and E_t is the electron- or hole-tunneling energy).

Thus we now consider a parallel two-site bridge with no couplings between the two bridge units as shown in Fig. 6.6. From eqs. (5.11) and (5.12) we find

$$T^{(dae)}_{tr(ne)} \approx \frac{2}{\Delta E_{CT}} \left[\frac{V^e_{d^* b_1^*} V^e_{a^* b_1^*} + V^e_{d^* b_2^*} V^e_{a^* b_2^*}}{\Delta E_{ET}} \right] \left[\frac{V^h_{db_1} V^h_{ab_1} + V^h_{db_2} V^h_{ab_2}}{\Delta E_{HT}} \right], \tag{6.21}$$

i.e., eight lowest-order DA exciton pathways (shown in Figs. 6.7 and 6.8), and

$$\begin{aligned} T^{(be)}_{tr(ne)} \approx & \left[\frac{V^e_{d^* b_1^*}}{\Delta E_{ET}} \right] \left[\frac{V^h_{db_1} V^h_{ab_1} + V^h_{db_2} V^h_{ab_2}}{\Delta E_{BE}} \right] \left[\frac{V^e_{a^* b_1^*}}{\Delta E_{ET}} \right] + \left[\frac{V^e_{d^* b_2^*}}{\Delta E_{ET}} \right] \left[\frac{V^h_{db_1} V^h_{ab_1} + V^h_{db_2} V^h_{ab_2}}{\Delta E_{BE}} \right] \left[\frac{V^e_{a^* b_2^*}}{\Delta E_{ET}} \right] \\ & + \left[\frac{V^h_{db_1}}{\Delta E_{HT}} \right] \left[\frac{V^e_{d^* b_1^*} V^e_{a^* b_1^*} + V^e_{d^* b_2^*} V^e_{a^* b_2^*}}{\Delta E_{BE}} \right] \left[\frac{V^h_{ab_1}}{\Delta E_{HT}} \right] + \left[\frac{V^h_{db_2}}{\Delta E_{HT}} \right] \left[\frac{V^e_{d^* b_1^*} V^e_{a^* b_1^*} + V^e_{d^* b_2^*} V^e_{a^* b_2^*}}{\Delta E_{BE}} \right] \left[\frac{V^h_{ab_2}}{\Delta E_{HT}} \right] \\ & + \left[\frac{V^e_{d^* b_1^*}}{\Delta E_{ET}} \right] \left[\frac{V^h_{db_1} V^e_{a^* b_1^*}}{\Delta E_{BE}} \right] \left[\frac{V^h_{ab_1}}{\Delta E_{HT}} \right] + \left[\frac{V^e_{d^* b_1^*}}{\Delta E_{ET}} \right] \left[\frac{V^h_{db_2} V^e_{a^* b_1^*}}{\Delta E_{BE}} \right] \left[\frac{V^h_{ab_2}}{\Delta E_{HT}} \right] \\ & + \left[\frac{V^e_{d^* b_2^*}}{\Delta E_{ET}} \right] \left[\frac{V^h_{db_1} V^e_{a^* b_2^*}}{\Delta E_{BE}} \right] \left[\frac{V^h_{ab_1}}{\Delta E_{HT}} \right] + \left[\frac{V^e_{d^* b_2^*}}{\Delta E_{ET}} \right] \left[\frac{V^h_{db_2} V^e_{a^* b_2^*}}{\Delta E_{BE}} \right] \left[\frac{V^h_{ab_2}}{\Delta E_{HT}} \right] \end{aligned} \tag{6.22}$$

$$+\left[\frac{V^h_{db_1}}{\Delta E_{HT}}\right]\left[\frac{V^e_{d^*b_1^*}V^h_{ab_1}}{\Delta E_{BE}}\right]\left[\frac{V^e_{a^*b_1^*}}{\Delta E_{ET}}\right]+\left[\frac{V^h_{db_1}}{\Delta E_{HT}}\right]\left[\frac{V^e_{d^*b_2^*}V^h_{ab_1}}{\Delta E_{BE}}\right]\left[\frac{V^e_{a^*b_2^*}}{\Delta E_{ET}}\right]$$
$$+\left[\frac{V^h_{db_2}}{\Delta E_{HT}}\right]\left[\frac{V^e_{d^*b_1^*}V^h_{ab_2}}{\Delta E_{BE}}\right]\left[\frac{V^e_{a^*b_1^*}}{\Delta E_{ET}}\right]+\left[\frac{V^h_{db_2}}{\Delta E_{HT}}\right]\left[\frac{V^e_{d^*b_2^*}V^h_{ab_2}}{\Delta E_{BE}}\right]\left[\frac{V^e_{a^*b_2^*}}{\Delta E_{ET}}\right],$$

i.e., sixteen lowest-order BE pathways (shown in Figs. 6.9 to 6.12).

If, in the system of Fig. 6.6, we set $V^e_{d^*b_1^*}=V^e$ and $V^e_{d^*b_2^*}=-V^e$ (with $V^e_{a^*b_1^*}=V^e_{a^*b_2^*}=V^e$, $V^h_{db_1}=V^h_{db_2}=V^h$ and $V^h_{ab_1}=V^h_{ab_2}=V^h$), then $T^{(dae)}_{tr(ne)}=0$ in eq. (6.21) (Figs. 6.7 and 6.8) and $T^{(be)}_{tr(ne)}=0$ in eq. (6.22) (Figs. 6.9 to 6.12). Therefore, in a parallel double-slit bridge, destructive interferences that reduce single ET $\left(T^e_{d^*a^*}\right)$ or HT $\left(T^h_{da}\right)$ interactions will also reduce the EnT coupling $T_{tr(ne)}$. Although couplings will depend on structure, this example demonstrates the power of triplet EnT pathway analysis.

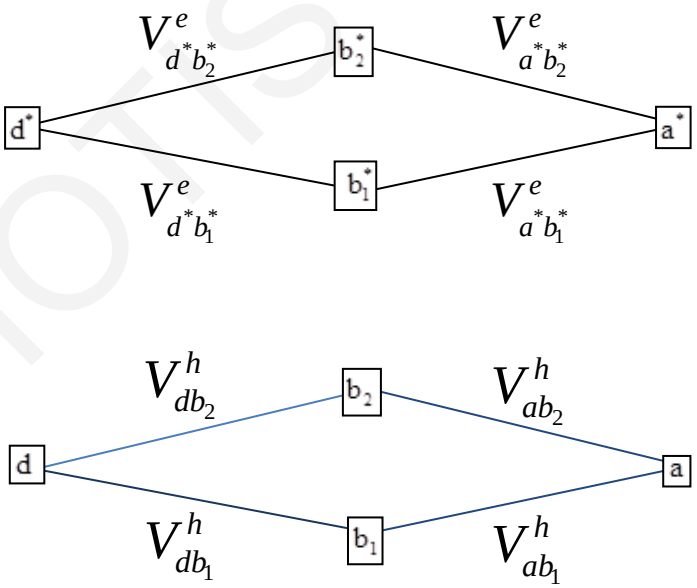

Figure 6.6: Nearest neighbor parallel two-bridge site-system without cross-talk that supports both ET (top, black) and HT (bottom blue) pathways. The color scheme is used in the following figures to distinguish between ET-mediated and HT-mediated exciton pathways.

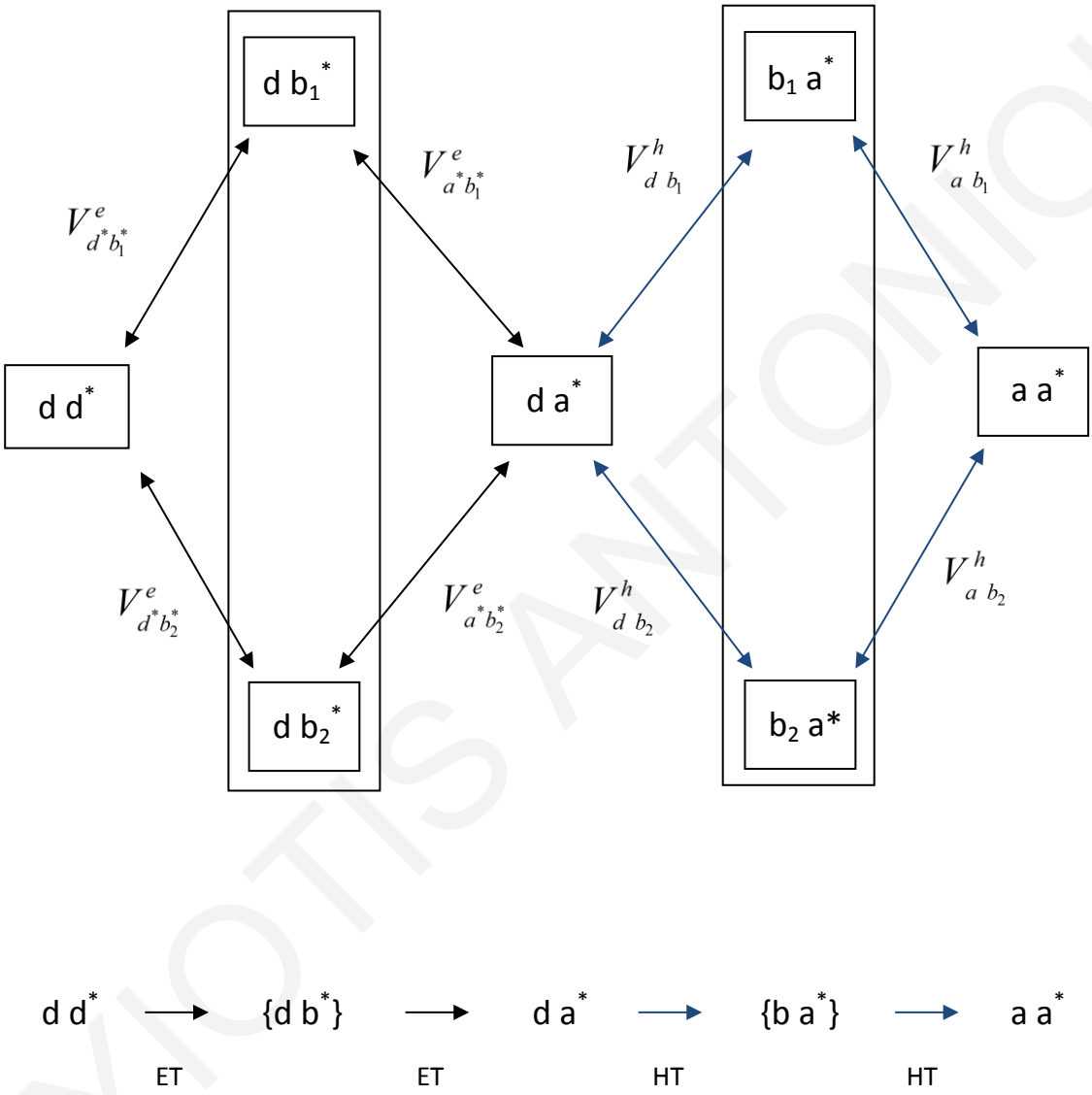

Figure 6.7: Lowest-order DA-CT exciton pathways for the parallel two-bridge-site system of Fig. 6.6 (eq. (6.21)). The diagrams show the four pathways that involve the $D^{+}BA^{-}$ intermediate.

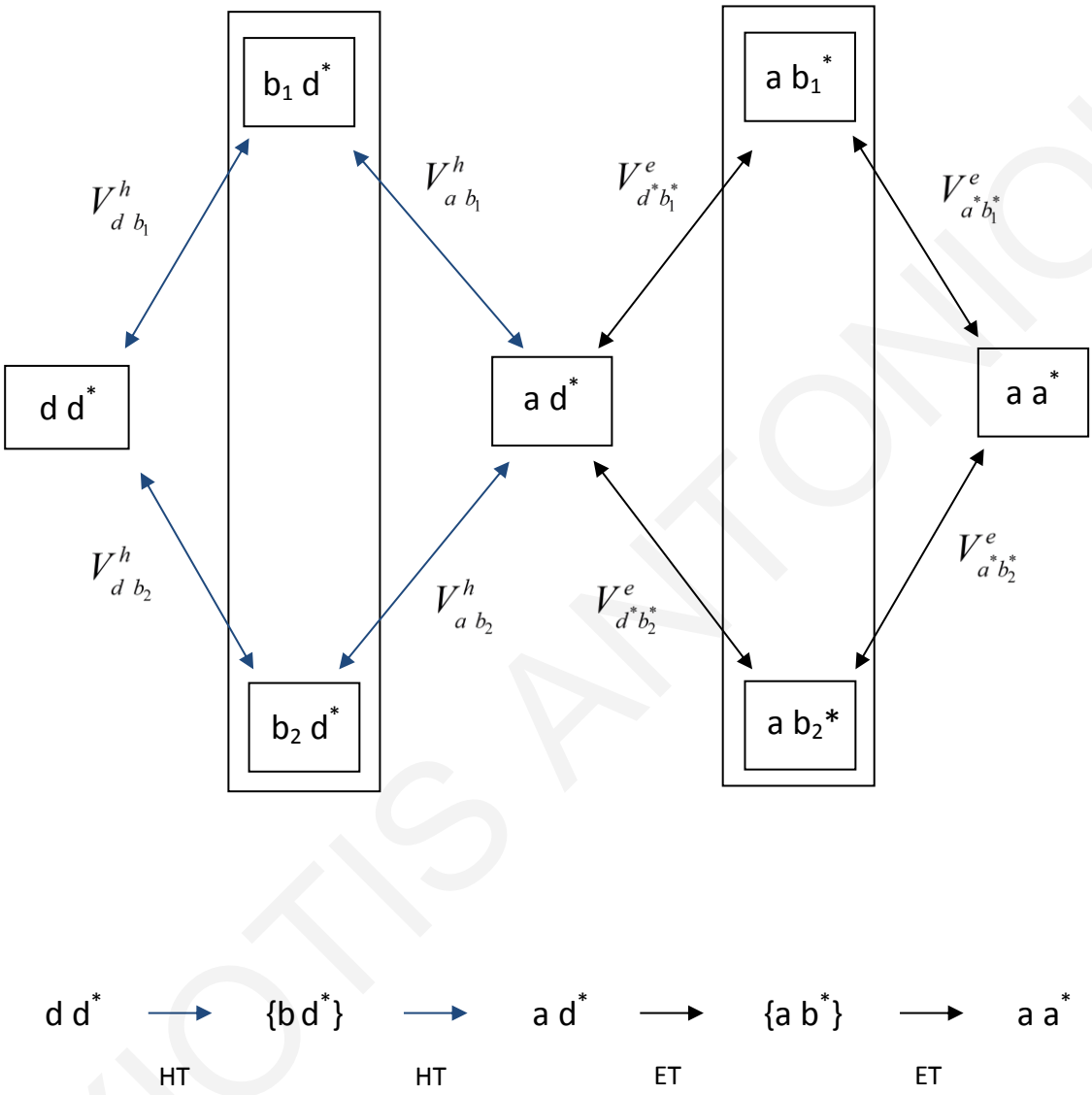

Figure 6.8: Lowest-order DA-CT exciton pathways for the parallel two-bridge-site system of Fig. 6.6 (eq. (6.21)). The diagrams show the four pathways that involve the $D^{-}BA^{+}$ intermediate.

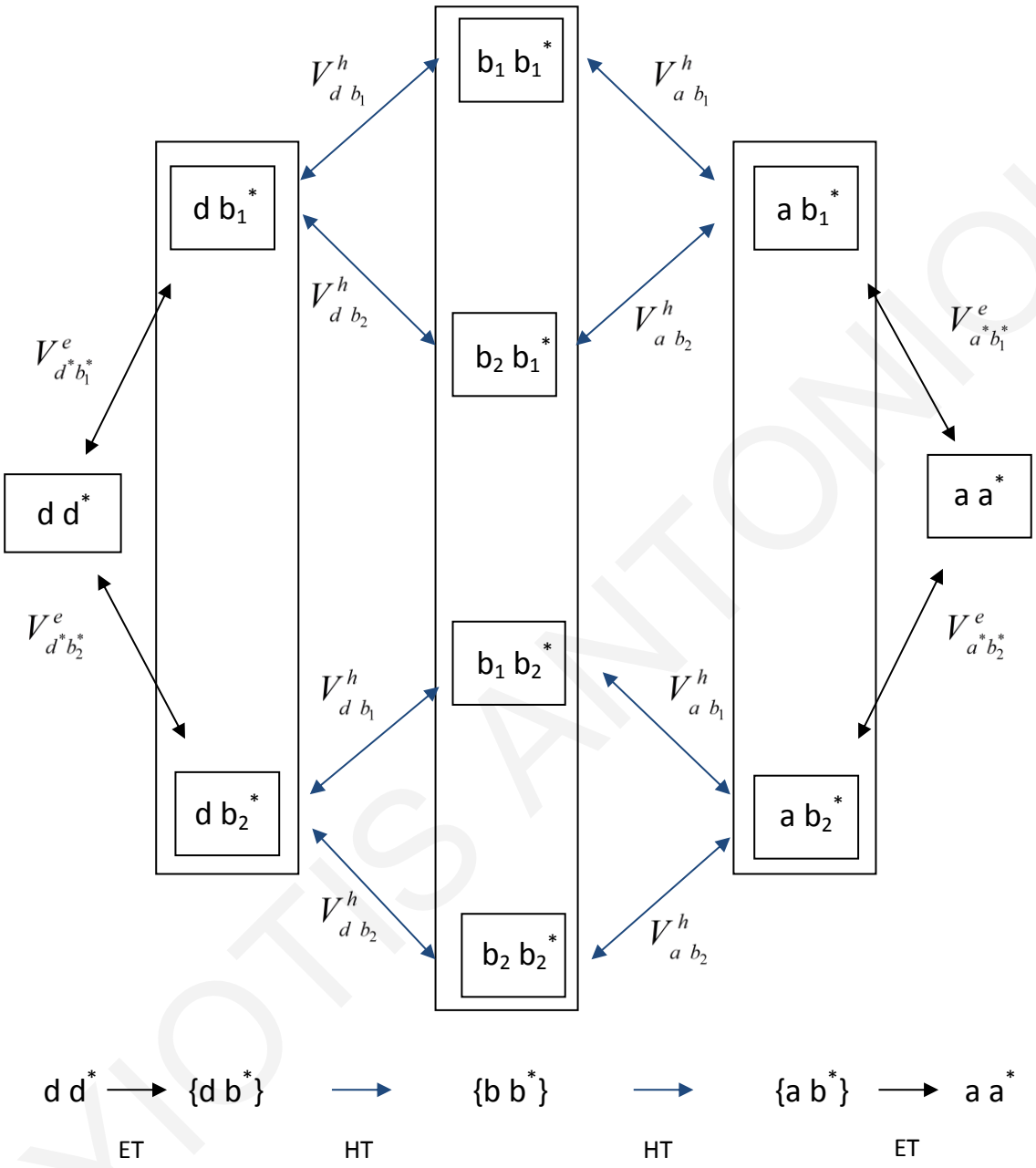

Figure 6.9: Lowest-order bridge-exciton pathways for the parallel two-bridge-site system of Fig. 6.6 (eq. (6.22)). The diagrams show the first and second terms of eq. (6.22) (four pathways).

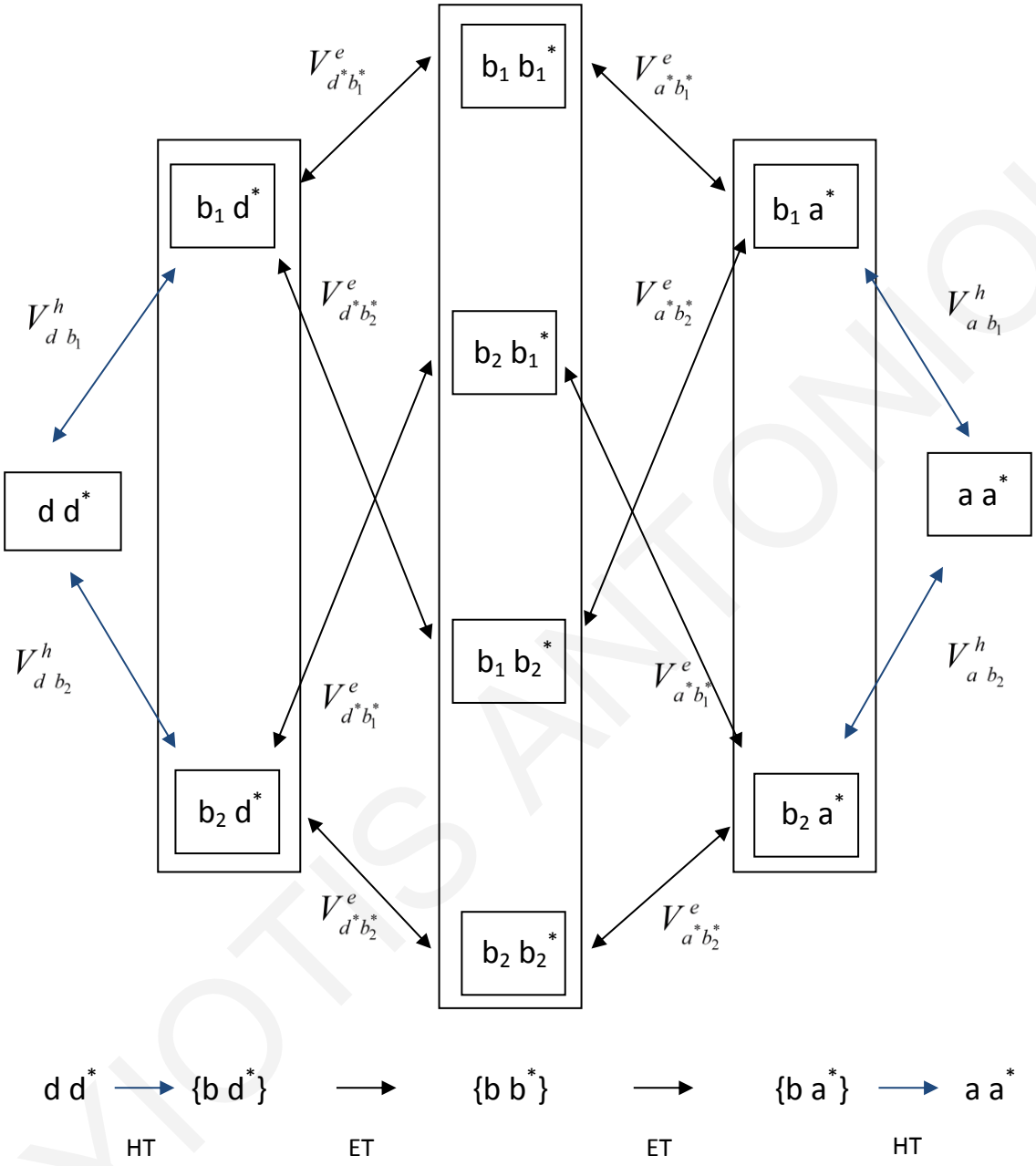

Figure 6.10: Lowest-order bridge-exciton pathways for the parallel two-bridge-site system of Fig. 6.6 (eq. (6.22)). The diagrams show the third and fourth terms of eq. (6.22) (four pathways).

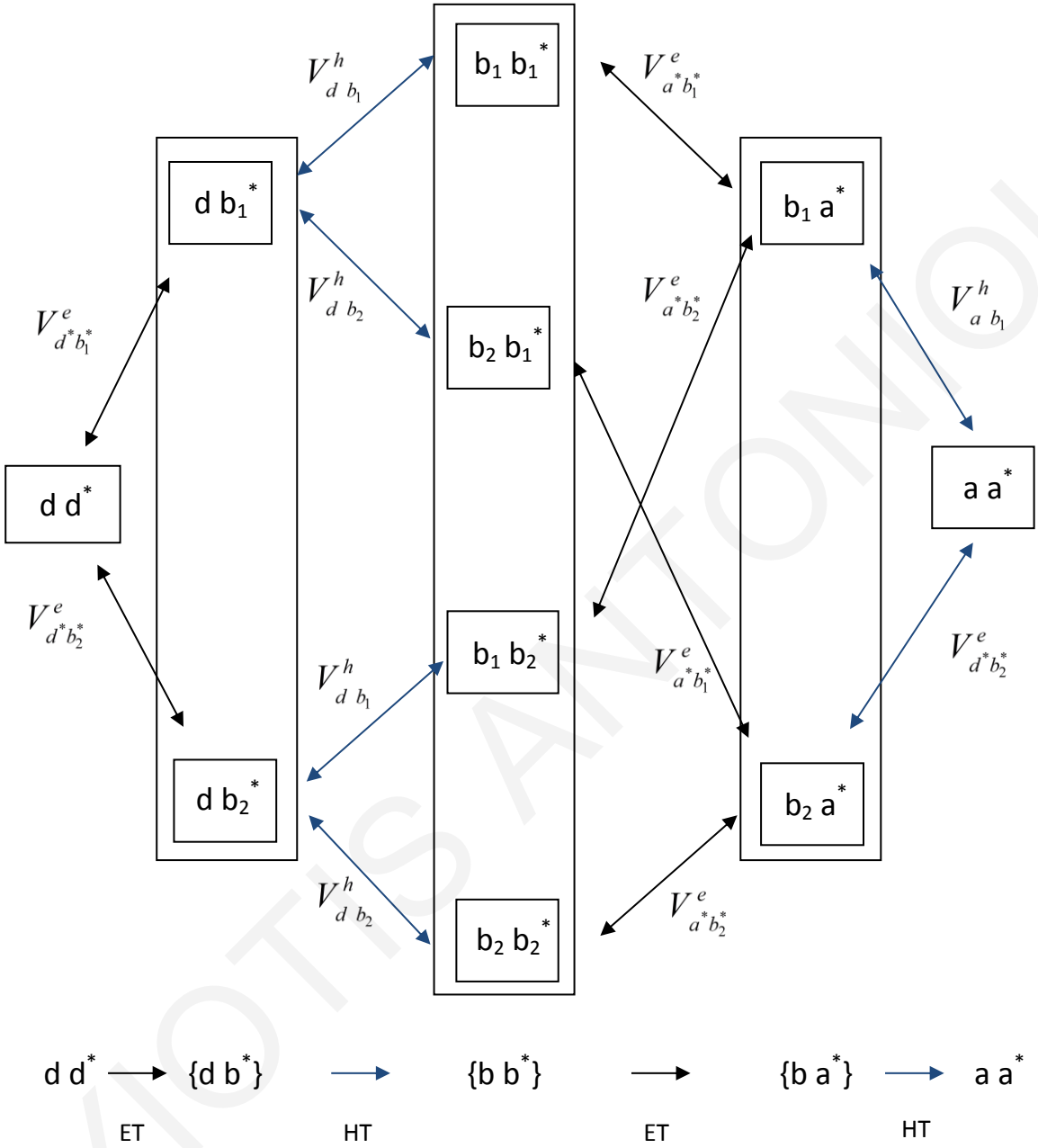

Figure 6.11: Lowest-order bridge-exciton pathways for the parallel two-bridge-site system of Fig. 6.6 (eq. (6.22)). The diagrams show the fifth to eighth terms of eq. (6.22) (four pathways).

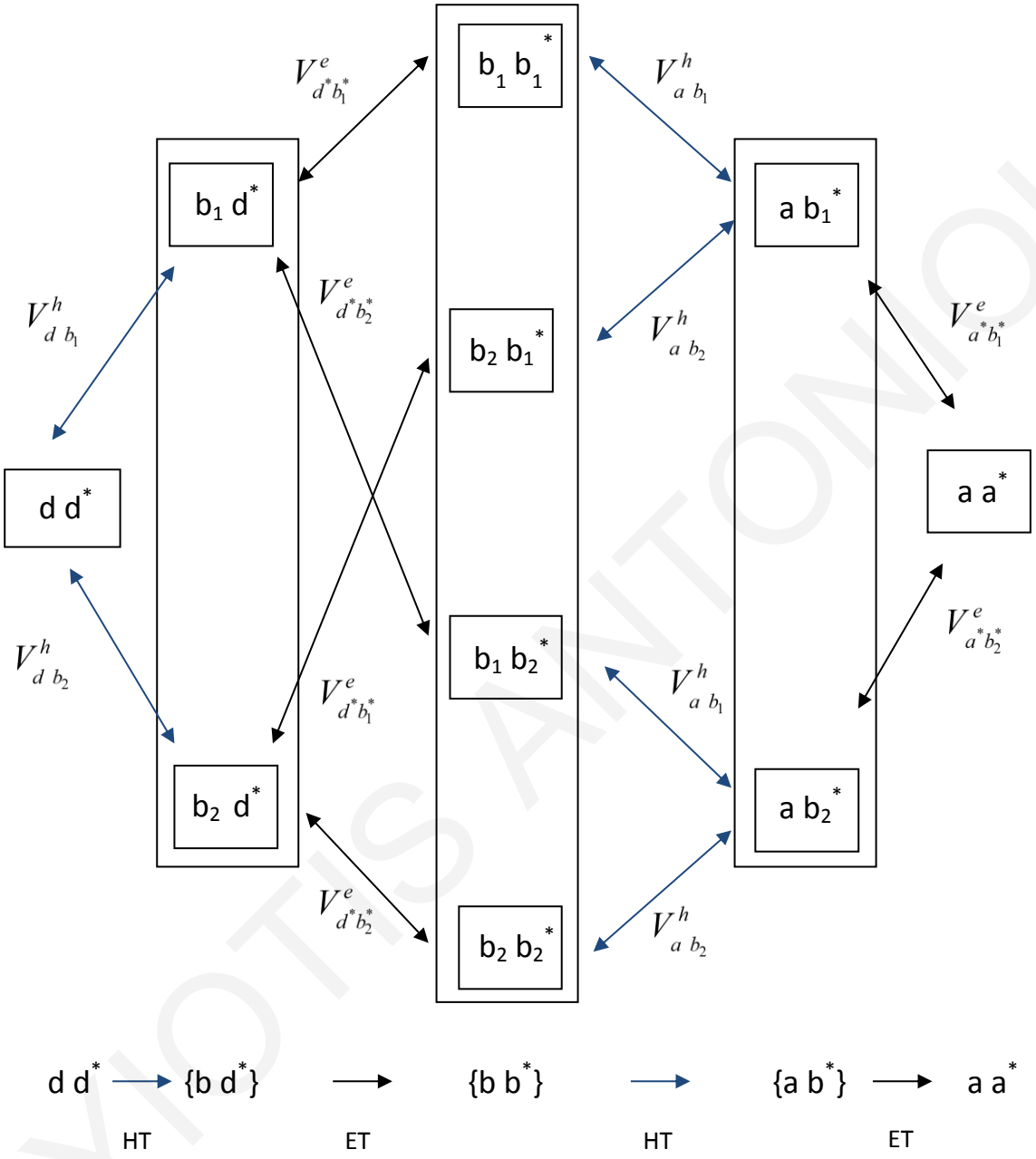

Figure 6.12: Lowest-order bridge-exciton pathways for the parallel two-bridge-site system of Fig. 6.6 (eq. (6.22)). The diagrams show the 9th to 12th terms of eq. (6.22) (four pathways).

6.2.4 *N*-Site Bridge

As the number of bridge sites increases, the contribution to the overall EnT coupling arising from BE pathways increases rapidly and dominates the coupling. For a bridge with *N*-sites, there are many classes of BE pathways distinguished by the number of bridge exciton states $\left|b_n, b_m^*\right\rangle$ that are visited to lowest order in $\hat{V}^e$ and $\hat{V}^h$. For a nearest-neighbor *N*-site bridge model (Fig. 6.13a), the lowest-order BE pathway class with the maximum number of BE states is shown in Fig. 6.13b. The total contribution to the EnT coupling arising from this BE pathway class is given by

$$T_{tr(ne)}^{(be)} \approx \left[\frac{V_{d^*b^*}^e V_{db}^h}{\Delta E_{ET}} + \frac{V_{db}^h V_{d^*b^*}^e}{\Delta E_{HT}}\right] \times BE \times \left[\frac{V_{a^*b^*}^e V_{ab}^h}{\Delta E_{HT}} + \frac{V_{ab}^h V_{a^*b^*}^e}{\Delta E_{ET}}\right], \tag{6.23}$$

where

$$BE \approx \binom{2N}{N} \frac{\left(V_{b^*b^*}^e\right)^{N-1}\left(V_{bb}^h\right)^{N-1}}{\left(\Delta E_{BE}\right)^{2N-1}}. \tag{6.24}$$

We assumed that $E_{db_j^*} \approx E_{db^*}$ ($E_{ab_j^*} \approx E_{ab^*}$), $E_{b_j d^*} \approx E_{bd^*}$ ($E_{b_j a^*} \approx E_{ba^*}$) and $E_{b_i b_j^*} \approx E_{bb^*}$. E_t and the energy gaps ΔE are defined as above. This energy denominator absorbs the distance dependent Coulomb attraction energies for the many virtual states. There are thus $\binom{2N}{N} \approx \exp\left[+1.4N\right]$ (for large *N*) bridge-exciton pathways in eq. (6.24).

For comparison, there are only two DA CT exciton pathways for the *N*-bridge-site system that contribute a coupling of

$$T_{tr(ne)}^{(dae)} \approx \frac{2}{\Delta E_{CT}} \left[\frac{V_{d^*b^*}^e \left(V_{b^*b^*}^e\right)^{N-1} V_{a^*b^*}^e}{\left(\Delta E_{ET}\right)^N}\right]\left[\frac{V_{db}^h \left(V_{bb}^h\right)^{N-1} V_{ab}^h}{\left(\Delta E_{HT}\right)^N}\right]. \tag{6.25}$$

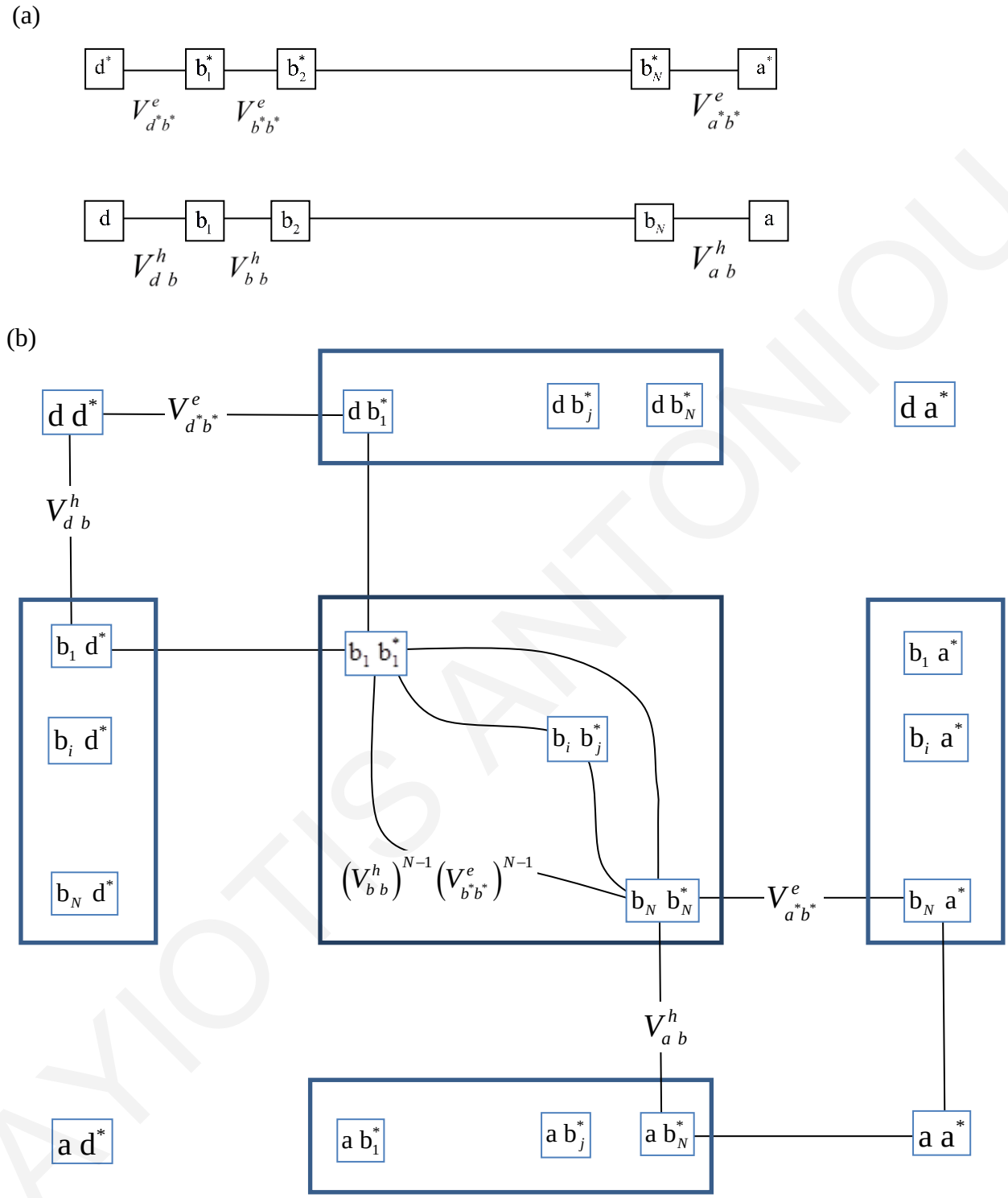

Figure 6.13: (a) Model of a linear *N*-site bridge with nearest-neighbor couplings that support through-bridge ET (top) and through-bridge HT (bottom). (b) Diagram showing the total contribution of those lowest-order BE pathways that visit the maximum number of BE states $\left|b_n, b_m^*\right\rangle$. The number of lowest-order $\left|b_1, b_1^*\right\rangle$-to-$\left|b_N, b_N^*\right\rangle$ paths within the BE subspace (central box) grows exponentially with *N*.

6.3 Double-Particle Exchange Energy Transfer Pathways Analysis in Local Basis

Here, we establish a pathway decomposition of the two-particle exchange components $\left(D^*A^*\left|DA\right.\right)$ of the total Dexter coupling (ignored in the previous Sections). The pathway analysis of $\left(D^*A^*\left|DA\right.\right)$ enables the development of structure function relations for the exchange interactions.

6.3.1 Dexter Energy Transfer through a Single Bridge Site

The exchange contribution to the D-to-A triplet EnT coupling (second term of eq. (5.2)), is given by

$$T_{tr(ex)} \equiv \left(D^*A^*\left|DA\right.\right) = \int d^3r_1 \int d^3r_2 \; S^e_{D^*A^*}\left(\vec{r}_1\right)\left(\frac{e^2}{4\pi\varepsilon_0\left|\vec{r}_1-\vec{r}_2\right|}\right) S^h_{DA}\left(\vec{r}_2\right) . \tag{6.26}$$

The $\left|D\right\rangle$, $\left|D^*\right\rangle$ and $\left|A\right\rangle$, $\left|A^*\right\rangle$ denote diabatic orbitals that, in the tunneling regime, are mostly localized on the D and A fragments with tails on B (see Chapter 5). These orbitals can be written in a basis of zeroth-order orbitals that are fully localized on D, B, or A fragments; i.e., $\left|D\right\rangle \simeq \left|d\right\rangle + \left|\delta^{br}_D\right\rangle$, $\left|D^*\right\rangle \simeq \left|d^*\right\rangle + \left|\delta^{br}_{D^*}\right\rangle$, $\left|A\right\rangle \simeq \left|a\right\rangle + \left|\delta^{br}_A\right\rangle$ and $\left|A^*\right\rangle \simeq \left|a^*\right\rangle + \left|\delta^{br}_{A^*}\right\rangle$, where $\left|d\right\rangle$ ($\left|d^*\right\rangle$) and $\left|a\right\rangle$ ($\left|a^*\right\rangle$) are the zeroth-order D-localized and A-localized basis orbitals and $\left|\delta^{br}\right\rangle$ are the bridge tails. In eq. (6.26) $S^e_{D^*A^*}\left(\vec{r}_1\right) = \psi_{D^*}\left(\vec{r}_1\right)\psi_{A^*}\left(\vec{r}_1\right)$ and $S^h_{DA}\left(\vec{r}_2\right) = \psi_D\left(\vec{r}_2\right)\psi_A\left(\vec{r}_2\right)$ are overlap densities for the electron and hole donor and acceptor molecular orbitals, respectively (which are assumed real). $\psi_{D^*}\left(\vec{r}_1\right) = \left\langle \vec{r}_1 \middle| D^* \right\rangle$, $\psi_{A^*}\left(\vec{r}_1\right) = \left\langle \vec{r}_1 \middle| A^* \right\rangle$, etc., are orbital wavefunctions.

We use the chemists notation for the two-electron integrals

$$\left(i^*j^*\left|k\ell\right.\right) = \int d^3r_1 \int d^3r_2 \; \psi_{i^*}\left(\vec{r}_1\right)\psi_{j^*}\left(\vec{r}_1\right)\left(\frac{e^2}{4\pi\varepsilon_0\left|\vec{r}_1-\vec{r}_2\right|}\right)\psi_k\left(\vec{r}_2\right)\psi_\ell\left(\vec{r}_2\right) . \tag{6.27}$$

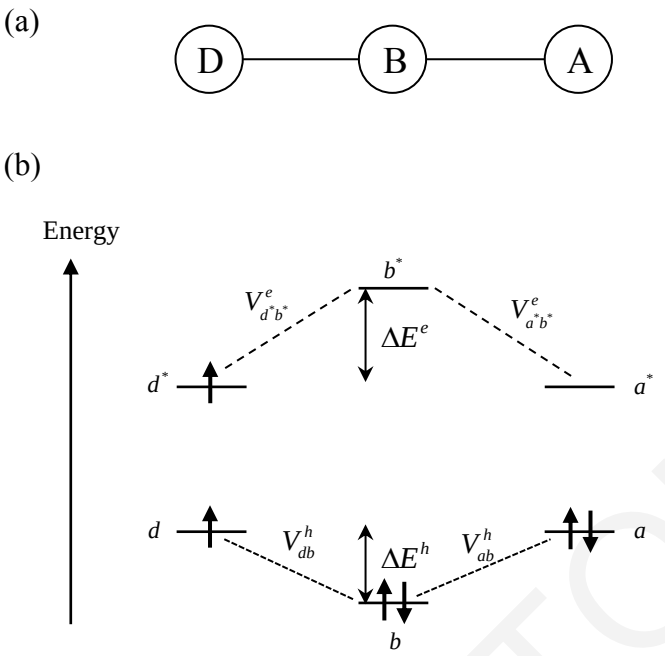

Figure 6.14: (a) D-B-A system with one bridge unit. (b) Model for comparing ET and HT donor-acceptor couplings to the triplet exciton (Dexter) donor-acceptor coupling.

A minimalistic D-B-A system model Hamiltonian consists of six zeroth-order orbitals, two for each site (Fig. 6.14) given by

$$\hat{H} = \hat{H}_D + \hat{H}_B + \hat{H}_A + \hat{V}_{\text{int}} \tag{6.28}$$

where,

$$\hat{H}_D = \varepsilon_d \left|d\right\rangle\left\langle d\right| + \varepsilon_{d^*} \left|d^*\right\rangle\left\langle d^*\right|, \tag{6.29a}$$

$$\hat{H}_B = \varepsilon_b \left|b\right\rangle\left\langle b\right| + \varepsilon_{b^*} \left|b^*\right\rangle\left\langle b^*\right|, \tag{6.29b}$$

$$\hat{H}_A = \varepsilon_a \left|a\right\rangle\left\langle a\right| + \varepsilon_{a^*} \left|a^*\right\rangle\left\langle a^*\right|, \tag{6.29c}$$

where ε_i, ε_{i^*} are the respective zeroth-order orbital energies for the ground and exited states. The interaction Hamiltonian $\hat{V}_{\text{int}} = \hat{V}^h + \hat{V}^e$ is given by

$$\hat{V}^h = V^h_{db}\left(\left|d\right\rangle\left\langle b\right| + \left|b\right\rangle\left\langle d\right|\right) + V^h_{ab}\left(\left|a\right\rangle\left\langle b\right| + \left|b\right\rangle\left\langle a\right|\right), \tag{6.30a}$$

$$\hat{V}^e = V^e_{d^*b^*}\left(\left|d^*\right\rangle\left\langle b^*\right| + \left|b^*\right\rangle\left\langle d^*\right|\right) + V^e_{a^*b^*}\left(\left|a^*\right\rangle\left\langle b^*\right| + \left|b^*\right\rangle\left\langle a^*\right|\right). \tag{6.30b}$$

The hole-mediated (V_{db}^{h}, V_{ab}^{h}) and electron-mediated ($V_{d^*b^*}^{e}$, $V_{a^*b^*}^{e}$) coupling elements are the donor-bridge and acceptor-bridge electronic interactions, and the direct D-to-A through-space interaction is assumed to be equal to zero ($V_{da}^{h} \approx 0$, $V_{d^*a^*}^{e} \approx 0$). We further assume that b and b^* orbitals are off resonance with d, d^*, a and a^* orbitals (Fig. 6.14). That is, all of the following values are much less than one $\left|V_{db}^{h}/\left(\varepsilon_b - \varepsilon_d\right)\right|$, $\left|V_{ab}^{h}/\left(\varepsilon_b - \varepsilon_a\right)\right|$, $\left|V_{d^*b^*}^{e}/\left(\varepsilon_{b^*} - \varepsilon_{d^*}\right)\right|$ and $\left|V_{a^*b^*}^{e}/\left(\varepsilon_{b^*} - \varepsilon_{a^*}\right)\right|$. As such, the D-to-A hole-mediated and electron-mediated couplings are weak through-bridge tunneling interactions.

In the electron and hole tunneling limit, we can use lowest-order perturbation theory in the donor-bridge and acceptor-bridge electronic interactions to describe the mixed D-B and B-A orbitals (i.e., $|D\rangle, |D^*\rangle, |A\rangle, |A^*\rangle$), identical to the lowest-order perturbation theory treatment for pure ET and HT [1-7]. Hence,

$$|D\rangle = |d\rangle - \frac{V_{db}^{h}}{\Delta E_{bd}^{h}}|b\rangle, \tag{6.31a}$$

$$|A\rangle = |a\rangle - \frac{V_{ab}^{h}}{\Delta E_{ba}^{h}}|b\rangle, \tag{6.31b}$$

and,

$$|D^*\rangle = |d^*\rangle + \frac{V_{d^*b^*}^{e}}{\Delta E_{b^*d^*}^{e}}|b^*\rangle, \tag{6.32a}$$

$$|A^*\rangle = |a^*\rangle + \frac{V_{a^*b^*}^{e}}{\Delta E_{b^*a^*}^{e}}|b^*\rangle. \tag{6.32b}$$

Here, $\Delta E_{ij}^{h} = \varepsilon_i - \varepsilon_j$ and $\Delta E_{i^*j^*}^{e} = \varepsilon_{i^*} - \varepsilon_{j^*}$. Substituting eq. (6.31) and (6.32) into eq. (6.26), and retaining terms up to fourth-order in the electronic couplings, we find the Dexter coupling up to fourth order in $V_{ij}/\Delta E_{ij}$

$$T_{tr(ex)} = \left(d^* a^* | da\right) + \sum_{i=1}^{4} T_{tr(ex)}(i). \tag{6.33}$$

In the equation above

$$T_{tr(ex)}(1) = -\left(\frac{V^h_{db}}{\Delta E^h_{bd}}\right)\left(d^*a^*\middle|ab\right) - \left(\frac{V^h_{ab}}{\Delta E^h_{ba}}\right)\left(d^*a^*\middle|db\right) + \left(\frac{V^e_{d^*b^*}}{\Delta E^e_{b^*d^*}}\right)\left(a^*b^*\middle|da\right) + \left(\frac{V^e_{a^*b^*}}{\Delta E^e_{b^*a^*}}\right)\left(d^*b^*\middle|da\right), \tag{6.34}$$

$$\begin{aligned} T_{tr(ex)}(2) = {} & \left(\frac{V^h_{db}}{\Delta E^h_{bd}}\right)\left(\frac{V^h_{ab}}{\Delta E^h_{ba}}\right)\left(d^*a^*\middle|bb\right) + \left(\frac{V^e_{d^*b^*}}{\Delta E^e_{b^*d^*}}\right)\left(\frac{V^e_{a^*b^*}}{\Delta E^e_{b^*a^*}}\right)\left(b^*b^*\middle|da\right) \\ & - \left(\frac{V^e_{a^*b^*}}{\Delta E^e_{b^*a^*}}\right)\left(\frac{V^h_{ab}}{\Delta E^h_{ba}}\right)\left(d^*b^*\middle|db\right) - \left(\frac{V^e_{a^*b^*}}{\Delta E^e_{b^*a^*}}\right)\left(\frac{V^h_{db}}{\Delta E^h_{bd}}\right)\left(d^*b^*\middle|ab\right) \\ & - \left(\frac{V^e_{d^*b^*}}{\Delta E^e_{b^*d^*}}\right)\left(\frac{V^h_{ab}}{\Delta E^h_{ba}}\right)\left(a^*b^*\middle|db\right) - \left(\frac{V^e_{d^*b^*}}{\Delta E^e_{b^*d^*}}\right)\left(\frac{V^h_{db}}{\Delta E^h_{bd}}\right)\left(a^*b^*\middle|ab\right), \end{aligned} \tag{6.35}$$

$$\begin{aligned} T_{tr(ex)}(3) = {} & \left(\frac{V^e_{a^*b^*}}{\Delta E^e_{b^*a^*}}\right)\left(\frac{V^h_{ab}}{\Delta E^h_{ba}}\right)\left(\frac{V^h_{db}}{\Delta E^h_{bd}}\right)\left(d^*b^*\middle|bb\right) \\ & + \left(\frac{V^e_{d^*b^*}}{\Delta E^e_{b^*d^*}}\right)\left(\frac{V^h_{ab}}{\Delta E^h_{ba}}\right)\left(\frac{V^h_{db}}{\Delta E^h_{bd}}\right)\left(a^*b^*\middle|bb\right) \\ & - \left(\frac{V^e_{a^*b^*}}{\Delta E^e_{b^*a^*}}\right)\left(\frac{V^e_{d^*b^*}}{\Delta E^e_{b^*d^*}}\right)\left(\frac{V^h_{ab}}{\Delta E^h_{ba}}\right)\left(b^*b^*\middle|db\right) \\ & - \left(\frac{V^e_{a^*b^*}}{\Delta E^e_{b^*a^*}}\right)\left(\frac{V^e_{d^*b^*}}{\Delta E^e_{b^*d^*}}\right)\left(\frac{V^h_{db}}{\Delta E^h_{bd}}\right)\left(b^*b^*\middle|ab\right), \end{aligned} \tag{6.36}$$

and

$$T_{tr(ex)}(4) = \left(\frac{V^e_{a^*b^*}}{\Delta E^e_{b^*a^*}}\right)\left(\frac{V^e_{d^*b^*}}{\Delta E^e_{b^*d^*}}\right)\left(\frac{V^h_{db}}{\Delta E^h_{bd}}\right)\left(\frac{V^h_{ab}}{\Delta E^h_{ba}}\right)\left(b^*b^*\middle|bb\right). \tag{6.37}$$

In simple electron tunneling, the lowest-order donor-acceptor coupling would be proportional to $V_{db}V_{ab}/\Delta E$ where ΔE is the tunneling energy gap between the quasi-degenerate donor and acceptor states and the nearest energy bridge orbital. In contrast, the lowest-order Dexter couplings contain two-electron integrals $\left(i^*j^*\middle|k\ell\right)$. The largest two-electron integrals describe Coulombic attraction between populations on the bridge and appear first in the fourth-order term $T_{tr(ex)}(4)$. Motivated by the neglect of differential

overlap (NDO) approximation, we could suggest that this fourth-order term dominates $T_{tr(ex)}$ because of its enhanced Coulomb integral and strongest overlap. In this approximation, $T_{tr(ex)} \approx T_{tr(ex)}(4)$. Interestingly, this term is the product of the bridge-mediated D-A ET tunneling matrix element and the HT tunneling matrix element

$$T^{e}_{d^*a^*} = \frac{V^{e}_{d^*b^*} V^{e}_{a^*b^*}}{\Delta E^{e}} \quad , \quad T^{h}_{da} = \frac{V^{h}_{db} V^{h}_{ab}}{\Delta E^{h}} \tag{6.38}$$

and the Coulomb integral $\left(b^*b^* \middle| bb\right)$, i.e.,

$$T_{tr(ex)}(4) = \left(\frac{T^{e}_{d^*a^*}}{\Delta E^{e}}\right)\left(\frac{T^{h}_{da}}{\Delta E^{h}}\right)\left(b^*b^* \middle| bb\right). \tag{6.39}$$

These expressions are the analogues of the lowest-order perturbation theory interactions for ET and HT [1-7], respectively. The hole and electron denominators are different, as there are two different "tunneling energies" rather than just one as would be the case in electron transfer. We assumed here that $\varepsilon_d = \varepsilon_a$ and $\varepsilon_{d^*} = \varepsilon_{a^*}$ such that $\Delta E^{h}_{bd} = \Delta E^{h}_{ba} = \Delta E^{h}$ and $\Delta E^{e}_{b^*d^*} = \Delta E^{e}_{b^*a^*} = \Delta E^{e}$.

6.3.2 Dexter Energy Transfer through a multi-site Bridge

Consider the multi-site linear bridges shown in Fig. 6.15. The total Hamiltonian is given by eq. (6.28), where the donor and acceptor Hamiltonians are

$$\hat{H}_D = \varepsilon_d \left|d\right\rangle\left\langle d\right| + \varepsilon_{d^*} \left|d^*\right\rangle\left\langle d^*\right|, \tag{6.40a}$$

$$\hat{H}_A = \varepsilon_a \left|a\right\rangle\left\langle a\right| + \varepsilon_{a^*} \left|a^*\right\rangle\left\langle a^*\right|, \tag{6.40b}$$

and the bridge Hamiltonian is

$$\hat{H}_B = \hat{H}^{h}_B + \hat{H}^{e}_B + \hat{V}^{h}_B + \hat{V}^{e}_B + \hat{V}^{eh}_B. \tag{6.41}$$

The bridge Hamiltonian is divided into electron, hole, and mixed electron-hole parts

$$\hat{H}^{h}_B = \sum_i \varepsilon_{b_i} \left|b_i\right\rangle\left\langle b_i\right| \quad , \quad \hat{H}^{e}_B = \sum_i \varepsilon_{b_i^*} \left|b_i^*\right\rangle\left\langle b_i^*\right|, \tag{6.42a}$$

$$\hat{V}_B^h = \sum_i \sum_j V_{b_i b_j}^h \left(\left| b_i \right\rangle \left\langle b_j \right| + \left| b_j \right\rangle \left\langle b_i \right| \right), \tag{6.42b}$$

$$\hat{V}_B^e = \sum_i \sum_j V_{b_i^* b_j^*}^e \left(\left| b_i^* \right\rangle \left\langle b_j^* \right| + \left| b_j^* \right\rangle \left\langle b_i^* \right| \right). \tag{6.42c}$$

We will assume that $\left| \left(\varepsilon_{b_i^*} - E_t^e \right) \right| \gg \left| \left(\varepsilon_{b_i} - E_t^h \right) \right|$ so that we may ignore electron-hole tunneling interaction, as is often assumed in ET and HT through large energy gap bridges [3,6,7,17].

The interaction Hamiltonian between donor (acceptor) and the bridge is $\hat{V}_{\text{int}} = \hat{V}^h + \hat{V}^e$ with

$$\hat{V}^h = \sum_i V_{db_i}^h \left(\left| d \right\rangle \left\langle b_i \right| + \left| b_i \right\rangle \left\langle d \right| \right) + \sum_i V_{ab_i}^h \left(\left| a \right\rangle \left\langle b_i \right| + \left| b_i \right\rangle \left\langle a \right| \right), \tag{6.43a}$$

$$\hat{V}^e = \sum_j V_{d^* b_j^*}^e \left(\left| d^* \right\rangle \left\langle b_j^* \right| + \left| b_j^* \right\rangle \left\langle d^* \right| \right) + \sum_j V_{a^* b_j^*}^e \left(\left| a^* \right\rangle \left\langle b_j^* \right| + \left| b_j^* \right\rangle \left\langle a^* \right| \right). \tag{6.43b}$$

In the tunneling limit, the donor and acceptor mixing onto the bridge is given by

$$\left| D \right\rangle \approx \left| d \right\rangle + \hat{G}^h \left(E_t^h \right) \hat{V}^h \left| d \right\rangle, \tag{6.44a}$$

$$\left| A \right\rangle \approx \left| a \right\rangle + \hat{G}^h \left(E_t^h \right) \hat{V}^h \left| a \right\rangle, \tag{6.44b}$$

and,

$$\left| D^* \right\rangle \approx \left| d^* \right\rangle + \hat{G}^e \left(E_t^e \right) \hat{V}^e \left| d^* \right\rangle, \tag{6.45a}$$

$$\left| A^* \right\rangle \approx \left| a^* \right\rangle + \hat{G}^e \left(E_t^e \right) \hat{V}^e \left| a^* \right\rangle, \tag{6.45b}$$

where $E_t^h = \varepsilon_d = \varepsilon_a$ and $E_t^e = \varepsilon_{d^*} = \varepsilon_{a^*}$ are the hole and electron tunneling energies, and $\hat{G}^h$, $\hat{G}^e$ are hole and electron bridge-Green's functions

$$\hat{G}^h \left(E \right) = \left(E \, \hat{I} - \left(\hat{H}_B^h + \hat{V}_B^h \right) \right)^{-1}, \tag{6.46a}$$

$$\hat{G}^e \left(E \right) = \left(E \, \hat{I} - \left(\hat{H}_B^e + \hat{V}_B^e \right) \right)^{-1}. \tag{6.46b}$$

Substituting eqs. (6.44) and (6.45) into eq. (6.26), we get the following terms for the exchange contribution to the Dexter coupling

$$T_{tr(ex)}(1) \approx \sum_{b_j} T_{b_j,a}\left(d^*a^*\left|db_j\right.\right) + \sum_{b_i} T_{b_i,d}\left(d^*a^*\left|b_ia\right.\right) + \sum_{b_j^*} S^{\dagger}_{b_j^*,a^*}\left(d^*b_j^*\left|da\right.\right) + \sum_{b_i^*} S^{\dagger}_{b_i^*,d^*}\left(b_i^*a^*\left|da\right.\right), \tag{6.47}$$

$$\begin{aligned} T_{tr(ex)}(2) \approx & \sum_{b_i}\sum_{b_j} T_{b_i,d}\,T_{b_j,a}\left(d^*a^*\left|b_ib_j\right.\right) + \sum_{b_j^*}\sum_{b_j} S^{\dagger}_{b_j^*,a^*}\,T_{b_j,a}\left(d^*b_j^*\left|db_j\right.\right) \\ & + \sum_{b_j^*}\sum_{b_i} S^{\dagger}_{b_j^*,a^*}\,T_{b_i,d}\left(d^*b_j^*\left|b_ia\right.\right) + \sum_{b_i^*}\sum_{b_j} S^{\dagger}_{b_i^*,d^*}\,T_{b_j,a}\left(b_i^*a^*\left|db_j\right.\right) \\ & + \sum_{b_i^*}\sum_{b_i} S^{\dagger}_{b_i^*,d^*}\,T_{b_i,d}\left(b_i^*a^*\left|b_ia\right.\right) + \sum_{b_i^*}\sum_{b_j^*} S^{\dagger}_{b_i^*,d^*}\,S^{\dagger}_{b_j^*,a^*}\left(b_i^*b_j^*\left|da\right.\right), \end{aligned} \tag{6.48}$$

$$\begin{aligned} T_{tr(ex)}(3) \approx & \sum_{b_j^*}\sum_{b_i}\sum_{b_j} S^{\dagger}_{b_j^*,a^*}\,T_{b_i,d}\,T_{b_j,a}\left(d^*b_j^*\left|b_ib_j\right.\right) \\ & + \sum_{b_i^*}\sum_{b_i}\sum_{b_j} S^{\dagger}_{b_i^*,d^*}\,T_{b_i,d}\,T_{b_j,a}\left(b_i^*a^*\left|b_ib_j\right.\right) \\ & + \sum_{b_i^*}\sum_{b_j^*}\sum_{b_j} S^{\dagger}_{b_i^*,d^*}\,S^{\dagger}_{b_j^*,a^*}\,T_{b_j,a}\left(b_i^*b_j^*\left|db_j\right.\right) \\ & + \sum_{b_i^*}\sum_{b_j^*}\sum_{b_i} S^{\dagger}_{b_i^*,d^*}\,S^{\dagger}_{b_j^*,a^*}\,T_{b_i,d}\left(b_i^*b_j^*\left|b_ia\right.\right), \end{aligned} \tag{6.49}$$

and

$$T_{tr(ex)}(4) \approx \sum_{b_i^*}\sum_{b_j^*}\sum_{b_i}\sum_{b_j} S^{\dagger}_{b_i^*,d^*}\,S^{\dagger}_{b_j^*,a^*}\left(b_i^*b_j^*\left|b_ib_j\right.\right)T_{b_i,d}\,T_{b_j,a}\,, \tag{6.50}$$

where $T_{i,j} = \langle i|\hat{G}^h\hat{V}^h|\,j\rangle$ and $S_{i,j} = \langle i|\hat{G}^e\hat{V}^e|\,j\rangle$.

For example, the fourth-order term (eq. (6.50)) includes only bridge Coulombic interactions, e.g., $\left(b_i^*b_i^*\left|b_jb_j\right.\right)$, $\left(b_i^*b_j^*\left|b_kb_k\right.\right)$, etc. If in this term we ignore the exchange interactions $\left(b_i^*b_j^*\left|b_ib_j\right.\right)$, where $i \neq j$, we get

$$T_{tr(ex)}(4) \approx \sum_{i=1}^{N} S^{\dagger}_{b_i^*,d^*}\,S^{\dagger}_{b_i^*,a^*}\left(b_i^*b_i^*\left|b_ib_i\right.\right)T_{b_i,d}\,T_{b_i,a} + \sum_{i\neq j}^{N} S^{\dagger}_{b_i^*,d^*}\,S^{\dagger}_{b_i^*,a^*}\left(b_i^*b_i^*\left|b_jb_j\right.\right)T_{b_j,d}\,T_{b_j,a}\,. \tag{6.51}$$

Here, N is the number of bridge sites. We can further expand $\hat{G}^h(E)=\hat{G}^h\left(E_t^h\right)$ and $\hat{G}^e(E)=\hat{G}^e\left(E_t^e\right)$ in the $S_{i,j}$ and $T_{i,j}$ terms in powers of $\hat{V}_B^h$ and $\hat{V}_B^e$, respectively. The corresponding Dyson expansions are

$$\hat{G}^h \approx \hat{g}^h + \hat{g}^h \hat{V}_B^h \hat{g}^h + \ldots \quad , \quad \hat{G}^e \approx \hat{g}^e + \hat{g}^e \hat{V}_B^e \hat{g}^e + \ldots \tag{6.52}$$

where $\hat{g}^h(E)=\left(E\hat{I}-\hat{H}_B^h\right)^{-1}$ and $\hat{g}^e(E)=\left(E\hat{I}-\hat{H}_B^e\right)^{-1}$.

Assuming identical nearest-neighbor interaction matrix elements in the chain, and retaining only the lowest-order terms in the Dyson expansions, we get perturbative approximations to the terms in eq. (6.51). For example, for the first term in eq. (6.51),

$$\sum_{i=1}^{N} S^{\dagger}_{b_i^*,d^*} S^{\dagger}_{b_i^*,a^*} \left(b_i^* b_i^* \middle| b_i b_i\right) T_{b_i,d}\, T_{b_i,a}\,, \tag{6.53}$$

we get

$$\sum_{i=1}^{N}\left(b_i^* b_i^* \middle| b_i b_i\right) \times \left(\frac{V^e_{d^*b_1^*}\left(V^e_{b^*b^*}\right)^{i-1}}{\left(\Delta E^e\right)^i}\right)\left(\frac{V^e_{a^*b_N^*}\left(V^e_{b^*b^*}\right)^{N-i}}{\left(\Delta E^e\right)^{N-i+1}}\right)\left(\frac{V^h_{db_1}\left(V^h_{bb}\right)^{i-1}}{\left(\Delta E^h\right)^i}\right)\left(\frac{V^h_{ab_N}\left(V^h_{bb}\right)^{N-i}}{\left(\Delta E^h\right)^{N-i+1}}\right). \tag{6.54}$$

In the language of tunneling pathways analysis, eq. (6.54) is the product of five terms summed over all bridge sites i: (1) the electron propagation amplitude from the donor to the bridge site i, (2) the electron propagation amplitude from bridge site i to the acceptor, (3) the hole propagation amplitude from the donor to the bridge site i, (4) the hole propagation amplitude from the bridge site i to the acceptor, and (5) the Coulombic attraction between populations (exciton binding energy) at bridge site i. The product terms in eq. (6.54) take the familiar (lowest-order pathway) form $\prod_i\left(V_{i,i+1}/\Delta E_i\right)$ where the numerator coupling elements reflect the structure and interactions of each bridging unit and the denominator energy gap reflects the barrier (at frozen nuclear geometry) for injecting an electron (or hole) onto bridge site i.

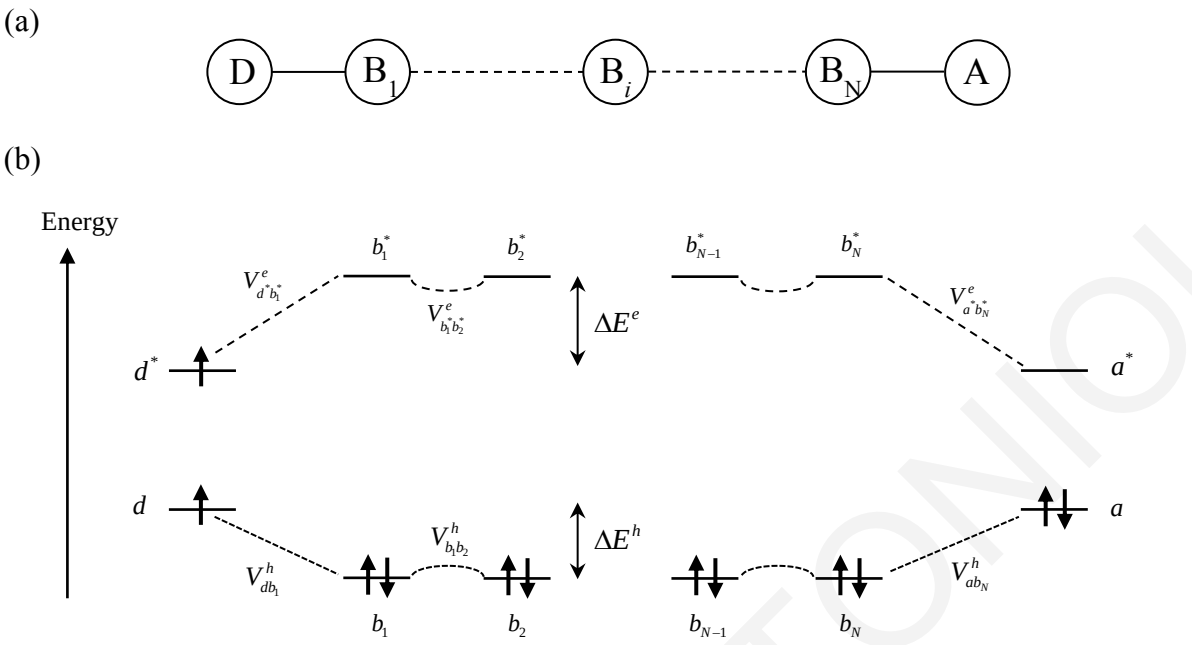

Figure 6.15: (a) D-B-A system with multiple bridge units. (b) The bridge is represented in a zeroth-order bonding and anti-bonding orbitals (one bonding and one anti-bonding orbital per bridge unit). These orbitals could be two-center bonds and anti-bonds.

6.3.3 Interferences among Dexter Coupling Pathways

Dexter EnT pathways interfere coherently, as do single ET pathways. We examine a model system with two parallel bridge sites that each support electron- and hole-coupling pathways (Fig. 6.16). In the total Hamiltonian, of eq. (6.28)

$$\hat{H}_B = \varepsilon_{b_1}\left|b_1\right\rangle\left\langle b_1\right| + \varepsilon_{b_1^*}\left|b_1^*\right\rangle\left\langle b_1^*\right| + \varepsilon_{b_2}\left|b_2\right\rangle\left\langle b_2\right| + \varepsilon_{b_2^*}\left|b_2^*\right\rangle\left\langle b_2^*\right|, \tag{6.55}$$

and $\hat{V}_{\text{int}} = \hat{V}^h + \hat{V}^e$, with

$$\begin{aligned}\hat{V}^h = {} & V^h_{db_1}\left(\left|d\right\rangle\left\langle b_1\right| + \left|b_1\right\rangle\left\langle d\right|\right) + V^h_{ab_1}\left(\left|a\right\rangle\left\langle b_1\right| + \left|b_1\right\rangle\left\langle a\right|\right) \\ & + V^h_{db_2}\left(\left|d\right\rangle\left\langle b_2\right| + \left|b_2\right\rangle\left\langle d\right|\right) + V^h_{ab_2}\left(\left|a\right\rangle\left\langle b_2\right| + \left|b_2\right\rangle\left\langle a\right|\right),\end{aligned} \tag{6.56a}$$

$$\begin{aligned}\hat{V}^e = {} & V^e_{d^*b_1^*}\left(\left|d^*\right\rangle\left\langle b_1^*\right| + \left|b_1^*\right\rangle\left\langle d^*\right|\right) + V^e_{a^*b_1^*}\left(\left|a^*\right\rangle\left\langle b_1^*\right| + \left|b_1^*\right\rangle\left\langle a^*\right|\right) \\ & + V^e_{d^*b_2^*}\left(\left|d^*\right\rangle\left\langle b_2^*\right| + \left|b_2^*\right\rangle\left\langle d^*\right|\right) + V^e_{a^*b_2^*}\left(\left|a^*\right\rangle\left\langle b_2^*\right| + \left|b_2^*\right\rangle\left\langle a^*\right|\right).\end{aligned} \tag{6.56b}$$

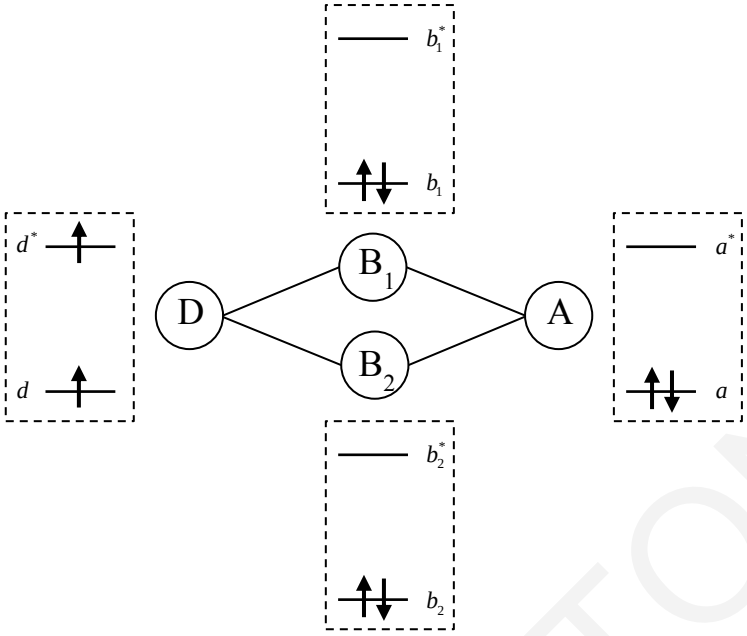

Figure 6.16: Double slit D-B-A system model for relating ET and HT donor-acceptor couplings to the triplet exciton (Dexter) donor-acceptor coupling. The bridge is represented in a local bonding and anti-bonding orbital representation. It is assumed that the two parallel bridge units are not coupled to each other by tunneling interactions.

Using the same approximations that led to eq. (6.54) we find

$$\begin{aligned} T_{tr(ex)} \approx & \left(\frac{V^e_{a^*b_1^*}}{\Delta E^e_1}\right)\left(\frac{V^e_{d^*b_1^*}}{\Delta E^e_1}\right)\left(b_1^*b_1^*\middle|b_1b_1\right)\left(\frac{V^h_{db_1}}{\Delta E^h_1}\right)\left(\frac{V^h_{ab_1}}{\Delta E^h_1}\right) \\ & + \left(\frac{V^e_{a^*b_2^*}}{\Delta E^e_2}\right)\left(\frac{V^e_{d^*b_2^*}}{\Delta E^e_2}\right)\left(b_2^*b_2^*\middle|b_2b_2\right)\left(\frac{V^h_{db_2}}{\Delta E^h_2}\right)\left(\frac{V^h_{ab_2}}{\Delta E^h_2}\right) \\ & + \left(\frac{V^e_{a^*b_1^*}}{\Delta E^e_1}\right)\left(\frac{V^e_{d^*b_1^*}}{\Delta E^e_1}\right)\left(b_1^*b_1^*\middle|b_2b_2\right)\left(\frac{V^h_{db_2}}{\Delta E^h_2}\right)\left(\frac{V^h_{ab_2}}{\Delta E^h_2}\right) \\ & + \left(\frac{V^e_{a^*b_2^*}}{\Delta E^e_2}\right)\left(\frac{V^e_{d^*b_2^*}}{\Delta E^e_2}\right)\left(b_2^*b_2^*\middle|b_1b_1\right)\left(\frac{V^h_{db_1}}{\Delta E^h_1}\right)\left(\frac{V^h_{ab_1}}{\Delta E^h_1}\right), \end{aligned} \tag{6.57}$$

which can be rewritten as

$$T_{tr(ex)} \approx \left(\frac{T^{e(1)}_{d^*a^*}}{\Delta E^e_1}\right)\left(b_1^* b_1^* \,|\, b_1 b_1\right)\left(\frac{T^{h(1)}_{da}}{\Delta E^h_1}\right) + \left(\frac{T^{e(2)}_{d^*a^*}}{\Delta E^e_2}\right)\left(b_2^* b_2^* \,|\, b_2 b_2\right)\left(\frac{T^{h(2)}_{da}}{\Delta E^h_2}\right) + \left(\frac{T^{e(1)}_{d^*a^*}}{\Delta E^e_1}\right)\left(b_1^* b_1^* \,|\, b_2 b_2\right)\left(\frac{T^{h(2)}_{da}}{\Delta E^h_2}\right) + \left(\frac{T^{e(2)}_{d^*a^*}}{\Delta E^e_2}\right)\left(b_2^* b_2^* \,|\, b_1 b_1\right)\left(\frac{T^{h(1)}_{da}}{\Delta E^h_1}\right), \tag{6.58}$$

where $T^{e(i)}_{d^*a^*} = \left(V^e_{d^*b_i^*} V^e_{a^*b_i^*}\right) \Big/ \Delta E^e_i$ and $T^{h(i)}_{da} = \left(V^h_{db_i} V^h_{ab_i}\right) \Big/ \Delta E^h_i$. If we retain only the largest two-electron integrals $\left(b_i^* b_i^* \,|\, b_i b_i\right)$, the first two terms survive and we get a coherent sum of two parallel Dexter pathway interactions

$$T_{tr(ex)} \approx \left(\frac{T^{e(1)}_{d^*a^*}}{\Delta E^e_1}\right)\left(b_1^* b_1^* \,|\, b_1 b_1\right)\left(\frac{T^{h(1)}_{da}}{\Delta E^h_1}\right) + \left(\frac{T^{e(2)}_{d^*a^*}}{\Delta E^e_2}\right)\left(b_2^* b_2^* \,|\, b_2 b_2\right)\left(\frac{T^{h(2)}_{da}}{\Delta E^h_2}\right). \tag{6.59}$$

This result may be generalized to the case of two parallel bridges denoted upper (U) and lower (L) with N_U and N_L sites, respectively

$$T_{tr(ex)} \approx \left(\frac{T^{e(L)}_{d^*a^*}}{\Delta E^e_L}\right)\left(\frac{T^{h(L)}_{da}}{\Delta E^h_L}\right)\sum_{i_L=1}^{N_L}\left(b_{i_L}^* b_{i_L}^* \,|\, b_{i_L} b_{i_L}\right) + \left(\frac{T^{e(U)}_{d^*a^*}}{\Delta E^e_U}\right)\left(\frac{T^{h(U)}_{da}}{\Delta E^h_U}\right)\sum_{i_U=1}^{N_U}\left(b_{i_U}^* b_{i_U}^* \,|\, b_{i_U} b_{i_U}\right). \tag{6.60}$$

The two-electron integrals in the above summation represent electron-hole attractions between bonding and anti-bonding charge densities, and are negative in value (i.e., exciton binding energies).

6.4 References

[1] V. May and O. Kühn, Charge and Energy Transfer Dynamics in Molecular Systems, Wiley-VCH, Weinheim, Germany, 2004.

[2] A. Nitzan, Chemical Dynamics in Condensed Phases, Oxford Univ. Press, Oxford, 2006.

[3] S. S. Skourtis and D. N. Beratan, Adv. Chem. Phys.,1999, 106, 377-452.

[4] S. Priyadarshy, S. S. Skourtis, S. M. Risser and D. N. Beratan, J. Chem. Phys., 1996, 104, 9473-9481.

[5] S. S. Skourtis, J. J. Regan and J. N. Onuchic, J. Phys. Chem., 1994, 98, 3379-3388.
[6] S. S. Skourtis, D. N. Beratan and J. N. Onuchic, Chem. Phys., 1993, 176, 501-520.
[7] S. S. Skourtis and J. N. Onuchic, Chem. Phys. Lett., 1993, 209, 171-177.
[8] D. N. Beratan, et al., Acc. Chem. Res., 2009, 42(10), 1669-1678.
[9] D. N. Beratan and S. S. Skourtis, Protein-mediated electron-transfer: pathways, orbital interactions, and contact maps. In Biological Electron-Transfer Chains: Genetics, Composition and Mode of operation, G. W. Canters and E. Vijgenboom, editors, Kluwer Academic Pub-lisher, Dordrecht, The Netherlands, pp. 9-27,1998.
[10] S. S. Skourtis and D. N. Beratan, J. Biol. Inorg. Chem., 1997, 2, 378-386.
[11] S. S. Skourtis and D. N. Beratan, J. Phys. Chem., 1997, 101, 1215-1234.
[12] J. N. Onuchic, S. M. Risser, S. S. Skourtis and David N. Beratan, The Design of starburst dendrimer electron transfer systems. In Molecular Electronics, M. Ratner and J. Jortner, editors, Iupac Chemistry for the 21st Century series, Blackwell Science, Oxford UK, pp. 369-379, 1997.
[13] S. S. Skourtis, J. N. Onuchic and D. N. Beratan, Inorg. Chim. Acta, 1996, 234, 167-175.
[14] S. S. Skourtis and S. Mukamel, Chem. Phys., 1995, 197, 367-387.
[15] W.B. Curry, M.D. Grabe, J.V. Kurnikov, S.S. Skourtis, D.N. Beratan, et al., J. Bioenerg. and Biomembr., 1995, 27, 285-293.
[16] S. S. Skourtis, D. H. Waldeck and D. N. Beratan, J. Phys. Chem. B, 2004, 108(40), 15511-15518.
[17] J. N. Onuchic and D. N. Beratan, J. Chem. Phys., 1990, 92(1), 722–733.

Chapter 7: Conclusions

The major objective of this Thesis was to further explore new theoretical/computational strategies that will enable the active control of electron transfer (ET) and energy transfer (EnT) reactions in molecular systems. We developed analytical frameworks based on donor (D) – bridge (B) – acceptor (A) molecular models, and employed numerical simulations and *ab initio* electronic structure computations of real molecules. The broader impact of this work on the research field is that it provides new powerful theoretical tools, for the ultimate task to control ET and EnT in molecular structures and materials. Specifically in Chapter 4, we established "design principles" for modifying specific ET molecules and experimental setups, in order to enhance the control of ET through application of infrared (IR) pulses. In Chapters 5 and 6 we developed a coupling-pathway theory for bridge-mediated triplet EnT, where we suggest improved formulas that take into account bridge-exciton contributions to EnT pathways which have been ignored until now in previous studies. We further used the formulation to demonstrate how to decompose the EnT coupling into coupling pathways, and to identify dominant through-bridge exciton pathways in EnT molecules.

In Chapter 4 I explored the feasibility of perturbing bridge-mediated ET with the application of a single IR pulse (for a realistic pulse-parameter regime), that selectively excites ET-active bridge vibrational modes. To describe the IR-perturbed ET reaction, I use a dissipative density matrix (Lindblad-type) model that takes into account the effects of vibrational relaxation. I suggested parameter regimes and molecular architectures that may enable the measurement of IR-pulse perturbations to bridge-mediated ET rates. The main focus of this study was on the fast ET rate regime (~ps) where the aim is to perturb ET "as the electron transfers". This is done by directly exciting an IR-active ET-active bridge mode with a subpsec period and a frequency above the mode continuum. I find that two important generic conditions need to be satisfied in order to have a measurable IR-perturbing effect on the ET rate "as the electron transfers". First, the bridge electronic state must be occupied with substantial probability during ET. This means, that the B state cannot create a very deep tunneling barrier for the transferring electron. Thus, the IR-perturbation effect is maximized for coherent resonant through-bridge tunneling. The second condition relates to the timescale-competition between ET and vibrational relaxation. If the timescale of ET and vibrational relaxation of the IR-excited B mode are

of the same order, the IR-induced ET rate perturbation is enhanced. In contrast, if the vibrational relaxation of the IR-excited B mode is faster than ET, the effects of the IR pulse on the ET rate as the electron transfers will be diminished. Finally, I have observed that for typical and moderate bridge electron-vibrational couplings, the IR-perturbation effect is substantial only for relatively strong IR fields that are accessible *via* surface enhanced infrared absorption settings.

In Chapter 5 we have developed a coupling pathway description for the bridge-mediated triplet EnT (Dexter) coupling. The most important result of our pathway analysis was the demonstration that bridge-exciton contributions to the overall triplet EnT coupling can be significant, and definitely cannot be ignored (as implicitly done by previous theories). Specifically, our theoretical and computational analysis showed that virtual bridge-exciton intermediate states dominate the triplet EnT coupling for long bridges and/or low tunneling-energy gap bridges. Further, the exponential sensitivity of the triplet EnT coupling to D-A distance and to bridge structure (and energetics), suggests that the bridge-mediated D-to-A triplet EnT rates and their directionality may be controlled by manipulating the bridge structure. The developed theory enables an atomic-level description for the origins of triplet EnT coupling, a necessary step toward controlling triplet EnT coupling interactions in a wide range of systems of current interest in energy science and in molecular biophysics. The single-particle coupling pathway analytical formulation introduced is sufficiently general to enable the further development of structure–function relations for triplet EnT interactions. This formulation was further used in Chapter 6 in the bridge-eigenstate basis in order to decompose and to identify the dominant through-bridge pathways for some D-B-A EnT systems. In addition to the single-particle coupling pathway framework, I further developed D-B-A models that take into account double-particle exchange contributions to illustrate exchange EnT pathways, which demonstrate strong analogies to ET pathways.

Appendix

Numerical code that solves the Liouville equation for $\hat{\sigma}(t)=\hat{\sigma}^{el}(t)\otimes\hat{\sigma}^{vi}(t)$ for modelling infrared-perturbed electron transfer

To perform the necessary calculations of Chapter 4 I developed an extensive numerical code that solves the Liouville equation (eq. (4.13)). The code is written in MATLAB and its present form is optimized for speed and computational memory usage. The numerical code incorporates D, B, A electronic states and two normal mode oscillators, one coupled to the bridge state and the other to acceptor state (see Fig. 4.4). Thus it includes in total $N=N_{el}\times N_{vib}$ vibronic states, where $N_{vib}=n_B\times n_A$, and n_B and n_A are the vibrational modes (states) of the first and second oscillator, respectively. Importantly, the code is readily expandable, and allows one to increase the number of electronic and vibrational states of the system. This gives us the flexibility to adjust the complexity of the D-B-A system model.

The structure of the code is based on five basic parts and is illustrated in Fig. A.1. The parts that construct the equations: (i) the DBA system Hamiltonian (eqs. (4.5)-(4.9)), (ii) the time dependent Hamiltonian of the IR field (eq. (4.10)), (iii) the dissipative part consisting of vibrational relaxation decay rates (eq. (4.12)), (iv) the Liouville equation (eq. (4.13)). The part that solve the equations and compute observables: (v) computes the time evolution of the D and A probabilities with and without the IR perturbation ($P_D(t)$, $P_D^{(IR)}(t)$ and $P_A(t)$, $P_A^{(IR)}(t)$, respectively) performing partial vibrational traces (Tr_{vib}) or electronic traces (Tr_{el}) of the total system density matrix $\hat{\sigma}(t)=\hat{\sigma}^{el}(t)\otimes\hat{\sigma}^{vi}(t)$. Translation from Hilbert space indices (states) to Liouville space indices (states) and vice versa is an essential procedure, and for this reason a function was created, build-in the code, which efficiently transforms the individual Hamiltonians from Hilbert to Liouville space.

All the Hamiltonians/Liouvilians are created using a nearest-neighbors approach. More precisely I build an array of indices of vibronic states that are coupled, and an array of the Hamiltonian (couplings) elements for these states. I do not store full matrices but only

create on the fly using the above arrays the elements that appear in the Liouville equation (eqs. (4.11) and (4.13)).

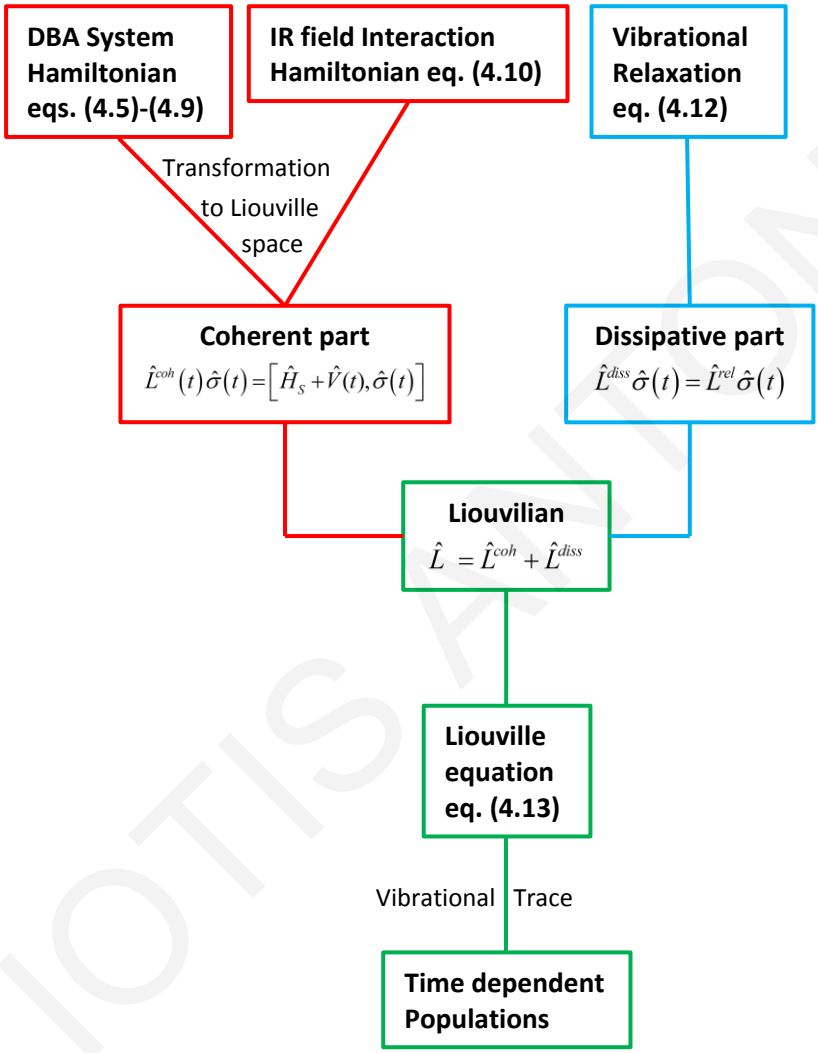

Figure A.1: Flowchart demonstrating the structure of the numerical code.